Prepared for:

National Institute for Coastal and

Marine Management (RWS/RIKZ)

Technical Advisory Committee on Water Defences (TAW-C)

Spectra in an estuary during a superstorm

August 1996

TUDelft

Delft University of Technology

delft hydraulics

H 2368

Spectra in an estuary during a superstorm

N. Booij, L.H. Holthuijsen, R.C. Ris and G. Ph. van Vledder

Executive's summary

In the framework of the HYDRA project a study was performed to obtain an understanding of nearshore wave conditions that can be expected during a severe storm in the Friesche Zeegat along the dikes of the Frisian mainland. To that end a 'superstorm' was defined and used as a boundary condition for flow and wave model computations. The specification of the superstorm was obtained by parameterizing the February 1953 storm followed by a modification of a few storm parameters (mostly intensifying the storm). The project consisted of the following main tasks:

1) flow model computations to obtain current velocities and water levels in the Friesche Zeegat,
2) wave model computations in the Friesche Zeegat, using the results of task 1.

The flow computations were carried out with three different models. First, the Continental Shelf Model (CSM) was used to obtain the current velocity and water level fields for the whole North Sea. The CSM model provided boundary conditions for the Waddenmodel. This second model was used to compute currents and water levels for the whole Dutch part of the Waddensea. Finally, the Friesche Zeegat flow model was nested in the Waddenmodel to compute current and water level fields in the Friesche Zeegat.

The wave model computations were carried out with two models. First, the third generation 'overall' SWAN wave model was used to compute the wave conditions in the Friesche Zeegat at the height of the storm, defined as the moment of time with the highest water level in the central part of the Friesche Zeegat. The SWAN model was also used for a sensitivity analysis to obtain an understanding of the effect of variations in boundary conditions, physics and numerics on the wave conditions in the Friesche Zeegat. The third generation 'overall' PHIDIAS wave model was used to compute the time variation of the wave conditions in the Friesche Zeegat for a period of 8 hours around the peak of the storm.

Prior to the wave model computations, two modifications to the SWAN model were carried out: nesting of computational grids and transformation of relative frequency spectra to absolute-frequency spectra.

The results of the flow computations indicate that at the peak of the superstorm the flow in the Waddensea is mainly from West to East. The results of the SWAN wave model computations indicate that the wave conditions along the Frisian dike are mainly determined by the local wind and by depth limitations on the tidal flats in the Waddensea. The offshore wave boundary condition has little or no effect on the nearshore wave conditions. In addition it was found that the effect of currents on the nearshore wave conditions was very small. Finally, the results of the instationary run with the PHIDIAS wave model indicate that the most severe nearshore wave conditions occur at the moment of high water and remain more or less constant for the next 4 hours.

The results of this study comprise a large amount of numerical and graphical results. The wave model results are presented as coloured contour plots for a number of wave parameters, cross sections of these wave parameters along three rays, and 1d- and 2d spectral plots. Only

a fraction of these results is included in this report. A full set of graphical results is available in a separate volume of this report.

Contents

List of tables

List of figures

List of figures (vervolg)

List of figures (vervolg)

1 Introduction

The present report describes the setup and results of the project 'Spectra in an estuary during a superstorm'. The purpose of this project was to develop an understanding of the relative importance of various phenomena during an extreme storm leading to the design wave conditions for dikes in estuaries. Further, basic material required for further verification of the models will be developed. This project was carried out jointly by DELFT HYDRAULICS and Delft University of Technology for the National Institute for Coastal and Marine Management of Rijkswaterstaat (RIKZ).

In the present study the Friesche Zeegat has been selected as the location for the above mentioned studies. The Friesche Zeegat is an estuary located between the Dutch wadden islands Ameland and Schiermonnikoog. Its location is shown in Figure 1.1. The bottom topography of the Friesche Zeegat is shown in Figure 1.2. The Friesche Zeegat has a complex topography and is characterized by a shallow outer delta which has a deep channel running north-south and curving eastwards towards the closure dam of the former Lauwers Sea.

The original scope of this project consisted of the following tasks:

A) Flow computations for a super storm,
B) Two-dimensional wave computations with the wave models SWAN and PHIDIAS.
C) Sensitivity analysis (parameters), with the SWAN model
D) Sensitivity analysis (wave spectra), with the SWAN model
E) Flow computations for verification study
F) Extension of SWAN functionality

During the execution of this project a number of modifications were made to the scope of work. The original scope of work for the flow computations contained the use of three models: CSM-8, ZUNOWAK and the Friesche Zeegat flow model. This sequence of flow models led to unreliable results in the Waddensea, which was due to a too crude schematization of the Waddensea in the ZUNOWAK model. Due to these problems the original scope of work was modified and the ZUNOWAK model was replaced by the curvi-linear Wadden model. Another modification was to merge task D into task C and to skip task E. The last modification was the addition of an extra case for the sensitivity study with the SWAN wave model. In this case the peak period of the incoming waves was set to a higher value.

The scope of work of this project was described by RIKZ in their Request For Proposal (RFP) of June 11, 1995. Based on this RFP DELFT HYDRAULICS and Delft University of Technology made a proposal for this study. This was formulated by DELFT HYDRAULICS in their letter of July 11, 1995, HK5508/H2368 to RIKZ, in which Delft University was contracted by DELFT HYDRAULICS for tasks B, C and F. On September 6, 1996, the project started as RIKZ contract RKZ-236.

The project was carried out in the period August 1995 and July 1996 as DELFT HYDRAULICS project H2368. The tasks B, C and E were performed by N. Booij, L.H. Holthuijsen and

R.C. Ris of Delft University of Technology. The tasks A, B were carried out by G.Ph. van Vledder, G.K.F.M van Banning, G. Hartsuiker and E.J. Ehrlich of DELFT HYDRAULICS.

The structure of this report is as follows. The methodology of this study is presented in Chapter 2. This includes a description of the superstorm and the various assumptions made in this project. Chapter 3 gives an overview of the flow computations that were made to obtain current velocities and water levels in the Friesche Zeegat. The results of the wave model computations are presented in Chapter 4. This includes a description of the various models, the model setup and a description of the computations that have been carried out. The main part of Chapter 4 covers the presentation of the computational results. Summary and conclusions for this study are given in Chapter 5. Finally, recommendations are given in Chapter 6.

2 Methodology

2.1 Introduction

This chapter describes the elements of the superstorm project. The wind field of the superstorm is described in Section 2.2. The wave boundary conditions are given in Section 2.3. Section 2.4 contains a description of the bottom topography used for the flow and wave model computations. The setup of the wave model computations is described in Section 2.5.

The present study aims to obtain an understanding of nearshore wave conditions that can be expected during a severe storm along the dikes of the Frisian main land along the Friesche Zeegat. To that end a 'superstorm' was defined and used as a boundary condition for flow and wave model computations. This superstorm is an adapted version of a parameterized February 1953 storm. Details thereof can be found in Section 2.3.

The wind fields of the superstorm were used as input for the flow modelling in the Friesche Zeegat to compute the current and water levels associated with a severe storm. The associated astronomical forcing was taken from the period of the February 1953 storm.

The wind fields and the current and water level fields were used as forcing and boundary conditions for the wave model computations. These computations were carried out with two models. First, the third generation SWAN model was used to compute the wave conditions in the Friesche Zeegat at the peak of the storm, defined as the moment of time with the highest water level in the Friesche Zeegat. This moment was chosen on the expectation that the wave conditions near the coast are mainly depth-dependent, such that the highest wave conditions at the coast occur at the moment of high water. In these computations only one aspect of wave-current interactions is taken into account, viz. current refraction and wave blocking. The effects of wave-induced currents are not taken into account.

The third generation wave model SWAN was also used for a sensitivity analysis to obtain an understanding of the effect of variations in boundary conditions, physics and numerics on the wave conditions in the Friesche Zeegat. An overview of the various conditions is described in Section 2.3 of this Chapter.

The third generation wave model PHIDIAS was used to compute the time variation of the wave conditions in the Friesche Zeegat for a period of 8 hours around the height of the storm to investigate the time variation of the wave conditions and to check the assumption that the highest nearshore wave conditions occur at the moment of high water.

For the analysis of the wave model results, three types of graphical output were made. First, contour plots of various wave parameters. Second, cross-sections of these wave parameters along three rays. Third, at 15 locations in the Friesche Zeegat, 1d and 2d-spectra were produced. In addition, tables of numerical results were produced. Due to the enormous amount of data plots, only a fraction of these results are included into this report. A full set of data is available in a separate volume to this report (DELFT HYDRAULICS, 1996).

2.2 Coordinate system and conventions

All coordinates are given with reference to the Paris coordinate system (the national grid in the Netherlands, Xp and Yp). Wave and wind directions are mostly given according to the nautical convention, i.e. the direction from which the wind and waves are coming with respect to North. Positive angles are given clockwise from North and are indicated as °N.

In the Paris system, the direction of the Xp-axis is taken towards the East and the Yp-axis is towards the North. In the specification of angles of grids, waves and winds, SWAN and PHIDIAS use the Cartesian or mathematical definition. In this system all directions are counted counter-clockwise from East. In addition, wind and wave direction are defined as the direction to which they are going.

In the present study a number of regular rectangular grids are used. They can have an arbitrary orientation. These grids are described in the HISWA/SWAN convention. In this convention they are characterized by the following parameters: X0, Y0, Lx, Ly, Dx, Dy, Mx, My and α. Here, X0 and Y0 represent the origin of the grid in the Paris coordinate system. Lx and Ly are the lengths of the sides of the grid and Dx and Dy are the sizes of the grid cells. Mx and My are the number of grid cells in x- and y-direction. α is the direction of the x-axis of the grid with respect to the Xp-axis.

2.3 Description of the superstorm

The superstorm is based on a modified '1953' storm. For the present project this storm was parameterized (Bijl, 1994), its intensity increased and the track of the storm was shifted somewhat to the North. Examples of computed wind fields at the peak of this storm are given in Figure 2.1a through Figure 2.1c. The time variation of the wind speed and direction is given in Table 2.1.

As can seen in the Figures 2.1a to 2.1c and in Table 2.1 the peak of the storm, in terms of wind speed, occurs at Feb. 1, 06:00 hrs. At that moment the wind speed is about 37 m/s with a direction of 313° N. During the superstorm the wind direction is slowly turning from west to north. An overview of the variation of the computed water level is also given in Table 2.1. These water levels have been computed with the Friesche Zeegat flow model. Details thereof are given in Chapter 3.

The results of the flow computations show that during the superstorm 2 moments of high water occur, viz. on Jan 31. 22:00 hrs and on Feb. 1, 08:00 hrs. The peak of the superstorm can be defined in various ways. One may choose the moment of time with the highest the wind speed or the moment with the highest water level. For the present study the latter criterion is used. Moreover, the first high water peak was chosen as the peak of the superstorm for which all computations were made.

2.4 Wave boundary conditions

The wave boundary conditions for the wave model computations with the SWAN and PHIDIAS models were provided by RIKZ on the basis of the wind and water level conditions at the -20 depth contour according to RIKZ (1995). In report the following relations have been used to derive the peak frequency T_p from the mean wave period T_{m01}: $T_{m02} = 0.9\ T_{m01}$ and $T_p = 1.55\ T_{m02}$.

Date and time	U (m/s)	Wdir (° N)	water level (cm)
5301 3116	23.50	273.05	141
5301 3117	25.12	278.93	184
5301 3118	26.74	284.04	258
5301 3119	28.42	288.44	328
5301 3120	30.10	292.37	385
5301 3121	31.78	295.86	426
5301 3122	33.05	298.67	443
5301 3123	34.31	301.27	438
5302 0100	35.58	303.68	426
5302 0101	36.09	305.39	412
5302 0102	36.59	307.05	390
5302 0103	37.10	308.66	365
5302 0104	37.15	310.03	353
5302 0105	37.19	311.40	357
5302 0106	37.24	312.77	374
5302 0107	36.68	313.72	400
5302 0108	36.12	314.70	414
5302 0109	35.56	315.72	409
5302 0110	34.79	316.81	390
5302 0111	34.01	317.95	359
5302 0112	33.24	319.14	315
5302 0113	31.97	320.11	260

Table 2.1 Variation of wind speed and wind direction and water level around the superstorm in the Friesche Zeegat.

Initially, the boundary wave direction was taken to be equal to the wind direction. This, however, was proved not workable, since then the mean wave direction was not directed into the Friesche Zeegat. To overcome this problem, the mean wave direction at the -20 m depth contour was 'forced' to a more northerly direction. The resulting wave boundary conditions are summarized in Table 2.2.

Date	Hs (m)	T_{m01} (s)	T_p (s)	θ_0 (° N)
5301 3116	5.24	8.24	11.49	310
5301 3117	5.68	8.58	11.97	310
5301 3118	6.50	9.18	12.81	310
5301 3119	7.28	9.71	13.55	310
5301 3120	7.96	10.16	14.17	310
5301 3121	8.34	10.40	14.51	310
5301 3122	8.54	10.52	14.68	310
5301 3123	8.53	10.51	14.66	310
5302 0100	8.44	10.46	14.59	310
5302 0101	8.34	10.40	14.51	310
5302 0102	8.14	10.27	14.33	310
5302 0103	7.92	10.13	14.13	310
5302 0104	7.80	10.05	14.02	310
5302 0105	7.81	10.06	14.03	311
5302 0106	8.01	10.19	14.22	312
5302 0107	8.25	10.34	14.42	313
5302 0108	8.41	10.44	14.56	314
5302 0109	8.35	10.40	14.51	315
5302 0110	8.25	10.34	14.42	316
5302 0111	7.95	10.15	14.16	317
5302 0112	7.42	9.81	13.68	319
5302 0113	6.78	9.37	13.07	320

Table 2.2 Variation of wave boundary conditions around the peak of the superstorm

2.5 Bottom topography

Prior to the flow and wave model computations a bottom topography was constructed. For the Friesche Zeegat a bottom topography was provided by RIKZ. This bottom is known under the name FZHAREN.BOD and it is shown in Figure 1.2. It is given on a rectangular grid with a grid size of 100 m. Numerical characteristics of this grid are given in Table 2.3.

x0 (m)	y0 (m)	x1 (m)	y1 (m)	mx	my	dx (m)	dy (m)	α (°)
185796	596082	31300	23900	313	239	100	100	10

Table 2.3 Characteristics of grid of bottom topography FZHAREN.

Inspection of this bottom topography showed a suspicious hole at location Xp = 211,500, Yp = 605,000. This hole is shown in Figure 2.2. This figure shows a detail of the FZHAREN bottom topography. The depth of this hole was about 20 m. For use in the wave model computations it was 'numerically' filled.

The bottom topography FZHAREN was also implemented in the Friesche Zeegat flow model. Comparison with the bottom topography as used in the Waddenmodel showed that the bottom FZHAREN missed some shallow parts near the Frisian coast. To that end the bottom FZHAREN was extended at a number of locations along the dike of the Frisian main land. An overview of these locations is shown in Figure 2.3.

The modified and extended bottom topography was used on the flow computations with the Friesche Zeegat flow model and in the wave model computations.

2.6 Wave model computations

Wave model computations have been carried out with both the SWAN model and the PHIDIAS model. The SWAN model has been applied in stationary mode whereas the PHIDIAS was applied in instationary mode for a period of 8 hours.

As described in Section 2.1 the peak of the storm was defined as the moment in time with the highest water level in the Friesche Zeegat. As can be seen in Table 2.1 this moment is January 31, 1995, 22:00 hrs. For this moment all SWAN computations have been carried out. In the present study the wave model computations have been carried out with different wave boundary conditions instead of those specified in Table 2.1. For most cases a lower peak period was used, only for case B6 the specified boundary condition was used.

The SWAN model has been used for a base case (the standard run) and for a number of variations. In the standard run the default settings of the SWAN were used. An overview of the various cases with variations in boundary conditions (B), physical processes (P) and numerics (N) is shown in Table 2.4.

An overview thereof is presented in Chapter 4. Detailed information on the choice of these variations and the numerical values of parameter settings of the SWAN model for each of these variations is also given in Chapter 4 (see Section 4.2.2).

The PHIDIAS wave model computations were performed for a period of 8 hours around the first high water of the storm. The first computational result is given for Jan. 31, 1953, 18:00 hrs, the last result is given for 1 February 1953, 02:00 hrs.

Case	Description	Type of variation
B1	Standard run	
B2	Wind turned off	B
B3	No incoming waves	B
B4	No current effects	B
B5	Wind direction 350°N	B
B6	Higher peak period	B
C3	Higher coefficient for depth induced wave breaking, γ_d = 0.85	P
C4	No bottom friction	P
C5	No triads	P
C6	Extra water level of .30 m	B
C9	WAM cycle 3 settings	P
C10	Bottom noise	B
C11	Higher spatial resolution	N
C12	Other frequency range	N
C13	Artificial bottom topography	B

Table 2.4 Overview of cases computed with the SWAN model

3 Flow Simulations

3.1 Introduction

A set of flow simulations has been carried out to generate water level and flow fields during a superstorm (a schematized 1953 storm), Task A of the project. To that end a number of different model lay-outs is used. To avoid mixing-up of model names and sizes a detailed description of all used tidal models is given in Appendix I. An overview of the location of all these models is given in Figure 3.1.

On the basis of the preliminary results of the simulations, it was decided to change the approach and to use a different sequence of mathematical models as originally planned. It turned out that the resolution of the ZUNOWAK model was not high enough to generate a consistent and reliable flow field in the Waddensea, leading to unacceptable boundary conditions for the Friesche Zeegat model. It was therefore decided to change the approach in such a way that the sequence of CSM, WADDEN model and Friesche Zeegat model would be used. It turned out that the resolution of the curvi-linear Wadden model was slightly lower than the Friesche Zeegat model. However, it was decided to run both models.

During the project another difficulty occurred, which was caused by inexperience in running nested models with both space varying wind and pressure fields. For large scale models it is automatically assumed that the boundary conditions are compensated for the difference between reference pressure and the actual pressure. This is completely correct and should be done during storm simulations. This may lead to an impact on the boundary conditions of large scale models. However, when nesting a model via time series in a large model with space varying wind and pressure fields, this compensation for pressure differences is already accounted for in these time series and should not be done again. So, two different simulation models should be used for the overall and for the nested models. The overall model has to be compensated at its boundaries for atmospheric pressure effects, the nested model should not be compensated for this effect as it is already incorporated in the time series which are used as boundary conditions.

In the following sections an overview will be given of the steps taken to arrive at a certain result, which is briefly discussed.

3.2 Flow simulations for the superstorm

The original model sequence, which was chosen to represent the water level and flow fields for the Friesche Zeegat Area, for the superstorm (modified 1953 storm) was the sequence CSM, ZUNOWAK-bol model and FZ-model. The following steps were executed in sequence and controlled.

1 The program WIND of Bijl (1994) was slightly adapted to include a start-up period of the super-storm. The inclusion of this warming-up period was necessary to avoid jumps in the input conditions for the flow models. The start-up period had a duration of 60 hours. During the first 48 hours (28 January, 0:00 hrs - 30 January, 0:00 hrs) the wind was set to zero values and the CSM model was run without wind forcing.

For the next 12 hours (30 January, 0:00 hrs - 30 January, 12:00 hrs) the wind speed increased linearly in time and the CSM model was run with wind forcing. The proper wind data were given for a 72 hour period from 30 January, 12:00 hrs till 2 February, 12:00 hours. Generation of wind- and pressure fields for the CSM model was in spherical coordinates. Examples of the applied wind and pressure fields have already been shown in the Figures 2.1a through 2.1c.

2 The CSM model was prepared for the generation of water level time series at output locations along the boundary of the ZUNOWAK model.

3 A simulation was made with the CSM model in purely astronomical mode for the superstorm simulation period, without wind and pressure effects. This was done to serve as a reference and to check the performance of the model.

4 A simulation was made with the CSM model with superstorm wind- and pressure fields as generated in step 1.

5 The generated time series of water levels along the boundary support points of the ZUNOWAK model, were inspected and transferred to the ZUNOWAK model, this was done for the simulation with and the simulation without the superstorm.

6 Wind and pressure fields for the ZUNOWAK model were generated every 3 hours.

7 The ZUNOWAK model was prepared for the generation of water level time series at output locations along the boundaries of the FZ-model.

8 A simulation was made with the ZUNOWAK model in purely astronomical mode for the superstorm simulation period, without wind and pressure effects. This was done to serve as a reference and to check the performance of the model.

9 A simulation was made with the ZUNOWAK model with superstorm wind- and pressure fields as generated in step 6. Some results are shown in the Figures 3.2a through 3.2c. A detail of the flow field in the Friesche Zeegat at the peak of the storm is shown in Figure 3.3. This figure clearly shows that the Friesche Zeegat has only a few grid points in the ZUNOWAK model.

10 The generated time series of water levels along the boundary support points of the Friesche Zeegat model, were inspected and transferred to the Friesche Zeegat model, this was done for the simulation with and the simulation without the superstorm.

11 Wind and pressure fields for the FZ-model were generated every 3 hours.

12 A simulation was made with the FZ-model in purely astronomical mode for the superstorm simulation period, without wind and pressure effects. This was done to serve as a reference and to check the performance of the model.

13 A simulation was made with the FZ-model with superstorm wind- and pressure fields as generated in step 11.

At this moment it was decided in mutual consultation with the Client to stop this line and to revise the scope of work, which lead to the following steps:

14 The CSM model was prepared for the generation of water level time series at output locations along the boundaries of the WADDEN model.

15 A simulation was made with the WADDEN model in purely astronomical mode for the superstorm simulation period, without wind and pressure effects. This was done to serve as a reference and to check the performance of the model.

16 A simulation was made with the CSM model with superstorm wind- and pressure fields as generated in step 1.

17 The generated time series of water levels along the boundary support points of the WADDEN model, were inspected and transferred to the WADDEN model.

18 The WADDEN model was prepared for the generation of water level time series at output locations along the boundaries of the FZ-model. Thereafter the WADDEN model was run to compute flow and water level fields. Examples of these fields are shown in the Figures 3.4a through 3.4c.

19 A simulation was made with the FZ-model with superstorm wind- and pressure fields as generated in step 11. Some results are shown in the Figures 3.5a through 3.5c.

20 Conversion of computational results to output grids readable by the various wave models. For the HISWA and SWAN model the results have to be converted to a regular rectangular grid.

21 Extension of the flow and water level field for the area south of Ameland. To avoid unrealistic high flow velocities, a check was performed on the flow velocities such that they do not exceed $0.8\ \sqrt{(g.h)}$, with h the local waterdepth.

It is noted that the various flow models have not been calibrated against measurements. This might have been possible when the models were run in astronomical mode. For the present project this was not deemed necessary since the main purpose is to get a general insight into the wave conditions during a superstorm.

It is further noted that in general the Waddenmodel has a courser grid than the Friesche Zeegat model. This, however, is not valid for the four corners of the Friesche Zeegat model.

4 Wave model computations

4.1 Introduction

This Chapter gives an overview of the set-up of and the results obtained with the SWAN and PHIDIAS wave model computations. The set-up and results of the SWAN wave model are presented in Section 4.2. The results of the PHIDIAS model are presented in Section 4.3.

Prior to the execution of the wave model computations with the SWAN wave model it was necessary to modify the functionality of the SWAN model. In view of the foreseen set-up of the SWAN model for the present study two modifications were realized (Task F). First, the option of nesting was included in SWAN. This task is described in DUT (1995a), 'Design of nesting in the 3rd generation spectral wave model SWAN'. A second modification was to introduce a transformation of spectra between relative and absolute frequencies. This task is described in DUT (1995b), 'Design of transformation of relative-frequency wave spectra to absolute-frequency spectra in the SWAN wave model'.

4.2 SWAN model results

4.2.1 Setup

The present SWAN computations have all been carried out with SWAN Cycle 1, version 20.86. After several typical test computations, some modifications were found to be required. A summary of these modifications is given in Appendix II of this report.

Two types of computational grids are distinguished. A geographic grid and a spectral grid. The geographical grid should be chosen such that it covers the area of interest. The spectral grid should be chosen such that it covers the range of frequencies that can be expected for the superstorm conditions.

Geographic grids

The cases have been computed with two different, overlapping computational grids (a fine grid nested in a coarse grid), except one case where an additional superfine grid has been added for case C11. The resolution of the course grid was 250 x 250 m^2. The resolution fine grid is 125 x 125 m^2. The resolution of the super fine grid is 50 x 50 m^2. Characteristics of the 3 grids are given in Table 4.1. The grids are shown in Figure 4.1.

	X0	Y0	Lx	Ly	Mx	My	dx	dy	α (°)
course	182000	62000	24000	31000	96	124	250	250	280
fine	183650	610645	13000	27750	104	222	100	100	280
extra fine	192077	610773	2500	21000	50	420	50	50	280

Table 4.1 Characteristics of SWAN computational grids

Spectral grid

The cases have been computed with a spectral frequency resolution of 1/0936 f in the range from 0.05 Hz to 0.8 Hz with 32 frequencies. The directional resolution was 10° over the full circle with 36 directions. For case C12, however, the frequency range was limited to the range 0.05 Hz - 0.5 Hz, with 27 frequencies.

Computational parameters

The user commands of SWAN require the choice of certain parameters to be set (or to rely on defaults settings). For this study all settings were chosen to be default except for the numerical schema. These settings are also given in the manual.

The computations were carried out with SWAN in third-generation mode for wind input, quadruplet interactions, triad interactions and white-capping. The quadruplet wave-wave interactions are computed with the Discrete Interaction Approximation (DIA of Hasselmann et al; 1985). The expressions of Cavaleri and Malanotte-Rizozoli (1981) for describing the linear growth of the wave component, which have been slightly modified by Tolman (1992), have been used in this study. The expression of Janssen (1989, 1991) is used for the exponential growth term in SWAN. The following coefficients were used with the expressions for the wind input:

- coefficient for determining the rate of dissipation $c_{ds1} = 4.5$;
- coefficient which determines the dependency of the white-capping on wave number $\delta = 0.5$.

In SWAN a spectral version of the depth-limited part of Battjes-Janssen (1978) wave breaking model is used. This is applied proportionately to the energy in each spectral component so that it does not affect the spectral form. The accompanying coefficients are:

- critical wave height at which an individual wave begins to break, $H_{crit} = \gamma_s$*depth, with breaking parameter gamma of $\gamma_s = 0.73$;
- coefficient for determining the rate of dissipation $\alpha = 1.0$.

The energy dissipation due to bottom friction can be described by three different expressions in SWAN, those of Hasselmann et al. (1973, JONSWAP) and of Collins (1972), and of Madsen et al. (1988). In this study the expression of Hasselmann et al. (1973, JONSWAP) is used with the following parameter:

- coefficient for the JONSWAP formulation for bottom friction $c_{fjon} = 0.067$ m^2s^{-3} (default value in SWAN).

In shallow water the triad interactions are of significant importance. These interactions result in the transfer of energy to higher frequencies. The expression in SWAN which is used in this study is based on equation (11) of Eldeberky and Battjes (1995). For application in this project, however, the strength of the interactions was reduced by 50%.

Output grids, lines and points

The output is provided on the coarse computational grid where it does not overlap the fine grid. Otherwise the output is on the fine computational grid. At several points along three lines, detailed information has been provided (in particular spectra). The main line runs from deep water through the tidal inlet along the axis of the main tidal channel. Halfway between the barrier islands and the main coast this line divides into three separate lines. One continues along the (curving) channel, one continues straight ahead to the main land and the last runs across the shoals to the west of the channel. These lines and the output locations are shown in Figure 4.2.

Parameters

The following parameters have been computed:

- Significant wave height,
- mean wave period (relative frequency in the plots and absolute frequency in quantitative form such as tables),
- peak period,
- directional spreading,
- mean direction,
- spectral narrowness or wave groupiness parameter,
- ratio of significant wave height over depth.

The definition of these parameters are given in Appendix III.

4.2.2 Review of cases

An overview of the cases computed with the SWAN model has already been given in Section 2.6. All of these cases are variations on the base case which has been computed with the default settings of the SWAN model. Below, these cases are described in more detail including the reasons for choosing particular settings.

B1 The base case. Peak period is 10.52 sec.

B2 Wind turned off. This case gives an indication to the effect of local wind on the wave conditions in the Waddensea.

B3 No incoming waves. Inspection of this case may indicate the effect of the local wind on the wave conditions in the Waddensea may be assessed.

B4 No currents. Are currents important for the wave conditions in the Friesche Zeegat.

B5 Other wind direction. Are the wave conditions in the Waddensea sensitive to variations in the wind direction.

B6 Higher peak period of 14.68 sec. This case was added to assess the consequences of using a lower peak period.

C3 Other coefficient for wave breaking. On the basis of recent work by Eldeberky and Battjes (1996) the default value 0.73 for γ_d was set to 0.85 to compensate for the use of the mean frequency in the dissipation formulation instead of the more commonly used peak frequency.

C4 No bottom friction. Based on work by Young (1995) and other researchers it is assumed that bottom friction has little or no effect in many shallow water applications. It was therefore decided to turn this effect off.

C5 No triads. In view of the ongoing discussions about the effect and importance of triad interactions in shallow water the triads were turned off.

C6 Extra water level of 0.3 m. In view of uncertainties in flow modelling, the water level was increased with 0.3 m for the whole grid. Current velocities where not affected.

C9 WAM cycle 3 settings. The default settings of SWAN contain WAM cycle 4 settings. To see the effects of other wind input and white-capping formulations the SWAN model was run with WAM cycle 3 settings.

C10 Bottom noise. In view of uncertainties with respect to the exact bottom topography the standard bottom topography was polluted with noise. For this case the local water depth was increased with 20% of its value multiplied with a number from uniform distribution in the range 0.8-1.2. The spatial scale of this pollution was computed on a scale of 2500 m. An overview of the bottom topography for this case is shown in Figure 4.3. The differences with respect to case B1 are shown in Figure 4.4.

C11 Higher spatial resolution. Since the main interest of this study is in the wave conditions near the dike of the Frisian main land an extra fine nest was defined for a small strip along the dike. This nest area has a grid size of 50 m. The location of this grid is shown in Figure 4.1. Its numerical characteristics are given in Table 4.1.

C12 Other frequency range. To see the effect of another frequency resolution, the highest model frequency was lowered from 0.8 Hz to 0.5 Hz. To retain the same frequency spacing as for the base case, the number of frequencies was lowered to 27.

C13 Artificial bottom topography. A case with an artificial bottom topography was defined to investigate the possibility that general conclusions may be drawn for schematic Waddensea situations. In view of experience in the WASP project an artificial bottom topography was defined with the following characteristics.

- a shallow Waddensea with a depth of 2 m
- a shallow area between the barrier island with a depth of 0 m.
- two barrier islands with width of 3 km and separated by 10 km
- a trench running from deep water to the dike of the main land.

For the wave computation an overall water level of 5 m was used. The precise locations of the dike and barrier islands was chosen such that the same computational grids could be used as for the base case. The rays and output locations are different from the base case. The bottom topography, rays and output locations for case C13 is shown in Figure 4.5.

4.2.3 The base case

The base case will be shown here in full (all available information). The input file for the SWAN computation is given in Appendix IV. Reference is made to section 2.1 where the main purpose of these computations is stated.

All geographic distributions (in a format of coloured contour plots) of the output parameters are given in Figures 4.6. The information along the output rays is provided in Figures 4.7 and the spectra are given in Figures 4.8. Numerical values of flow, depth and wave parameters at the output locations of the base case and all variations are given in the Tables 4.2.1 through 4.2.10.

The waves penetrate from the deep water to the barrier islands while dissipating some energy (although shoaling will delay the decrease in significant wave height somewhat). The dissipation is also indicated by the value of the ratio of significant wave height over depth which is equal to about 0.4 (contour Figure 4.6.8; a value often considered to be the maximum attainable in gentle slope conditions). At the western lateral boundary the significant wave height is unrealistically low (Figure 4.6.8) because the boundary condition there is "no waves". This absence of wave energy penetrates into the computational area under an angle of approximately 30° (arriving at the eastern of Ameland, thus avoiding penetration of the tidal inlet).

The waves arriving at the tidal inlet will dissipate considerable energy at the shoals at the entrance (see contour Figure 4.6.2 and ray Figure 4.7.1). This is clearly visible in the decrease of the significant wave height. In fact, the location of the outer delta and of the shoals is readily discernable in the contour line plots of the significant wave height (Figure 4.6.2).

The waves then penetrate into the area behind the barrier, in particular into the main tidal channel (this effect is also visible in the differences of the significant wave height along the three rays, Figures 4.7.1, 4.7.2 and 4.7.3). This seems to be a penetration of the waves from deep water but actually it is the effect of wave generation in the channel(s) that is seen. Outside the channel the generation is rather limited, resulting in higher waves in the channel(s) than outside the channel(s). The base case is not enough to arrive at this conclusion. It is only obvious when this case is compared with case B3 (no deep water waves and only local wind generation).

The local generation in the western part of the tidal flats (south of Ameland) is limited in the computation because of the same boundary problems as in deep water. The wave conditions along the dike of the main land is therefore not reliable at the western side of the computational area from the western boundary to location 16. From this location in eastern direction, the significant wave height just offshore increases from about 1.5 m to about 2 m further east (where the water is also deeper).

The shift at the entrance from dissipating deep water waves to the local generating of waves is also visible in the shift of the peak frequency from the deep water waves (at about 10.5 s) to the locally generated waves (4.6 s; Figure 4.6.4). This is very obvious in the spectra (Figure 4.8.3) of location 3 (where the deep water waves still dominate), station 4 (where the two wave fields are equally relevant) and location 5 (where the locally generated waves

dominate). Since the two peak frequencies differ considerably, the change in value in the transition zone is rather abrupt as shown by the steep gradients in the values in Figure 4.8.1.

The mean wave period is shifting gradually from the deep water value to the value of the local wind sea. It increases slightly from the deep water boundary to the tidal inlet (it is speculated that this is a shoaling effect). Over the tidal flats the waves seem to arrive fairly quickly at an equilibrium state because both the significant wave height and the mean wave period remain nearly constant. Moreover, the ratio of significant wave height over depth is nearly constant at a value between 0.35 and 0.4. However, the deep water waves can penetrate fairly far across the tidal flats. For instance, at location 14 the low frequency energy is clearly visible in the spectrum (Figure 4.8.14). This penetration seems to occur only in the areas directly exposed to the tidal gap (shadowing by the islands in other areas, compare the spectra at locations 8 and 14 with the spectra at locations 10 and 11). This penetration of the deep water waves complicates the directional behaviour of the waves near the exposed part of the dike of the main land (between locations 15 and 10, say). The locally generated waves propagate roughly in the wind direction (WNW) whereas the deep water waves travel from North. East of location 10, the directional behaviour is uni-modal. In the channels the equilibrium state is more complex: the significant wave height and the mean period are slightly higher than over the tidal flats but the directional width is more narrow (compare ray 1 and ray 2: contour Figures 4.6.5 and ray Figures 4.8.1, 4.8.2 and 4.8.3; indicating probably a drain of energy to the sides of the channel and / or an absence of wave energy from the sides with shallow water).

The directional spreading of the waves increases dramatically beyond the shoals at the tidal inlet (see Figure 4.6.5). Refraction apparently creates cross-seas here. Over the tidal flats the directional spreading is typically 30° (Figure 4.6.5) which is the normal value for wind generated waves. In the main channel and near the mainland dike the width decreases to about 20°, probably due to refraction. The directional width of the deep water waves decreases similarly near the mainland dike, see the spectra in Figure 4.8.15.

The frequency spectrum is obviously wide where the spectrum is bi-modal (the value of kappa is low). This is the case in the transition area from swell dominated sea to the wind sea dominated sea. Before and after, the narrowness indicates a uni-modal spectrum, in agreement with the shape of the computed spectra.

4.2.4 Variations

To investigate uncertainties in the state-of-the-art of wave modelling and in the boundary conditions (waves, currents, bathymetry etc.), the computations have been repeated for several variations in these aspects. They can be divided into three classes:

(1) variations in wave, wind, current and bathymetry conditions (cases B2, B3, B4, B5, B6, C10 and C13),
(2) variations in physics (cases C3, C4, C5, C6 and C9) and
(3) variations in numerics (cases C11 and C12). The following comments ignore the areas where the computed wave field is disturbed by improper boundary conditions (western boundary in particular).

No comments = no effect

Variations in wave, wind and current conditions

No wind (B2):
The significant wave decreases significantly from about 0.5 - 1.0 m in the inlet and the western tidal flats to about 2 m at the eastern tidal flats (this includes the areas directly off the mainland dike; see Figure 4.9). This larger difference at the eastern flats is probably due to the larger fetches and the greater depths in the area.

The peak period is obviously constant as there is no locally generated sea exists to "take over", except at the entrance of the main channel where the swell splits into two fields with different "dissipation and triad histories" (see locations 5 an 6, in Figure 4.9 and their spectra, Figure 4.10 and 4.11). The one travelling to SSE with higher frequencies and the on travelling to SSW with lower frequencies. Locally the high-frequency wave field dominates, shifting the peak frequency around locations 5 and 6.

The mean wave period decreases due to the absence of the locally generates waves which are high-frequency waves (see spectrum Figure 4.11) but this wave period does not decrease to the deep water value probably due to (low-frequency) dissipation and triad interactions.

The directional spreading (Figure 4.12) varies more than in the base case (the locally generated waves tend to suppress refraction effects in the base case) and more cross seas occur. In general the sea conditions are more confused.

The mean direction clearly shows which parts of the tidal flats and the dike are exposed to the deep water conditions (the shadowing effect of the islands, Figure 4.13). The deep water waves apparently travel along the main channel to the eastern tidal flats.

The spectral narrowness nearly constant, except at the entrance of the main channel where the spectrum is bimodal (see comments on "peak period").

The ratio of significant wave height over depth is decreasing because the wind cannot maintain the dissipation rates as in the base case.

Zero waves (B3):
The significant wave height is due only to the local wind and the differences with the base case south of location 5 are practically zero. Apparently the wave field over the tidal flat but also in the channels away from the tidal inlet is dominated by the wind. All other parameters are equally dominated south of location 4 by the local wind except the spectral narrowness, which in the presence of swell increases (broader spectrum, spectrum Figure 4.14).

No current (B4):
The pattern of the significant wave height over the tidal flats and along the mainland dike shifts slightly to the west (Figure 4.15). This is hardly noticeable along the rays (see Figure 4.16 for ray 1). The absence of currents makes the relative period equal to the absolute period. This complicates the comparison of periods and spectral narrowness because the wave period at the deep water boundary is not corrected for this. Differences with the base case are therefore almost entirely due to this effect. Directional effects of the currents

are very small (typically less than 5° for both the mean wave direction and the directional spreading).

Wind from 350° (B5):
The pattern of the significant wave height turns slightly west due to a turning of the sheltering effects of the islands (the waves are slightly lower south of the tip of Schiermonnikoog and south of the tip of Ameland) and of the shoals at the tidal inlet. The directional spreading is slightly larger over the tidal flats because of the larger difference between the initial wave direction and the local wind direction. The mean wave direction over the flats turn with the changed wind direction.

Higher peak period (B6):
The results for case b6 show that differences with the base case mainly occur in deep water. This can be seen in the ray plots (Figures 4.17, 4.18 and 4.19). South of station 3 the results are almost identical to those of the base case. North of Station 3 the differences are noticeable for the peak period, the mean wave period and the kappa parameters. South of station 3, differences are only noticeable for the kappa parameters.

The contour plots of integrated wave parameters are show that north of Schiermonnikoog the Hs/d (see Figure 4.20) ratio is somewhat higher for case B6 than for the base case.

Inspection of the spectra shows that significant differences occur for the stations 1, 2, 3 and 4 (see Figures 4.21 and 4.22). The effect of triad interactions can be seen clearly in the frequency spectrum for station 4. For both the base case (B1) and the current case, a secondary peak arises at twice the peak frequency. For station 5 (see Figure 4.23) the two secondary peaks have almost the same position, which is due to the effect of wind on the growth of the waves. For the stations closer to the coast it can be seen that some swell penetrates into the Waddensea up to the coast of the Frisian main land (e.g. for location 8, Figure 4.24).

Variations in physics

Gamma 0.85 (C3):
The significant wave height increases slightly (roughly between 5 and 12%) but less than the change in gamma (16%). The frequency spectrum becomes broader probably because the mean period (which normalizes the narrowness) decreases slightly. That in its turn is possibly because the white-capping retains the high-frequency tail of the spectrum but not the low-frequency part (spectrum Figure 4.25).

No bottom friction (C4):
The significant wave height increases slightly. Over the flats and in the channels the differences are of the order of a few centimetres (less than 0.10 m). The frequency spectrum is slightly broader because slightly more swell penetrates into the tidal area (see Figure 4.26 and spectral Figure 4.27).

No triads (C5):
The significant wave height increases slightly in the outer delta. The differences there are of the order of 0.10 m (Figure 4.28). The mean wave period increases somewhat in the outer delta due to less "triad pumping" from low frequencies to high frequencies (spectral

Figure 4.29 and 4.30). The differences are of the order of 0.5 s to 1.0 s. The absence of this high-frequency energy there decreases the width of the frequency spectrum (the value of kappa increases).

Deeper water (C6):
All differences are practically zero although the significant wave height and the mean wave period do increase with a few percent (less than about 5%).

WAM Cycle 3 (C9):
The significant wave height is about 0.20 m higher in deep water and about 0.10 to 0.40 m lower over the flats (Figure 4.31). This seems to indicate that the wave growth is slightly slower for young sea states and slightly faster for more mature sea states (the bottom dissipation is not changed). This is probably due to the fact that the WAM cycle 3 and cycle 4 wave growth formulations are not tuned in the SWAN model.

Bottom noise (C10):
Only in the deep water part does the significant wave height vary somewhat (about 0.10 m to 0.20 m). Otherwise the differences are less than 0.05 m. With hindsight it can be concluded that the current method of adding noise to the bottom topography is unrealistic. It would have been better to shift the position of sand banks and channels in a random way.

Variations in numerics

Superfine (C11):
The significant wave height along the mainland dike is locally about 0.16 m lower (see ray Figure 4.32). The mean wave period is slightly higher at this location (difference of 0.1 s).

Lower high freq (C12):
The significant wave height increases slightly (order of 0.10 to 0.05 m). The reason may well be the dependency of the quadruplet interaction on the treatment of the high-frequency tail (Banner and Young effect).

Artificial bottom (C13):
The results are essentially similar to the results in the real case: the swell penetrates just inside the tidal area where the local wind sea takes over (see shift of peak frequency). The swell does penetrate all the way to the mainland dike but its significance is minor. In this artificial case the refraction effects are very visible: part of the swell reflects on the (west) side of the main channel (see Figures 4.33 and 4.34). This is visible in the directional spreading which increases dramatically on the west of the channel. In the spectra the reflected energy is well visible at location 14 (towards SSE), see Figure 4.35. The three peaks in the two-dimensional spectrum there are remarkable. It is speculated that the high-frequency peak from the swell direction is generated by triad interactions (perhaps enhanced by local wind generation). The other high-frequency peak is probably pure wind sea, perhaps turned off the wind direction due to refraction.

4.3 PHIDIAS model results

4.3.1 Model setup

The PHIDIAS wave model is an instationary third generation wind-wave model. The model can be used for the computation for the wind-waves in deep, intermediate and shallow water, optionally in the presence of time varying current and water level fields. Descriptions and applications of the wave model can be found in DELFT HYDRAULICS (1994b) and in Van Vledder et al. (1994).

The PHIDIAS wave model is in many things similar to the SWAN wave model. The main differences between the versions of the two model which have been used in the present study are:

- PHIDIAS solves the action balance equation in a time-dependent way, whereas SWAN uses a sweep technique to arrive a stationary solution;
- PHIDIAS does not model the effect of triad interactions, whereas this source term is present in the SWAN wave model;
- PHIDIAS uses WAM cycle 3 physics whereas SWAN applies WAM cycle 4 physics.

For the present study version 1.1 of the PHIDIAS wave model was used.

The PHIDIAS model was run on the same grid as the course grid of the SWAN computations. Nesting was not applied in the PHIDIAS computation. The spectral resolution was as follows: 30 frequencies in the range 0.05 Hz - 0.8 Hz on a logarithmic grid. The directional resolution was 15° with 24 direction bins over the full circle.

The wave boundary conditions were obtained from RIKZ, they have already been given in Section 2.4. Wind and flow data were updated every hour. Output of wave model results is presented in the same way as for the SWAN wave model computations. The PHIDIAS input file is given in Appendix V.

4.3.2 Results of instationary run

The results are given for 9 moments of time. These times are summarized in Table 4.3 together with the time code used in the flow computations. Numerical results of the instationary PHIDIAS run are summarized in the Tables 4.4.1 through 4.4.10. Some graphical results are presented in this report.

The results of the computations indicate that spatial characteristics of the wave field are surprisingly similar to those obtained with the SWAN model. This can be seen in the Figures 4.3.6, 4.3.7 and 4.3.8, which shows the spatial distribution of the significant wave height, mean wave period and peak period. The spatial distribution of the peak period (see Figure 4.38) shows some unexpected high values near the coast of the Frisian mainland. The computed spectra are similar to those obtained with the SWAN wave model (see e.g. Figure 4.39). For nearshore locations, however, some strange phenomena occur in the computed spectra, see e.g. Figure 4.40. At present, the origin of these phenomena is not clear.

Date and time	Time code
530131 1800	T03
530131 1900	T04
530131 2000	T05
530131 2100	T06
530131 2200	T07
530131 2300	T08
530201 0000	T09
530201 0100	T10
530201 0200	T11

Table 4.3 Time codes of PHIDIAS wave model results

The time variation of these parameters shows that the significant wave height is rapidly increasing from T03 to T07 and then remains more or less constant till time T13. In the offshore points the wave heights slightly decrease, whereas they are still increasing for the deep water points in ray 2, which runs through the deep channel, the Zoutkamperlaag. The highest significant wave heights are found at time T11 for the near shore locations. The mean wave period has a similar behaviour as the significant wave height. A rapid increase from T03 to T07 whereafter they remain more or less constant. The numerical values of the peak period are more or less constant for all times, indicating that the 'take over' of the local wind sea over the offshore wave conditions takes place at more or less the same locations. The computed values of the Hs/d ratio are constant for the deep water offshore location and for the shallow near shore locations. The only exception is for the locations 10, 11 and 12 in Ray 2, where the waves may become somewhat higher because they are dependent on the local water depth.

5 Summary and conclusions

In this study flow and wave model computations have been carried out for the Friesche Zeegat to determine nearshore wave conditions along the dikes of the Frisian mainland during a superstorm. The superstorm was provided by RIKZ and consists of an adapted February 1953 storm. This 1953 storm has been parameterized and its parameters have been modified to strengthen the storm intensity and to shift the path to the North.

It is noted that conclusions that are formulated below are only valid for the superstorm conditions used in this study and for the Friesche Zeegat. The conclusions are not necessarily valid in general for the transformation of offshore wave conditions to nearshore wave conditions in estuaries. Despite this limitations, a large amount of information has been obtained that can be of use in further studies.

The bottom topography for the flow and wave model computations was obtained from RIKZ. This bottom was modified in two areas. First, a hole in the bottom at the end the Zoutkamperlaag was smoothed. Second, the bottom was extended southwards along the dike of the Frisian mainland by information from the bottom topography already available in the Wadden model.

The flow model computations have been carried out with three numerical flow models. First, the CSM-8 North Sea flow model was applied to determine flow and water level fields for the North Sea. In these computations astronomical boundary conditions have been used which are valid for the 1953 storm. In addition, the modified wind field was used to compute storm effects on the current and water level conditions. The results of the CSM-8 model were used as a boundary condition for a nested curvi-linear model covering the Waddensea. This model, the Waddenmodel, provided boundary conditions for the Friesche Zeegat flow model which was nested into the Waddenmodel. The coupling between the various flow models was via time series of water levels.

The coupling between the various models was not easy because of the strong wind forcing. This was especially noticeable at the corner points of the various grids and along the land-sea boundaries. In addition, in preliminary computations, double counting of pressure corrections led to severe problems before a satisfactory solution was found.

The results of the flow computations show that during the superstorm high water two peaks occur in the water level. In addition it was found that the flow in the Waddensea during the superstorm was from West to East. This result was not expected, it is, however, due to the strong westerly winds during the superstorm.

The computed current and water level fields were used as a boundary condition for the wave model computations, thus accounting for wave-current interactions as current-induced refraction and wave blocking. Effects of the wave field on the current field were not taken into account.

Since the Friesche Zeegat flow model has no active computational points south of Ameland, the flow and water level field for this area was constructed by copying flow information from the most westerly active line south of Ameland.

The SWAN wave model computations were carried out for the moment of time of the first peak of high water. This consisted of a base case model run for which the SWAN model was run with its default settings. Thereafter, the SWAN model was run for 14 other cases in which variations on boundary conditions, physical settings and numerical settings were applied.

The results of the SWAN wave model computations indicate that the wave conditions along the dikes of the Frisian mainland are mainly due to the effect of the local wind. The offshore boundary conditions have only a small effect on the nearshore wave conditions. This is due to the strong filtering effect of the shallow banks in the middle of the Friesche Zeegat. Some effects can be seen in the occurrence of low frequency energy near the dikes. This can best be seen by comparing the results for the cases B1 and B6. Near the coast the waves are mainly depth-limited and an equilibrium exists between energy gain by wind input and dissipation by depth-limited wave breaking. The effect of the currents on the wave conditions is hardly noticeable. This can be explained by the fact that the mean wave direction is more or less perpendicular to the current direction. The use of a more northerly wind direction gave essentially the same results as described above.

Bottom friction has little or no effect on the nearshore wave conditions. This was verified by turning its effect off. This result supports the conclusion that in areas with a complex bottom topography with many shallow areas, the effect of bottom friction is much smaller than dissipation effects by depth-limited wave breaking.

The effect of triad interactions was only noticeable in the shallow areas in the centre of the Friesche Zeegat. They have no effect on the nearshore wave conditions. In this area the water was very shallow and the waves relatively high. In the coastal zone, with a width of 1 km, the effect of triad interactions was not noticeable, probably because the waves have lost almost all of their energy. This was checked by turning them off in one of the variations. Closer to the Frisian coast the effect of triad interactions is not clear. This is because the scale of the computational grid is large compared to the spatial scale on which triads are assumed to have effect. One may therefore conclude that the effect of triads in these region may be omitted when computing nearshore wave conditions for superstorm conditions in an estuary. This result should be interpreted with care. Since the parameterization of the triad interactions is still in development, it may be possible that future and improved parameterizations may show different results in which its effects are more visible.

One variation with another formulation for wind generation (WAM cycle 3) indicates that some uncertainty exists in the proper wind formulation.

The use of a finer spatial grid gives somewhat smoother results in the area in front of the dikes, but its effect is small. Similarly, the use of a smaller frequency range hardly changes the results of the computations.

The effect of changing the peak period for the wave boundary condition on the main conclusions of this study is small.

The PHIDIAS model was applied for a period of 8 hours around the first high water peak. During this period the wind speed was still increasing and its direction slowly turning to the North. The results of the wave model computations indicate that the wave conditions in the Waddensea were increasing significantly in the period prior to the first peak of the storm

(in terms of water level) and that they stayed more or less constant during the following four hours. This result is not in line with the assumption (or expectation) that the highest nearshore wave conditions occur only at the moment of high water. In the shallow nearshore areas the wave height remains more or less constant because they are depth-limited, whereas in the relatively deep Zoutkamperlaag the wave height increases. The present results can be explained by noting that although the water level is already decreasing the wind speed is still increasing. The combined effects keep the nearshore wave conditions high.

6 Recommendations

Based on the results of this study the following recommendations for further studies and adaptions to the wave models for superstorm-like studies in the Friesche Zeegat can be made. These recommendations are divided into the following groups: storm specification, flow modelling, wave modelling and wave model settings.

Storm specification

- Use wind boundary conditions for other storm conditions, such that strong north-south currents occur through the tidal inlet. It is expected that then wave-current effects such as wave blocking and wave guiding are better visible. In the present study, an initially unexpected east-west current occurred in the Waddensea.

Flow modelling

- Omit the rectangular Friesche Zeegat flow model and use a nested curvi-linear Waddenmodel instead.

Wave modelling

- Include side wave boundary conditions to decrease the areas which are affected by side effects.
- Include other variations for the sensitivity analysis, for instance:
  - one with a more realistic 'bottom noise' in which locations of sand banks and channels are shifted in position,
  - turn depth and/or current refraction off.
- Produce spectra for other locations where interesting phenomena occur, for instance in the area between the islands of Ameland and Schiermonnikoog.
- Extend the period for the instationary run to cover also the second high water peak.
- Refresh the flow field every 15 minutes, in the present instationary run a time step of 1 hour was used.
- Investigate the effects of instationarity versus a series of stationary runs.
- Include two-way wave-current effects, viz. wave-driven currents, possibly only significant for smaller wind speeds
- Use a curvi-linear wave model in combination with a nested curvi-linear Waddenmodel.
- Improve wind input source term.

General

- Use one bottom topography for flow and wave computations.

SWAN wave model

- Use one convention for output wave directions.
- Include conversion of wave boundary condition in the presence of currents on the wave boundaries from absolute frequencies to relative frequencies.

PHIDIAS wave model

- Include WAM cycle 4 physics.
- Include source term for triad interactions.

References

Battjes, J.A., J.P.F.M. Janssen, 1978: Energy loss and set-up due to breaking of random waves, Proc. 16th Int. Conf. Coastal Engineering, Hamburg, 569-587.

Battjes, J.A. and G.Ph. van Vledder, 1984: Verification of Kimura's theory for wave group statistics. Proc. 19th Int. Conf. on Coastal Engineering. 642-648.

Bijl, W., 1994: Testing program 'Wind'. Report of Ministry of Transport, Public Works and Water Management, National Institute for Coastal and Marine Management/RIKZ, prepared for the EG*EPOCH project.

Cavaleri, L., P. Malanotte-Rizzoli, 1981: Wind wave prediction in shallow water, Theory and applications, J. Geophys. Res. 86, No. C11, 10, 961-10, 973.

Collins, J.I., 1972: Prediction of shallow water spectra, J. Geophys. Res. 77, 15, 2693-2707.

DELFT HYDRAULICS, 1994a: A curvi-linear model for the Dutch Waddensea (in Dutch), Report H2202.

DELFT HYDRAULICS, 1994b: Verification of PHIDIAS against shallow water wave data, Report H1914.

DELFT HYDRAULICS, 1996: Spectra in an estuary during a superstorm. Contour plots, ray plots and wave spectra. Appendix to report H2368.

DUT, 1995a: Design of nesting in the 3rd generation spectral wave model SWAN, N. Booij and R. Padilla-Hernandez. Report 8-95 Delft University of Technoloy, Fac. of Civil Engineering.

DUT, 1995b: Design of transformation of relative-frequency wave spectra to absolute-frequency spectra in the SWAN model, N. Booij. Report 10-95 Delft University of Technology, Fac. of Civil Engineering.

Eldeberky, Y. and J.A. Battjes, 1995: Parameterization of triad interactions in wave energy models. Proc. of Int. Conference Coastal Dynamics '95, Gdansk, Poland.

Eldeberky, Y. and J.A. Battjes, 1996: Spectral modelling of wave breaking: Application to Boussinesq equations. J. of Geophys. Res., Vol. 101, No. C1, 1253-1264.

Hasselmann, K., et al., 1973: Measurement of wind-wave growth and swell decay during the joint North Sea Wave Project (JONSWAP), Erganzungsheft zur Deutchen Hydrographischen Zeitschrift, 12.

Hasselmann, S., K. Hasselmann, J.H. Allender and T.P. Barnett, 1985: Computations and parameterizations of the linear energy transfer in a gravity wave spectrum, Part I. Parameterizations of the non-linear transfer for application in wave models. J. Phys. Oceanogr., 15, No. 11, 1378-1391.

Holthuijsen, L.H., N. Booij and R,C, Ris, 1993: A spectral wave model for the coastal zone. Proc. Int. Conf WAVES '93, New Orleans, 630-641.

Holthuijsen, L.H., N. Booij, R.C. Ris, 1996: User manual for the program SWAN Cycle 1, Simulation of WAves in the Near-shore, Faculty of Civil Engineering, Delft University of Technology, the Netherlands.

Janssen, P.A.E.M., 1989: Wave induced stress and the drag of air flow over sea waves, J. Phys. Oceanogr., 19, 745-754.

Janssen, P.A.E.M., 1991: Quasi-linear theory of wind-wave generation applied to wave forecasting, J. Phys. Oceanogr., 21, 1631-1642.

Kuik, A.J., G.Ph. van Vledder and L.H. Holthuijsen, 1988: A routine method for the analysis of pitch-and-roll buoy wave data. J. Phys. Oceanogr., Vol. 18, 1020-1034.

Madsen, O.S., Y.K. Poon, H.C. Graber, 1988: Spectral wave attenuation by bottom friction: theory, Proc. 21th Int. Conf. Coastal Engineering, Malaga, Spain, 492-504.

RIKZ, 1995: Golfrandvoorwaarden langs de Nederlandse kust op relatief diep water. Report RIKZ-95.024.

Ris, R.C., L.H. Holthuijsen and N. Booij, 1994: A spectral model for waves in the near shore zone. Proc. 24th Int. Conf. on Coastal Engineering, 68-78.

Tolman, H.J., 1992: Effects of numerics on the physics in a third-generation wind-wave model, J. Phys. Oceanogr., 22, 1095-1111.

Van Vledder, G. Ph., M.J.F. Stive and J.G. de Ronde, 1994b: Performance of a spectral wind-wave model in shallow water. Proc. 24th Int. Conf. Coastal Eng., 761-774.

Voogt, L., 1984: A tidal model of the North Sea based on the JONSWAP-1976 measuring campaign (in Dutch). Rijkswaterstaat, Report WWKZ-842.006.

loc	b1	b2	b3	b4	b5	b6	c3	c4	c5	c6	c9	c10	c11	c12	c13
1	1.540	1.540	1.540	.000	1.540	1.540	1.540	1.540	1.540	1.540	1.540	1.540	.000	1.540	.000
2	1.510	1.510	1.510	.000	1.510	1.510	1.510	1.510	1.510	1.510	1.510	1.510	.000	1.510	.000
3	.960	.960	.960	.000	.960	.960	.960	.960	.960	.960	.960	.960	.000	.960	.000
4	.780	.780	.780	.000	.780	.780	.780	.780	.780	.780	.780	.780	.000	.780	.000
5	.270	.270	.270	.000	.270	.270	.270	.270	.270	.270	.270	.270	.000	.270	.000
6	.440	.440	.440	.000	.440	.440	.440	.440	.440	.440	.440	.440	.000	.440	.000
7	1.090	1.090	1.090	.000	1.090	1.090	1.090	1.090	1.090	1.090	1.090	1.090	.000	1.090	.000
8	1.060	1.060	1.060	.000	1.060	1.060	1.060	1.060	1.060	1.060	1.060	1.060	1.060	1.060	.000
10	.850	.850	.850	.000	.850	.850	.850	.850	.850	.850	.850	.850	.000	.850	.000
11	.970	.970	.970	.000	.970	.970	.970	.970	.970	.970	.970	.970	.960	.970	.000
12	.610	.610	.610	.000	.610	.610	.610	.610	.610	.610	.610	.610	.610	.610	.000
14	1.150	1.150	1.150	.000	1.150	1.150	1.150	1.150	1.150	1.150	1.150	1.150	.000	1.150	.000
15	.810	.810	.810	.000	.810	.810	.810	.810	.810	.810	.810	.810	.810	.810	.000

Table 4.2.1 Current speed in x-direction at all output location and for all cases with SWAN

loc	b1	b2	b3	b4	b5	b6	c3	c4	c5	c6	c9	c10	c11	c12	c13
1	.400	.400	.400	.000	.400	.400	.400	.400	.400	.400	.400	.400	.000	.400	.000
2	.350	.350	.350	.000	.350	.350	.350	.350	.350	.350	.350	.350	.000	.350	.000
3	.280	.280	.280	.000	.280	.280	.280	.280	.280	.280	.280	.280	.000	.280	.000
4	.110	.110	.110	.000	.110	.110	.110	.110	.110	.110	.110	.110	.000	.110	.000
5	.040	.040	.040	.000	.040	.040	.040	.040	.040	.040	.040	.040	.000	.040	.000
6	-.090	-.090	-.090	.000	-.090	-.090	-.090	-.090	-.090	-.090	-.090	-.090	.000	-.090	.000
7	.130	.130	.130	.000	.130	.130	.130	.130	.130	.130	.130	.130	.000	.130	.000
8	-.010	-.010	-.010	.000	-.010	-.010	-.010	-.010	-.010	-.010	-.010	-.010	-.010	-.010	.000
10	-.160	-.160	-.160	.000	-.160	-.160	-.160	-.160	-.160	-.160	-.160	-.160	.000	-.160	.000
11	-.070	-.070	-.070	.000	-.070	-.070	-.070	-.070	-.070	-.070	-.070	-.070	-.060	-.070	.000
12	.020	.020	.020	.000	.020	.020	.020	.020	.020	.020	.020	.020	.020	.020	.000
14	.150	.150	.150	.000	.150	.150	.150	.150	.150	.150	.150	.150	.000	.150	.000
15	.300	.300	.300	.000	.300	.300	.300	.300	.300	.300	.300	.300	.300	.300	.000

Table 4.2.2 Current speed in y-direction at all output location and for all cases with SWAN

loc	b1	b2	b3	b4	b5	b6	c3	c4	c5	c6	c9	c10	c11	c12	c13
1	27.040	27.040	27.040	27.040	27.040	27.040	27.040	27.040	27.040	27.340	27.040	25.420	-1000.000	27.040	22.000
2	21.090	21.090	21.090	21.090	21.090	21.090	21.090	21.090	21.090	21.390	21.090	18.590	-1000.000	21.090	16.520
3	10.840	10.840	10.840	10.840	10.840	10.840	10.840	10.840	10.840	11.140	10.840	10.930	-1000.000	10.840	14.520
4	13.170	13.170	13.170	13.170	13.170	13.170	13.170	13.170	13.170	13.470	13.170	12.590	-1000.000	13.170	13.030
5	19.420	19.420	19.420	19.420	19.420	19.420	19.420	19.420	19.420	19.720	19.420	20.260	-1000.000	19.420	11.540
6	19.070	19.070	19.070	19.070	19.070	19.070	19.070	19.070	19.070	19.370	19.070	20.140	-1000.000	19.070	10.540
7	5.470	5.470	5.470	5.470	5.470	5.470	5.470	5.470	5.470	5.770	5.470	5.500	-1000.000	5.470	9.550
8	4.630	4.630	4.630	4.630	4.630	4.630	4.630	4.630	4.630	4.930	4.630	4.620	4.640	4.630	9.150
10	12.390	12.390	12.390	12.390	12.390	12.390	12.390	12.390	12.390	12.690	12.390	12.900	-1000.000	12.390	7.000
11	12.090	12.090	12.090	12.090	12.090	12.090	12.090	12.090	12.090	12.390	12.090	12.860	12.110	12.090	7.000
12	7.170	7.170	7.170	7.170	7.170	7.170	7.170	7.170	7.170	7.470	7.170	7.430	7.100	7.170	7.000
14	5.360	5.360	5.360	5.360	5.360	5.360	5.360	5.360	5.360	5.660	5.360	5.350	-1000.000	5.360	7.000
15	3.750	3.750	3.750	3.750	3.750	3.750	3.750	3.750	3.750	4.050	3.750	3.730	3.740	3.750	7.000

Table 4.2.3 Water depth at all output location and for all cases with SWAN

loc	b1	b2	b3	b4	b5	b6	c3	c4	c5	c6	c9	c10	c11	c12	c13
1	8.380	8.210	2.130	8.390	8.330	8.630	8.440	8.410	8.380	8.400	8.560	8.360	-10.000	8.370	7.650
2	7.340	6.870	3.070	7.450	7.360	7.390	7.590	7.520	7.320	7.370	7.600	7.140	-10.000	7.280	6.120
3	3.870	3.580	3.200	4.070	4.000	3.930	4.350	3.940	3.990	3.980	3.790	3.970	-10.000	3.780	3.980
4	3.960	3.170	3.150	4.150	3.850	3.980	4.360	4.050	4.240	4.060	3.730	3.900	-10.000	4.090	3.320
5	2.520	1.130	2.700	2.580	2.680	2.470	2.670	2.520	2.610	2.590	2.340	2.530	-10.000	2.600	3.130
6	2.560	1.130	2.620	2.640	2.620	2.550	2.740	2.600	2.730	2.630	2.390	2.570	-10.000	2.660	3.040
7	2.020	1.040	2.010	2.070	1.990	2.020	2.280	2.060	2.160	2.110	1.870	2.030	-10.000	2.130	2.910
8	1.770	1.000	1.770	1.800	1.760	1.770	2.020	1.800	1.900	1.870	1.630	1.770	1.700	1.870	2.840
10	2.500	.700	2.510	2.630	2.360	2.500	2.620	2.550	2.700	2.560	2.190	2.530	-10.000	2.590	2.560
11	2.270	.450	2.280	2.410	2.230	2.270	2.370	2.310	2.470	2.330	1.970	2.280	2.100	2.350	2.560
12	2.030	.340	2.050	2.170	2.180	2.030	2.110	2.080	2.190	2.080	1.800	2.040	1.870	2.090	2.550
14	1.870	.890	1.880	2.020	1.900	1.860	2.000	1.920	1.970	1.950	1.800	1.880	-10.000	1.910	2.380
15	1.470	.610	1.460	1.550	1.520	1.480	1.590	1.510	1.570	1.560	1.380	1.460	1.450	1.500	2.250

Table 4.2.4 Significant wave height at all output location and for all cases with SWAN

loc	b1	b2	b3	b4	b5	b6	c3	c4	c5	c6	c9	c10	c11	c12	c13
1	8.050	8.190	2.360	8.540	8.140	9.750	7.840	8.080	8.050	8.010	7.440	8.080	-10.000	8.010	8.660
2	8.320	8.840	3.220	8.740	8.460	8.910	8.160	8.380	8.510	8.360	7.620	7.890	-10.000	8.310	7.020
3	5.270	6.930	3.660	5.460	5.600	5.910	5.630	5.350	5.920	5.360	5.870	5.440	-10.000	5.700	5.060
4	4.960	6.870	4.020	5.380	5.360	5.200	5.260	5.090	5.140	5.030	5.110	4.960	-10.000	4.770	4.370
5	3.410	4.700	3.570	3.730	3.790	3.380	3.560	3.440	3.360	3.480	3.320	3.410	-10.000	3.190	4.190
6	3.340	4.680	3.430	3.810	3.650	3.330	3.510	3.380	3.350	3.410	3.210	3.350	-10.000	3.150	4.160
7	2.900	4.690	2.880	3.450	3.360	2.900	3.220	2.990	2.930	3.010	3.170	2.910	-10.000	2.840	4.110
8	2.690	4.930	2.680	3.210	3.020	2.690	2.980	2.760	2.700	2.800	2.980	2.690	2.780	2.670	4.130
10	3.310	4.120	3.320	3.880	3.340	3.310	3.420	3.370	3.320	3.370	3.130	3.340	-10.000	3.210	3.910
11	3.060	3.200	3.070	3.670	3.250	3.060	3.150	3.100	3.070	3.110	2.870	3.070	3.090	2.960	3.940
12	3.050	3.050	3.060	3.490	3.300	3.050	3.140	3.110	3.060	3.100	2.900	3.060	3.050	2.940	3.990
14	2.840	4.740	2.770	3.390	3.320	2.860	3.190	2.960	2.880	2.960	3.160	2.840	-10.000	2.890	3.570
15	2.570	6.270	2.530	2.950	3.030	2.580	2.830	2.670	2.590	2.680	2.890	2.550	2.680	2.530	3.450

Table 4.2.5 Mean wave period Tm02 at all output location and for all cases with SWAN

loc	b1	b2	b3	b4	b5	b6	c3	c4	c5	c6	c9	c10	c11	c12	c13
1	10.900	10.900	4.590	10.900	10.900	14.140	10.900	10.900	10.900	10.900	10.900	10.900	-10.000	10.110	10.900
2	10.900	10.900	5.450	10.900	10.900	14.140	10.900	10.900	10.900	10.900	10.900	10.900	-10.000	11.010	10.900
3	10.900	10.900	5.450	10.900	10.900	14.140	10.900	10.900	10.900	10.900	10.900	10.900	-10.000	11.010	10.900
4	10.870	10.870	6.490	10.870	10.870	15.390	10.870	10.870	10.870	10.870	10.870	10.870	-10.000	10.990	10.870
5	4.590	5.460	5.000	4.590	5.460	4.590	4.590	4.590	4.590	4.590	4.200	4.590	-10.000	4.700	5.460
6	4.590	5.460	5.000	5.000	5.460	4.590	5.000	4.590	4.590	4.590	4.590	4.590	-10.000	4.700	5.460
7	5.000	11.900	5.000	5.000	5.000	5.000	5.460	5.000	5.000	5.000	5.000	5.000	-10.000	5.100	5.460
8	5.000	11.900	5.000	5.000	5.000	5.000	5.460	5.000	5.000	5.000	5.000	5.000	5.000	5.100	5.460
10	5.460	12.990	5.460	5.460	5.000	5.460	5.460	5.460	5.460	5.460	5.000	5.460	-10.000	5.560	5.460
11	5.000	5.460	5.000	5.000	4.590	5.000	5.460	5.460	5.460	5.460	5.000	5.000	5.000	5.100	5.950
12	5.000	4.590	5.000	5.460	4.590	5.000	5.460	5.000	5.000	5.000	5.000	5.000	5.000	5.100	5.950
14	4.590	11.900	5.000	5.000	5.000	4.590	5.000	4.590	5.000	4.590	4.590	4.590	-10.000	4.700	5.000
15	4.590	11.900	4.590	5.000	4.590	4.590	4.590	4.590	4.590	4.590	4.590	4.590	4.590	4.700	5.000

Table 4.2.6 Peak period at all output location and for all cases with SWAN

loc	b1	b2	b3	b4	b5	b6	c3	c4	c5	c6	c9	c10	c11	c12	c13
1	26.340	25.790	31.600	26.200	25.850	25.460	26.430	26.390	26.340	26.390	27.560	26.430	-10.000	26.390	25.120
2	23.520	22.910	29.640	23.820	23.670	22.840	23.670	23.560	23.510	23.550	24.640	23.060	-10.000	23.610	23.560
3	24.140	22.150	29.680	27.510	22.850	22.250	25.490	23.870	21.370	24.080	23.190	23.150	-10.000	23.450	24.250
4	26.370	27.360	24.740	27.560	27.800	26.250	27.210	26.360	25.640	26.310	27.230	26.210	-10.000	26.690	29.510
5	32.610	27.070	30.490	33.080	23.980	32.970	32.600	32.650	33.450	32.430	34.120	32.490	-10.000	32.730	33.050
6	33.800	29.180	31.360	31.020	28.450	34.270	34.840	34.070	34.700	33.830	37.590	34.200	-10.000	34.540	32.110
7	29.660	25.710	27.990	28.500	27.330	30.000	30.930	29.640	30.190	29.880	32.870	29.930	-10.000	30.060	30.700
8	26.220	24.450	24.920	26.110	26.770	26.450	27.720	26.350	26.570	26.580	28.620	26.460	25.920	26.660	29.440
10	23.120	16.220	22.850	23.270	28.560	23.220	23.260	22.840	24.050	23.140	23.800	23.040	-10.000	23.670	26.070
11	22.880	16.940	22.760	22.990	31.220	22.900	23.360	22.650	23.830	22.880	23.960	22.860	21.660	23.560	24.120
12	19.320	12.290	19.230	21.110	28.130	19.320	19.290	19.120	20.100	19.180	19.530	19.250	17.220	19.500	23.010
14	30.400	33.480	28.400	27.270	26.780	30.930	32.230	30.730	31.450	30.850	32.200	30.310	-10.000	31.600	33.900
15	25.330	15.640	24.470	24.470	23.550	25.580	27.790	24.850	26.330	26.170	27.080	25.090	25.330	26.940	28.780

Table 4.2.7 Directional spreading at all output location and for all cases with SWAN

loc	b1	b2	b3	b4	b5	b6	c3	c4	c5	c6	c9	c10	c11	c12	c13
1	319.000	320.000	267.000	319.000	321.000	319.000	319.000	319.000	319.000	319.000	318.000	319.000	1269.000	319.000	322.000
2	325.000	327.000	293.000	323.000	329.000	325.000	325.000	325.000	325.000	325.000	324.000	326.000	1269.000	325.000	326.000
3	329.000	336.000	300.000	324.000	340.000	331.000	329.000	329.000	330.000	329.000	329.000	330.000	1269.000	329.000	334.000
4	314.000	326.000	304.000	311.000	332.000	315.000	315.000	314.000	313.000	315.000	317.000	313.000	1269.000	314.000	328.000
5	309.000	336.000	305.000	312.000	346.000	309.000	309.000	309.000	308.000	309.000	310.000	309.000	1269.000	309.000	316.000
6	306.000	359.000	305.000	308.000	348.000	305.000	306.000	306.000	305.000	306.000	307.000	306.000	1269.000	305.000	311.000
7	309.000	2.000	307.000	308.000	349.000	309.000	312.000	310.000	309.000	310.000	313.000	309.000	1269.000	310.000	309.000
8	309.000	7.000	308.000	307.000	347.000	309.000	312.000	311.000	309.000	310.000	314.000	310.000	310.000	310.000	309.000
10	306.000	318.000	306.000	304.000	334.000	306.000	306.000	306.000	305.000	306.000	306.000	306.000	1269.000	306.000	300.000
11	300.000	312.000	300.000	297.000	336.000	300.000	300.000	300.000	299.000	300.000	300.000	300.000	301.000	300.000	299.000
12	313.000	319.000	313.000	308.000	342.000	313.000	314.000	313.000	313.000	313.000	314.000	313.000	313.000	314.000	298.000
14	310.000	4.000	308.000	305.000	346.000	310.000	313.000	312.000	310.000	311.000	312.000	310.000	1269.000	311.000	301.000
15	314.000	5.000	313.000	311.000	347.000	314.000	318.000	315.000	315.000	315.000	318.000	314.000	314.000	316.000	298.000

Table 4.2.8 Mean wave direction at all output location and for all cases with SWAN

loc	b1	b2	b3	b4	b5	b6	c3	c4	c5	c6	c9	c10	c11	c12	c13
1	.640	.650	.550	.650	.640	.650	.640	.640	.640	.640	.650	.640	-1.000	.640	.660
2	.670	.670	.610	.670	.670	.560	.650	.670	.680	.670	.710	.660	-1.000	.690	.610
3	.530	.490	.590	.470	.490	.490	.490	.540	.730	.540	.530	.530	-1.000	.530	.490
4	.380	.460	.590	.340	.410	.370	.390	.390	.560	.390	.450	.390	-1.000	.400	.250
5	.350	.200	.560	.430	.490	.310	.330	.320	.320	.340	.310	.360	-1.000	.400	.280
6	.450	.260	.570	.530	.450	.430	.410	.430	.450	.440	.410	.450	-1.000	.480	.420
7	.360	.420	.530	.440	.380	.310	.310	.290	.360	.340	.300	.350	-1.000	.360	.510
8	.360	.440	.500	.400	.360	.320	.300	.290	.360	.340	.310	.360	.350	.360	.530
10	.510	.370	.570	.530	.480	.500	.470	.490	.500	.500	.510	.510	-1.000	.510	.410
11	.540	.300	.560	.560	.570	.540	.520	.520	.550	.540	.550	.550	.540	.560	.460
12	.530	.280	.550	.550	.570	.530	.510	.510	.530	.520	.550	.540	.530	.560	.470
14	.300	.420	.530	.380	.320	.230	.270	.220	.320	.270	.220	.300	-1.000	.280	.480
15	.380	.410	.530	.410	.350	.310	.340	.310	.390	.360	.310	.400	.400	.380	.570

Table 4.2.9 Spectral narrowness (kappa) at all output location and for all cases with SWAN

loc	b1	b2	b3	b4	b5	b6	c3	c4	c5	c6	c9	c10	c11	c12	c13
1	.310	.300	.080	.310	.310	.320	.310	.310	.310	.310	.320	.330	-10.000	.310	.350
2	.350	.330	.150	.350	.350	.380	.360	.360	.350	.340	.360	.380	-10.000	.340	.370
3	.360	.330	.300	.380	.370	.360	.400	.360	.370	.360	.350	.360	-10.000	.350	.270
4	.300	.240	.240	.320	.290	.300	.330	.310	.320	.300	.280	.310	-10.000	.310	.260
5	.130	.060	.140	.130	.140	.130	.140	.130	.130	.130	.120	.120	-10.000	.130	.270
6	.130	.060	.140	.140	.140	.130	.140	.140	.140	.140	.130	.130	-10.000	.140	.290
7	.370	.190	.370	.380	.360	.370	.420	.380	.400	.370	.340	.370	-10.000	.390	.300
8	.380	.220	.380	.390	.380	.380	.440	.390	.410	.380	.350	.380	.370	.400	.310
10	.200	.060	.200	.210	.190	.200	.210	.210	.220	.200	.180	.200	-10.000	.210	.370
11	.190	.040	.190	.200	.180	.190	.200	.190	.200	.190	.160	.180	.170	.190	.370
12	.280	.050	.290	.300	.300	.280	.290	.290	.300	.280	.250	.270	.260	.290	.360
14	.350	.170	.350	.380	.350	.350	.370	.360	.370	.340	.340	.350	-10.000	.360	.340
15	.390	.160	.390	.410	.400	.390	.420	.400	.420	.380	.370	.390	.390	.400	.320

Table 4.2.10 Hs/d ratio at all output location and for all cases with SWAN

loc	t03	t04	t05	t06	t07	t08	t09	t10	t11
1	1.190	1.490	1.650	1.660	1.540	1.360	1.170	1.010	.880
2	1.320	1.550	1.640	1.630	1.510	1.330	1.180	1.060	.960
3	.850	.920	.980	1.000	.960	.900	.840	.790	.750
4	.720	.760	.800	.850	.770	.600	.490	.440	.370
5	.100	.180	.200	.220	.270	.290	.320	.280	.260
6	.680	.740	.550	.480	.430	.420	.410	.390	.350
7	.720	.890	1.030	1.090	1.100	1.080	1.080	1.080	1.080
8	.700	.870	.990	1.060	1.070	1.050	1.050	1.050	1.050
10	1.070	1.340	1.240	1.050	.860	.670	.560	.530	.470
11	.980	1.270	1.220	1.120	.990	.830	.730	.690	.630
12	.710	.840	.750	.680	.610	.520	.470	.440	.420
14	.700	.840	1.000	1.110	1.150	1.130	1.110	1.080	1.080
15	.470	.530	.640	.760	.810	.800	.780	.750	.750

Table 4.4.1 Current speed in x-direction at all output locations around first peak

loc	t03	t04	t05	t06	t07	t08	t09	t10	t11
1	.200	.280	.360	.400	.400	.370	.320	.280	.260
2	.090	.160	.250	.320	.350	.340	.300	.260	.250
3	-.310	-.240	-.050	.140	.270	.360	.370	.340	.390
4	-.540	-.490	-.270	-.070	.100	.220	.240	.240	.310
5	-1.230	-1.100	-.500	-.110	.040	.170	.230	.240	.320
6	-.830	-.850	-.440	-.230	-.090	-.010	.020	.020	.070
7	-.240	-.150	-.010	.080	.130	.150	.140	.140	.150
8	-.190	-.150	-.080	-.040	-.010	.000	.000	-.010	.000
10	-.340	-.360	-.300	-.230	-.150	-.080	-.040	-.030	.000
11	-.170	-.200	-.150	-.110	-.070	-.030	.010	.030	.050
12	.050	.040	.030	.020	.020	.020	.010	.010	.010
14	-.140	-.080	.000	.090	.150	.160	.150	.130	.140
15	.040	.130	.200	.270	.310	.310	.300	.290	.290

Table 4.4.2 Current speed in y-direction at all output locations around first peak

loc	t03	t04	t05	t06	t07	t08	t09	t10	t11
1	25.140	25.850	26.430	26.850	27.020	27.000	26.880	26.760	26.560
2	19.240	19.970	20.560	21.000	21.180	21.150	21.020	20.900	20.700
3	8.800	9.580	10.210	10.670	10.860	10.830	10.710	10.600	10.410
4	11.060	11.860	12.530	13.010	13.210	13.200	13.080	12.970	12.790
5	17.060	17.930	18.650	19.180	19.400	19.400	19.300	19.190	19.040
6	16.490	17.380	18.130	18.680	18.930	18.950	18.850	18.750	18.620
7	2.910	3.830	4.600	5.170	5.430	5.460	5.380	5.290	5.170
8	2.040	2.980	3.760	4.340	4.620	4.660	4.590	4.510	4.400
10	9.720	10.620	11.450	12.080	12.380	12.450	12.370	12.290	12.180
11	9.230	10.130	11.010	11.660	12.000	12.090	12.030	11.960	11.870
12	4.300	5.190	6.120	6.790	7.150	7.260	7.210	7.150	7.070
14	2.750	3.750	4.550	5.110	5.350	5.360	5.260	5.180	5.060
15	1.090	2.130	2.980	3.600	3.860	3.850	3.740	3.650	3.550

Table 4.4.3 Water depth at all output locations around first peak (PHIDIAS)

loc	t03	t04	t05	t06	t07	t08	t09	t10	t11
1	6.660	7.440	8.040	8.380	8.520	8.510	8.460	8.370	8.250
2	5.910	6.530	7.020	7.290	7.480	7.510	7.500	7.450	7.390
3	3.180	3.520	3.740	3.930	4.160	4.190	4.070	4.020	3.980
4	3.160	3.550	3.650	3.820	4.210	4.280	4.360	4.230	4.240
5	1.410	1.870	2.220	2.590	2.810	2.870	2.930	2.900	2.930
6	1.460	1.940	2.260	2.570	2.830	2.860	2.910	2.870	2.890
7	1.150	1.500	1.680	1.940	2.190	2.220	2.220	2.150	2.120
8	.850	1.220	1.440	1.680	1.900	1.940	1.930	1.870	1.840
10	1.540	1.970	2.200	2.480	2.850	2.960	3.040	3.040	3.070
11	1.280	1.670	1.890	2.220	2.630	2.730	2.870	2.880	2.870
12	1.070	1.450	1.610	1.900	2.200	2.280	2.370	2.380	2.400
14	1.100	1.490	1.670	1.930	2.160	2.170	2.140	2.100	2.080
15	.520	.870	1.250	1.510	1.680	1.680	1.610	1.600	1.570

Table 4.4.4 Significant wave height at all output locations around first peak (PHIDIAS)

loc	t03	t04	t05	t06	t07	t08	t09	t10	t11
1	7.000	7.410	7.950	8.140	8.240	8.290	8.240	8.160	8.000
2	7.420	8.000	8.440	8.570	8.630	8.600	8.520	8.430	8.310
3	5.110	5.350	5.940	5.920	5.450	5.490	5.730	5.650	5.520
4	4.270	4.540	4.850	4.960	5.010	5.230	5.300	5.270	5.260
5	2.390	2.700	3.050	3.400	3.560	3.650	3.700	3.680	3.710
6	2.230	2.590	2.950	3.270	3.440	3.490	3.510	3.470	3.490
7	2.040	2.400	2.700	2.930	2.970	3.020	2.990	2.940	2.900
8	1.730	2.130	2.420	2.680	2.750	2.800	2.760	2.700	2.650
10	2.300	2.520	2.770	3.130	3.440	3.620	3.710	3.690	3.730
11	2.080	2.290	2.490	2.860	3.190	3.390	3.530	3.550	3.560
12	1.980	2.290	2.470	2.800	3.070	3.210	3.300	3.310	3.330
14	2.000	2.440	3.440	2.940	2.900	2.950	3.540	2.870	2.840
15	1.670	2.210	2.430	2.650	2.740	2.760	2.700	2.690	2.660

Table 4.4.5 Mean wave period at all output locations around first peak (PHIDIAS)

loc	t03	t04	t05	t06	t07	t08	t09	t10	t11
1	9.550	9.550	10.470	10.470	10.470	10.470	10.470	10.470	10.470
2	9.550	10.470	10.470	10.470	10.470	10.470	10.470	10.470	10.470
3	9.550	10.470	10.470	10.470	10.470	10.470	10.470	10.470	10.470
4	9.550	10.470	10.470	10.470	10.470	10.470	10.470	10.470	10.470
5	3.450	4.160	4.160	4.560	5.000	5.000	5.000	5.000	5.000
6	3.790	4.160	4.560	4.560	5.000	5.000	5.000	5.000	5.000
7	4.160	4.560	4.560	5.000	5.000	5.000	5.000	5.000	5.000
8	3.790	4.560	4.560	5.000	5.000	5.000	5.000	5.000	5.000
10	4.160	4.560	5.000	5.480	5.480	5.480	5.480	5.480	5.480
11	4.160	4.560	4.560	5.000	5.480	5.480	5.480	5.480	5.480
12	3.790	4.160	4.560	5.000	5.000	5.480	5.480	5.480	5.480
14	3.790	4.160	18.230	5.000	5.000	5.000	20.000	5.000	4.560
15	3.790	4.160	4.560	5.000	5.000	4.560	4.560	4.560	4.560

Table 4.4.6 Relative peak period at all output locations around first peak (PHIDIAS)

loc	t03	t04	t05	t06	t07	t08	t09	t10	t11
1	26.940	26.640	26.580	26.580	26.610	26.670	26.850	26.950	27.120
2	26.140	25.500	25.080	24.520	24.420	24.570	24.720	24.790	24.950
3	27.330	26.030	24.540	24.090	25.310	24.900	24.590	24.640	24.720
4	30.590	30.240	29.660	27.950	26.780	26.260	26.330	26.790	26.770
5	35.780	36.690	37.690	34.990	32.980	31.660	30.560	30.160	29.720
6	43.570	36.410	38.500	36.860	34.850	33.650	32.650	32.590	32.260
7	30.550	31.440	36.720	35.330	32.830	31.700	31.600	32.000	31.610
8	25.160	26.430	30.440	30.430	29.480	28.730	28.100	28.720	28.410
10	25.830	29.840	39.760	35.510	29.900	32.090	30.110	31.340	33.570
11	24.240	23.730	24.760	26.390	26.340	26.990	30.480	32.440	30.320
12	23.330	22.610	22.310	21.670	21.940	21.880	22.240	22.380	22.690
14	27.500	37.860	60.460	38.900	31.380	30.250	59.480	30.660	30.180
15	29.120	50.870	27.480	29.770	28.020	28.230	32.390	27.140	25.720

Table 4.4.7 Diretional spreading at all output locations around first peak (PHIDIAS)

loc	t03	t04	t05	t06	t07	t08	t09	t10	t11
1	323.000	324.000	324.000	319.000	319.000	319.000	319.000	319.000	318.000
2	326.000	327.000	327.000	324.000	324.000	323.000	323.000	323.000	323.000
3	327.000	329.000	331.000	328.000	325.000	325.000	326.000	326.000	326.000
4	306.000	309.000	313.000	312.000	310.000	310.000	310.000	311.000	310.000
5	305.000	309.000	311.000	310.000	309.000	311.000	312.000	313.000	314.000
6	298.000	303.000	308.000	305.000	304.000	305.000	306.000	308.000	309.000
7	298.000	301.000	308.000	308.000	307.000	309.000	310.000	312.000	313.000
8	298.000	301.000	309.000	308.000	307.000	309.000	310.000	312.000	312.000
10	298.000	299.000	300.000	303.000	304.000	304.000	305.000	305.000	305.000
11	290.000	293.000	296.000	297.000	298.000	298.000	297.000	296.000	298.000
12	307.000	310.000	312.000	313.000	314.000	314.000	314.000	315.000	315.000
14	293.000	295.000	283.000	301.000	304.000	307.000	290.000	309.000	311.000
15	303.000	305.000	307.000	306.000	306.000	308.000	308.000	311.000	313.000

Table 4.4.8 Mean wave direction (°N) at all output locations around first peak (PHIDIAS)

loc	t03	t04	t05	t06	t07	t08	t09	t10	t11
1	.650	.650	.640	.640	.640	.640	.640	.640	.650
2	.650	.650	.670	.680	.670	.680	.680	.680	.680
3	.690	.710	.730	.710	.690	.670	.680	.670	.650
4	.560	.580	.680	.640	.510	.480	.450	.460	.420
5	.280	.310	.270	.260	.290	.290	.310	.310	.340
6	.380	.440	.380	.400	.430	.430	.430	.440	.450
7	.430	.410	.250	.260	.290	.310	.310	.310	.320
8	.450	.400	.310	.280	.240	.260	.300	.290	.320
10	.500	.400	.130	.280	.360	.310	.400	.400	.470
11	.570	.560	.490	.360	.430	.410	.410	.410	.520
12	.560	.550	.540	.530	.530	.520	.520	.530	.530
14	.440	.200	.460	.200	.300	.300	.480	.320	.340
15	.190	.280	.380	.360	.350	.340	.370	.370	.380

Table 4.4.9 Spectral narrowness at all output locations around first peak (PHIDIAS)

loc	t03	t04	t05	t06	t07	t08	t09	t10	t11
1	.260	.290	.300	.310	.320	.320	.310	.310	.310
2	.310	.330	.340	.350	.350	.350	.360	.360	.360
3	.360	.370	.370	.370	.380	.390	.380	.380	.380
4	.290	.300	.290	.290	.320	.320	.330	.330	.330
5	.080	.100	.120	.130	.140	.150	.150	.150	.150
6	.090	.110	.120	.140	.150	.150	.150	.150	.160
7	.390	.390	.370	.370	.400	.410	.410	.410	.410
8	.420	.410	.380	.390	.410	.420	.420	.410	.420
10	.160	.190	.190	.200	.230	.240	.250	.250	.250
11	.140	.170	.170	.190	.220	.230	.240	.240	.240
12	.250	.280	.260	.280	.310	.310	.330	.330	.340
14	.400	.400	.370	.380	.400	.410	.410	.410	.410
15	.480	.410	.420	.420	.430	.440	.430	.440	.440

Table 4.4.10 Ration Hs/d at all output locations around first peak (PHIDIAS)

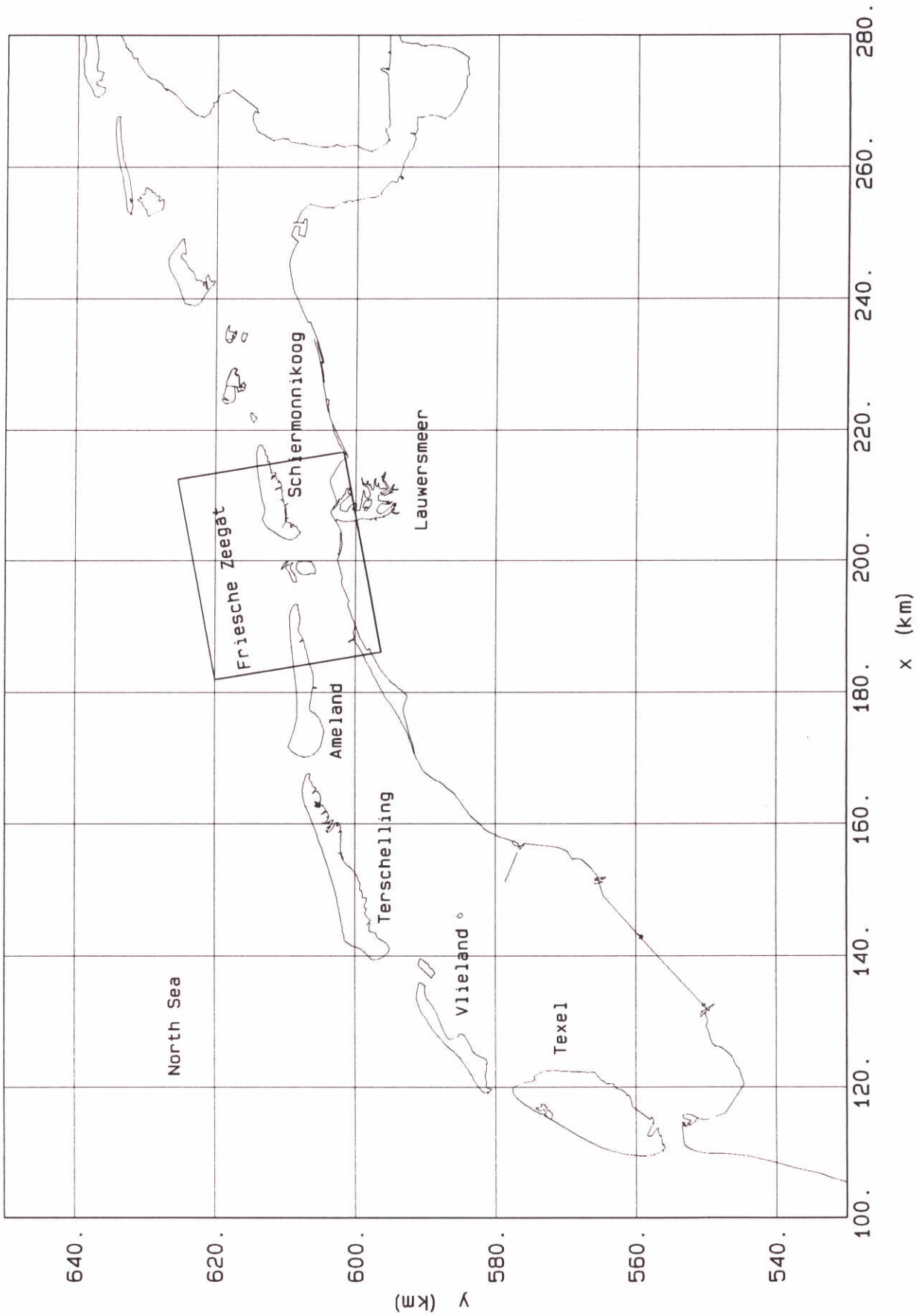

Overview of Dutch Waddencoast
and location of Friesche Zeegat
Coordinates in Paris system

superstorm

DELFT HYDRAULICS/DELFT UNIVERSITY OF TECHNOLOGY | H2368 | Fig. 1.1

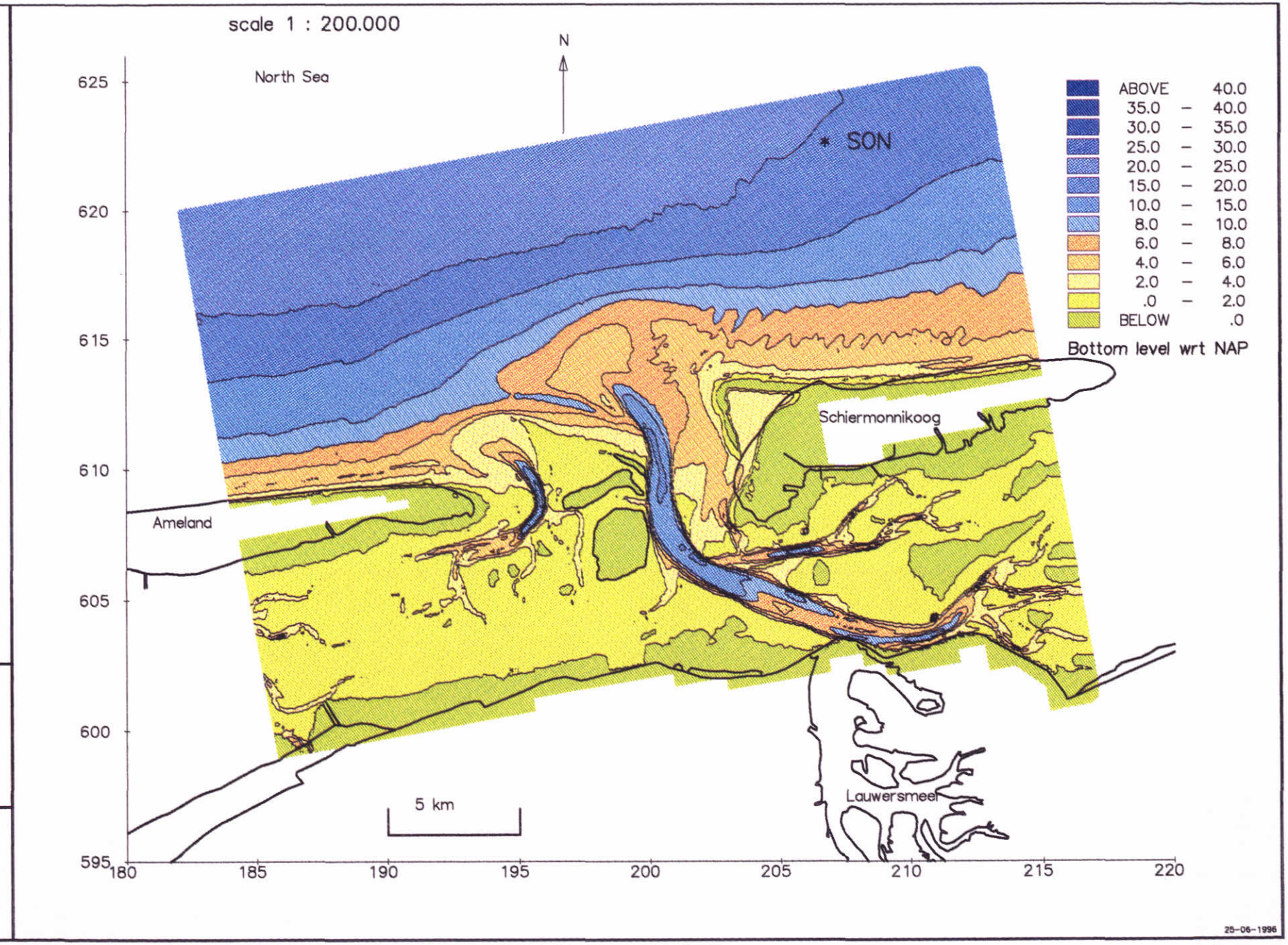

Bottom topography Friesche Zeegat

File : FZHAREN.BOD

DELFT HYDRAULICS + Delft University of Technology

H2368	superstorm	SWAN
Fig. 1.2		

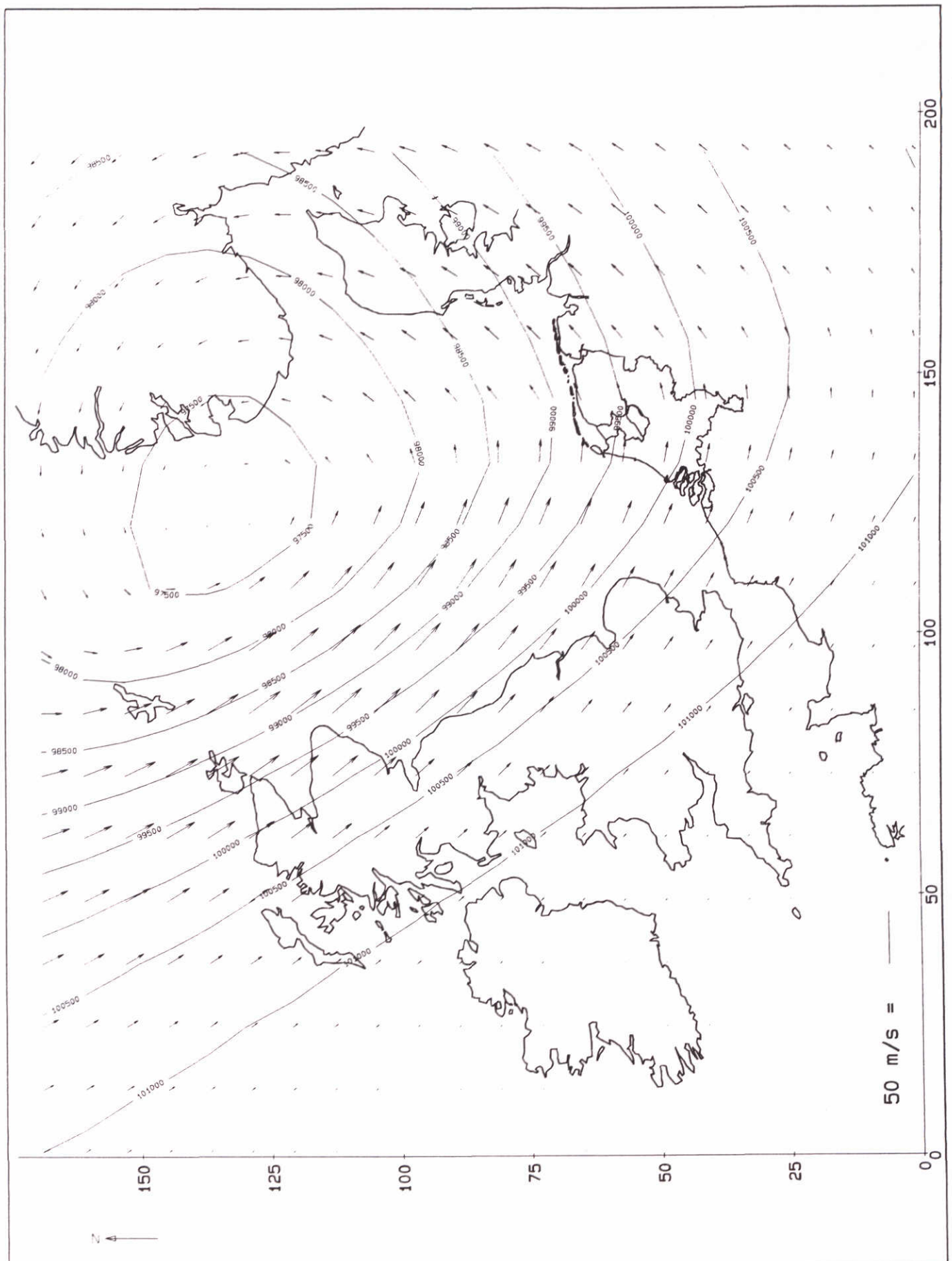
SCHEMATIZED STORM
WIND VECTORS AND ISOBARS (N/m 2)
TIME : 1953-01-31 12: 00
50 m/s =
N
CSM-8
DELFT HYDRAULICS
H-2368
Fig. 2.1a

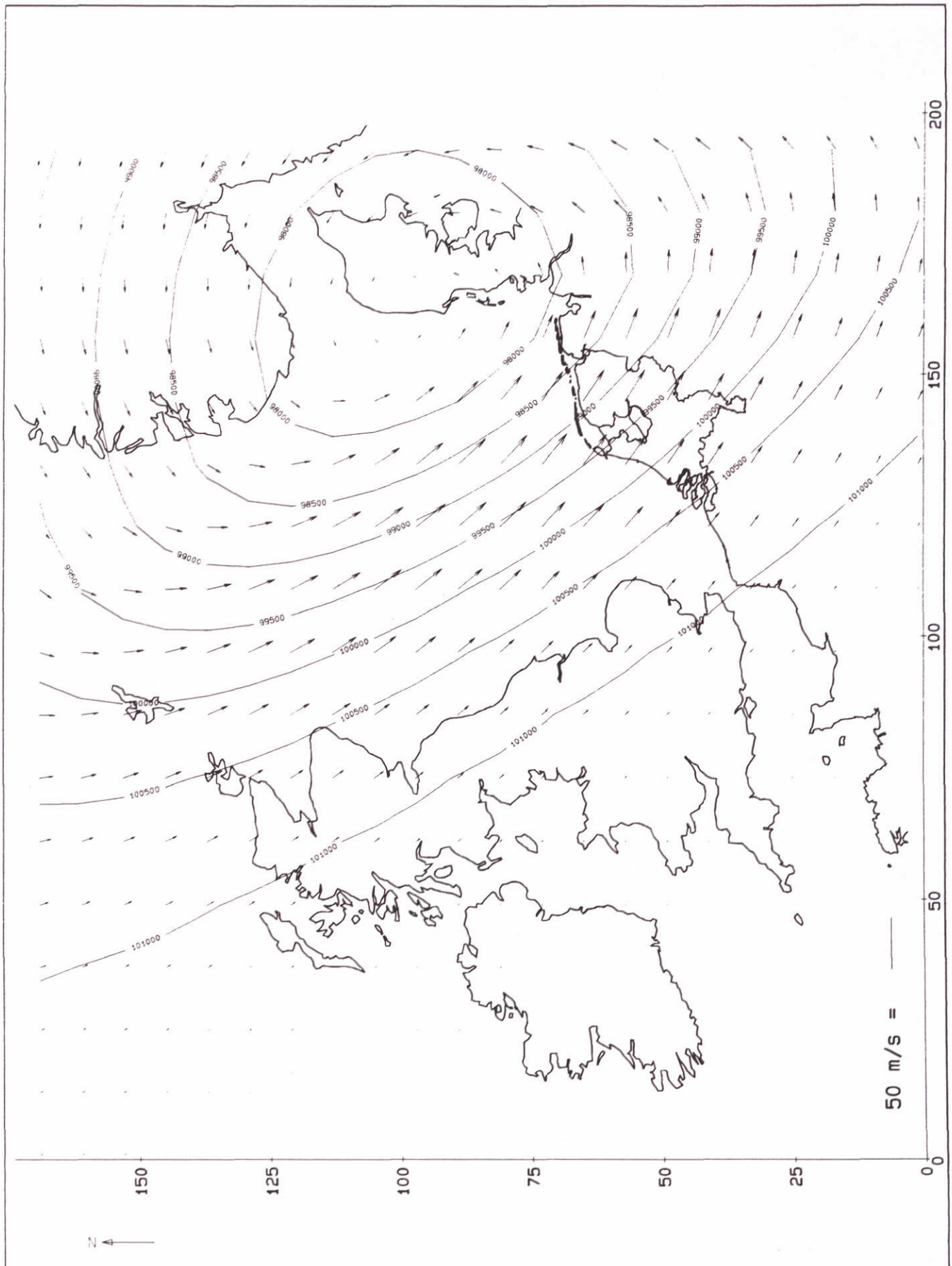

SCHEMATIZED STORM
WIND VECTORS AND ISOBARS (N/m^2)
TIME : 1953-02-01 00:00

CSM-8

DELFT HYDRAULICS

H-2368

Fig. 2.1b

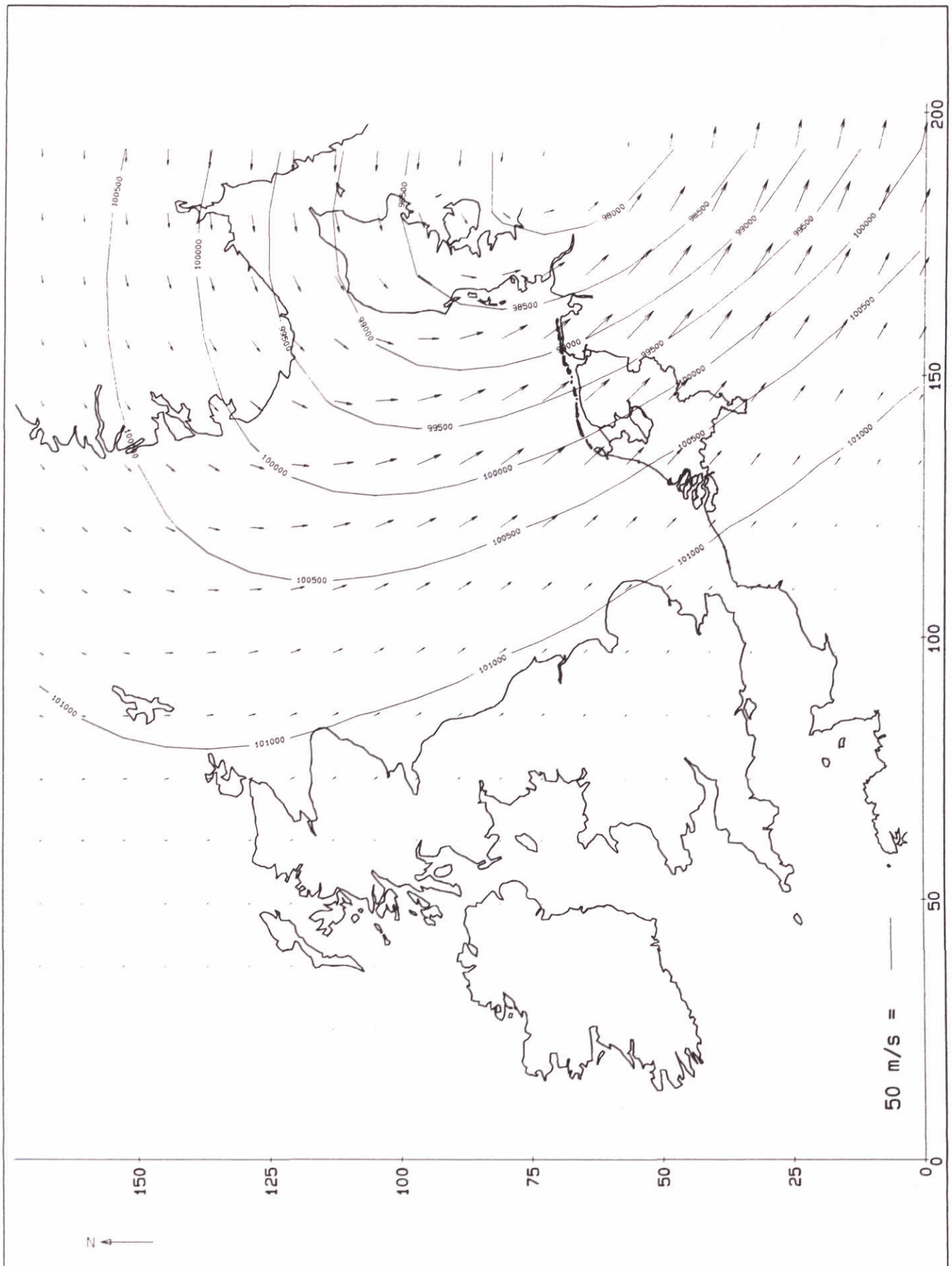

SCHEMATIZED STORM
WIND VECTORS AND ISOBARS (N/m^2)
TIME : 1953-02-01 12: 00

CSM-8

DELFT HYDRAULICS

H-2368

Fig. 2.1c

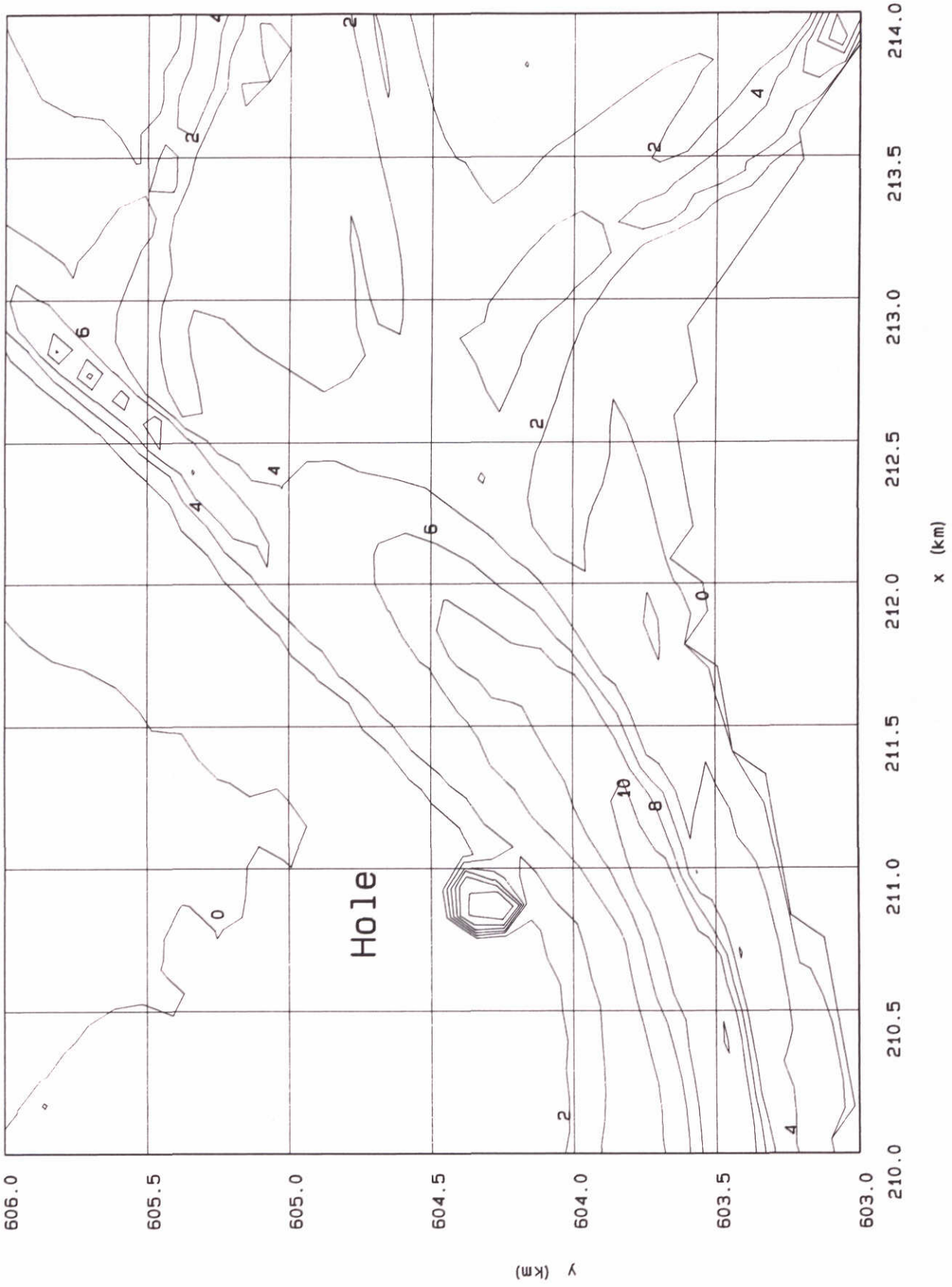

Detail of bottom file FZHAREN
showing the hole

DELFT HYDRAULICS/DELFT UNIVERSITY OF TECHNOLOGY | H2368 | Fig. 2.2

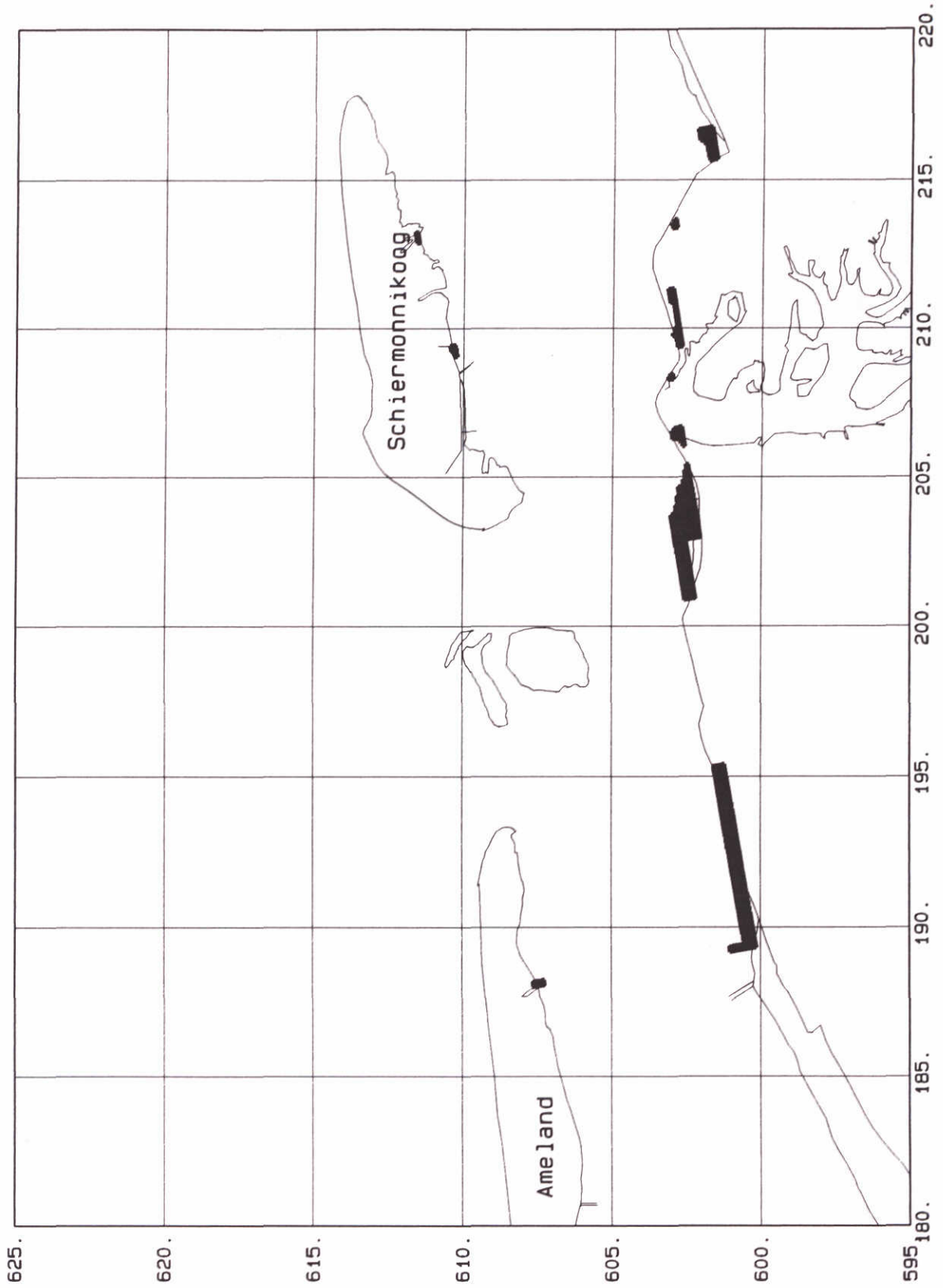

Locations where bottom topography FZHAREN.BOD
was extended with information from the Waddenmodel

DELFT HYDRAULICS/DELFT UNIVERSITY OF TECHNOLOGY | H2368 | Fig. 2.3

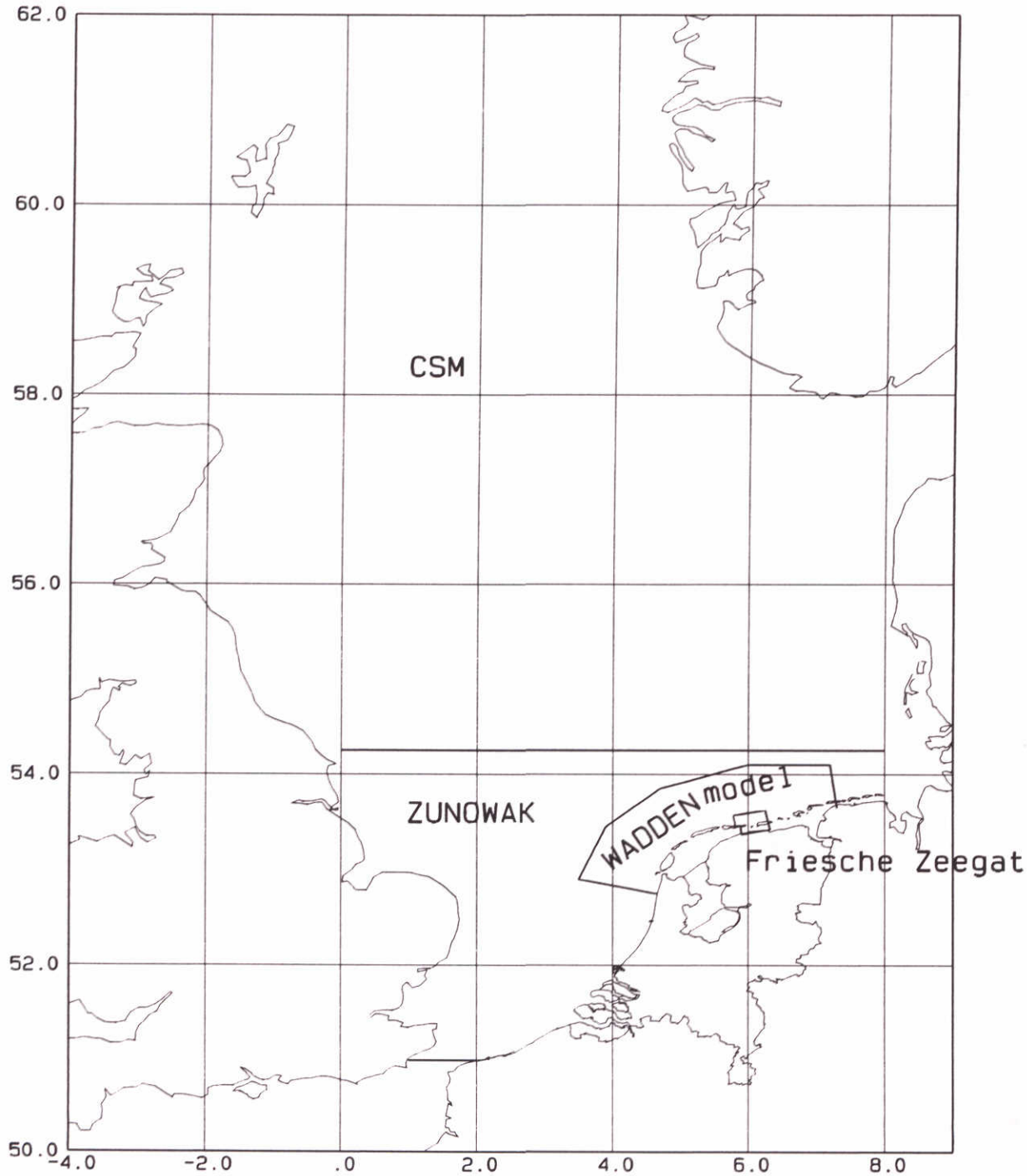

Overview of flow models used in the superstorm project
CSM, ZUNOWAK, WADDEN model and Friesche Zeegat model

DELFT HYDRAULICS/DELFT UNIVERSITY OF TECHNOLOGY | H2368 | Fig. 3.1

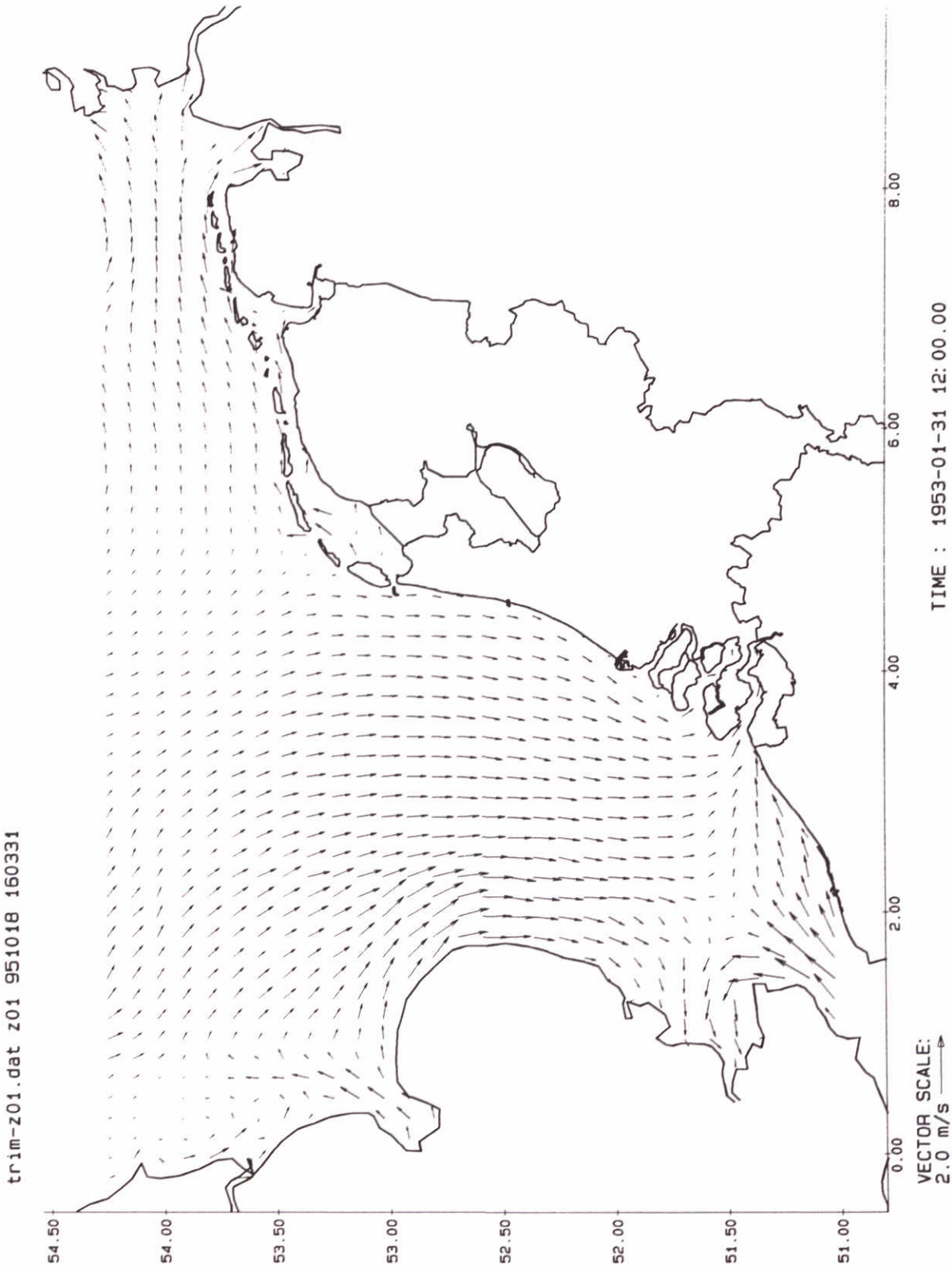

ZUNOWAK-BOL MODEL
VELOCITY FIELD z01

1995-10-18
17:03:42

DELFT HYDRAULICS

Fig. 3.2a

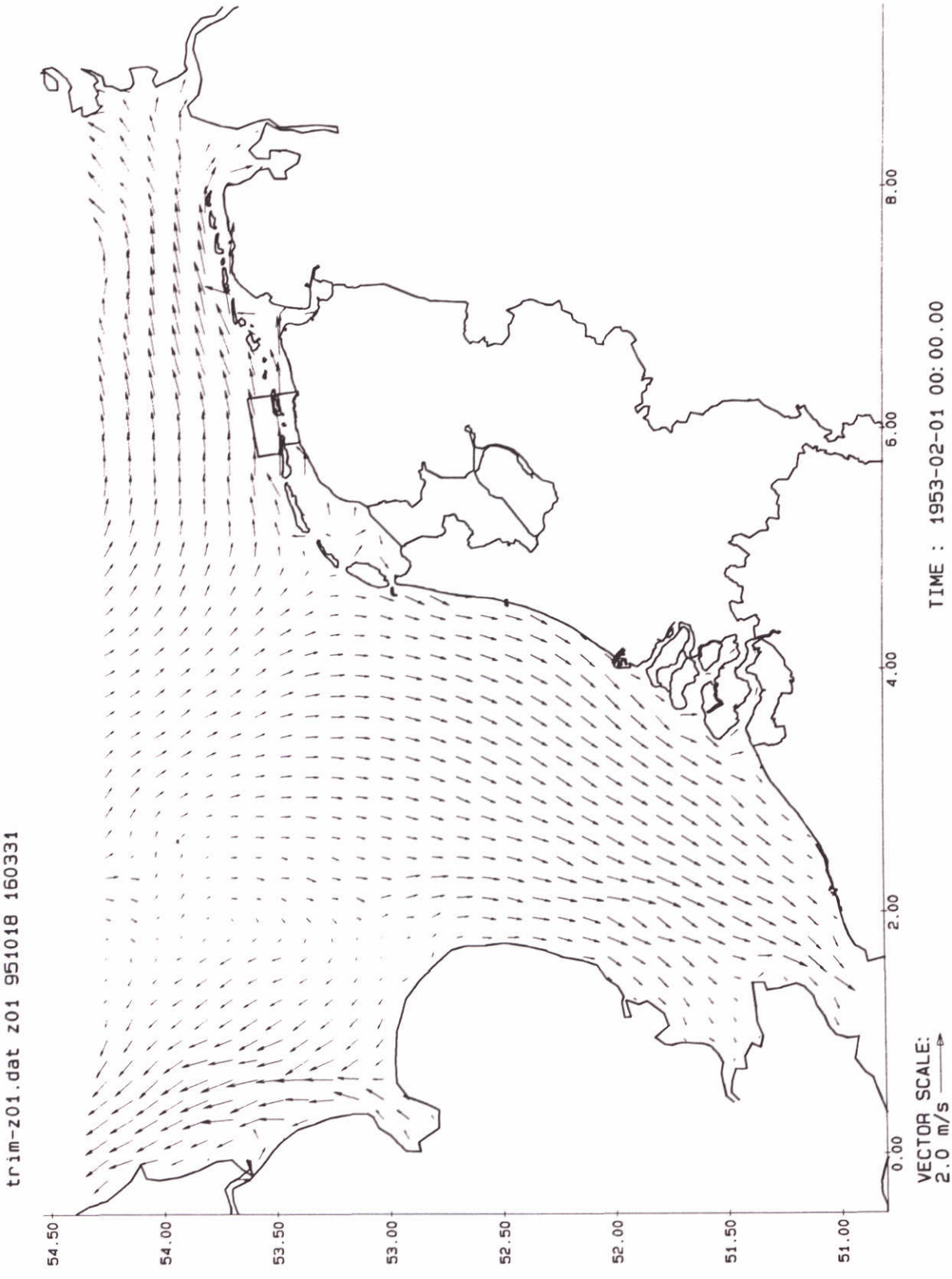

ZUNOWAK-BOL MODEL
VELOCITY FIELD z01

1995-10-18
17:03:53

DELFT HYDRAULICS

Fig. 3.2b

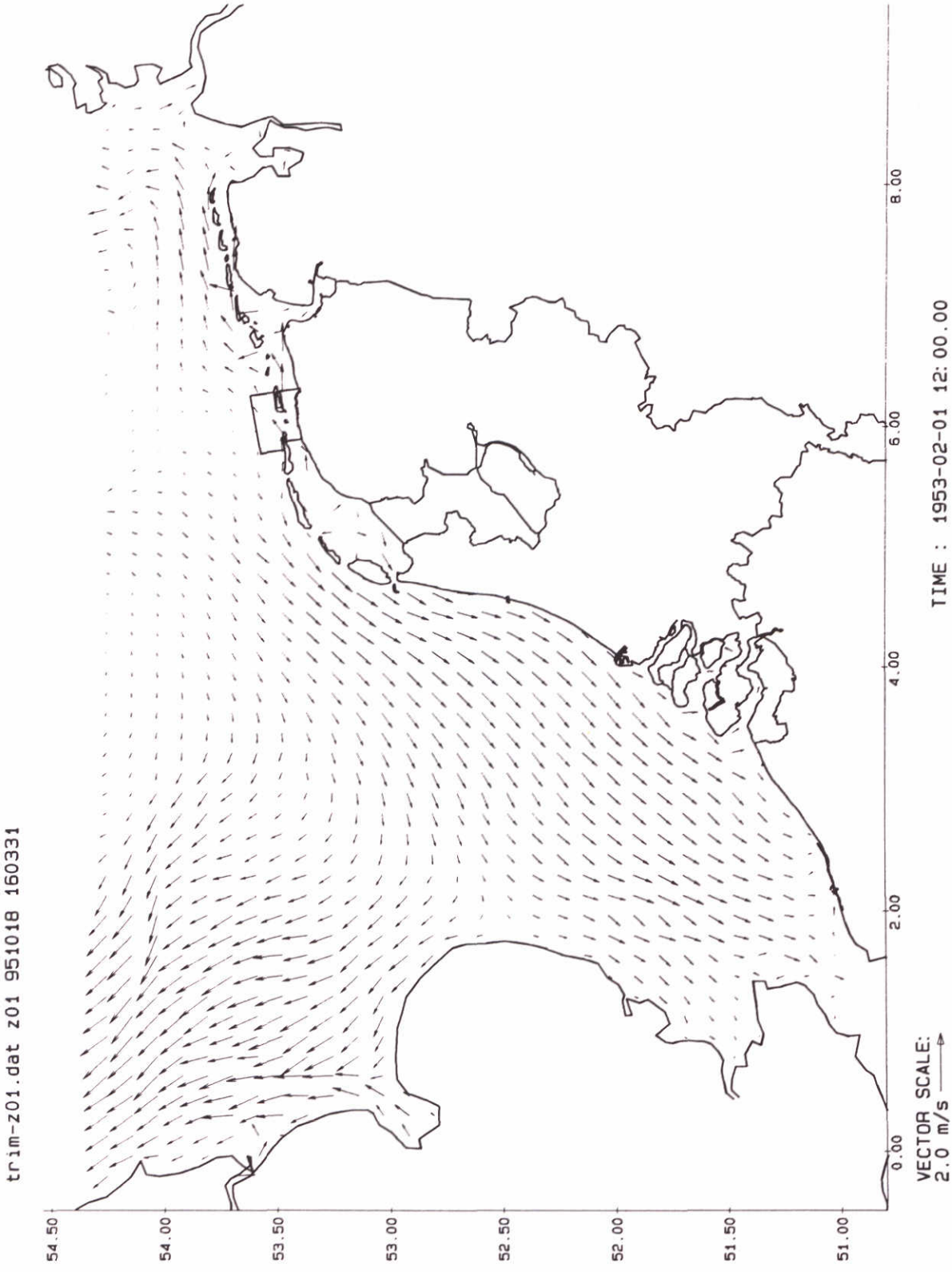

ZUNOWAK-BOL MODEL
VELOCITY FIELD z01

1995-10-18
17:08:19

DELFT HYDRAULICS

Fig. 3.2c

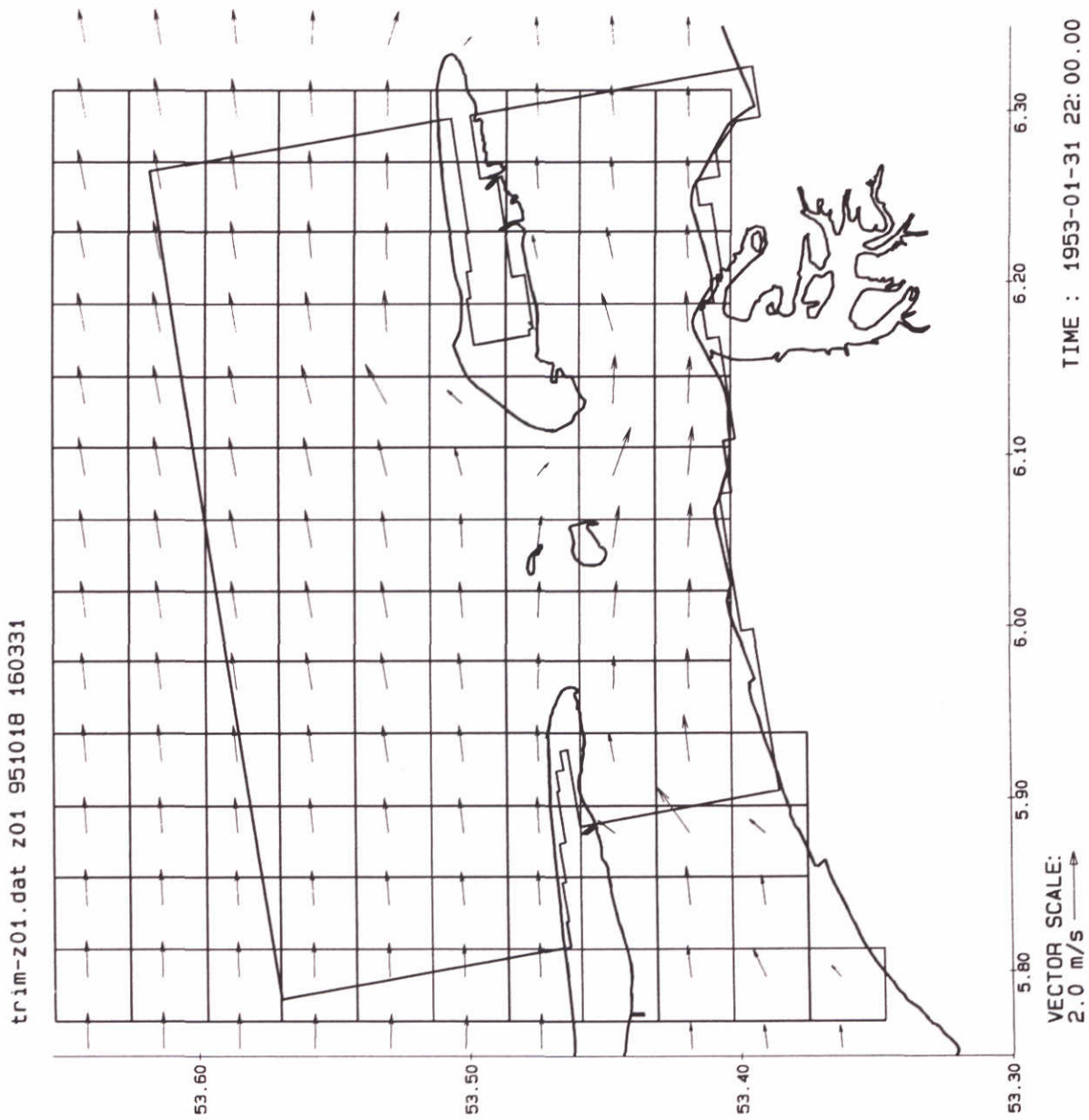

ZUNOWAK-BOL MODEL
VELOCITY FIELD z01

1995-10-18
17:03:51

DELFT HYDRAULICS

Fig. 3.3

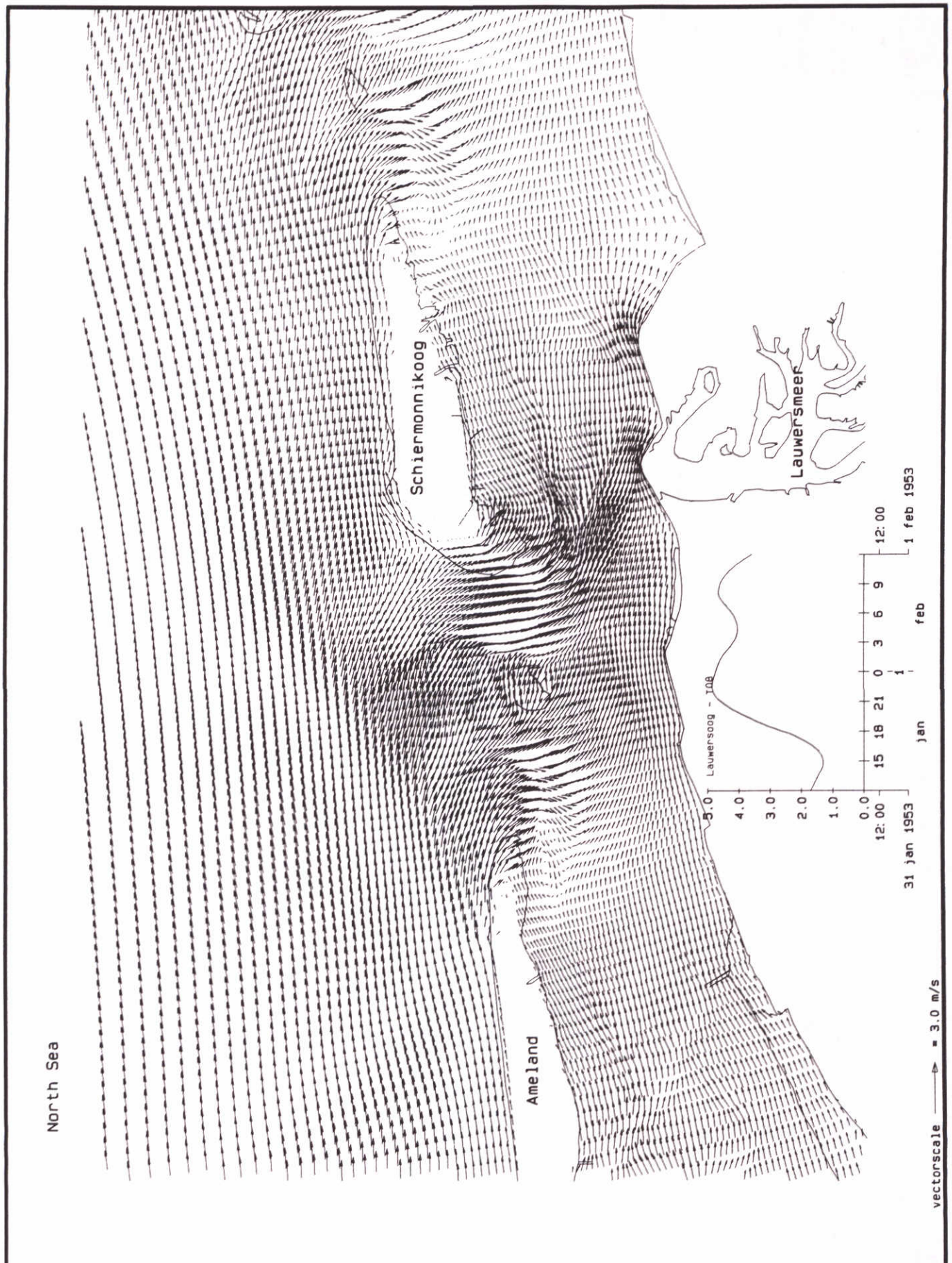

TIDAL MODEL DUTCH WADDENSEA, 1953 storm	T08	UV04
VELOCITY PATTERN AT 18.00 hr - FRIESCHE ZEEGAT	31 January 1953	
DELFT HYDRAULICS	H2368	Fig. 3.4a

TIDAL MODEL DUTCH WADDENSEA, 1953 storm	T08	UV06
VELOCITY PATTERN AT 22.00 hr - FRIESCHE ZEEGAT	31 January 1953	
DELFT HYDRAULICS	H2368	Fig. 3.4b

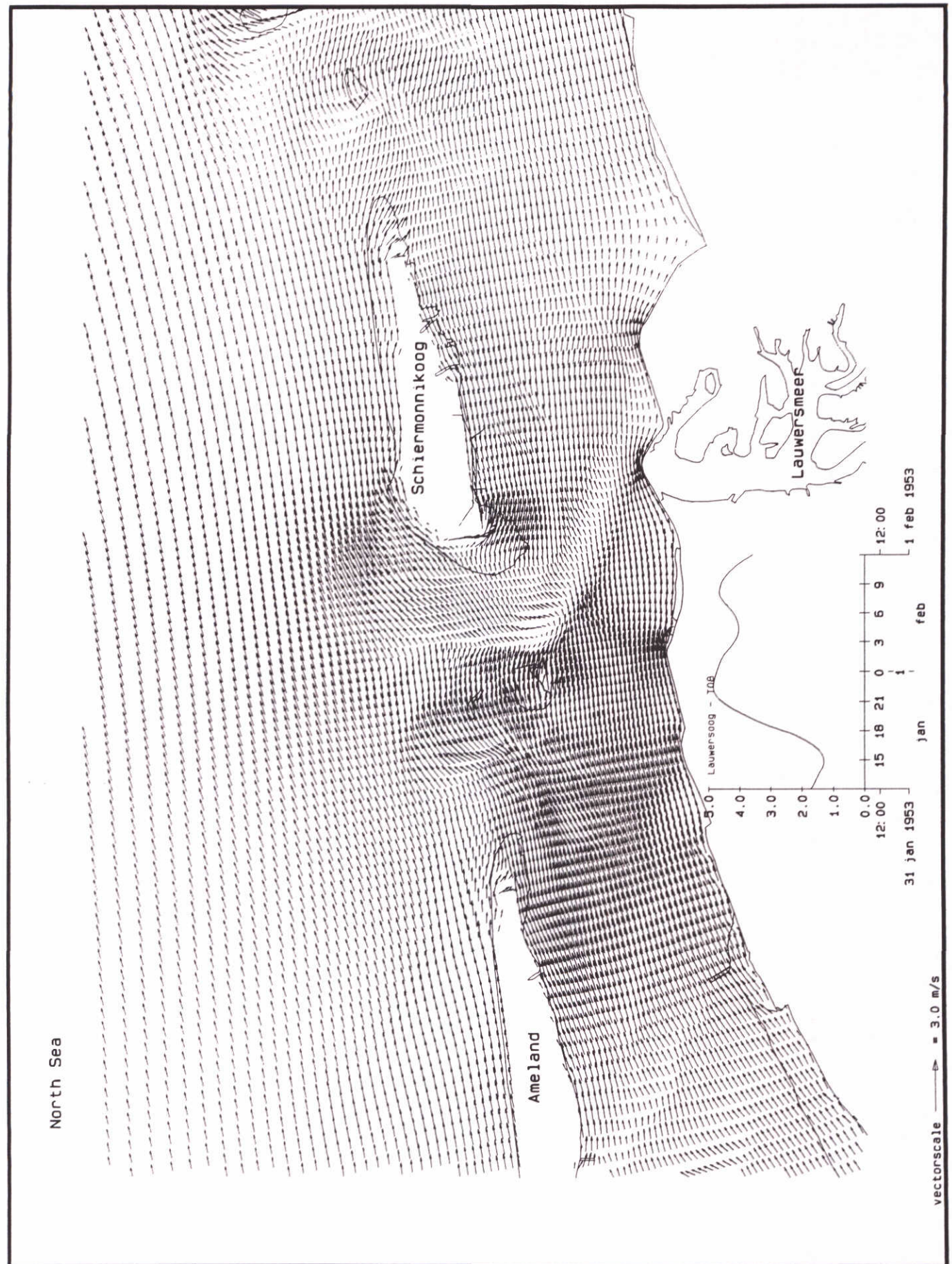

TIDAL MODEL DUTCH WADDENSEA, 1953 storm	T08	UV08
VELOCITY PATTERN AT 02.00 hr - FRIESCHE ZEEGAT	1 February 1953	
DELFT HYDRAULICS	H2368	Fig. 3.4c

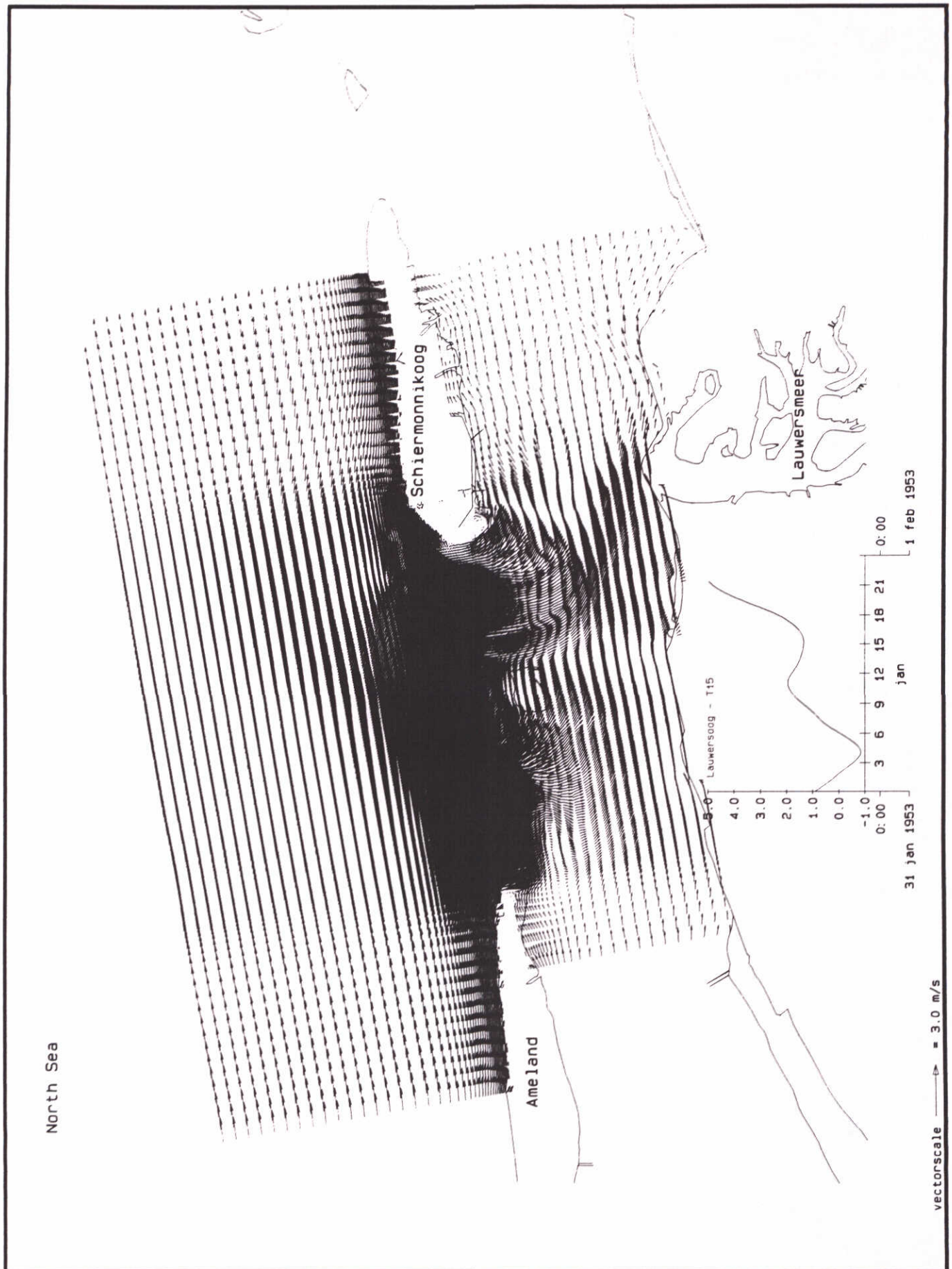

TIDAL MODEL FRIESCHE ZEEGAT, 1953 STORM	T15	UV10
VELOCITY PATTERN AT 18.00 hr	31 January 1953	
DELFT HYDRAULICS	H2368	Fig. 3.5a

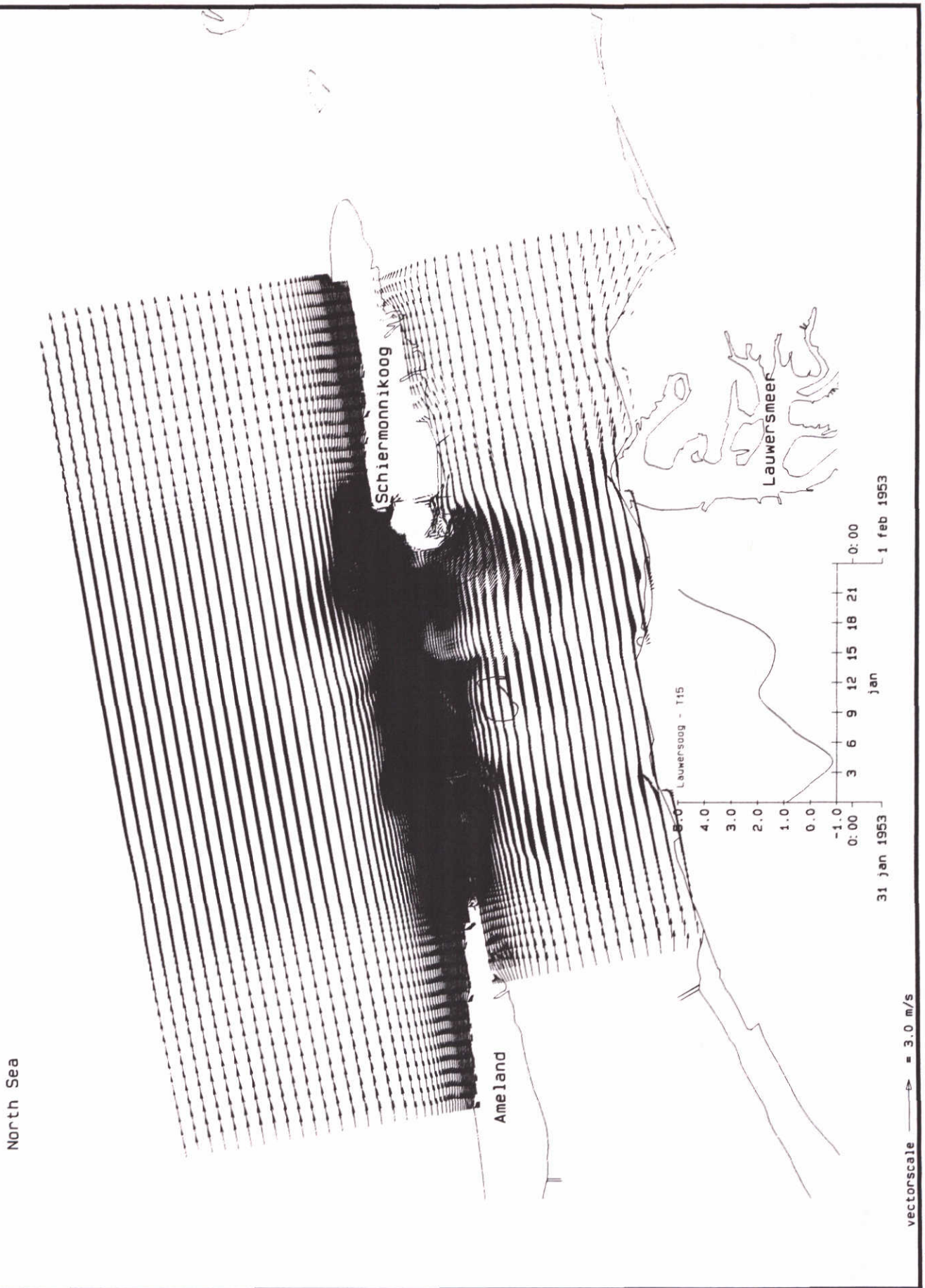

TIDAL MODEL FRIESCHE ZEEGAT, 1953 STORM	T15	UV12
VELOCITY PATTERN AT 22.00 hr	31 January 1953	
DELFT HYDRAULICS	H2368	Fig. 3.5b

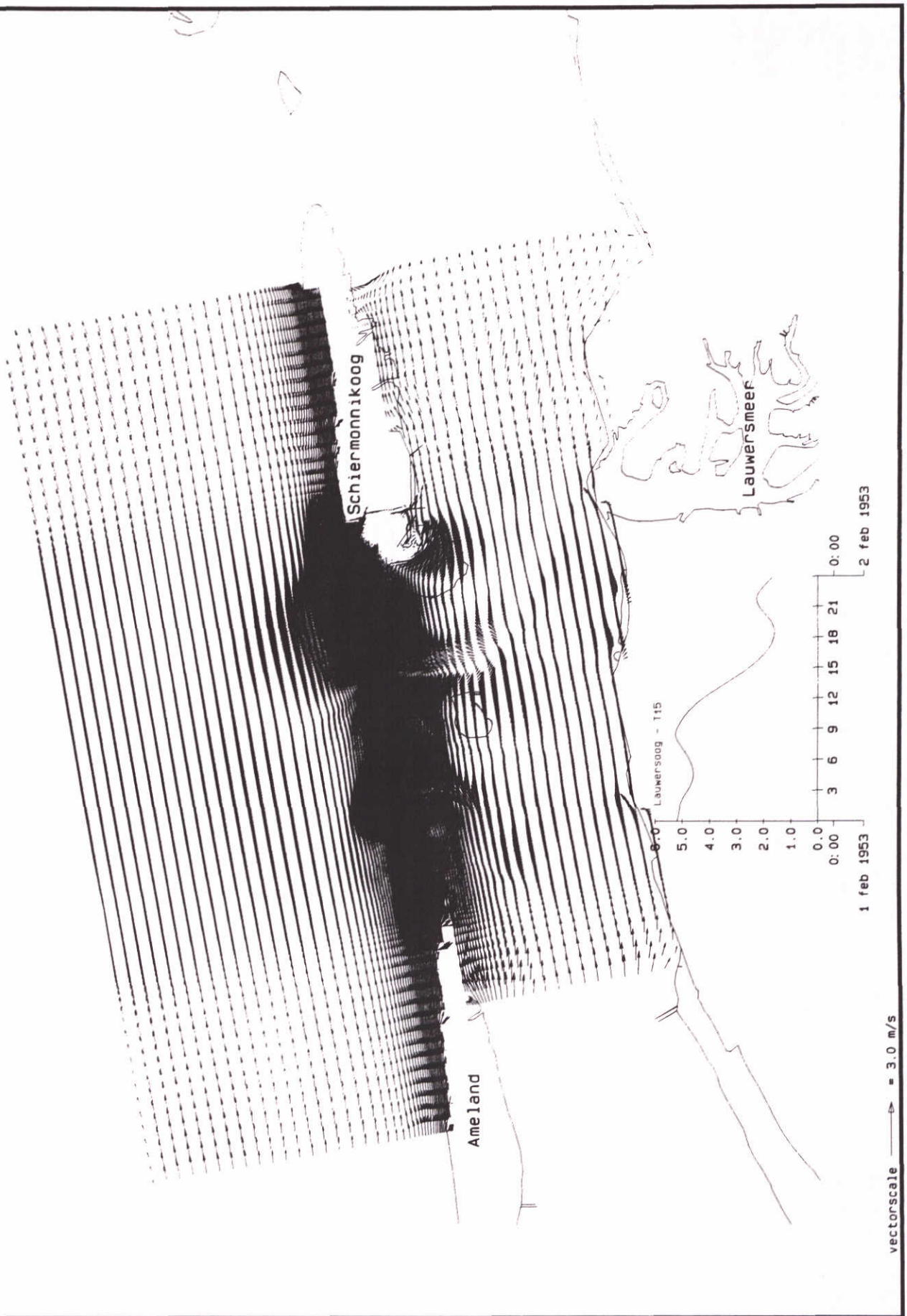

TIDAL MODEL FRIESCHE ZEEGAT, 1953 STORM	T15	UV14
VELOCITY PATTERN AT 02.00 hr	1 February 1953	
DELFT HYDRAULICS	H2368	Fig. 3.5c

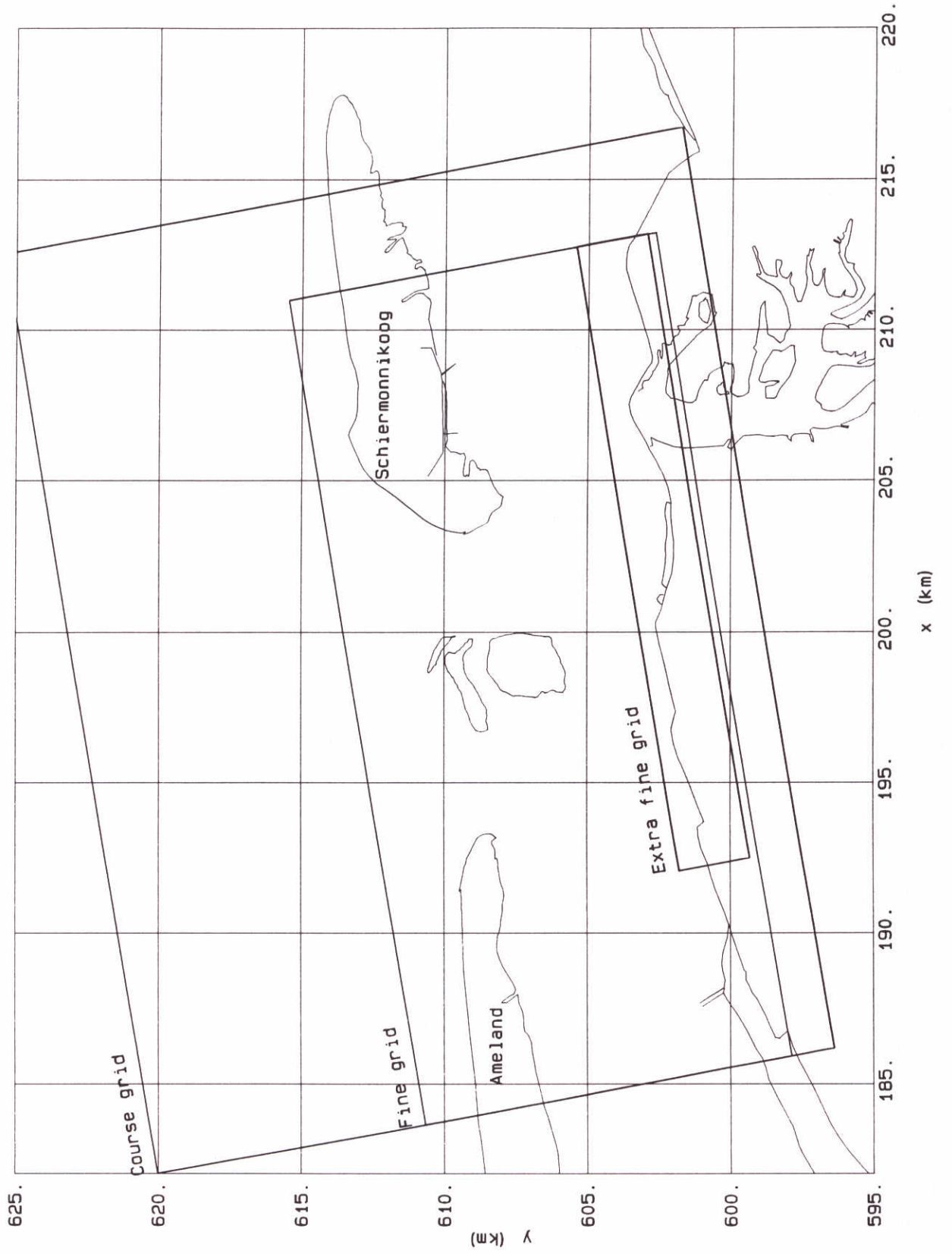

Location of computational grids used for SWAN computations

DELFT HYDRAULICS/DELFT UNIVERSITY OF TECHNOLOGY | H2368 | Fig. 4.1

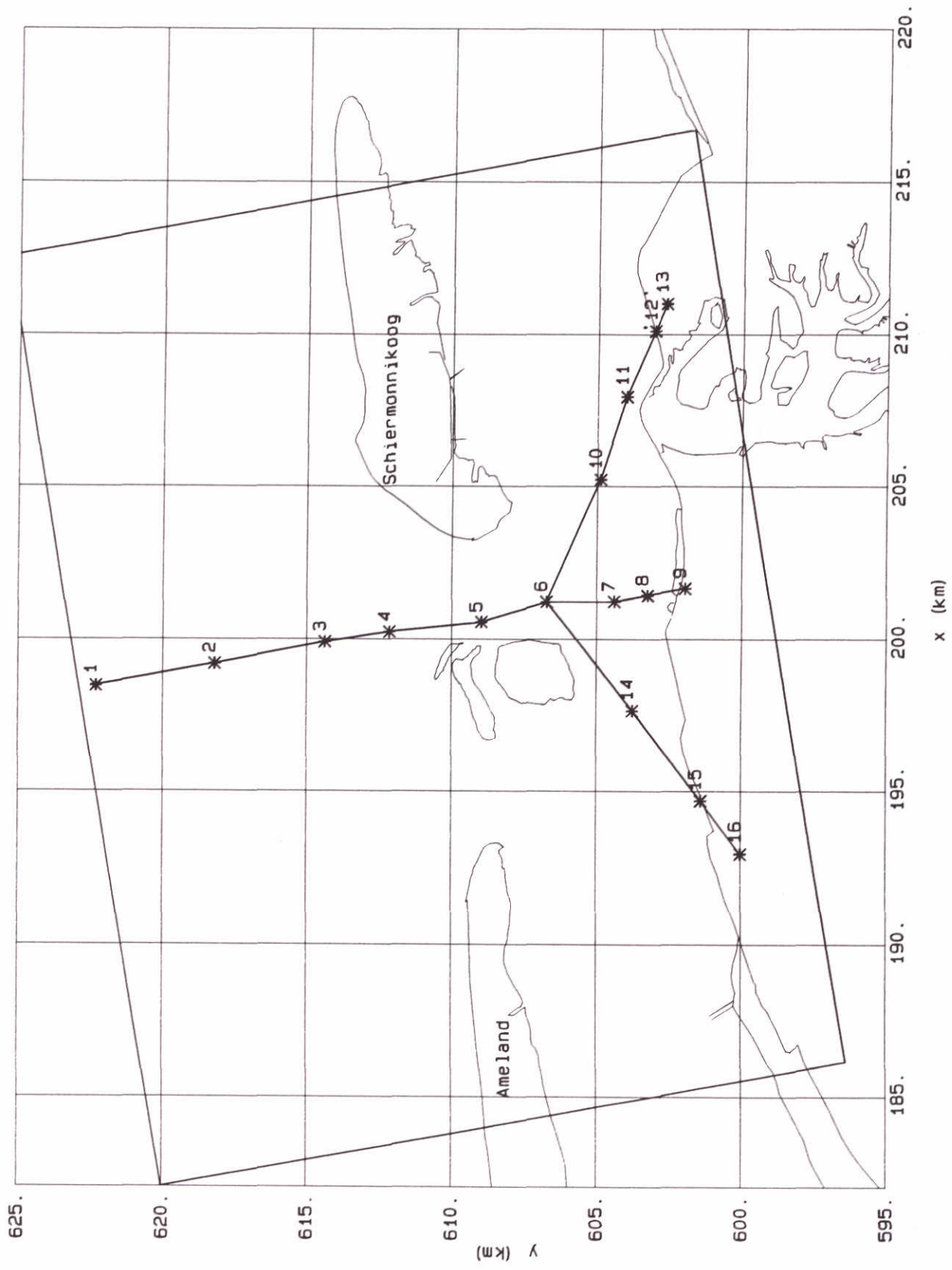

Location of output points and output rays

DELFT HYDRAULICS/DELFT UNIVERSITY OF TECHNOLOGY | H2368 | Fig. 4.2

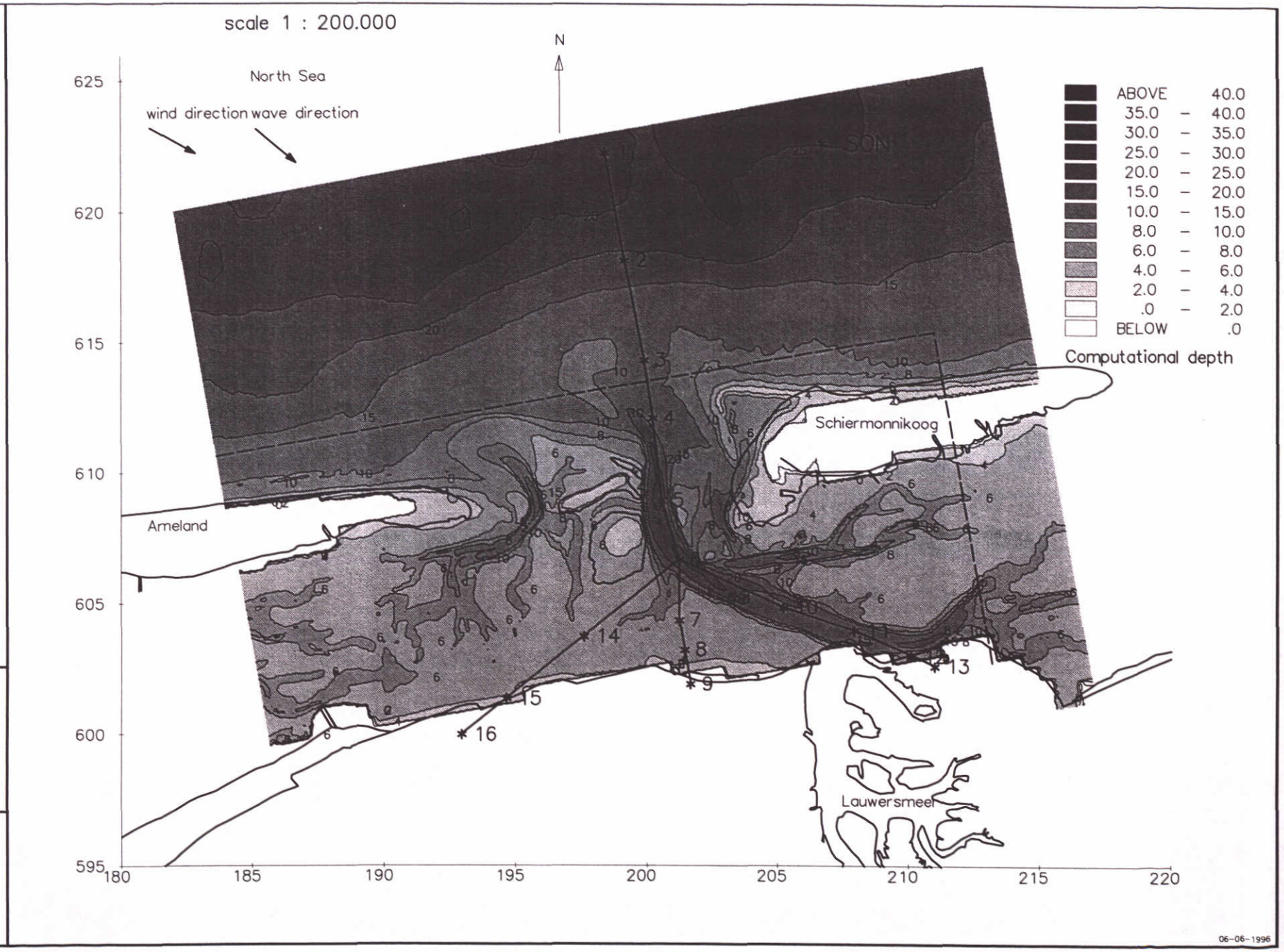

Wave model results Friesche Zeegat

SWAN wave model, course + fine grid , bottom noise

Computational depth (m)

case c10	SWAN
superstorm	
H2368	Fig. 4.3

DELFT HYDRAULICS + Delft University of Technology

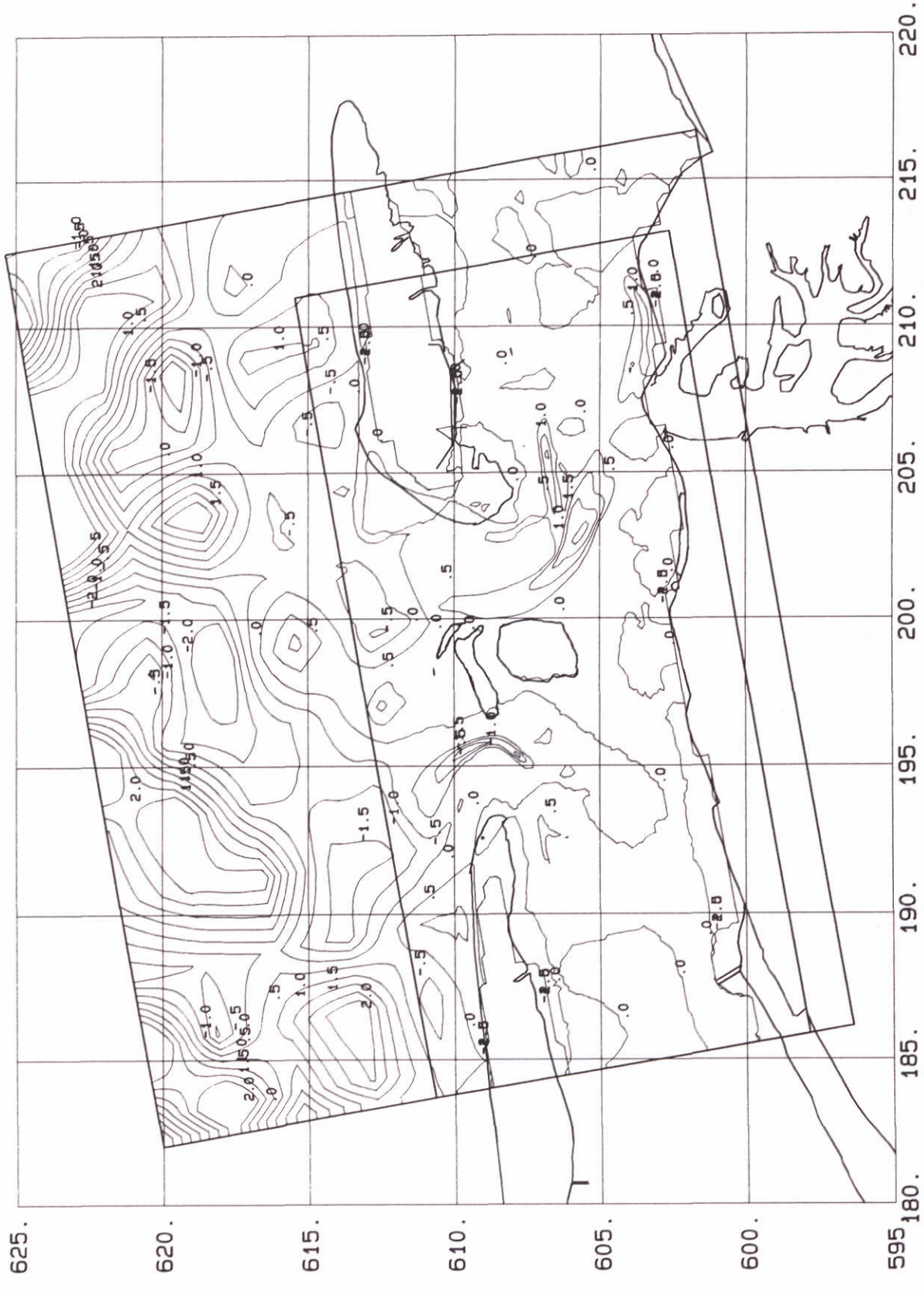

Differences bottom of the cases C10 and B1 Case C10, bottom noise	$c10_f d$	$c10_c d$
	superstorm	
DELFT HYDRAULICS/DELFT UNIVERSITY OF TECHNOLOGY	H2368	Fig. 4.4

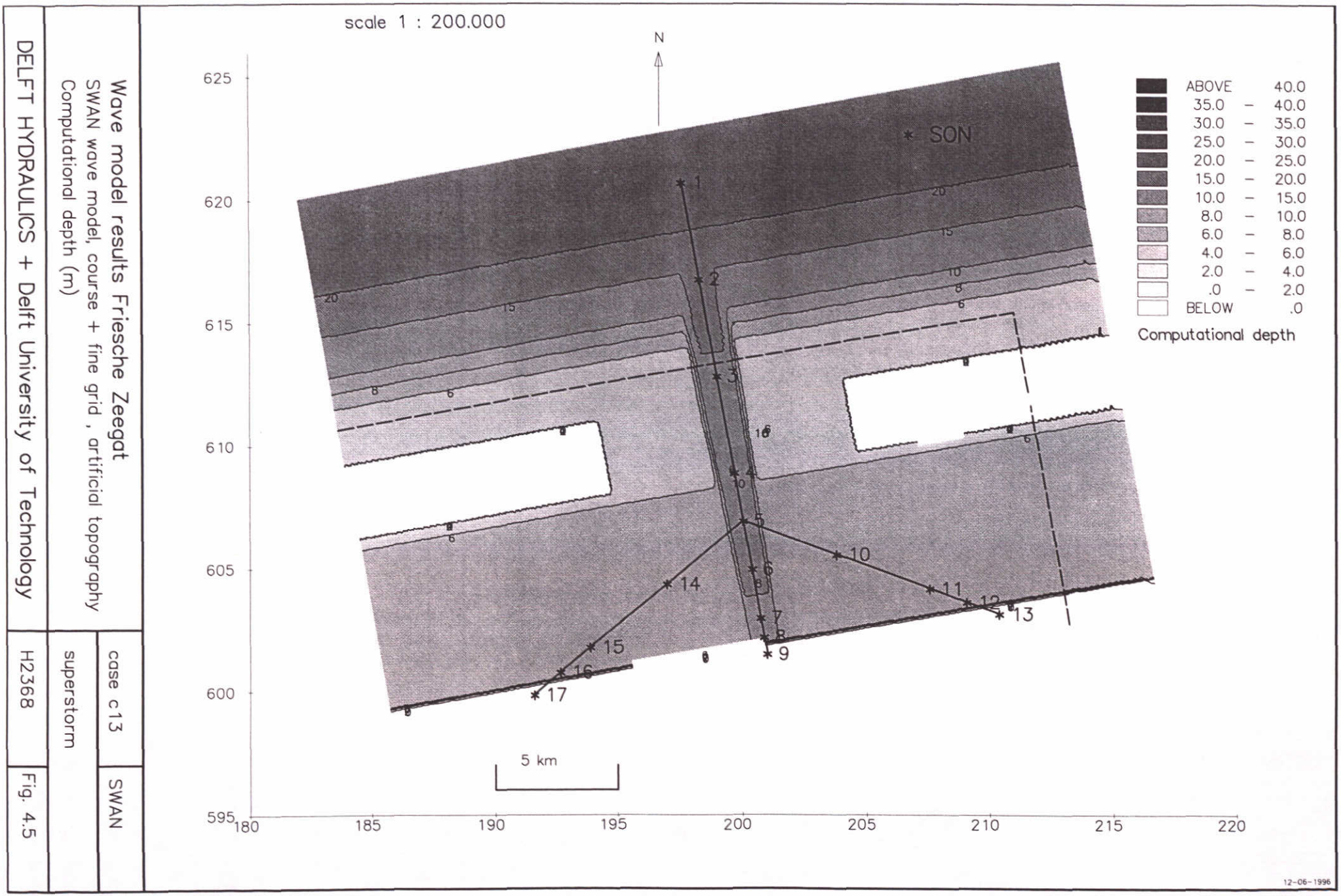

Wave model results Friesche Zeegat

SWAN wave model, course + fine grid , artificial topography

Computational depth (m)

DELFT HYDRAULICS + Delft University of Technology	case c13	SWAN
H2368	superstorm	
Fig. 4.5		

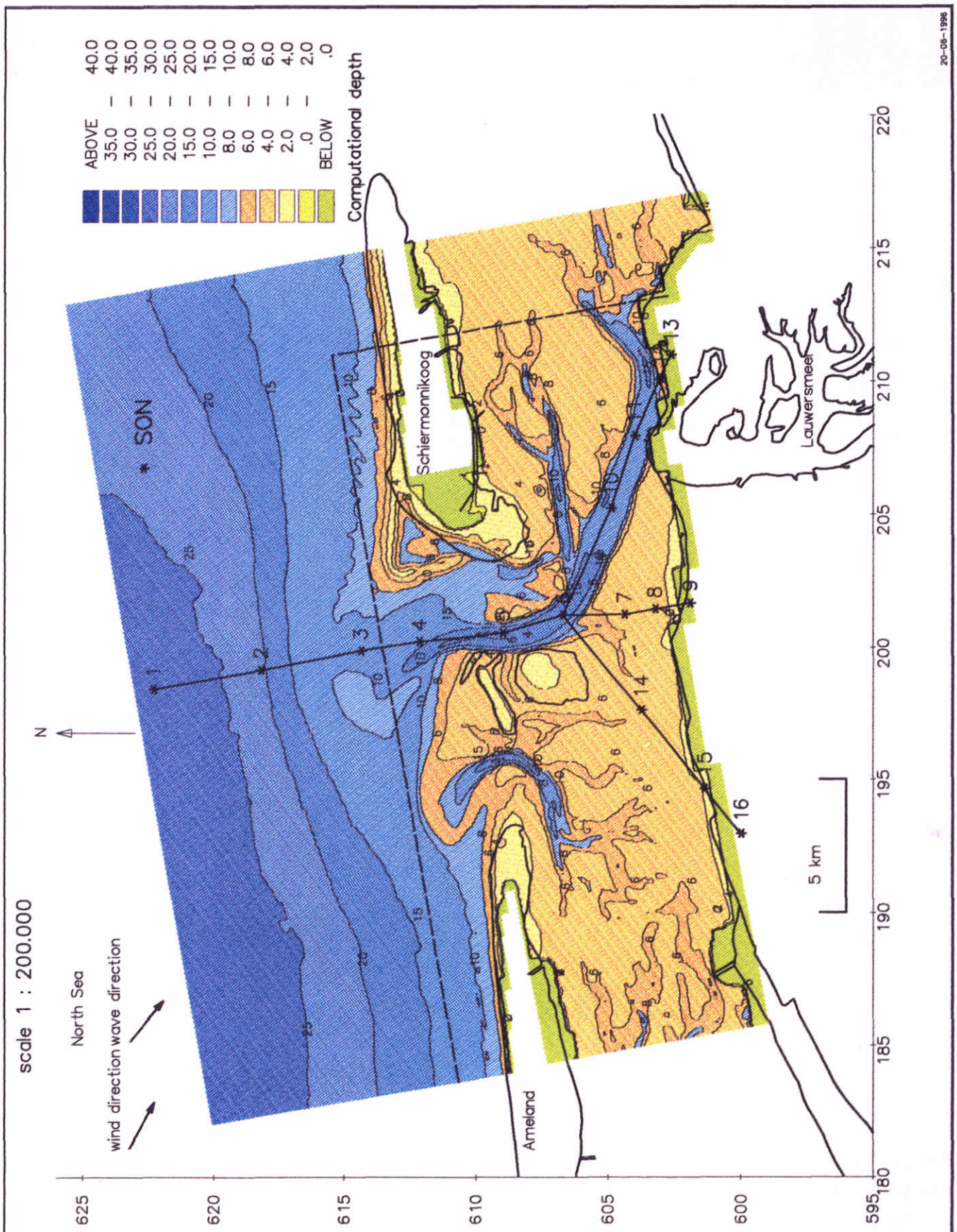

Wave model results Friesche Zeegat SWAN wave model, course + fine grid , base case Computational depth (m)	case b1	SWAN
	superstorm	
DELFT HYDRAULICS + Delft University of Technology	H2368	Fig. 4.6.1

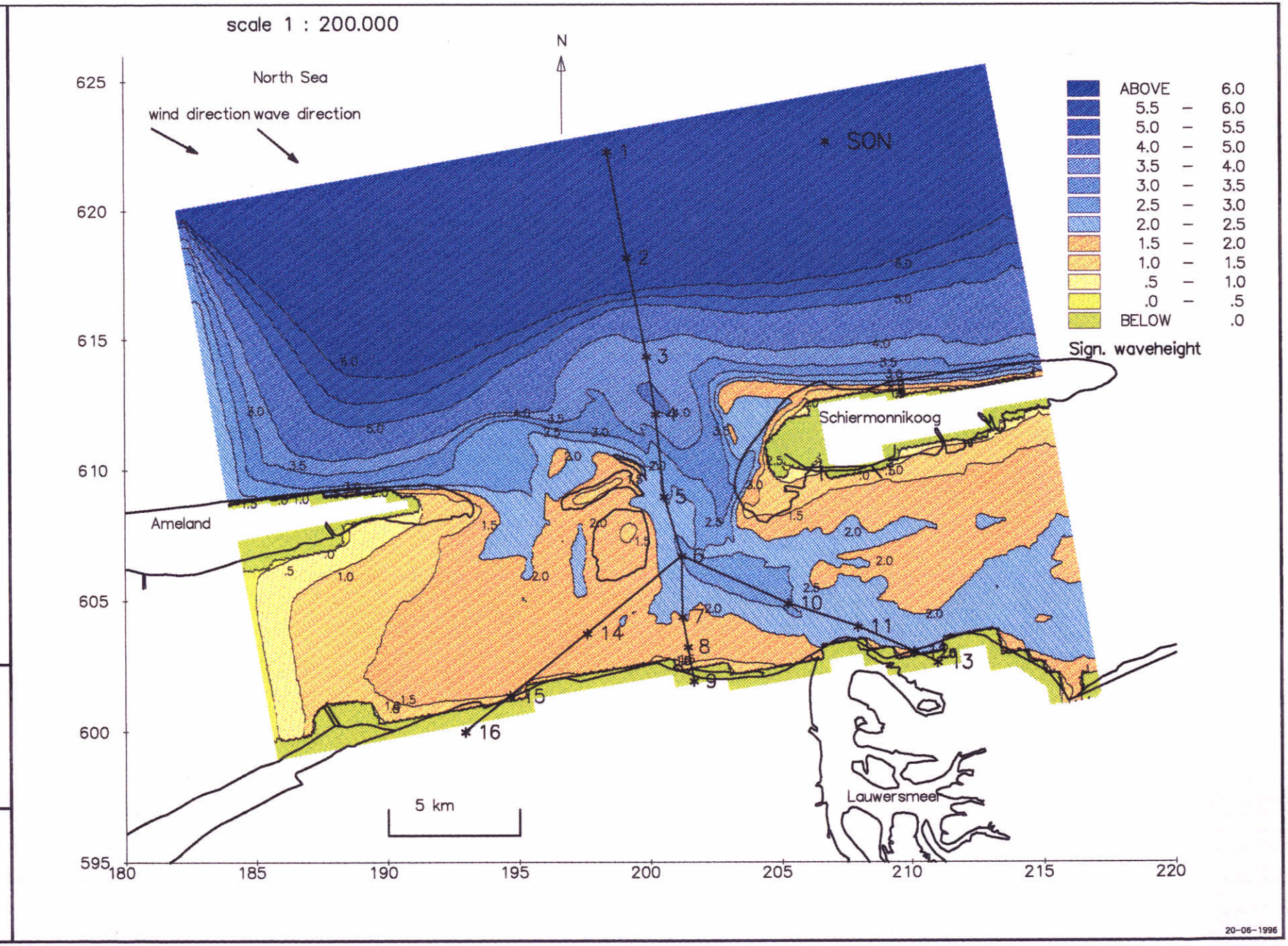

Wave model results Friesche Zeegat

SWAN wave model, course + fine grid , base case

Significant wave height (m)

case b1	SWAN
superstorm	
H2368	Fig. 4.6.2

DELFT HYDRAULICS + Delft University of Technology

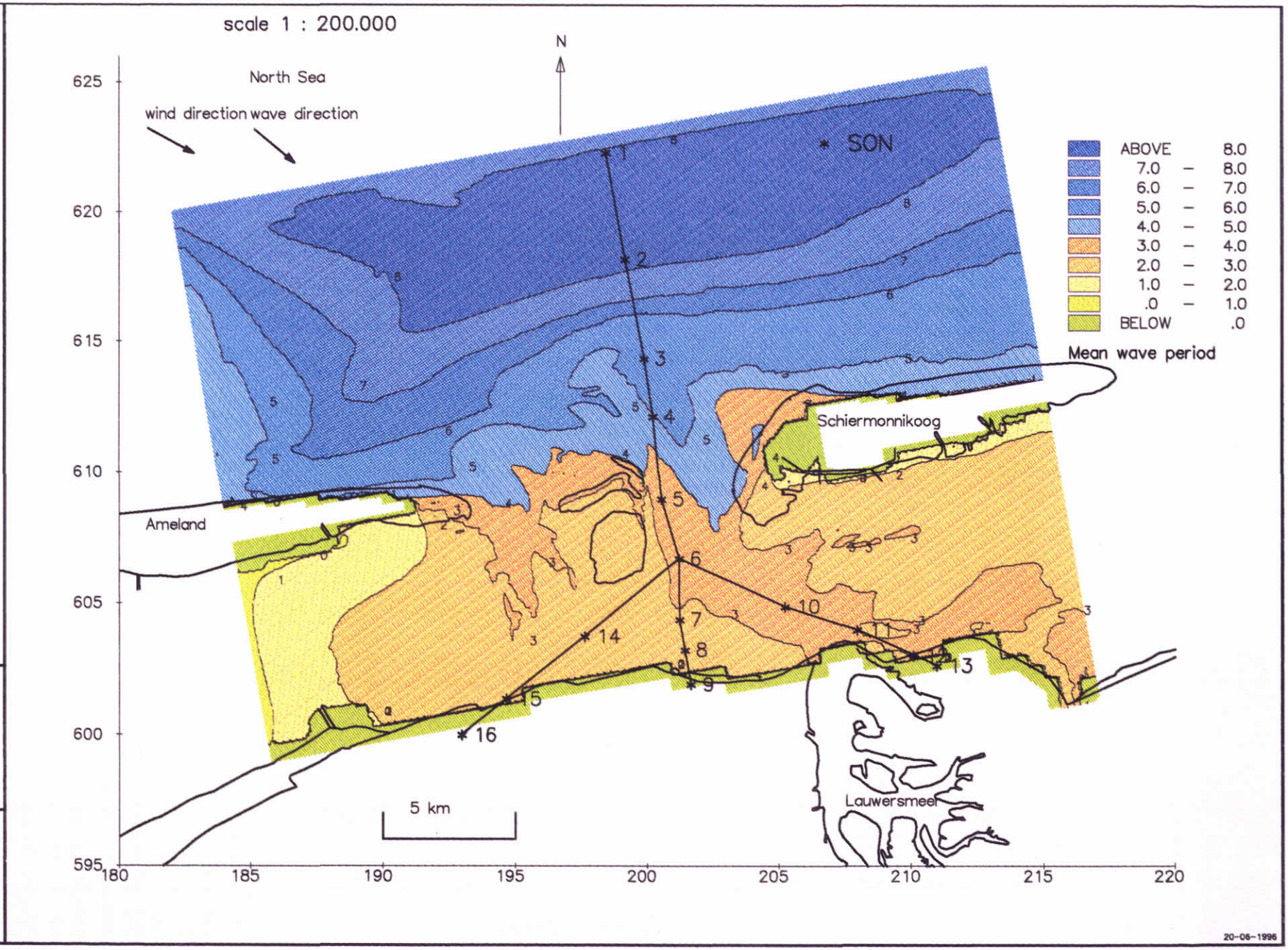

Wave model results Friesche Zeegat

SWAN wave model, course + fine grid , base case

Mean wave period T_{m02} (s)

case b1	SWAN
superstorm	
H2368	Fig. 4.6.3

DELFT HYDRAULICS + Delft University of Technology

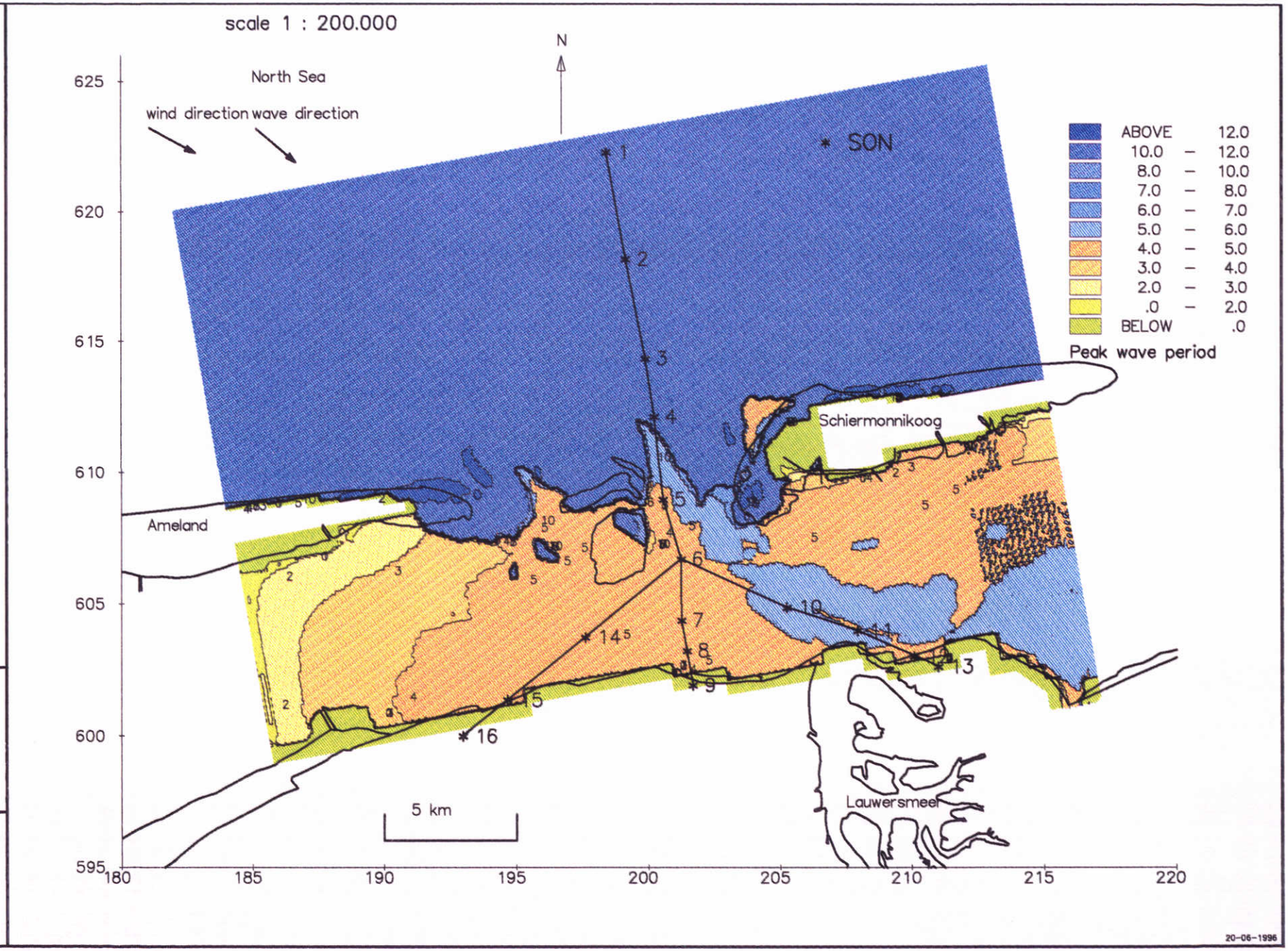

Wave model results Friesche Zeegat

SWAN wave model, course + fine grid , base case

Peak wave period RT_p (s)

case b1	SWAN
superstorm	
H2368	Fig. 4.6.4

DELFT HYDRAULICS + Delft University of Technology

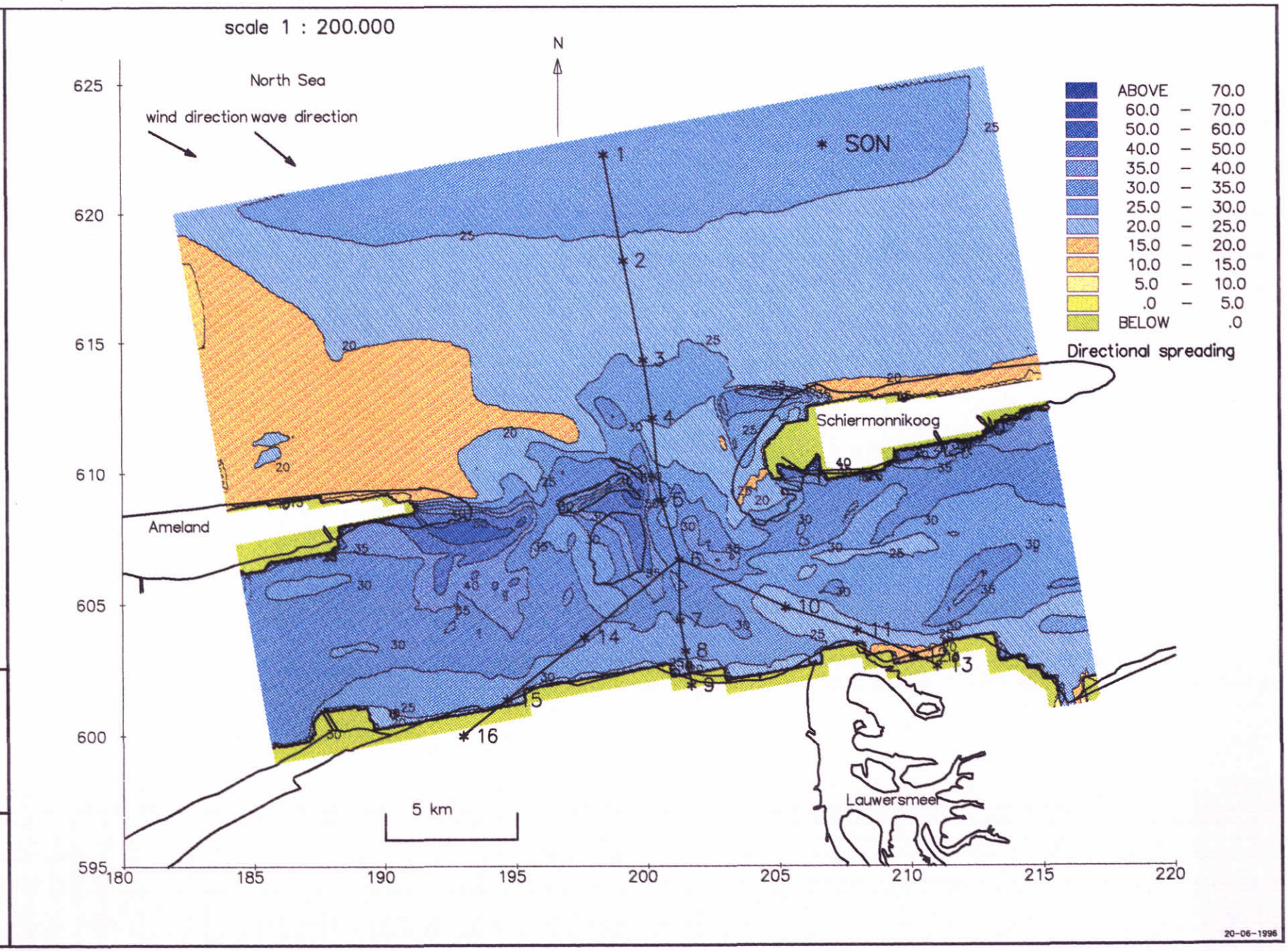

Wave model results Friesche Zeegat

SWAN wave model, course + fine grid , base case

Directional spreading (deg)

case b1	SWAN
superstorm	
H2368	Fig. 4.6.5

DELFT HYDRAULICS + Delft University of Technology

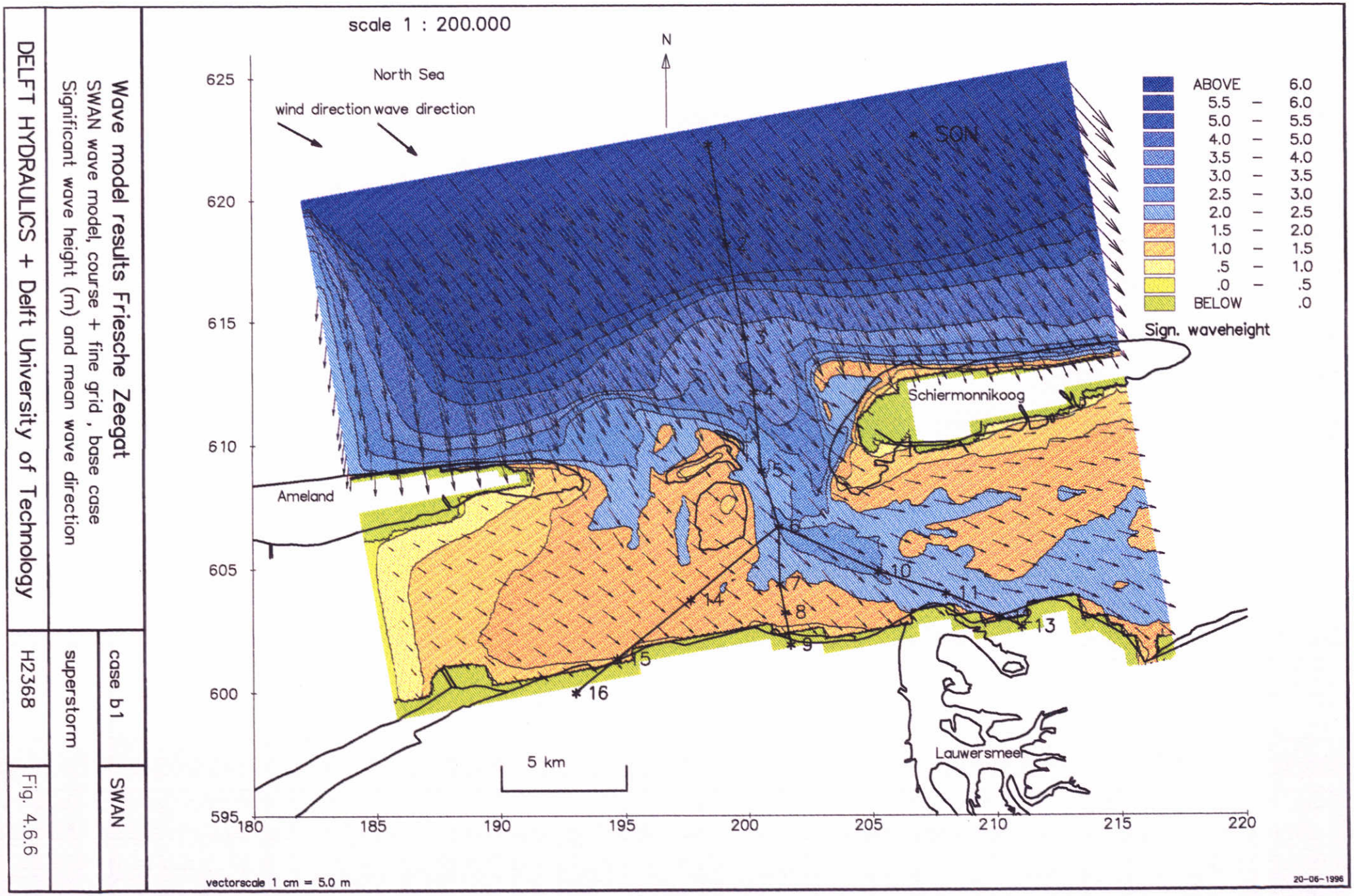

Wave model results Friesche Zeegat

SWAN wave model, course + fine grid , base case

Significant wave height (m) and mean wave direction

DELFT HYDRAULICS + Delft University of Technology		case b1
H2368	superstorm	SWAN
Fig. 4.6.6		

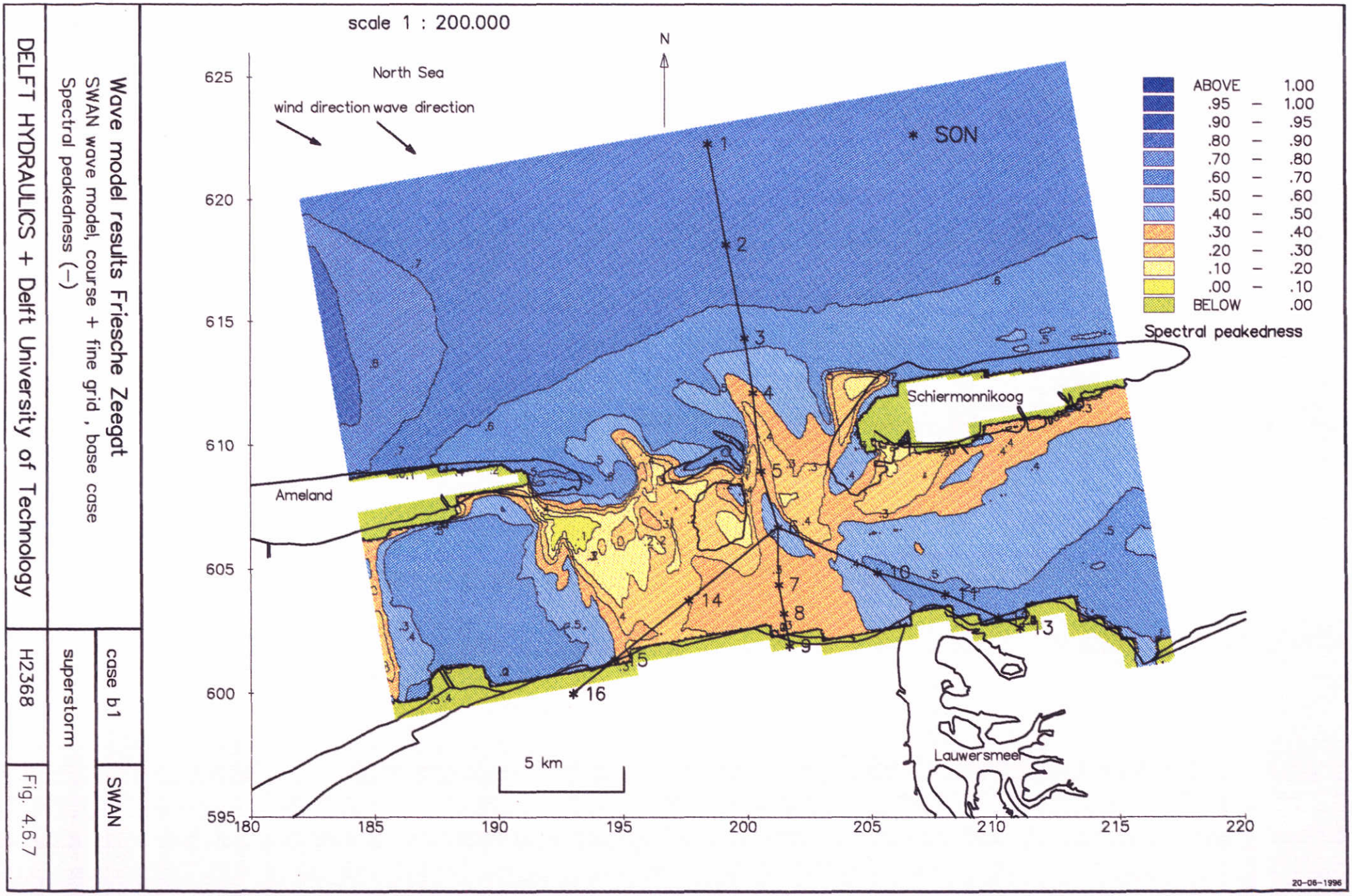

Wave model results Friesche Zeegat

SWAN wave model, course + fine grid , base case

Spectral peakedness (–)

case b1	SWAN
superstorm	
H2368	Fig. 4.6.7

DELFT HYDRAULICS + Delft University of Technology

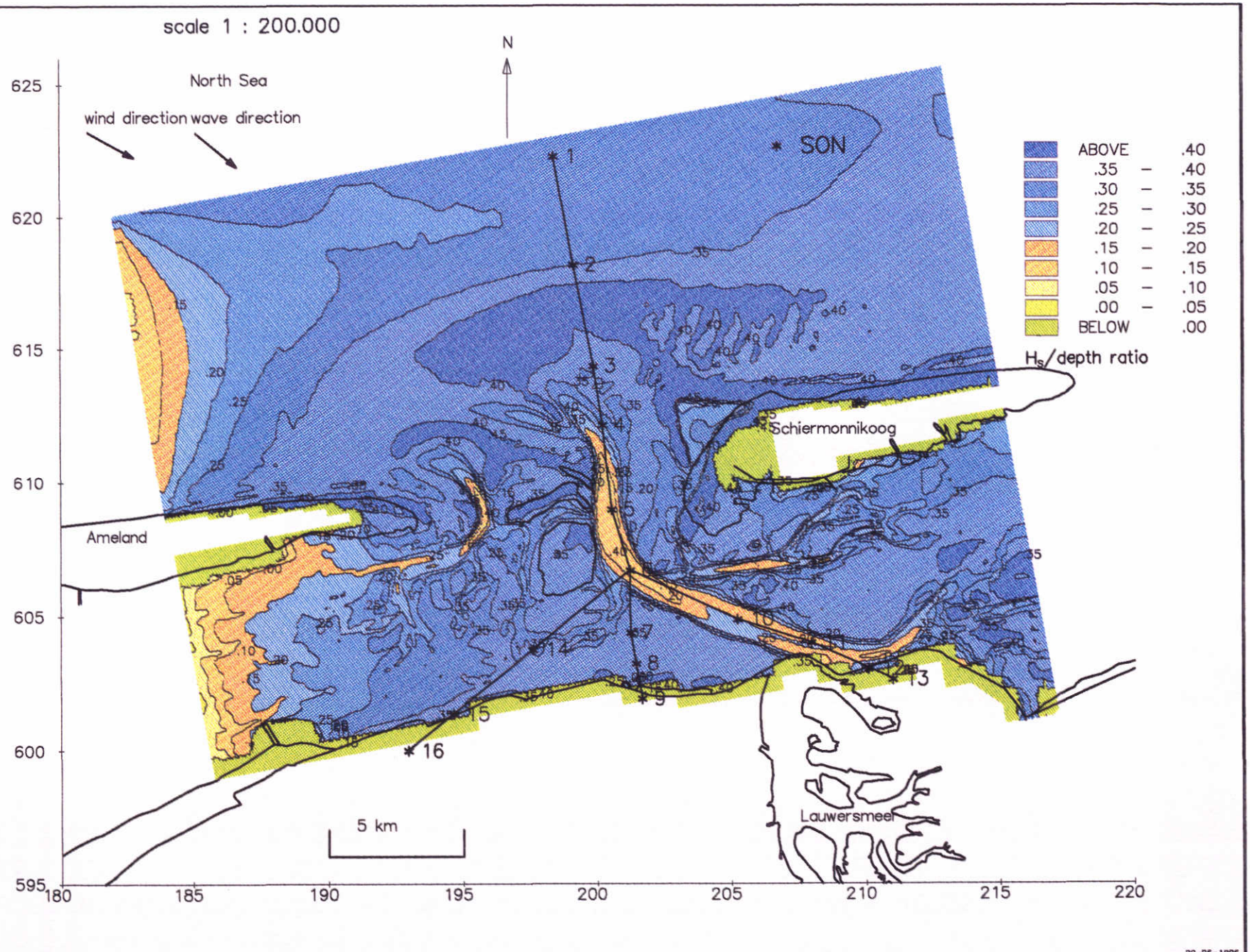

Wave model results Friesche Zeegat

SWAN wave model, course + fine grid , base case

H_s/depth ratio (-)

SWAN	case b1
superstorm	
H2368	Fig. 4.6.8

DELFT HYDRAULICS + Delft University of Technology

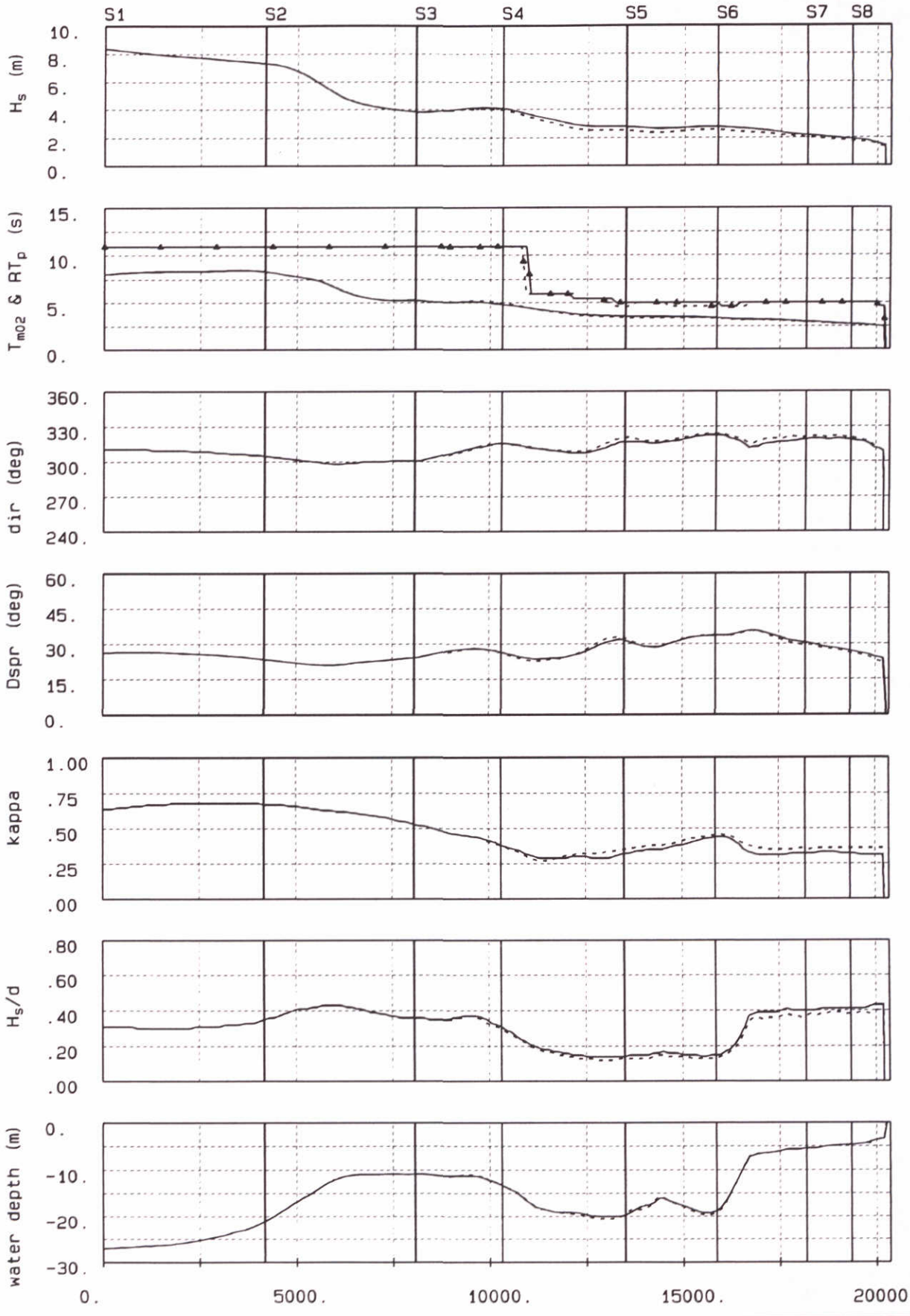

Wave parameters along rays in Friesche Zeegat SWAN wave model computation, Standard run Coarse grid (solid line), fine grid (dashed line)	Ray 1	Case b1
	Superstorm	
DELFT HYDRAULICS/DELFT UNIVERSITY OF TECHNOLOGY	H2368	Fig. 4.7.1

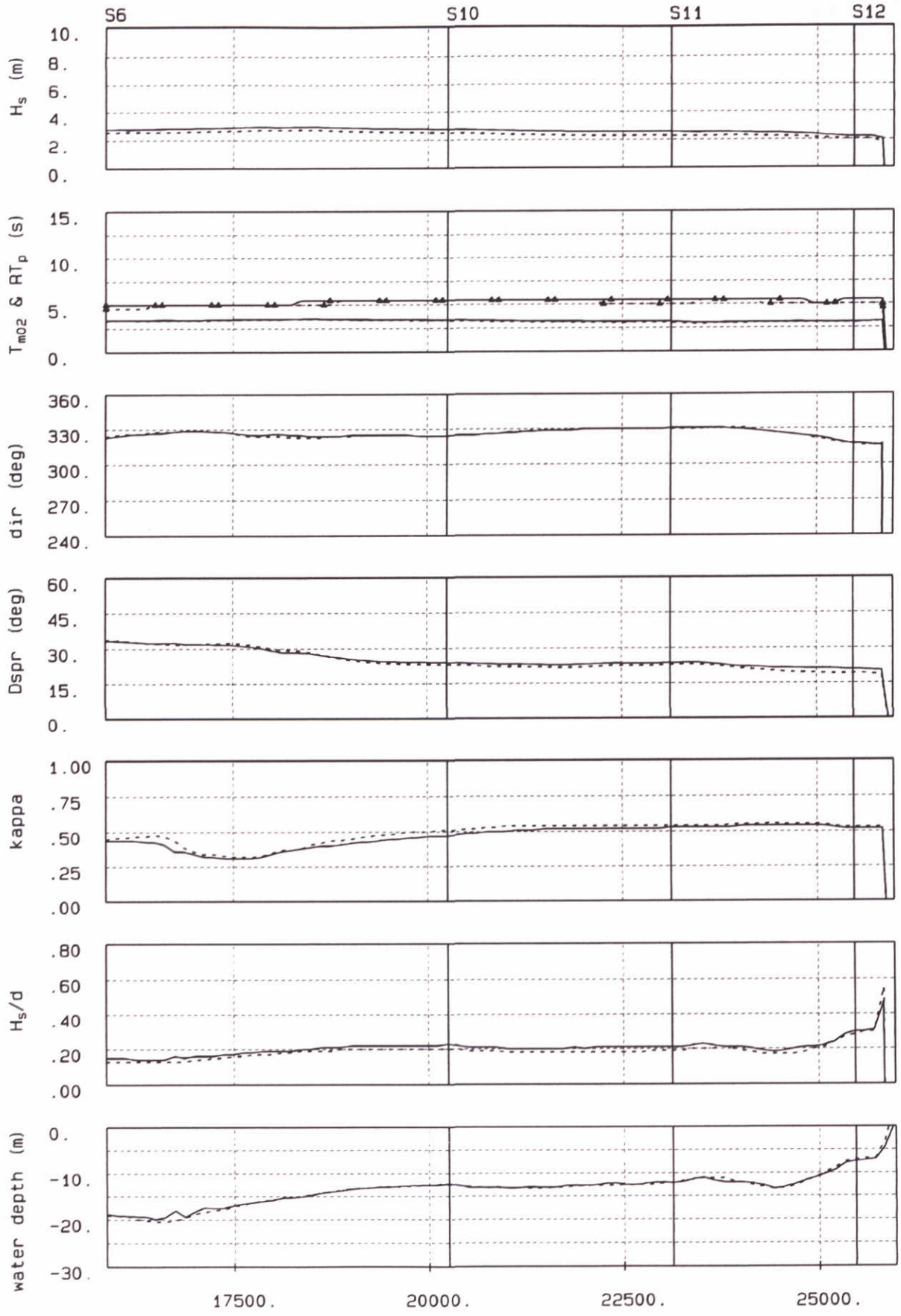

Wave parameters along rays in Friesche Zeegat SWAN wave model computation, Standard run Coarse grid (solid line), fine grid (dashed line)	Ray 2	Case b1
	Superstorm	
DELFT HYDRAULICS/DELFT UNIVERSITY OF TECHNOLOGY	H2368	Fig. 4.7.2

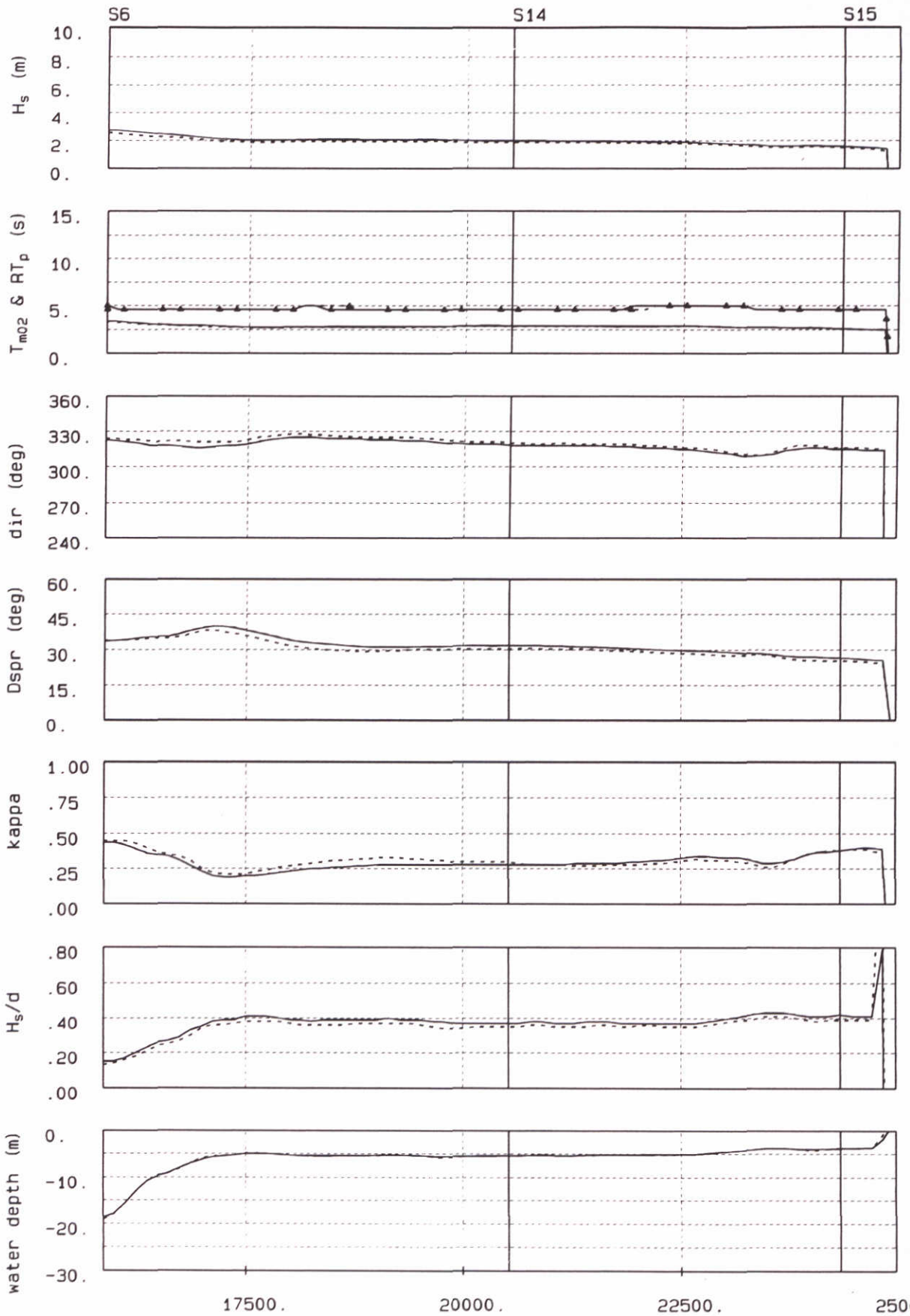

Wave parameters along rays in Friesche Zeegat SWAN wave model computation, Standard run Coarse grid (solid line), fine grid (dashed line)	Ray 3	Case b1
	Superstorm	
DELFT HYDRAULICS/DELFT UNIVERSITY OF TECHNOLOGY	H2368	Fig. 4.7.3

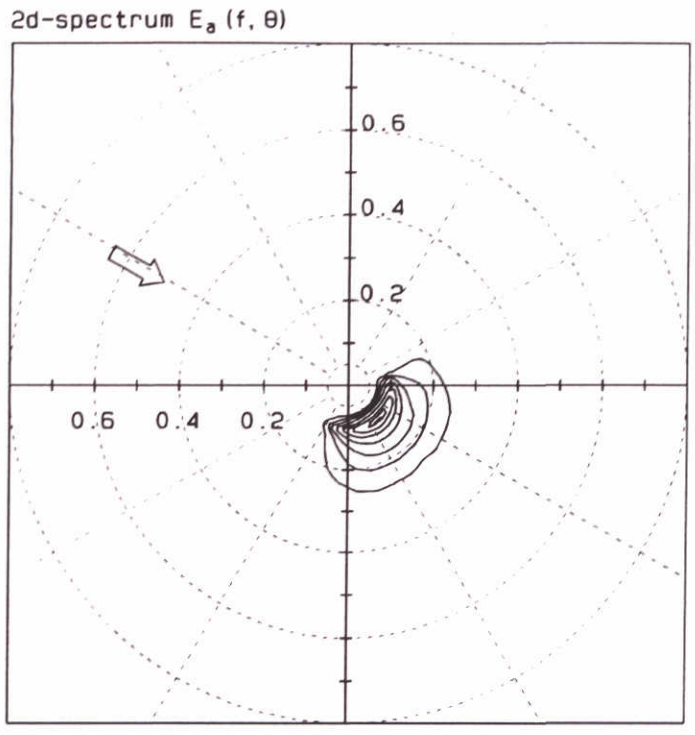

Contour levels:

0.99	$E_{a,max}$
0.90	$E_{a,max}$
0.50	$E_{a,max}$
0.25	$E_{a,max}$
0.125	$E_{a,max}$
0.0625	$E_{a,max}$
0.03125	$E_{a,max}$
0.01	$E_{a,max}$

⇨ Wind direction

Wind speed = 32.9 (m/s)

Wind direction = 299. (^{o}N)

Freq. range .05- .80 (Hz)

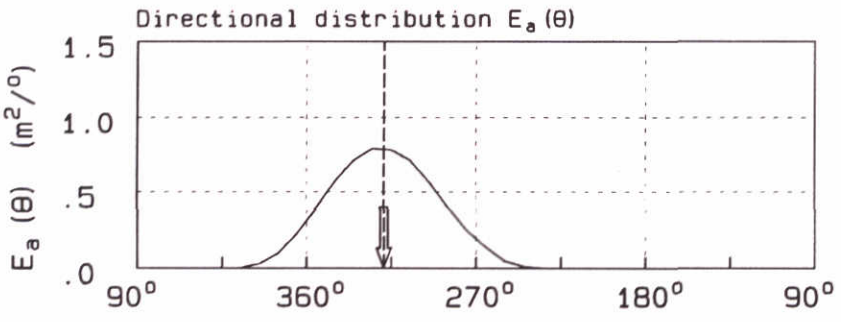

⇩ Mean wave direction

——— Case b1-c

..... Case b1-c

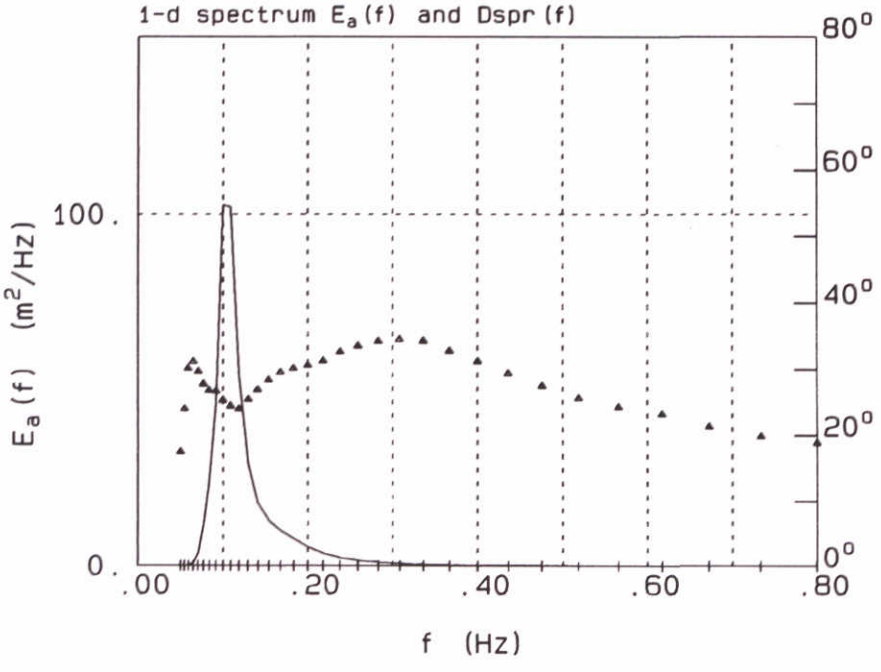

Parameters of $E_a(f)$

f_p	=	.10 (Hz)
Emax	=	102.60 (m^2/Hz)
H_s	=	8.38 (m)
T_{m02}	=	8.05 (s)
T_p	=	10.00 (s)
Dir	=	319.00 (^{o}N)
Dspr	=	26.34 (^{o})
kappa	=	.64
depth	=	27.04 (m)

Wave spectra in Friesche Zeegat computed by SWAN Case b1-c: standard run Location 1 x=198447.5 , y=622306.4		b1-c
	Superstorm	
DELFT HYDRAULICS/DELFT UNIVERSITY OF TECHNOLOGY	H2368	Fig. 4.8.1

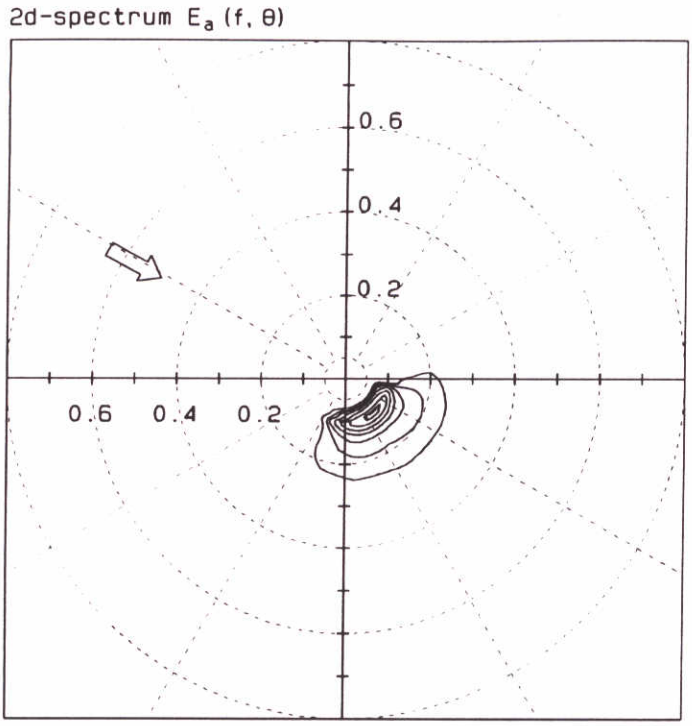

Contour levels:

0.99	$E_{a,max}$
0.90	$E_{a,max}$
0.50	$E_{a,max}$
0.25	$E_{a,max}$
0.125	$E_{a,max}$
0.0625	$E_{a,max}$
0.03125	$E_{a,max}$
0.01	$E_{a,max}$

⇨ Wind direction

Wind speed = 32.9 (m/s)

Wind direction = 299. (^{0}N)

Freq. range .05- .80 (Hz)

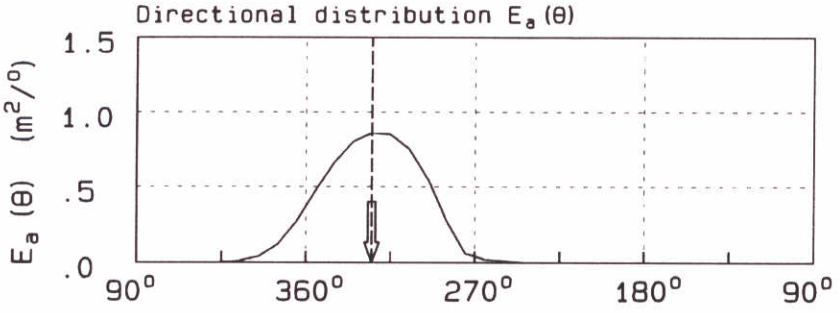

⇩ Mean wave direction

——— Case b1-c

..... Case b1-c

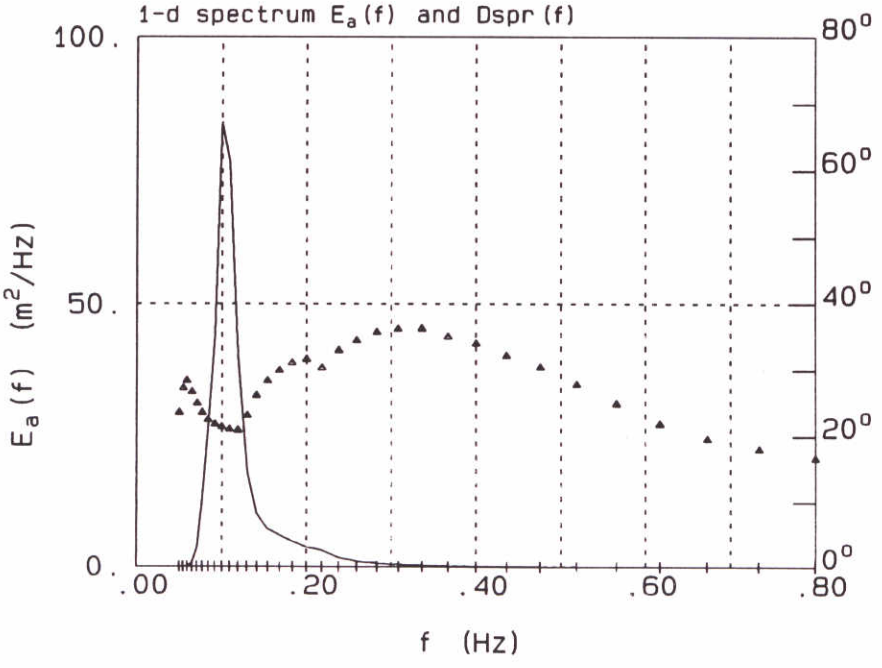

Parameters of $E_a(f)$

f_p	=	.10 (Hz)
Emax	=	84.10 (m^2/Hz)
H_s	=	7.34 (m)
T_{m02}	=	8.32 (s)
T_p	=	10.00 (s)
Dir	=	325.00 (^{0}N)
Dspr	=	23.52 (^{0})
kappa	=	.67
depth	=	21.09 (m)

Wave spectra in Friesche Zeegat computed by SWAN Case b1-c: standard run Location 2 x=199178.8 , y=618195.3		b1-c
	Superstorm	
DELFT HYDRAULICS/DELFT UNIVERSITY OF TECHNOLOGY	H2368	Fig. 4.8.2

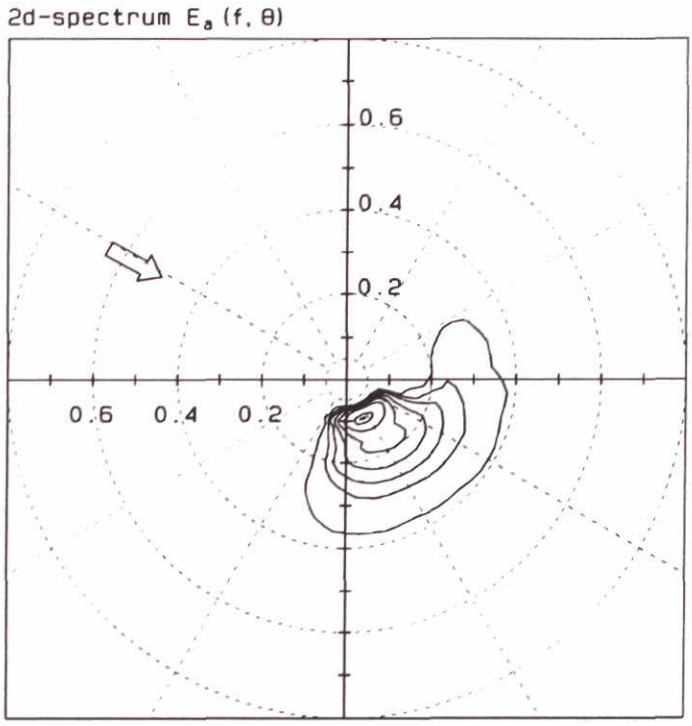

Contour levels:

0.99	$E_{a,max}$
0.90	$E_{a,max}$
0.50	$E_{a,max}$
0.25	$E_{a,max}$
0.125	$E_{a,max}$
0.0625	$E_{a,max}$
0.03125	$E_{a,max}$
0.01	$E_{a,max}$

⇨ Wind direction

Wind speed = 32.8 (m/s)

Wind direction = 299. (^oN)

Freq. range .05- .80 (Hz)

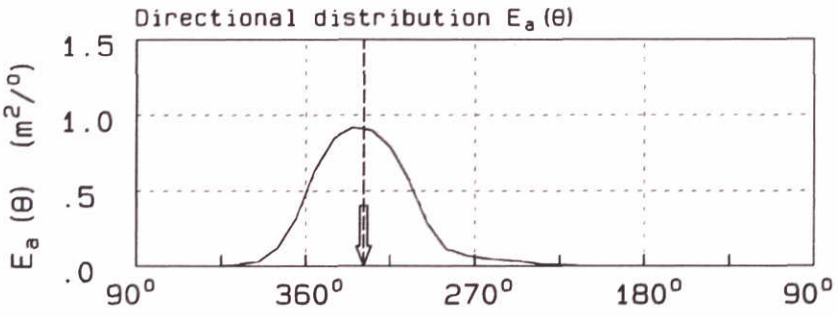

⇩ Mean wave direction

——— Case b1-c

..... Case b1-c

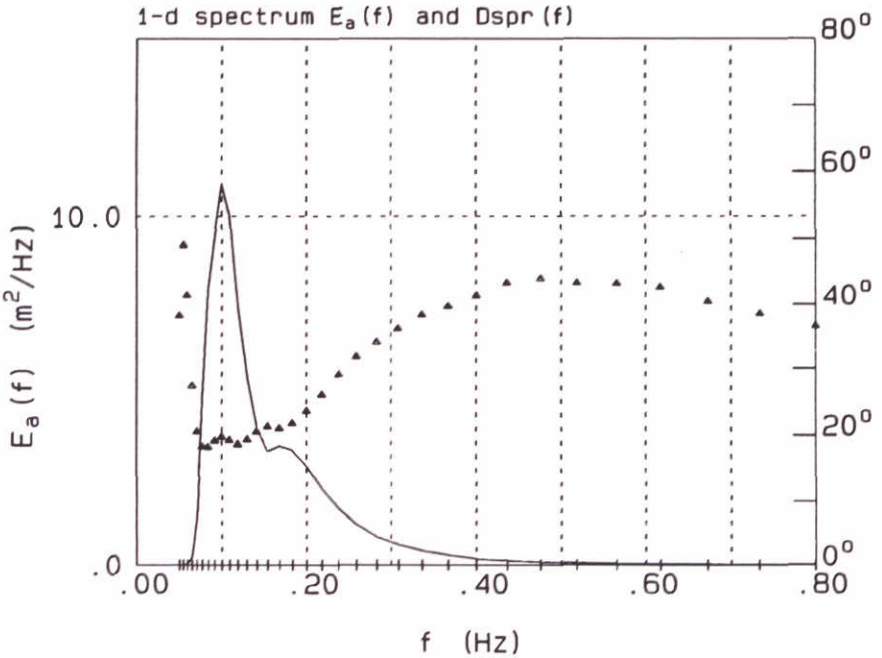

Parameters of $E_a(f)$

f_p	=	.10 (Hz)
Emax	=	10.89 (m^2/Hz)
H_s	=	3.87 (m)
T_{m02}	=	5.27 (s)
T_p	=	10.00 (s)
Dir	=	329.00 (^oN)
Dspr	=	24.14 (^{o})
kappa	=	.53
depth	=	10.84 (m)

Wave spectra in Friesche Zeegat computed by SWAN Case b1-c: standard run Location 3 x=199901.6 , y=614374.6		b1-c
	Superstorm	
DELFT HYDRAULICS/DELFT UNIVERSITY OF TECHNOLOGY	H2368	Fig. 4.8.3

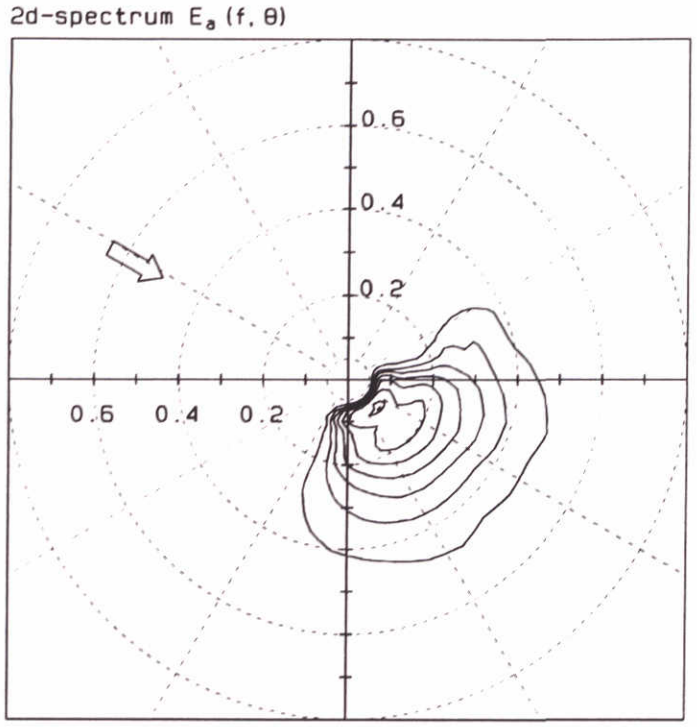

Contour levels:

0.99	$E_{a,max}$
0.90	$E_{a,max}$
0.50	$E_{a,max}$
0.25	$E_{a,max}$
0.125	$E_{a,max}$
0.0625	$E_{a,max}$
0.03125	$E_{a,max}$
0.01	$E_{a,max}$

⇨ Wind direction

Wind speed = 32.9 (m/s)

Wind direction = 299. (^oN)

Freq. range .05- .80 (Hz)

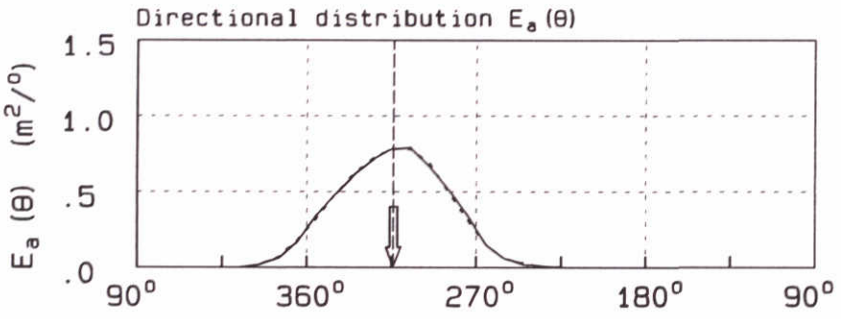

⇩ Mean wave direction

——— Case b1-f

..... Case b1-c

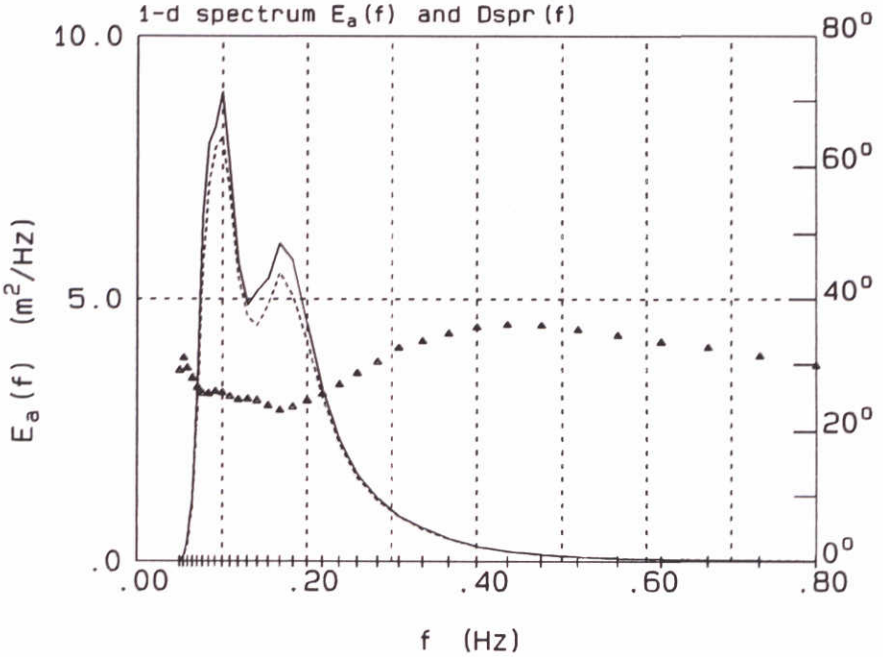

Parameters of $E_a(f)$

f_p	=	.10 (Hz)
Emax	=	8.92 (m^2/Hz)
H_s	=	3.96 (m)
T_{m02}	=	4.96 (s)
T_p	=	10.00 (s)
Dir	=	314.00 (^oN)
Dspr	=	26.37 (^{o})
kappa	=	.38
depth	=	13.17 (m)

Wave spectra in Friesche Zeegat computed by SWAN Case b1-f: standard run Location 4 x=200240.0 , y=612150.0		b1-f
	Superstorm	
DELFT HYDRAULICS/DELFT UNIVERSITY OF TECHNOLOGY	H2368	Fig. 4.8.4

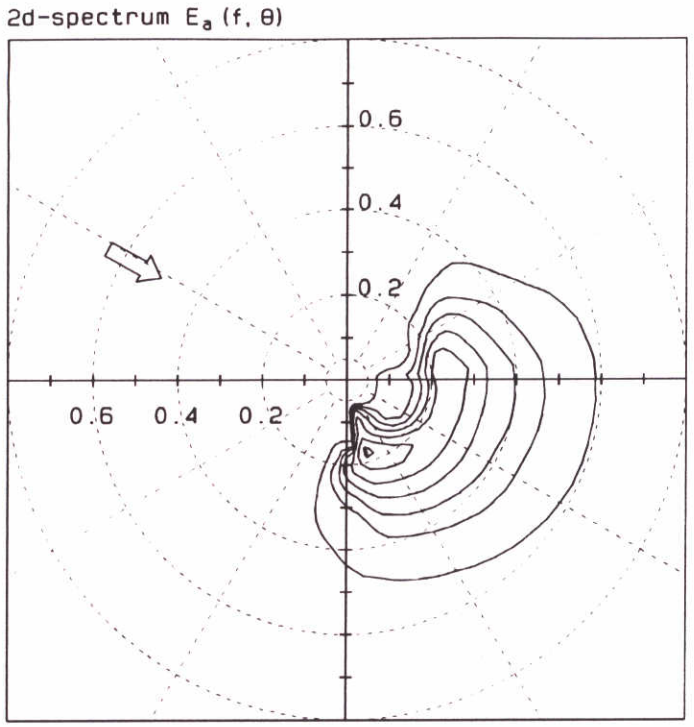

Contour levels:

0.99	$E_{a,max}$
0.90	$E_{a,max}$
0.50	$E_{a,max}$
0.25	$E_{a,max}$
0.125	$E_{a,max}$
0.0625	$E_{a,max}$
0.03125	$E_{a,max}$
0.01	$E_{a,max}$

⇨ Wind direction

Wind speed = 32.9 (m/s)

Wind direction = 299. (^oN)

Freq. range .05- .80 (Hz)

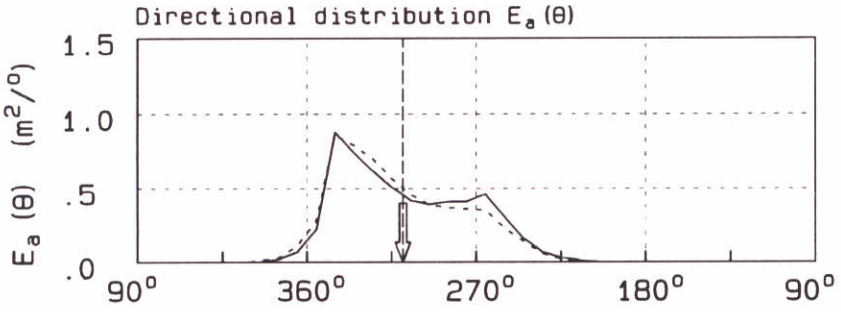

⇩ Mean wave direction

——— Case b1-f

..... Case b1-c

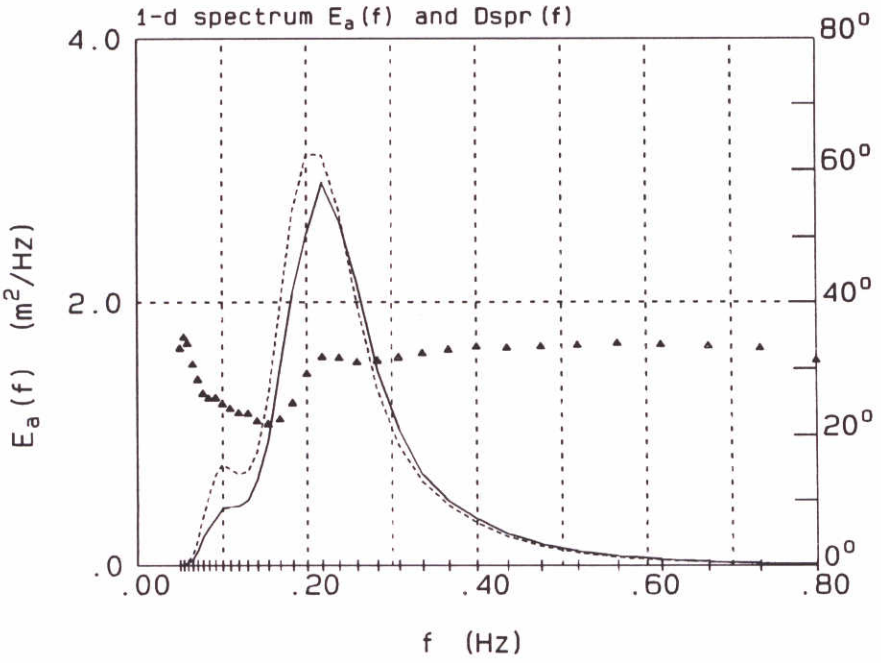

Parameters of $E_a(f)$

f_p	=	.22 (Hz)
Emax	=	2.91 (m^2/Hz)
H_s	=	2.52 (m)
T_{m02}	=	3.41 (s)
T_p	=	4.59 (s)
Dir	=	309.00 (^oN)
Dspr	=	32.61 (^{o})
kappa	=	.35
depth	=	19.42 (m)

Wave spectra in Friesche Zeegat computed by SWAN Case b1-f: standard run Location 5 x=200567.2 , y=608977.0		b1-f
	Superstorm	
DELFT HYDRAULICS/DELFT UNIVERSITY OF TECHNOLOGY	H2368	Fig. 4.8.5

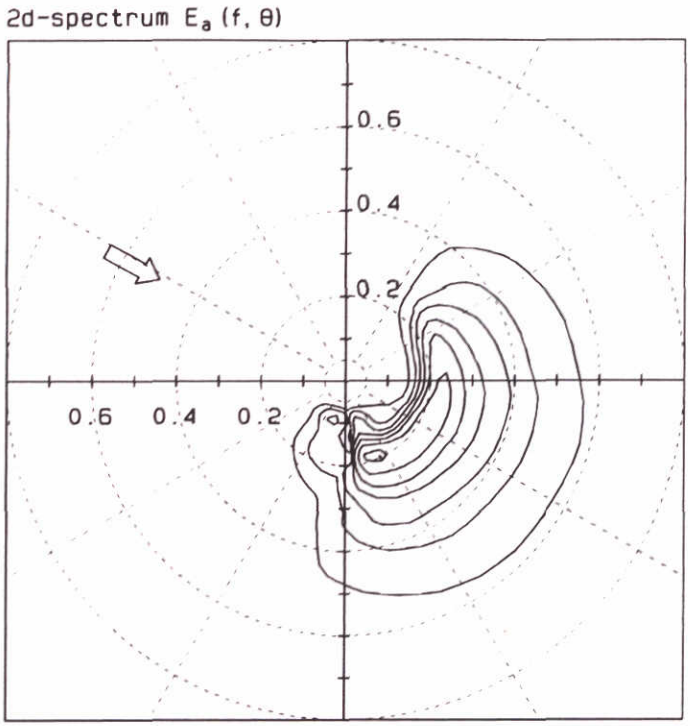

Contour levels:

0.99	$E_{a,max}$
0.90	$E_{a,max}$
0.50	$E_{a,max}$
0.25	$E_{a,max}$
0.125	$E_{a,max}$
0.0625	$E_{a,max}$
0.03125	$E_{a,max}$
0.01	$E_{a,max}$

⇨ Wind direction

Wind speed = 32.9 (m/s)

Wind direction = 299. (°N)

Freq. range .05- .80 (Hz)

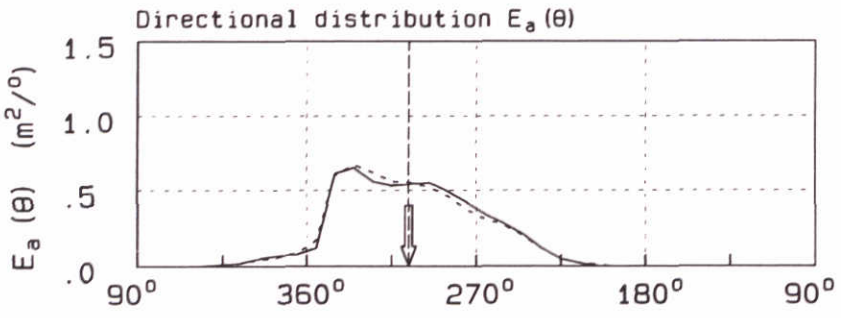

⇩ Mean wave direction

——— Case b1-f

..... Case b1-c

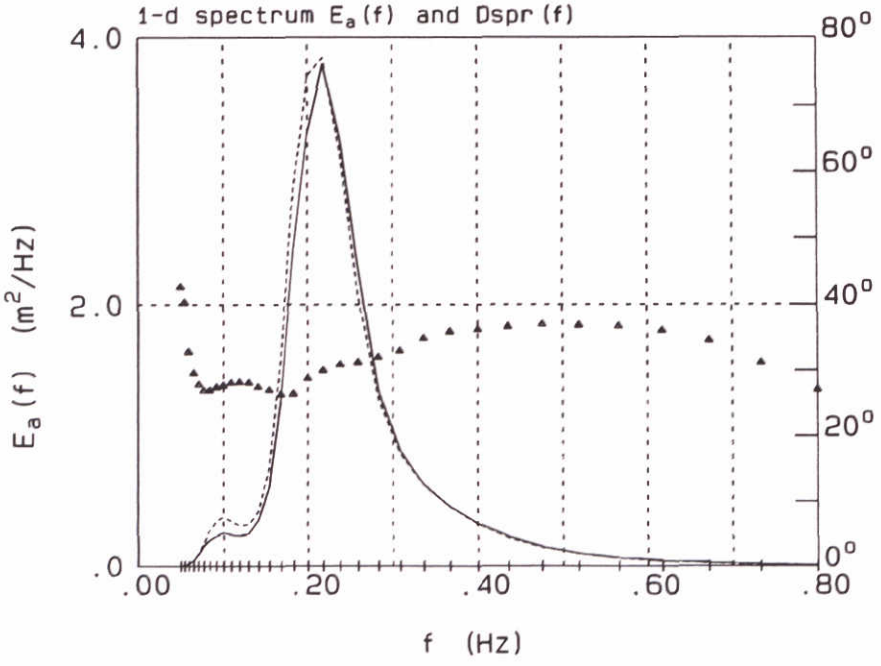

Parameters of $E_a(f)$

f_p	=	.22 (Hz)
Emax	=	3.80 (m^2/Hz)
H_s	=	2.56 (m)
T_{m02}	=	3.34 (s)
T_p	=	4.59 (s)
Dir	=	306.00 (°N)
Dspr	=	33.80 (°)
kappa	=	.45
depth	=	19.07 (m)

Wave spectra in Friesche Zeegat computed by SWAN Case b1-f: standard run Location 6 x=201245.3 , y=606717.0		b1-f
	Superstorm	
DELFT HYDRAULICS/DELFT UNIVERSITY OF TECHNOLOGY	H2368	Fig. 4.8.6

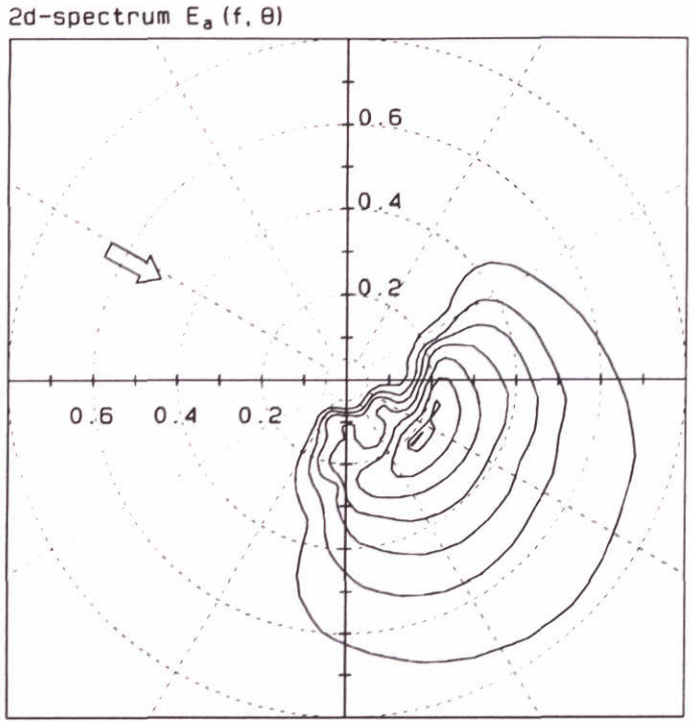

Contour levels:

0.99	$E_{a,max}$
0.90	$E_{a,max}$
0.50	$E_{a,max}$
0.25	$E_{a,max}$
0.125	$E_{a,max}$
0.0625	$E_{a,max}$
0.03125	$E_{a,max}$
0.01	$E_{a,max}$

⇨ Wind direction

Wind speed = 33.0 (m/s)

Wind direction = 298. (^{o}N)

Freq. range .05- .80 (Hz)

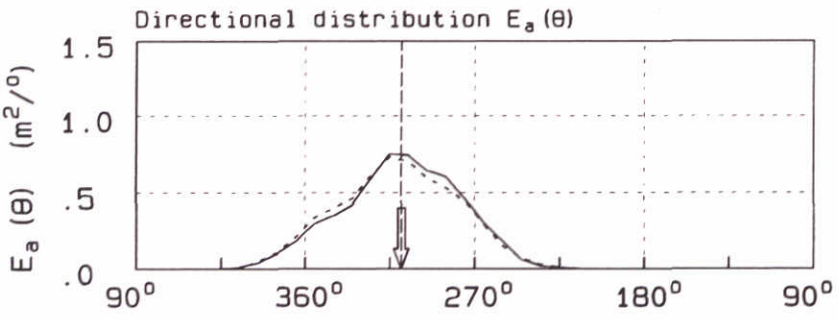

⇩ Mean wave direction

——— Case b1-f

..... Case b1-c

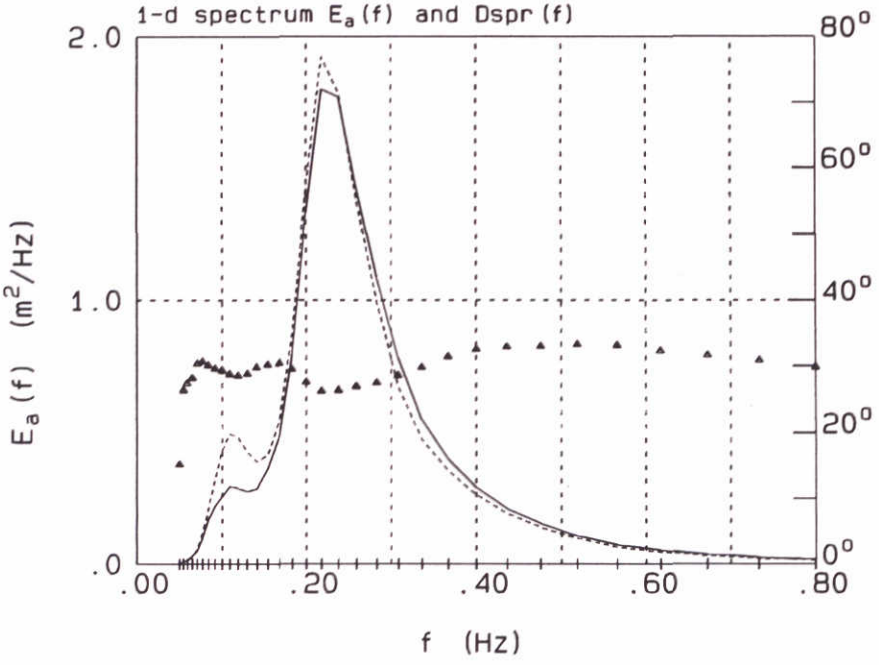

Parameters of $E_a(f)$

f_p	=	.22 (Hz)
Emax	=	1.80 (m^2/Hz)
H_s	=	2.02 (m)
T_{m02}	=	2.90 (s)
T_p	=	4.59 (s)
Dir	=	309.00 (^{o}N)
Dspr	=	29.66 (^{o})
kappa	=	.36
depth	=	5.47 (m)

Wave spectra in Friesche Zeegat computed by SWAN Case b1-f: standard run Location 7 x=201254.5 , y=604392.7		b1-f
	Superstorm	
DELFT HYDRAULICS/DELFT UNIVERSITY OF TECHNOLOGY	H2368	Fig. 4.8.7

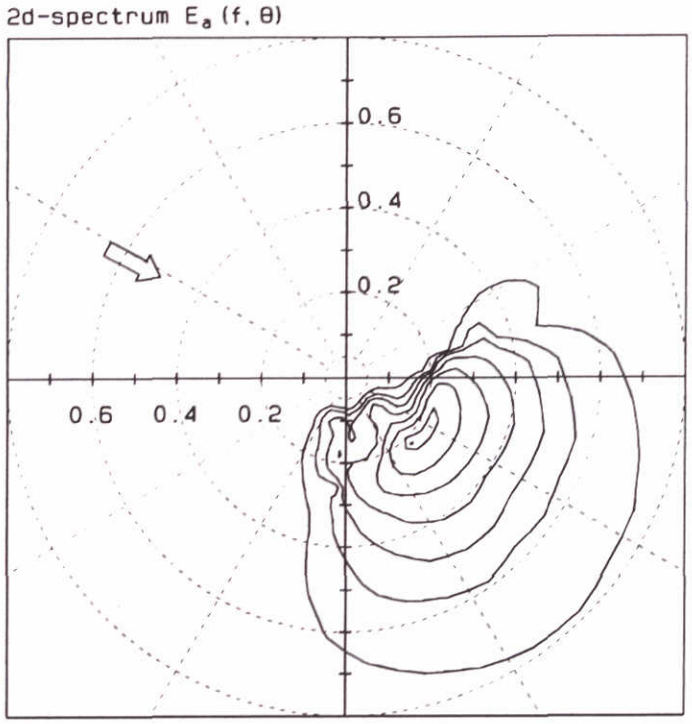

Contour levels:

0.99	$E_{a,max}$
0.90	$E_{a,max}$
0.50	$E_{a,max}$
0.25	$E_{a,max}$
0.125	$E_{a,max}$
0.0625	$E_{a,max}$
0.03125	$E_{a,max}$
0.01	$E_{a,max}$

⇨ Wind direction

Wind speed = 33.0 (m/s)

Wind direction = 298. (^{o}N)

Freq. range .05- .80 (Hz)

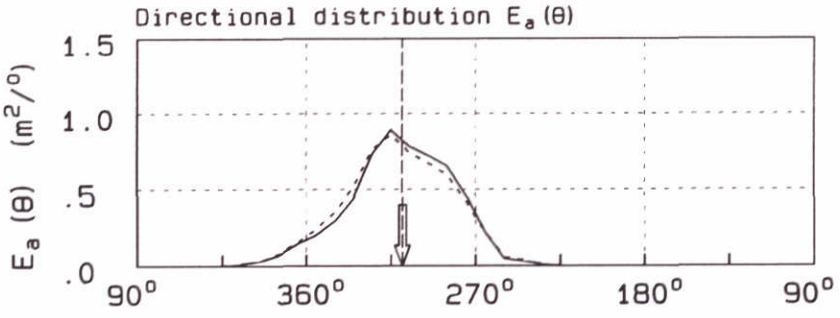

⇩ Mean wave direction

——— Case b1-f

..... Case b1-c

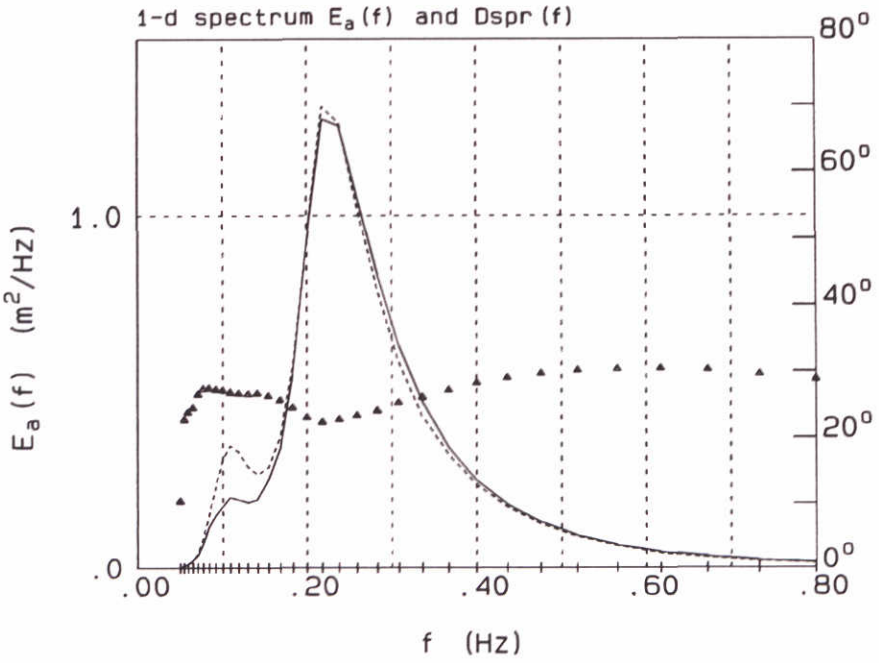

Parameters of $E_a(f)$

f_p	=	.22 (Hz)
Emax	=	1.27 (m^2/Hz)
H_s	=	1.77 (m)
T_{m02}	=	2.69 (s)
T_p	=	4.59 (s)
Dir	=	309.00 (^{o}N)
Dspr	=	26.22 (^{o})
kappa	=	.36
depth	=	4.63 (m)

Wave spectra in Friesche Zeegat computed by SWAN Case b1-f: standard run Location 8 x=201457.1 , y=603243.0		b1-f
	Superstorm	
DELFT HYDRAULICS/DELFT UNIVERSITY OF TECHNOLOGY	H2368	Fig. 4.8.8

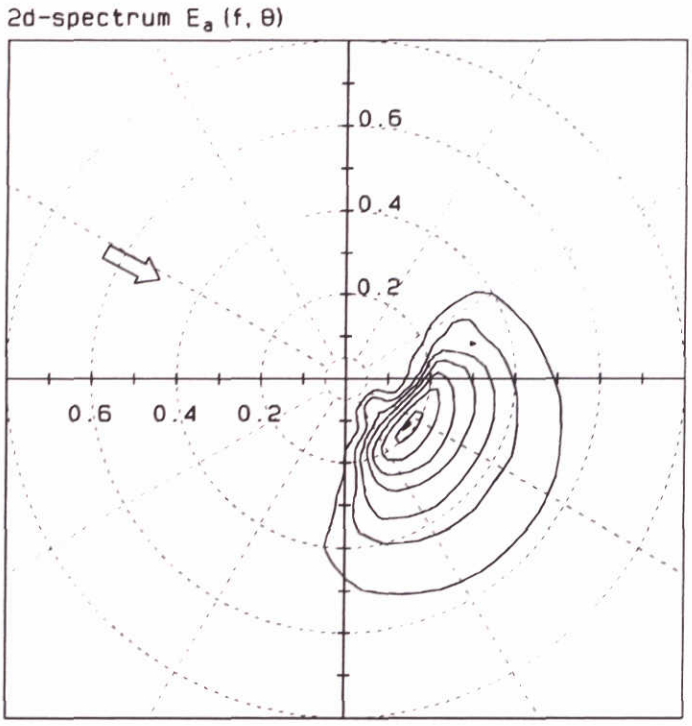

Contour levels:

0.99	$E_{a,max}$
0.90	$E_{a,max}$
0.50	$E_{a,max}$
0.25	$E_{a,max}$
0.125	$E_{a,max}$
0.0625	$E_{a,max}$
0.03125	$E_{a,max}$
0.01	$E_{a,max}$

⇨ Wind direction

Wind speed = 32.7 (m/s)

Wind direction = 298. (°N)

Freq. range .05- .80 (Hz)

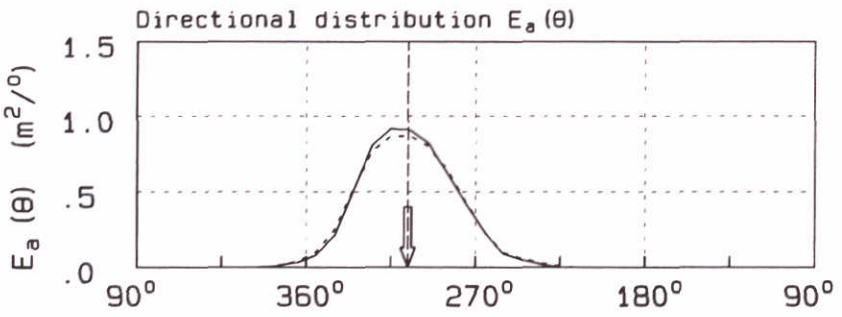

⇩ Mean wave direction

——— Case b1-f

..... Case b1-c

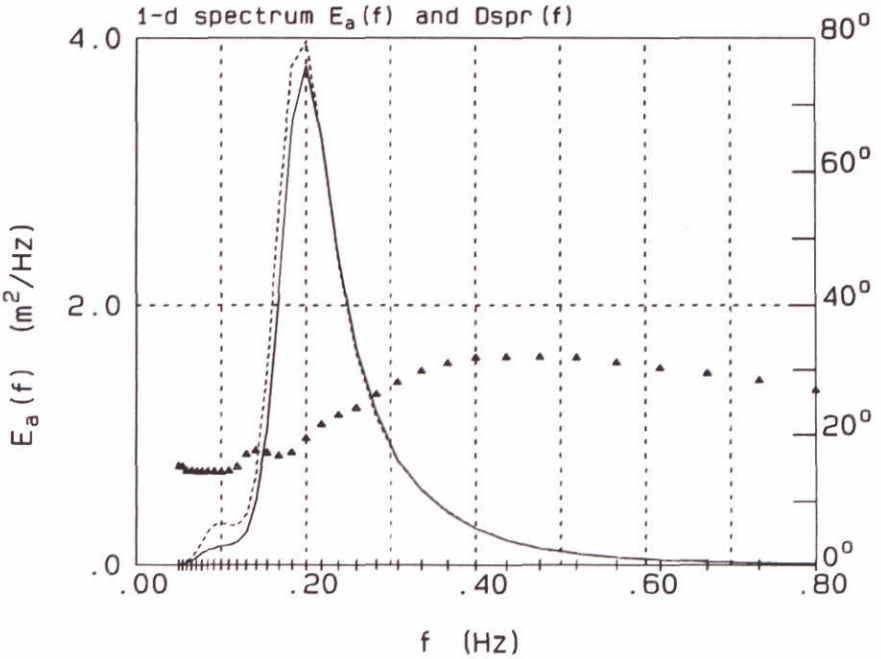

Parameters of $E_a(f)$

f_p	=	.20 (Hz)
Emax	=	3.79 (m^2/Hz)
H_s	=	2.50 (m)
T_{m02}	=	3.31 (s)
T_p	=	5.00 (s)
Dir	=	306.00 (°N)
Dspr	=	23.12 (°)
kappa	=	.51
depth	=	12.39 (m)

Wave spectra in Friesche Zeegat computed by SWAN Case b1-f: standard run Location 10 x=205235.8 , y=604887.4		b1-f
	Superstorm	
DELFT HYDRAULICS/DELFT UNIVERSITY OF TECHNOLOGY	H2368	Fig. 4.8.10

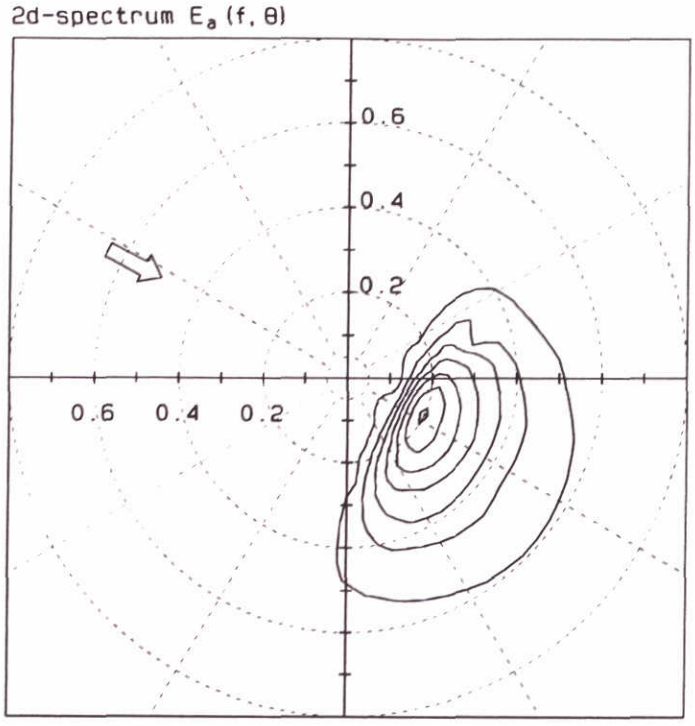

Contour levels:

0.99	$E_{a,max}$
0.90	$E_{a,max}$
0.50	$E_{a,max}$
0.25	$E_{a,max}$
0.125	$E_{a,max}$
0.0625	$E_{a,max}$
0.03125	$E_{a,max}$
0.01	$E_{a,max}$

⇨ Wind direction

Wind speed = 32.5 (m/s)

Wind direction = 298. (^{0}N)

Freq. range .05- .80 (Hz)

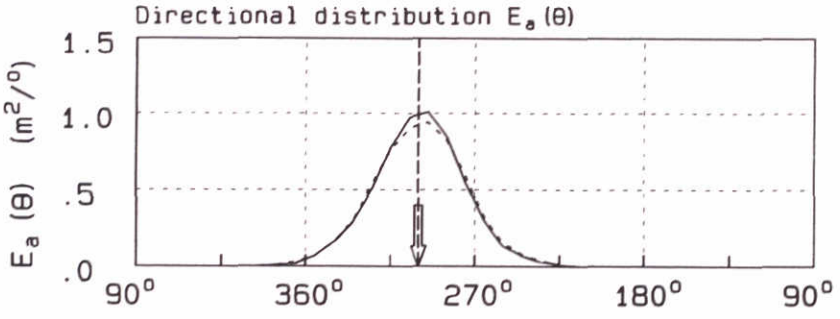

⇩ Mean wave direction

——— Case b1-f

..... Case b1-c

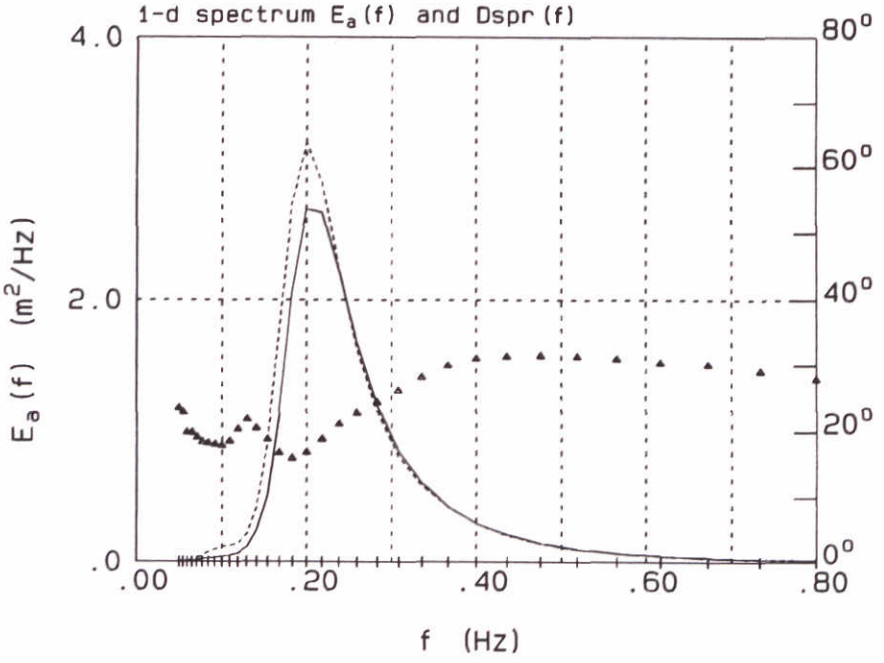

Parameters of $E_a(f)$

f_p	=	.20 (Hz)
Emax	=	2.68 (m^2/Hz)
H_s	=	2.27 (m)
T_{m02}	=	3.06 (s)
T_p	=	5.00 (s)
Dir	=	300.00 (^{0}N)
Dspr	=	22.88 (^{0})
kappa	=	.54
depth	=	12.09 (m)

Wave spectra in Friesche Zeegat computed by SWAN Case b1-f: standard run Location 11 x=207966.2 , y=604002.3		b1-f
	Superstorm	
DELFT HYDRAULICS/DELFT UNIVERSITY OF TECHNOLOGY	H2368	Fig. 4.8.11

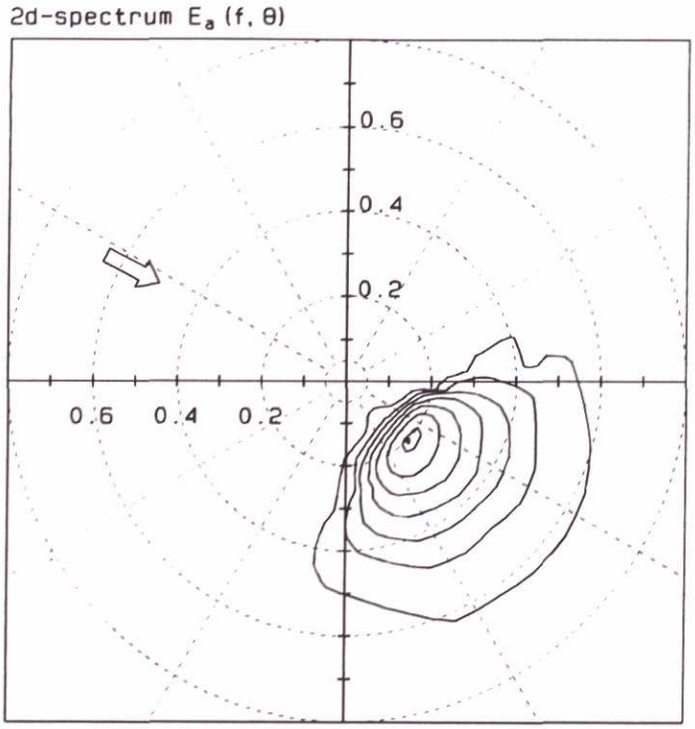

Contour levels:

0.99	$E_{a,max}$
0.90	$E_{a,max}$
0.50	$E_{a,max}$
0.25	$E_{a,max}$
0.125	$E_{a,max}$
0.0625	$E_{a,max}$
0.03125	$E_{a,max}$
0.01	$E_{a,max}$

⇨ Wind direction

Wind speed = 32.3 (m/s)

Wind direction = 297. (^{0}N)

Freq. range .05- .80 (Hz)

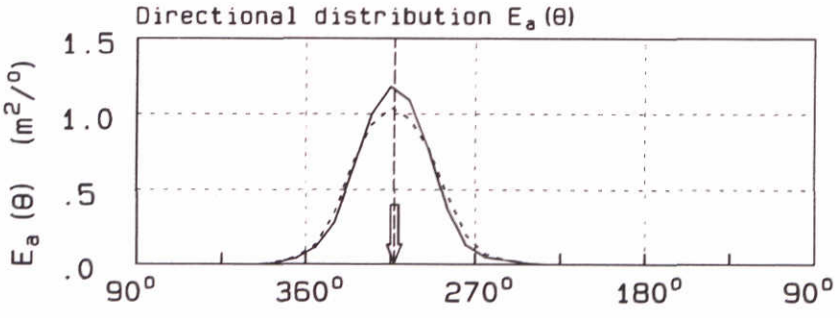

⇩ Mean wave direction

——— Case b1-f

..... Case b1-c

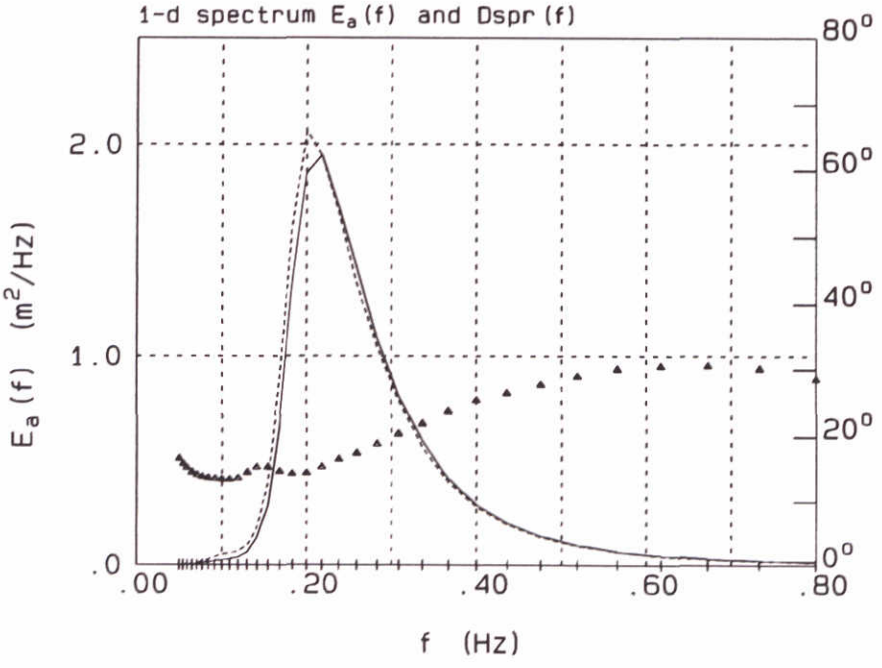

Parameters of $E_a(f)$

f_p	=	.22 (Hz)
Emax	=	1.95 (m^2/Hz)
H_s	=	2.03 (m)
T_{m02}	=	3.05 (s)
T_p	=	4.59 (s)
Dir	=	313.00 (^{0}N)
Dspr	=	19.32 (^{0})
kappa	=	.53
depth	=	7.17 (m)

Wave spectra in Friesche Zeegat computed by SWAN Case b1-f: standard run Location 12 x=210108.0 , y=603044.0		b1-f
	Superstorm	
DELFT HYDRAULICS/DELFT UNIVERSITY OF TECHNOLOGY	H2368	Fig. 4.8.12

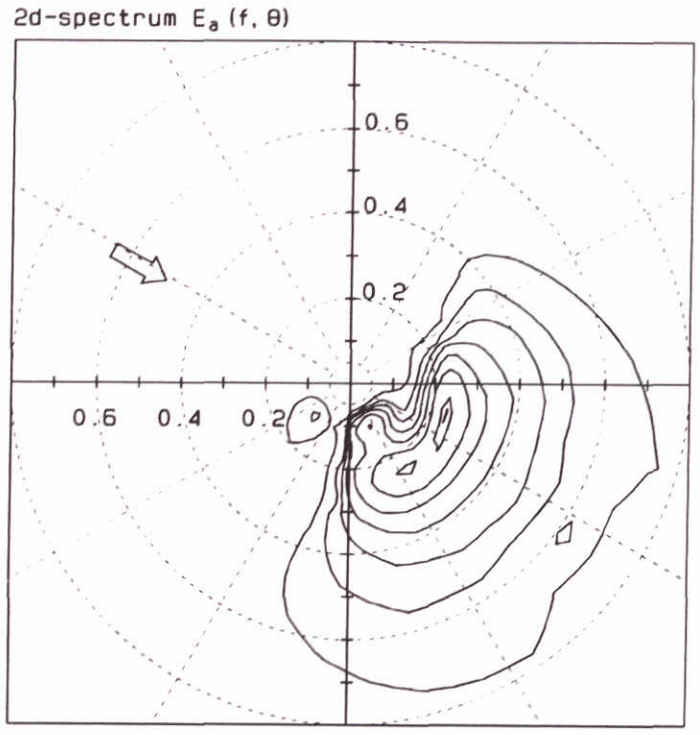

Contour levels:

0.99	$E_{a,max}$
0.90	$E_{a,max}$
0.50	$E_{a,max}$
0.25	$E_{a,max}$
0.125	$E_{a,max}$
0.0625	$E_{a,max}$
0.03125	$E_{a,max}$
0.01	$E_{a,max}$

⇨ Wind direction

Wind speed = 33.2 (m/s)

Wind direction = 299. (^{0}N)

Freq. range .05- .80 (Hz)

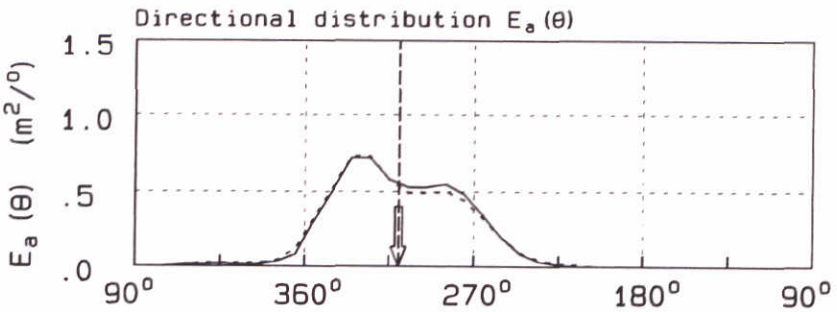

⇩ Mean wave direction

——— Case b1-f

..... Case b1-c

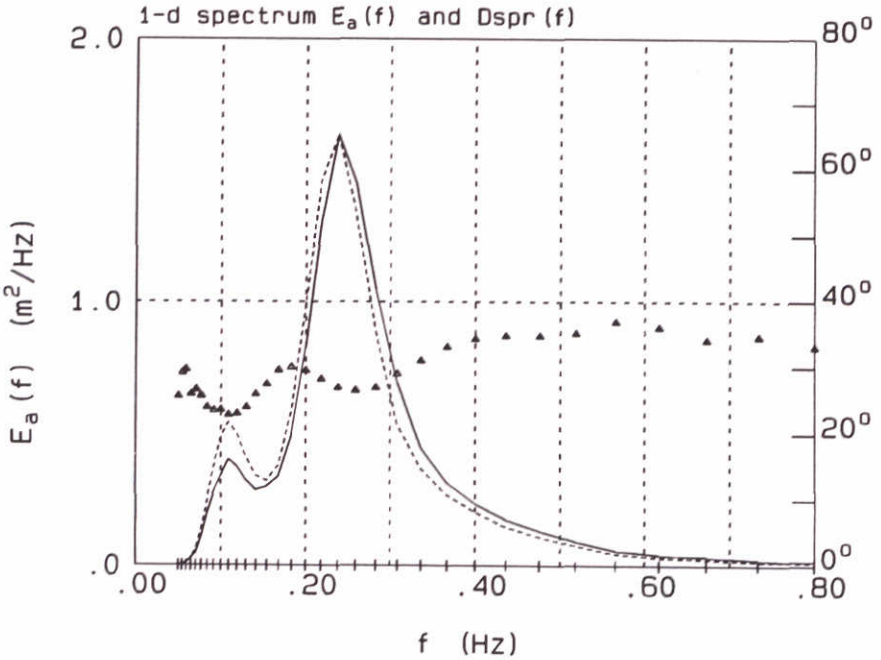

Parameters of $E_a(f)$

f_p	=	.24 (Hz)
Emax	=	1.63 (m^2/Hz)
H_s	=	1.87 (m)
T_{m02}	=	2.84 (s)
T_p	=	4.20 (s)
Dir	=	310.00 (^{0}N)
Dspr	=	30.40 (^{0})
kappa	=	.30
depth	=	5.36 (m)

Wave spectra in Friesche Zeegat computed by SWAN Case b1-f: standard run Location 14 x=197643.6 , y=603756.0		b1-f
	Superstorm	
DELFT HYDRAULICS/DELFT UNIVERSITY OF TECHNOLOGY	H2368	Fig. 4.8.14

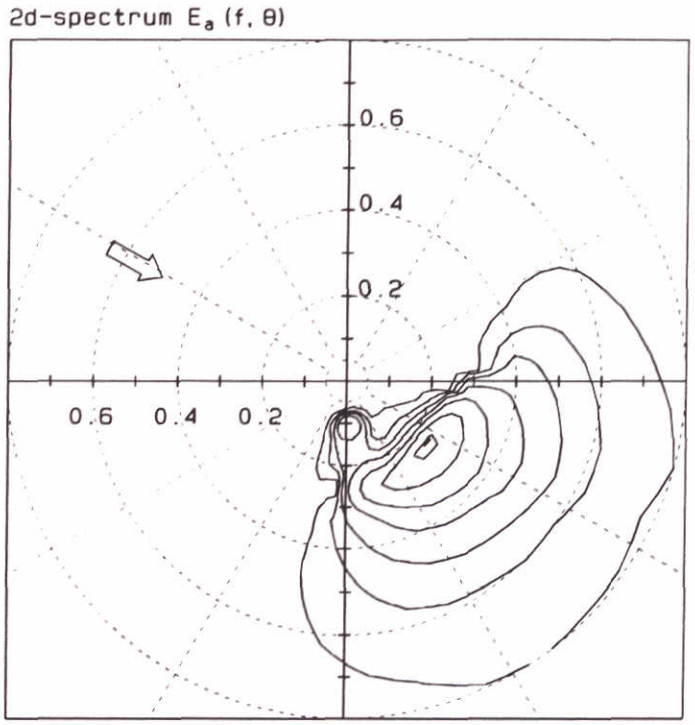

Contour levels:

0.99	$E_{a,max}$
0.90	$E_{a,max}$
0.50	$E_{a,max}$
0.25	$E_{a,max}$
0.125	$E_{a,max}$
0.0625	$E_{a,max}$
0.03125	$E_{a,max}$
0.01	$E_{a,max}$

⇨ Wind direction

Wind speed = 33.4 (m/s)

Wind direction = 299. (^{0}N)

Freq. range .05- .80 (Hz)

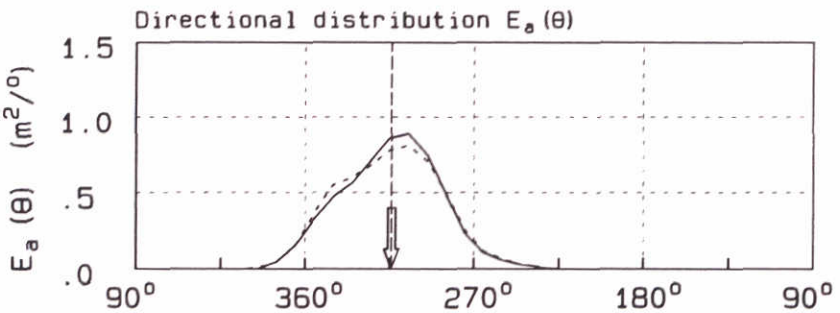

⇩ Mean wave direction

——— Case b1-f

..... Case b1-c

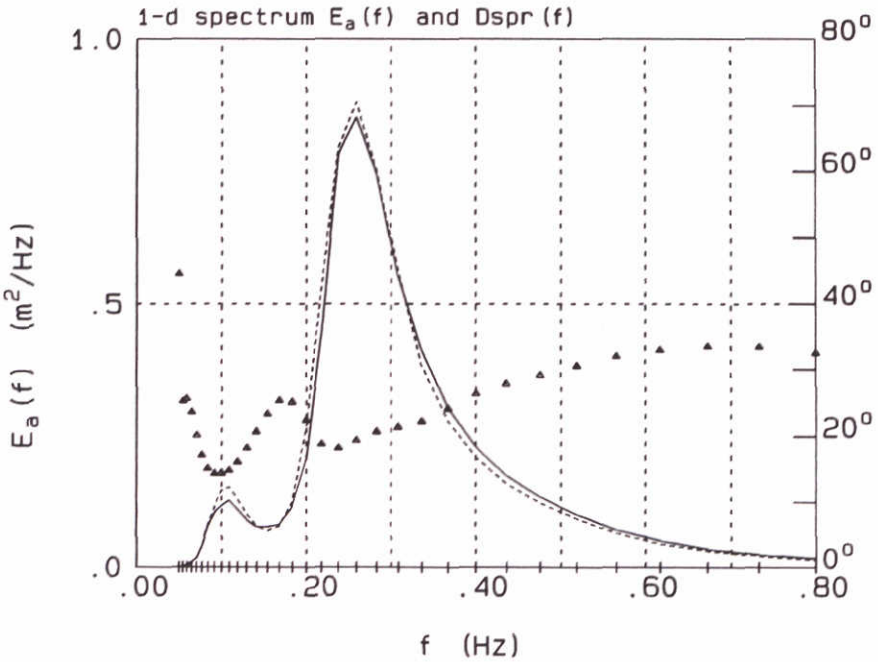

Parameters of $E_a(f)$

f_p	=	.26 (Hz)
Emax	=	.85 (m^2/Hz)
H_s	=	1.47 (m)
T_{m02}	=	2.57 (s)
T_p	=	3.86 (s)
Dir	=	314.00 (^{0}N)
Dspr	=	25.33 (^{0})
kappa	=	.38
depth	=	3.75 (m)

Wave spectra in Friesche Zeegat computed by SWAN Case b1-f: standard run Location 15 x=194679.2 , y=601371.6		b1-f
	Superstorm	
DELFT HYDRAULICS/DELFT UNIVERSITY OF TECHNOLOGY	H2368	Fig. 4.8.15

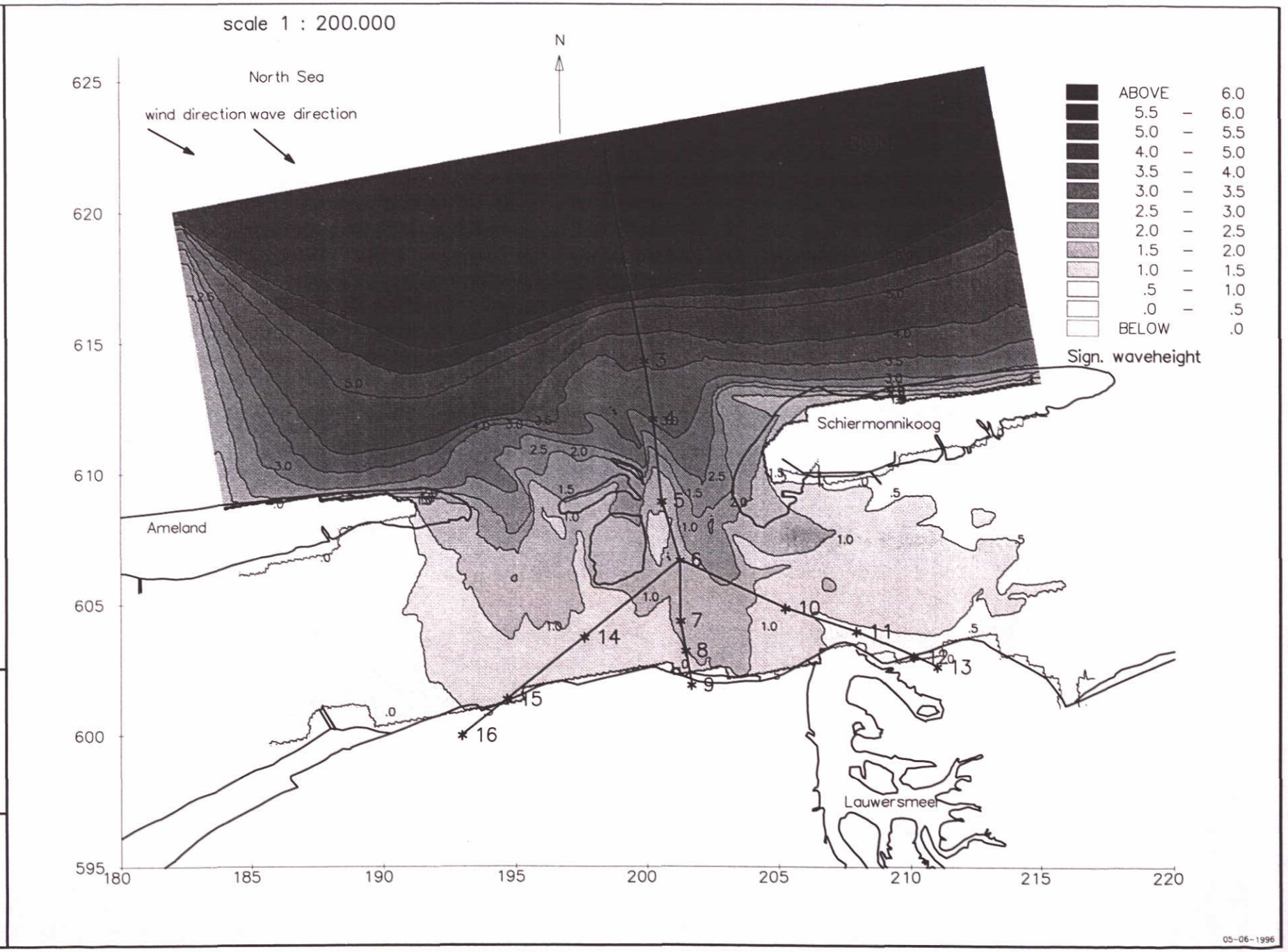

Wave model results Friesche Zeegat

SWAN wave model, course + fine grid , no wind

Significant wave height (m)

case b2	SWAN
superstorm	
H2368	Fig. 4.9

DELFT HYDRAULICS + Delft University of Technology

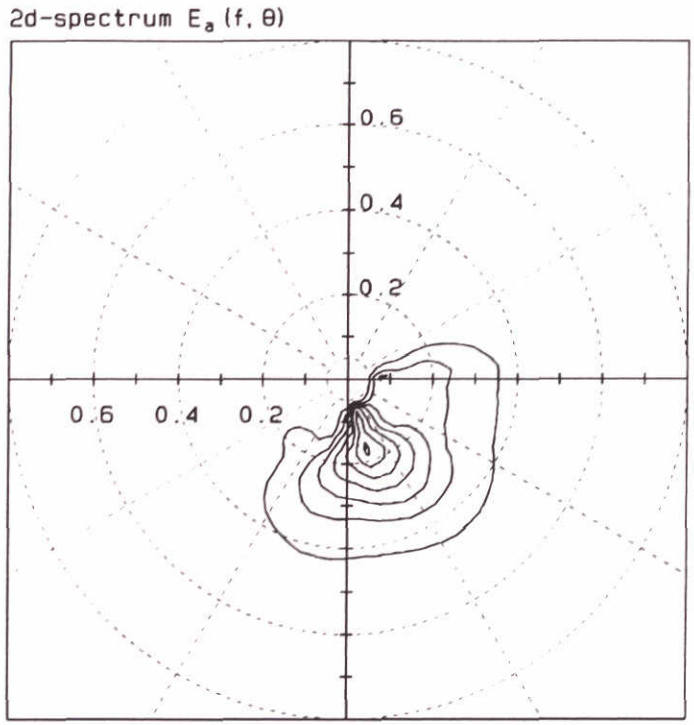

Contour levels:

0.99	$E_{a,max}$
0.90	$E_{a,max}$
0.50	$E_{a,max}$
0.25	$E_{a,max}$
0.125	$E_{a,max}$
0.0625	$E_{a,max}$
0.03125	$E_{a,max}$
0.01	$E_{a,max}$

⇨ Wind direction

Wind speed = .0 (m/s)

Wind direction = 299. (°N)

Freq. range .05- .80 (Hz)

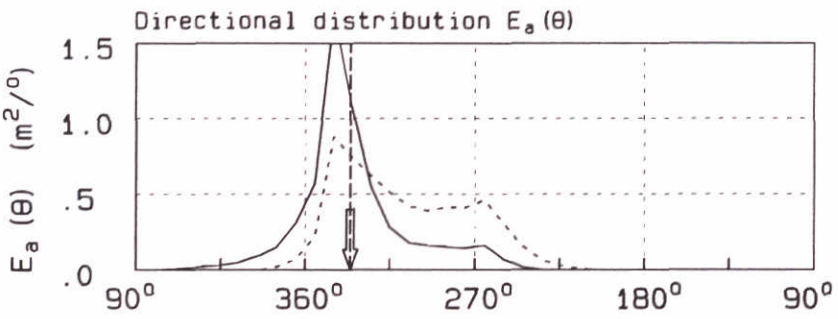

⇩ Mean wave direction

——— Case b2-f

····· Case b1-f

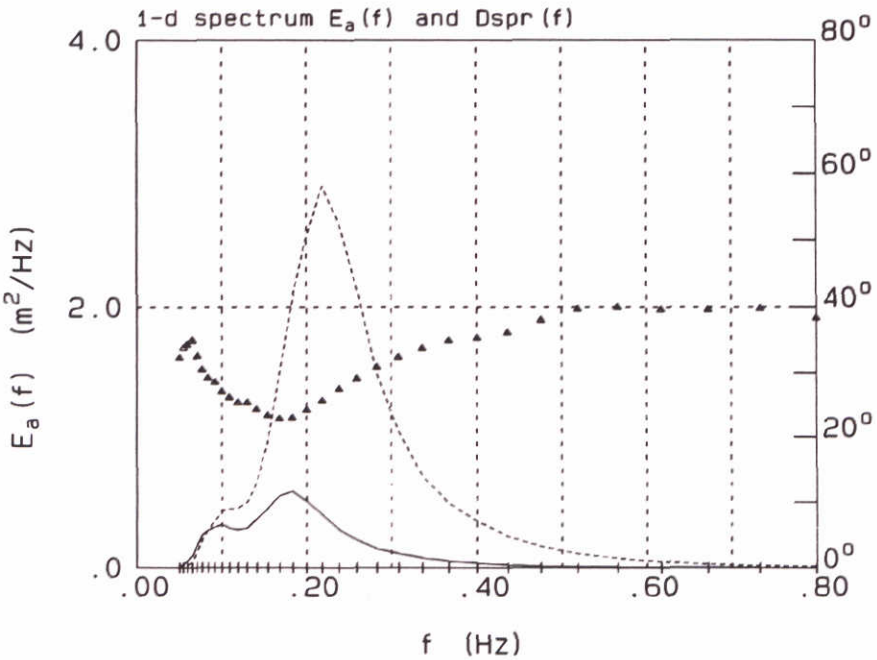

Parameters of $E_a(f)$

f_p	=	.18 (Hz)
Emax	=	.58 (m^2/Hz)
H_s	=	1.13 (m)
T_{m02}	=	4.70 (s)
T_p	=	5.46 (s)
Dir	=	336.00 (°N)
Dspr	=	27.07 (°)
kappa	=	.20
depth	=	19.42 (m)

Wave spectra in Friesche Zeegat computed by SWAN Case b2-f: no wind Location 5 x=200567.2 , y=608977.0		b2-f
	Superstorm	
DELFT HYDRAULICS/DELFT UNIVERSITY OF TECHNOLOGY	H2368	Fig. 4.10

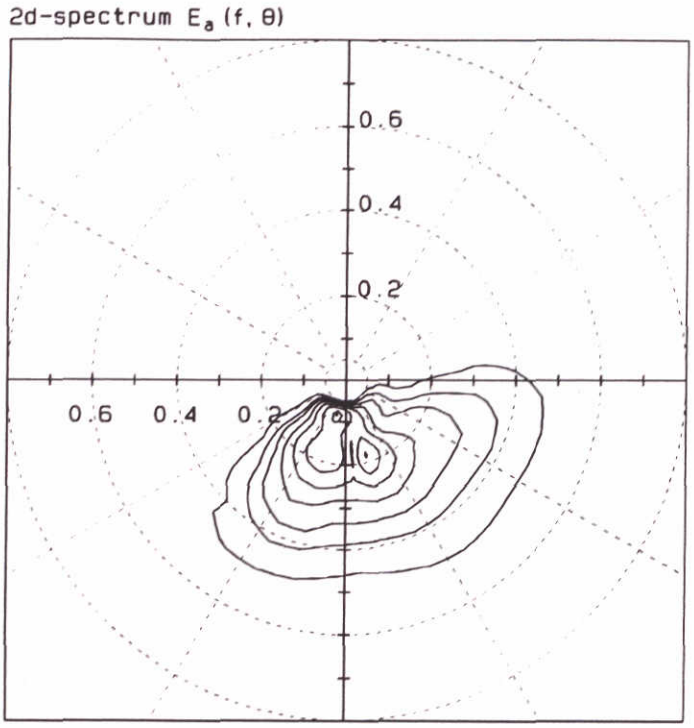

Contour levels:

0.99	$E_{a,max}$
0.90	$E_{a,max}$
0.50	$E_{a,max}$
0.25	$E_{a,max}$
0.125	$E_{a,max}$
0.0625	$E_{a,max}$
0.03125	$E_{a,max}$
0.01	$E_{a,max}$

⇨ Wind direction

Wind speed = .0 (m/s)

Wind direction = 299. (°N)

Freq. range .05- .80 (Hz)

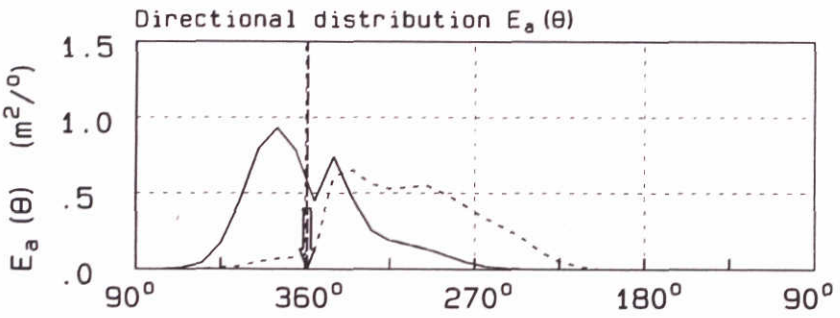

⇩ Mean wave direction

——— Case b2-f

..... Case b1-f

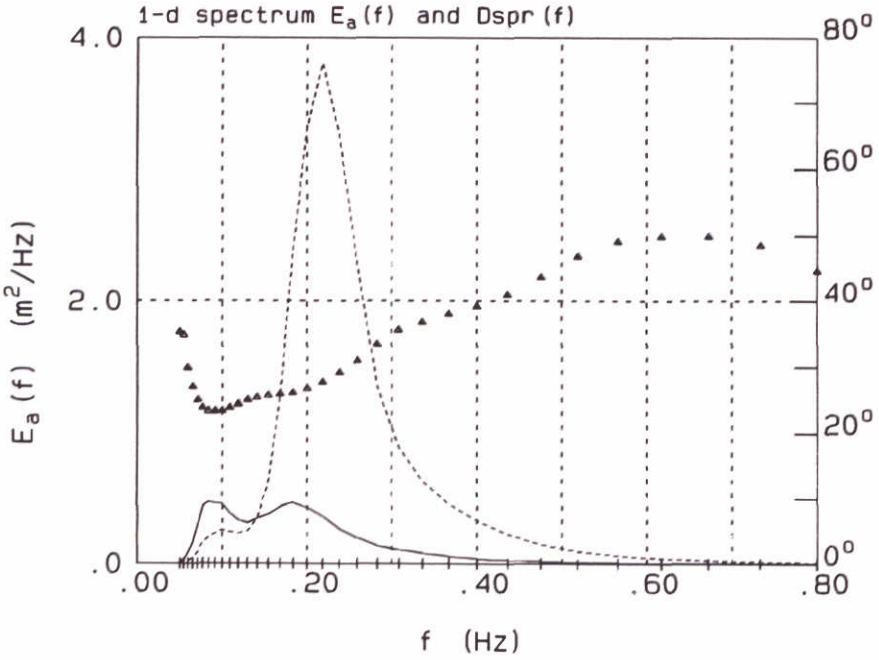

Parameters of $E_a(f)$

f_p	=	.08 (Hz)
Emax	=	.47 (m^2/Hz)
H_s	=	1.13 (m)
T_{m02}	=	4.68 (s)
T_p	=	11.90 (s)
Dir	=	359.00 (°N)
Dspr	=	29.18 (°)
kappa	=	.26
depth	=	19.07 (m)

Wave spectra in Friesche Zeegat computed by SWAN Case b2-f: no wind Location 6 x=201245.3 , y=606717.0		b2-f
	Superstorm	
DELFT HYDRAULICS/DELFT UNIVERSITY OF TECHNOLOGY	H2368	Fig. 4.11

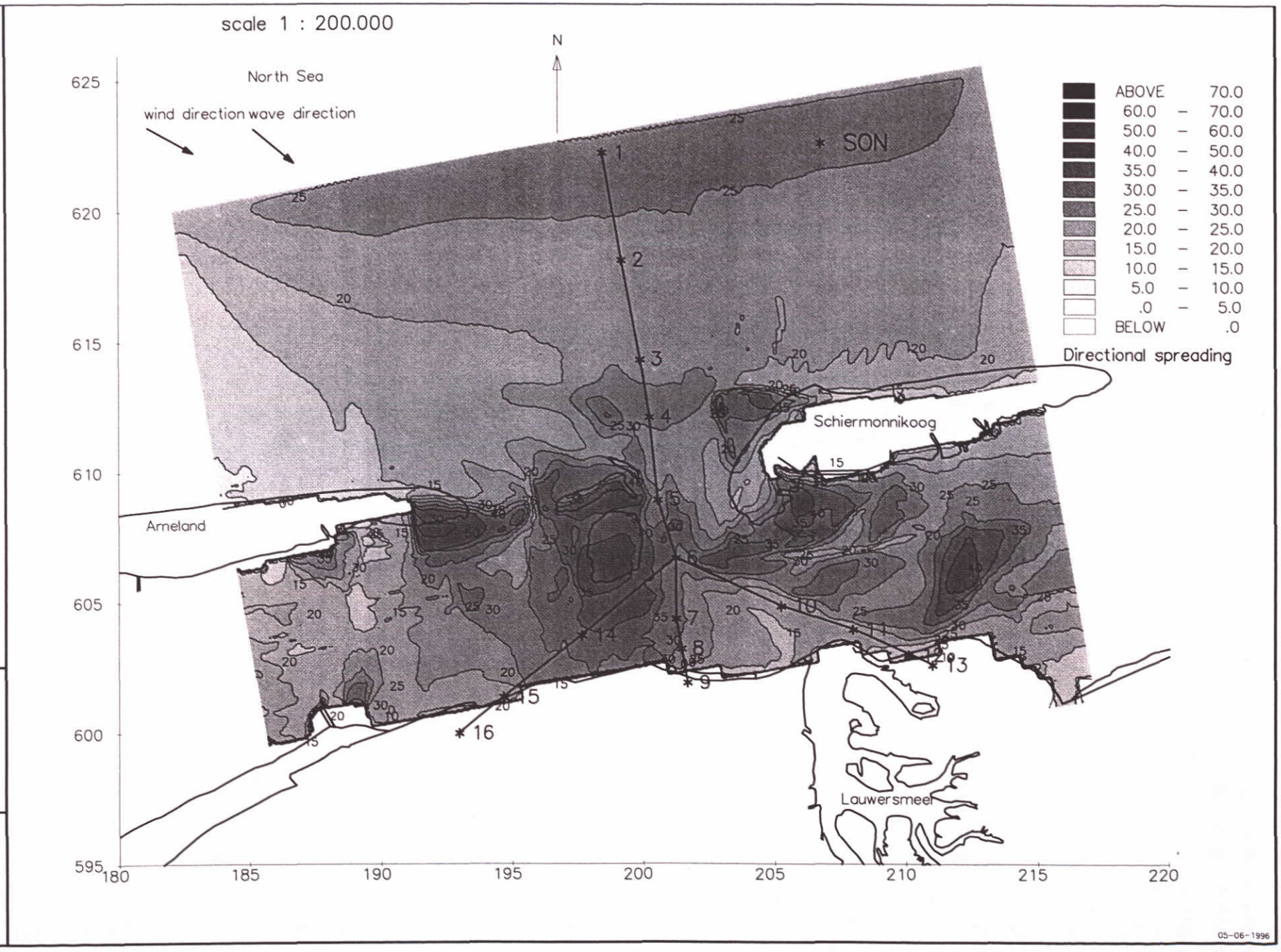

Wave model results Friesche Zeegat

SWAN wave model, course + fine grid , no wind

Directional spreading (deg)

case b2	SWAN
superstorm	
H2368	Fig. 4.12

DELFT HYDRAULICS + Delft University of Technology

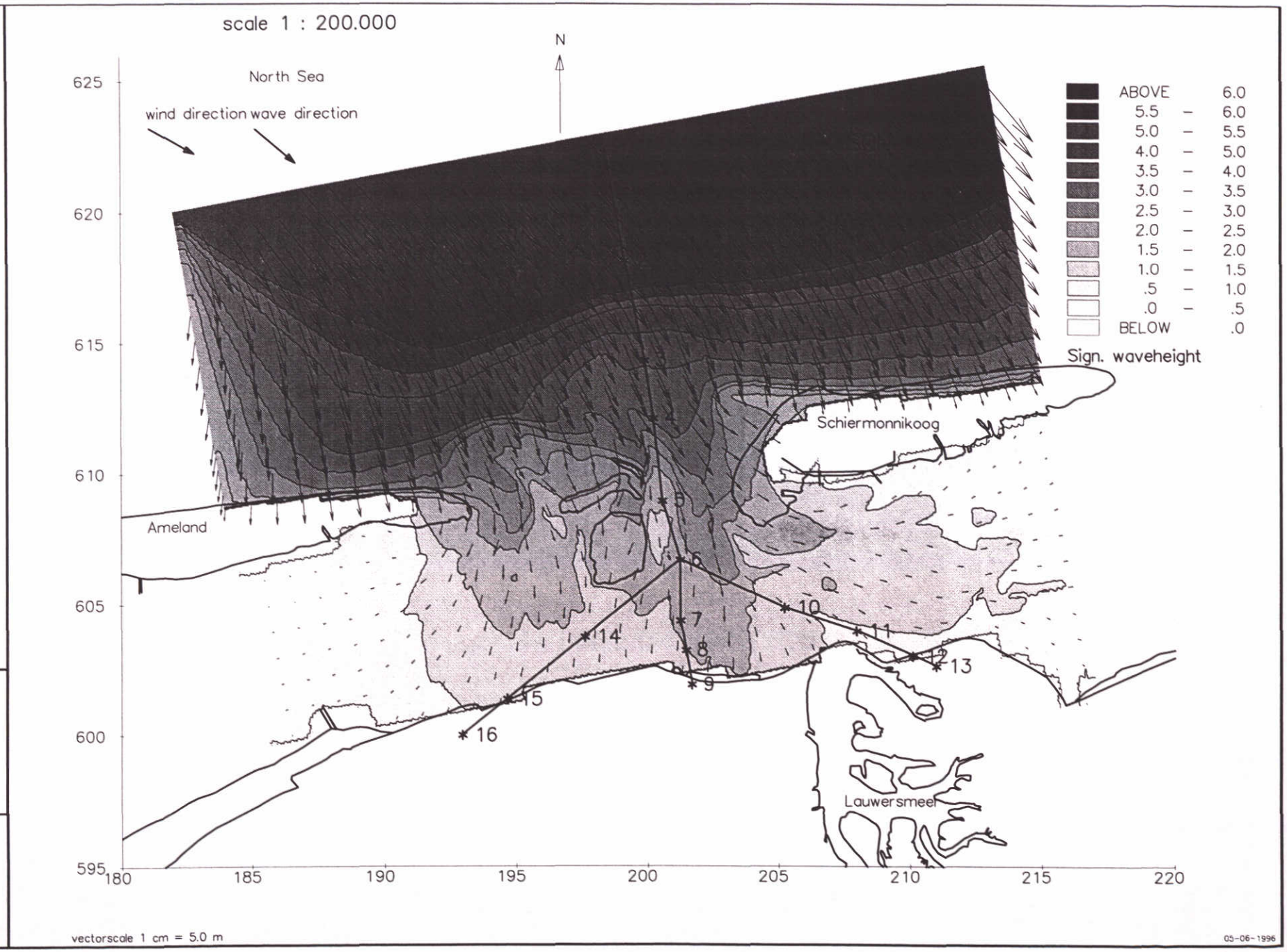

Wave model results Friesche Zeegat
SWAN wave model, course + fine grid , no wind
Significant wave height (m) and mean wave direction

case b2	SWAN
superstorm	
H2368	Fig. 4.13

DELFT HYDRAULICS + Delft University of Technology

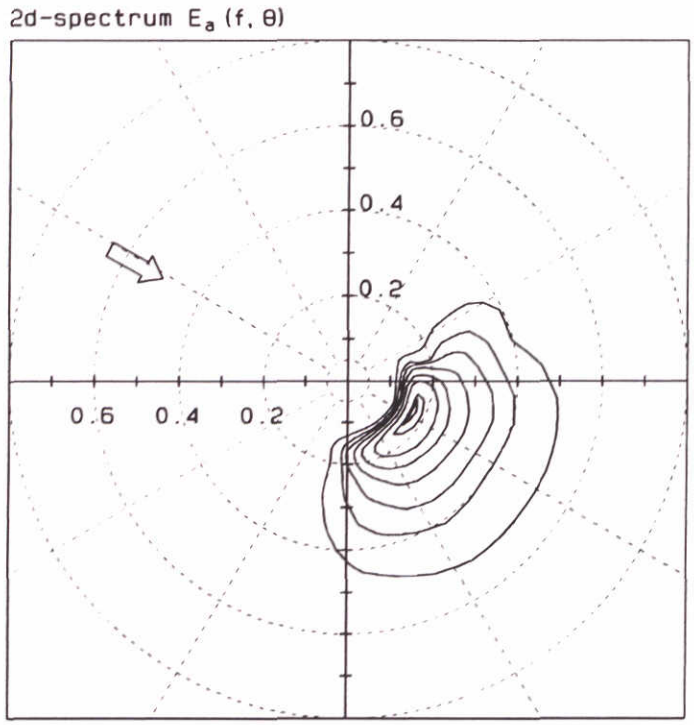

Contour levels:

0.99	$E_{a,max}$
0.90	$E_{a,max}$
0.50	$E_{a,max}$
0.25	$E_{a,max}$
0.125	$E_{a,max}$
0.0625	$E_{a,max}$
0.03125	$E_{a,max}$
0.01	$E_{a,max}$

⇨ Wind direction

Wind speed = 32.9 (m/s)

Wind direction = 299. (°N)

Freq. range .05- .80 (Hz)

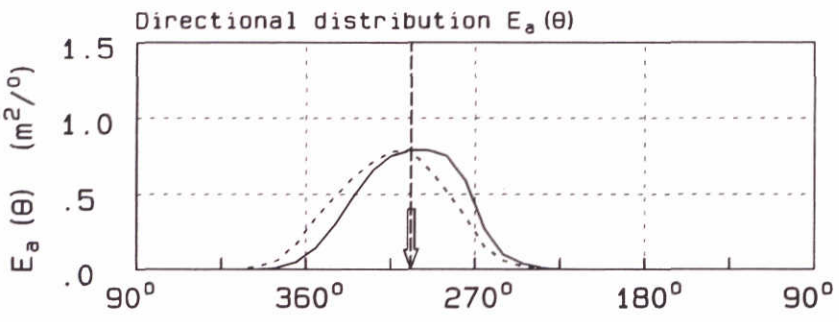

⇩ Mean wave direction

——— Case b3-f

..... Case b1-f

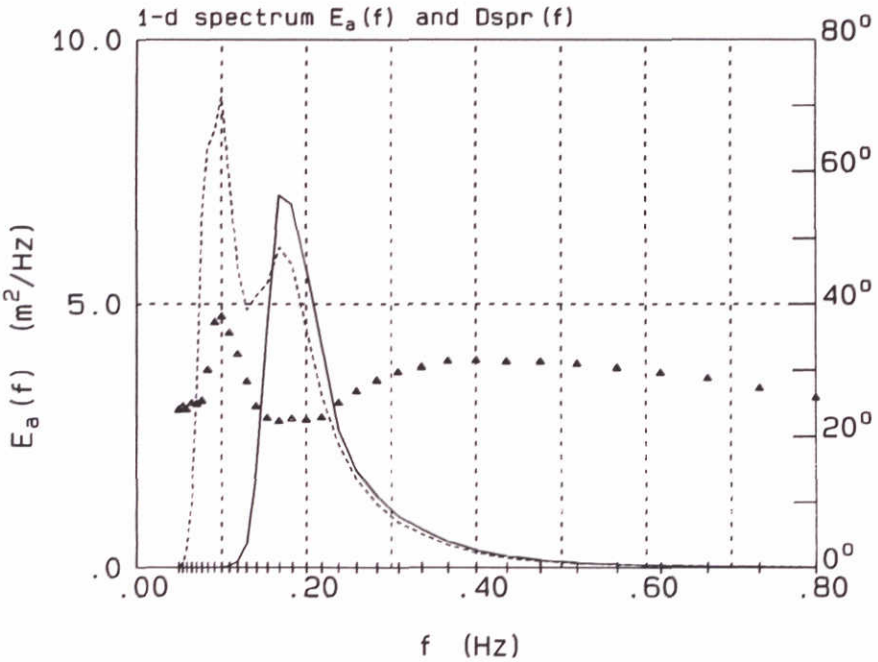

Parameters of $E_a(f)$

f_p	=	.17 (Hz)
Emax	=	7.06 (m^2/Hz)
H_s	=	3.15 (m)
T_{m02}	=	4.02 (s)
T_p	=	5.95 (s)
Dir	=	304.00 (°N)
Dspr	=	24.74 (°)
kappa	=	.59
depth	=	13.17 (m)

Wave spectra in Friesche Zeegat computed by SWAN Case b3-f: zero wave boundary Location 4 x=200240.0 , y=612150.0		b3-f
	Superstorm	
DELFT HYDRAULICS/DELFT UNIVERSITY OF TECHNOLOGY	H2368	Fig. 4.14

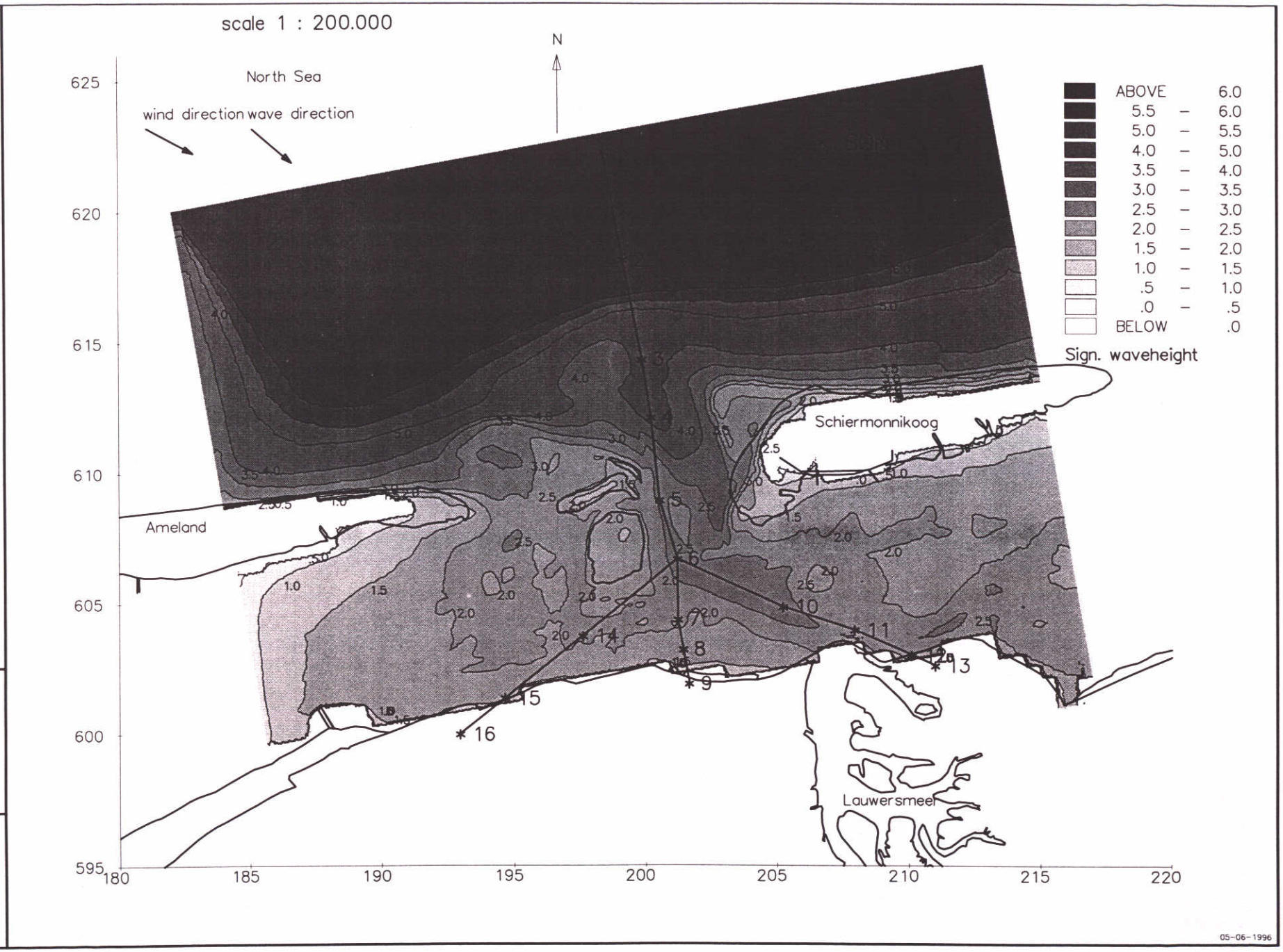

Wave model results Friesche Zeegat

SWAN wave model, course + fine grid , no current

Significant wave height (m)

case b4	SWAN
superstorm	
H2368	Fig. 4.15

DELFT HYDRAULICS + Delft University of Technology

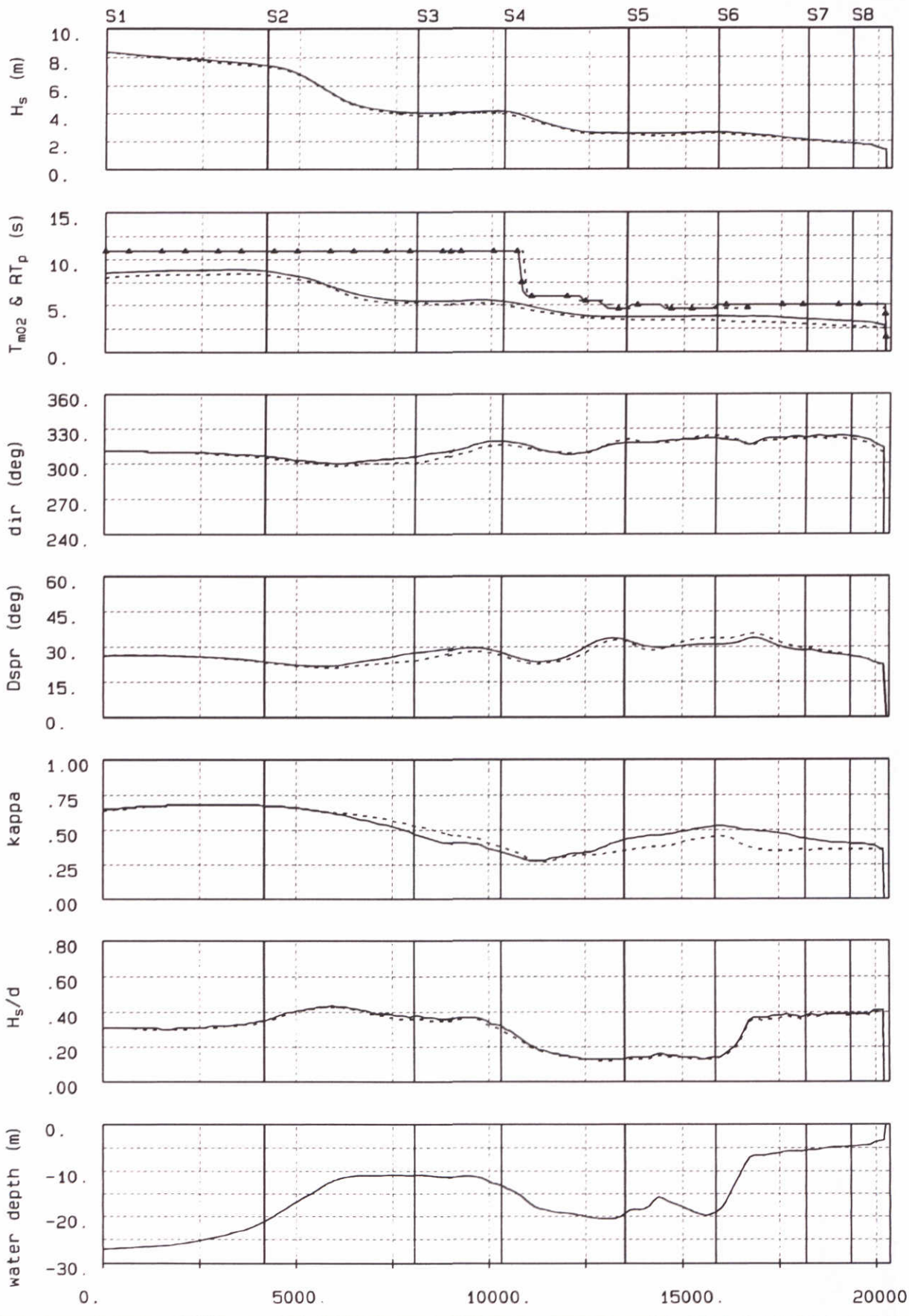

Wave parameters along rays in Friesche Zeegat SWAN wave model computation, no current Case b4 (solid line), Case b1 (dashed line)	Ray 1	Case b4
	Superstorm	
DELFT HYDRAULICS/DELFT UNIVERSITY OF TECHNOLOGY	H2368	Fig. 4.16

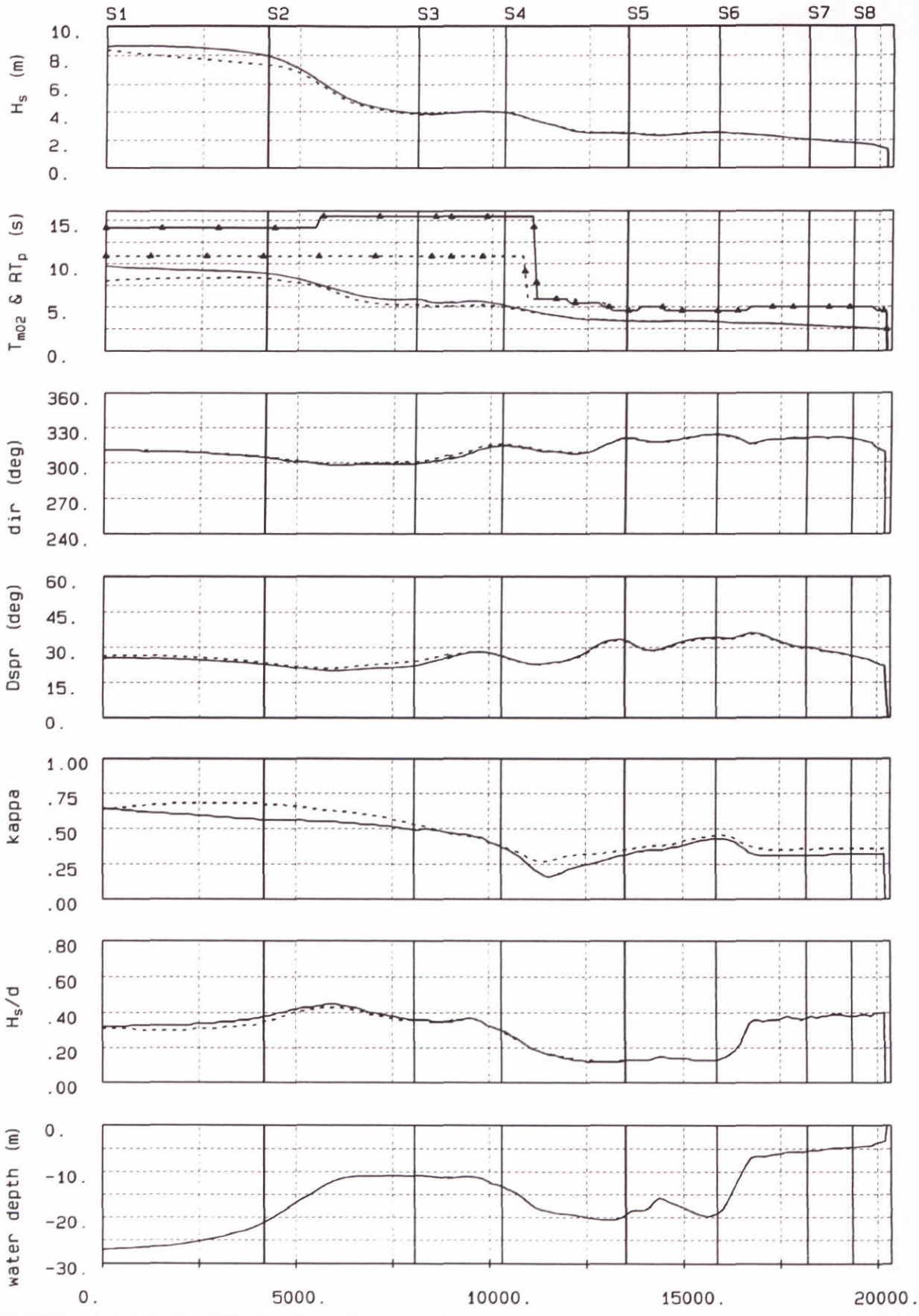

Wave parameters along rays in Friesche Zeegat SWAN wave model computation, Higher peak period Case b6 (solid line), Case b1 (dashed line)	Ray 1	Case b6
	Superstorm	
DELFT HYDRAULICS/DELFT UNIVERSITY OF TECHNOLOGY	H2368	Fig. 4.17

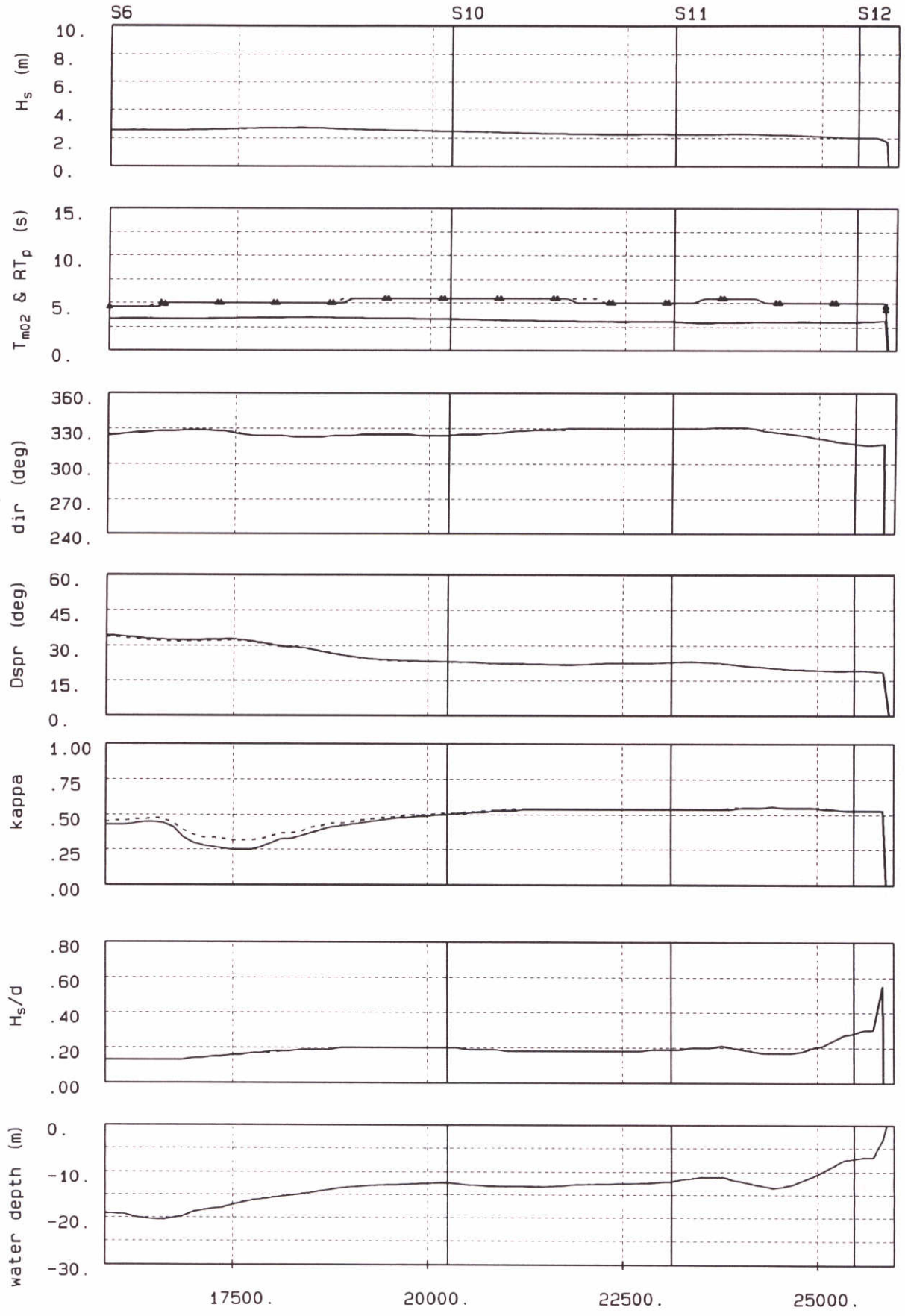

Wave parameters along rays in Friesche Zeegat SWAN wave model computation, Higher peak period Case b6 (solid line), Case b1 (dashed line)	Ray 2	Case b6
	Superstorm	
DELFT HYDRAULICS/DELFT UNIVERSITY OF TECHNOLOGY	H2368	Fig. 4.18

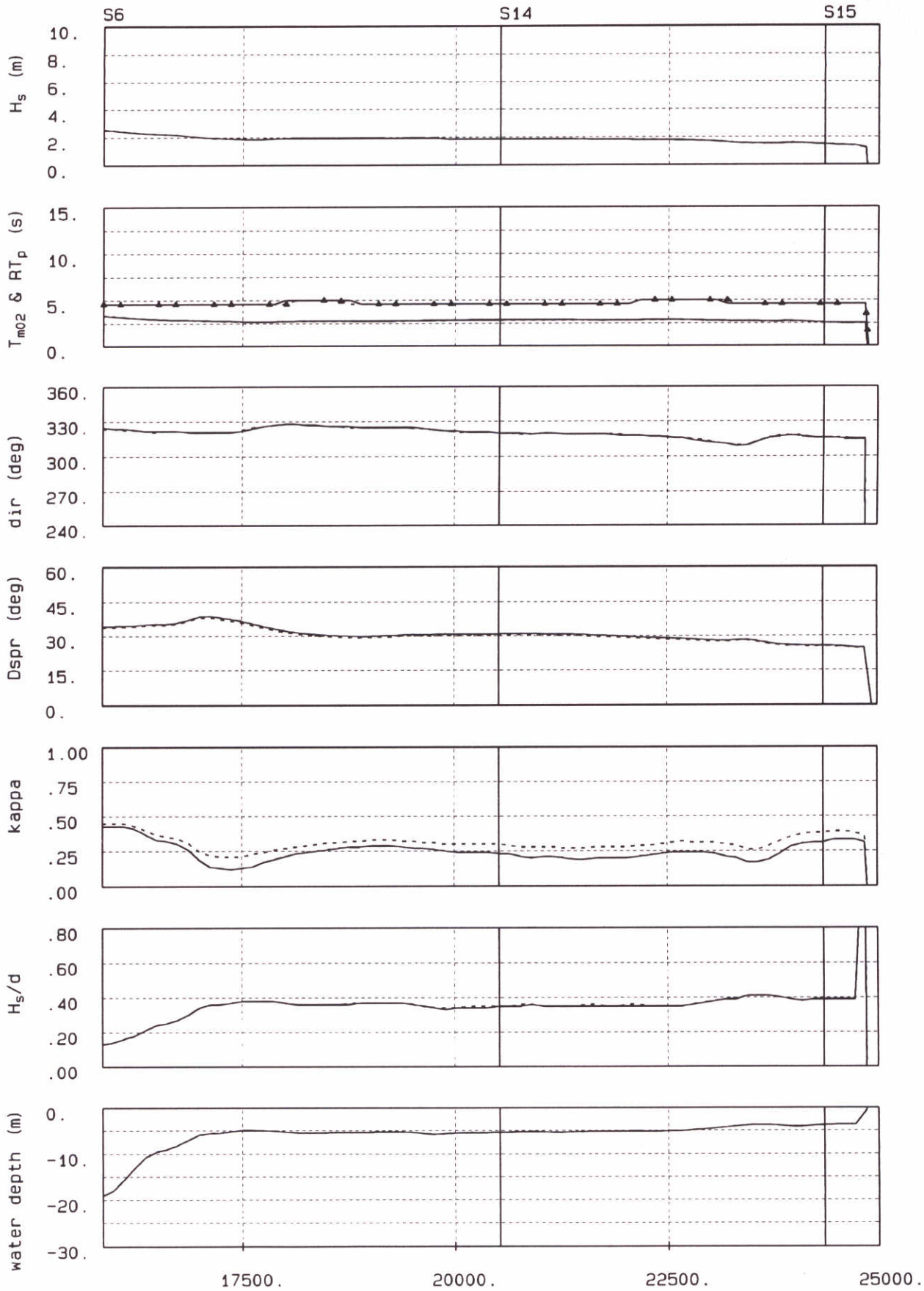

Wave parameters along rays in Friesche Zeegat SWAN wave model computation, Higher peak period Case b6 (solid line), Case b1 (dashed line)	Ray 3	Case b6
	Superstorm	
DELFT HYDRAULICS/DELFT UNIVERSITY OF TECHNOLOGY	H2368	Fig. 4.19

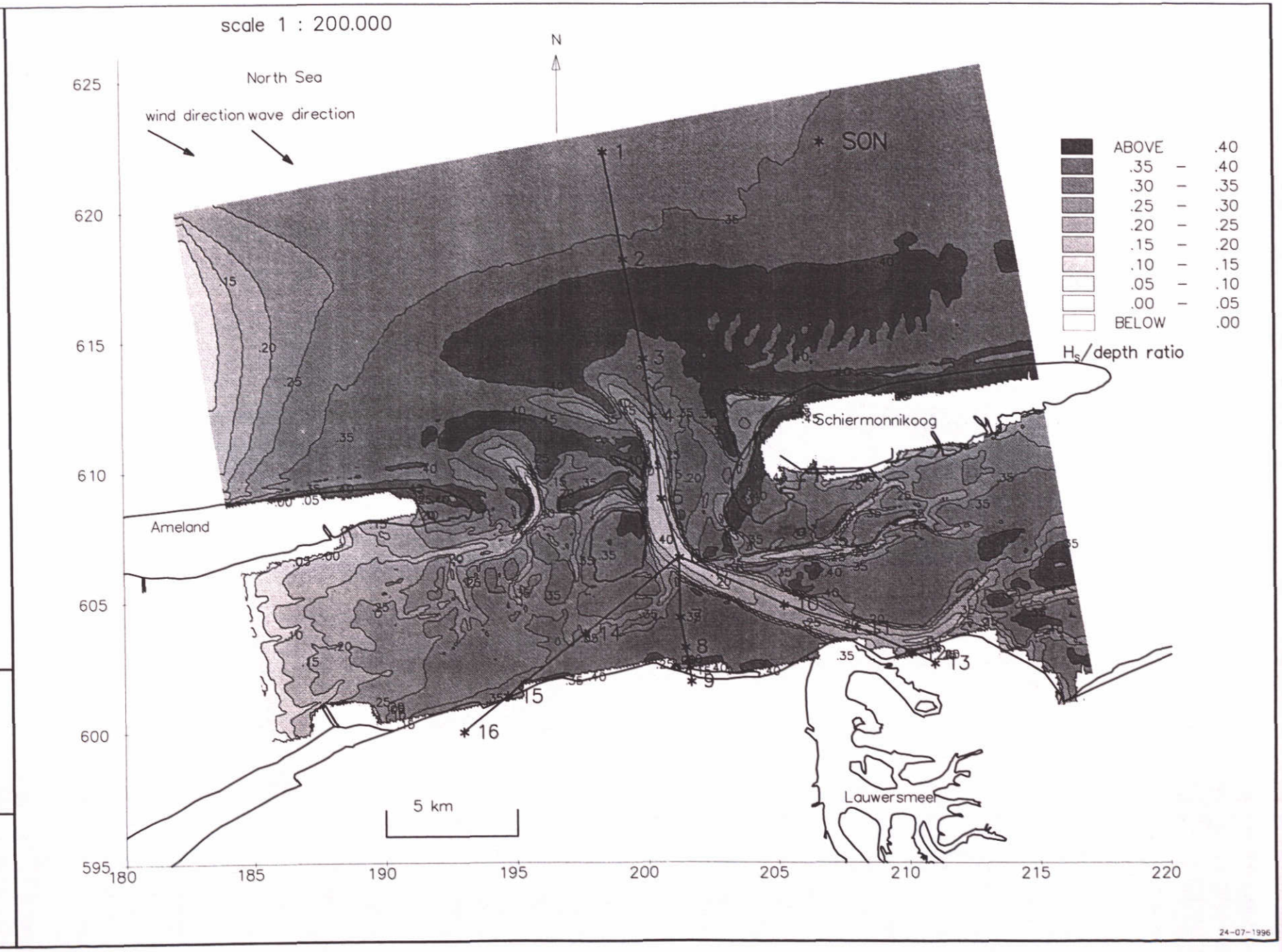

Wave model results Friesche Zeegat

SWAN wave model, course + fine grid , base case

H_s/depth ratio (–)

case b6	SWAN
superstorm	
H2368	Fig. 4.20

DELFT HYDRAULICS + Delft University of Technology

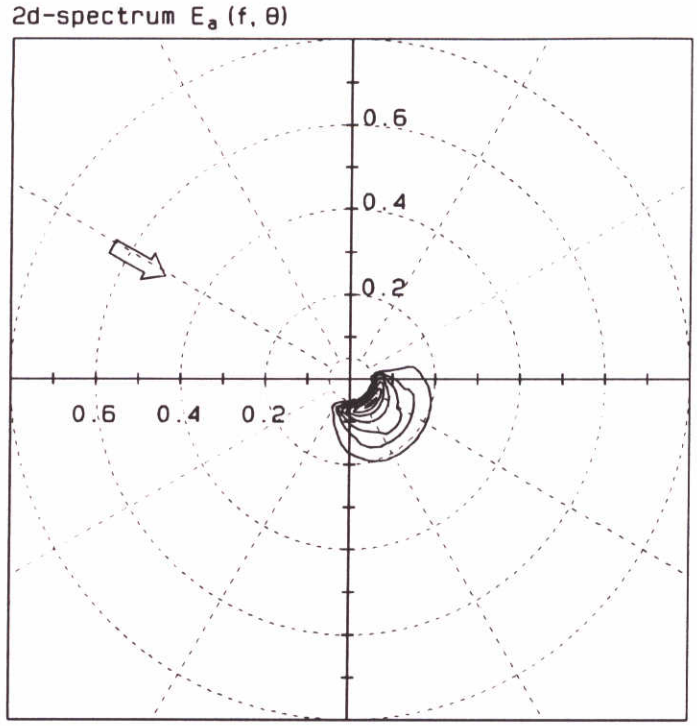

Contour levels:

0.99	$E_{a,max}$
0.90	$E_{a,max}$
0.50	$E_{a,max}$
0.25	$E_{a,max}$
0.125	$E_{a,max}$
0.0625	$E_{a,max}$
0.03125	$E_{a,max}$
0.01	$E_{a,max}$

⇨ Wind direction

Wind speed = 32.9 (m/s)

Wind direction = 299. (^{o}N)

Freq. range .05- .80 (Hz)

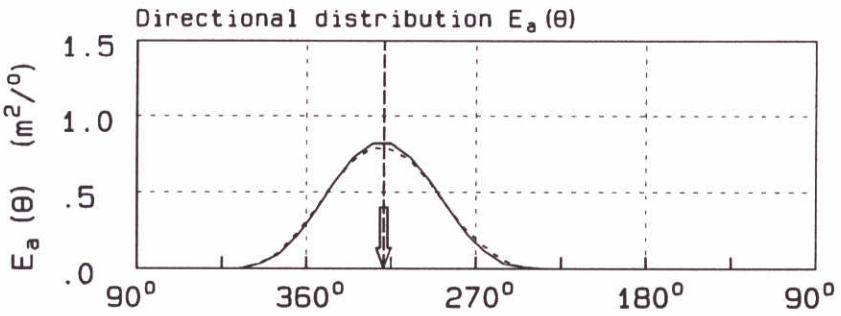

⇩ Mean wave direction

——— Case b6-c

..... Case b1-c

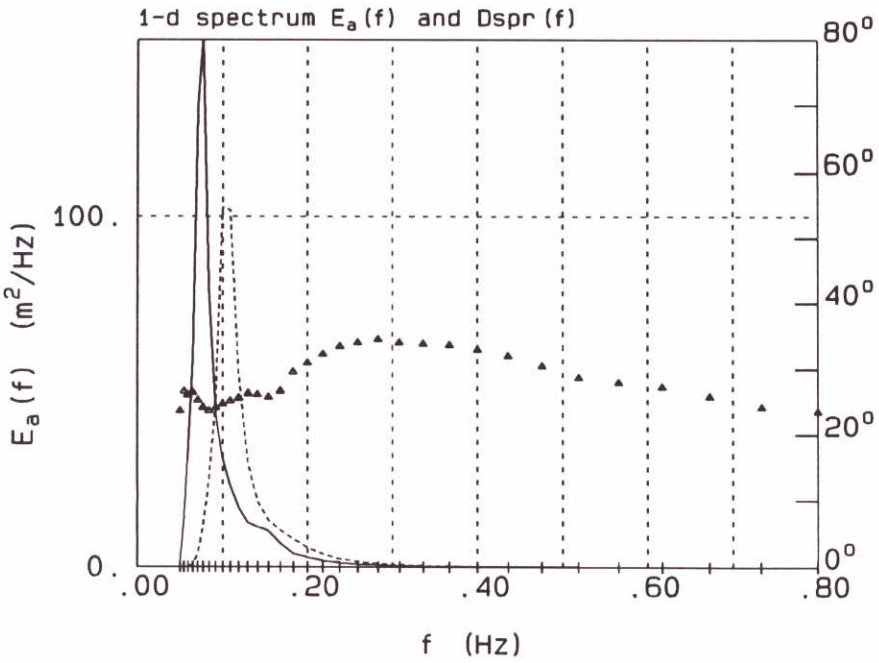

Parameters of $E_a(f)$

f_p	=	.08 (Hz)
Emax	=	151.20 (m^2/Hz)
H_s	=	8.63 (m)
T_{m02}	=	9.75 (s)
T_p	=	12.99 (s)
Dir	=	319.00 (^{o}N)
Dspr	=	25.46 (^{o})
kappa	=	.65
depth	=	27.04 (m)

Wave spectra in Friesche Zeegat computed by SWAN Case b6-c: Higher peak period Location 1 x=198447.5 , y=622306.4		b6-c
	Superstorm	
DELFT HYDRAULICS/DELFT UNIVERSITY OF TECHNOLOGY	H2368	Fig. 4.21

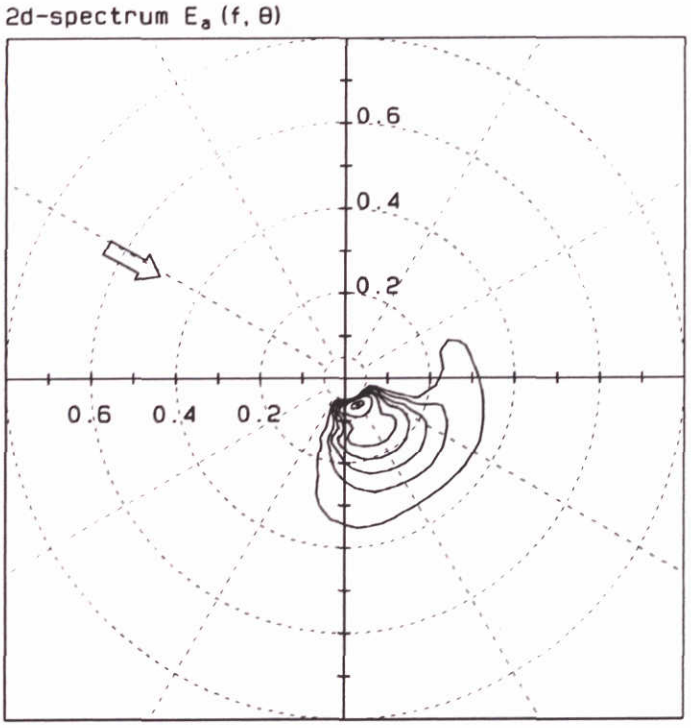

Contour levels:

0.99	$E_{a,max}$
0.90	$E_{a,max}$
0.50	$E_{a,max}$
0.25	$E_{a,max}$
0.125	$E_{a,max}$
0.0625	$E_{a,max}$
0.03125	$E_{a,max}$
0.01	$E_{a,max}$

⇨ Wind direction

Wind speed = 32.8 (m/s)

Wind direction = 299. (^oN)

Freq. range .05- .80 (Hz)

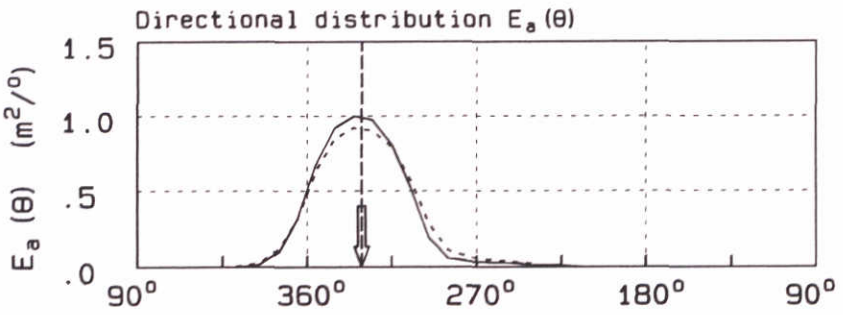

⇩ Mean wave direction

——— Case b6-c

..... Case b1-c

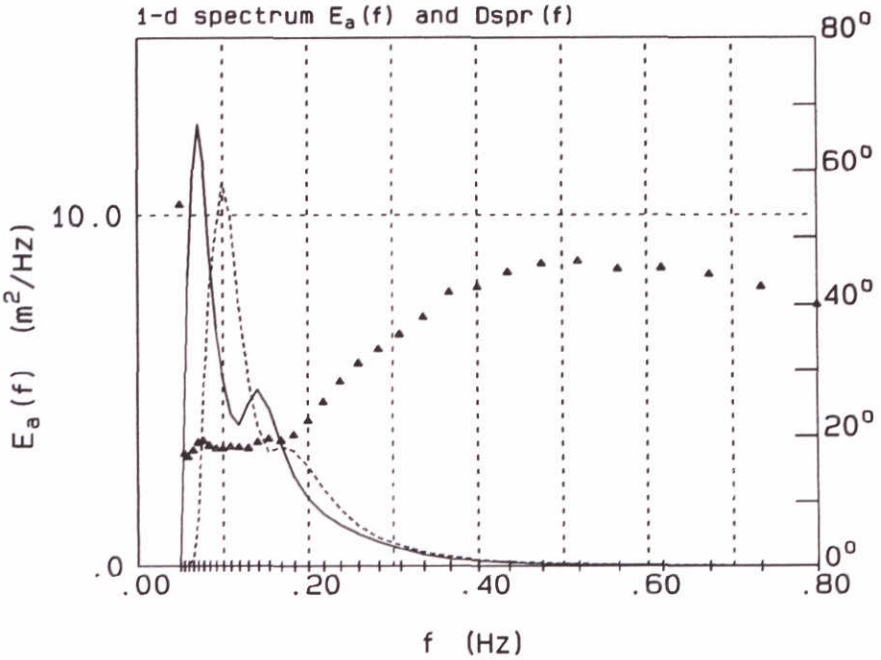

Parameters of $E_a(f)$

f_p	=	.07 (Hz)
Emax	=	12.59 (m^2/Hz)
H_s	=	3.93 (m)
T_{m02}	=	5.91 (s)
T_p	=	14.09 (s)
Dir	=	331.00 (^oN)
Dspr	=	22.25 (^{o})
kappa	=	.49
depth	=	10.84 (m)

Wave spectra in Friesche Zeegat computed by SWAN Case b6-c: Higher peak period Location 3 x=199901.6 , y=614374.6		b6-c
	Superstorm	
DELFT HYDRAULICS/DELFT UNIVERSITY OF TECHNOLOGY	H2368	Fig. 4.22

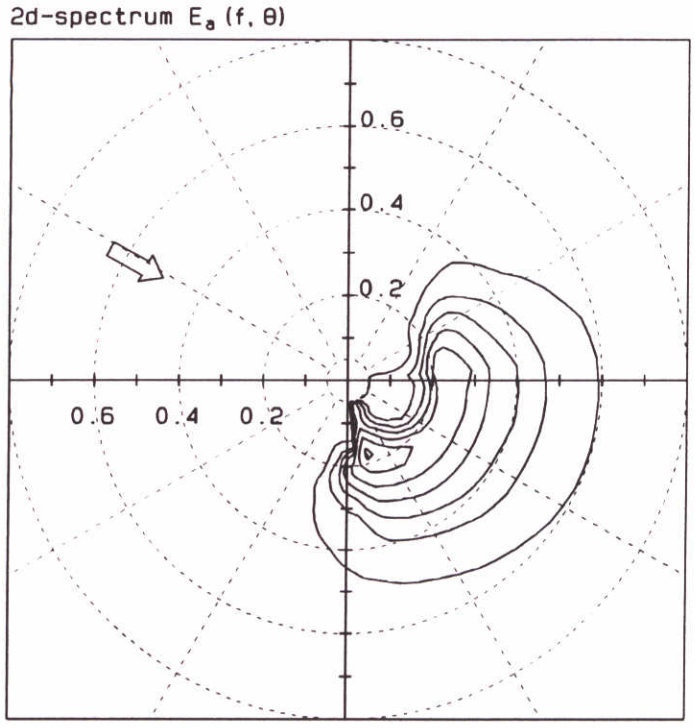

Contour levels:

0.99	$E_{a,max}$
0.90	$E_{a,max}$
0.50	$E_{a,max}$
0.25	$E_{a,max}$
0.125	$E_{a,max}$
0.0625	$E_{a,max}$
0.03125	$E_{a,max}$
0.01	$E_{a,max}$

⇨ Wind direction

Wind speed = 32.9 (m/s)

Wind direction = 299. (^{0}N)

Freq. range .05- .80 (Hz)

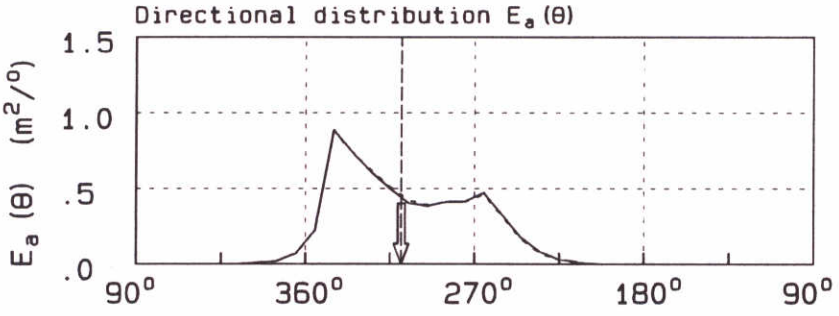

⇩ Mean wave direction

——— Case b6-f

..... Case b1-f

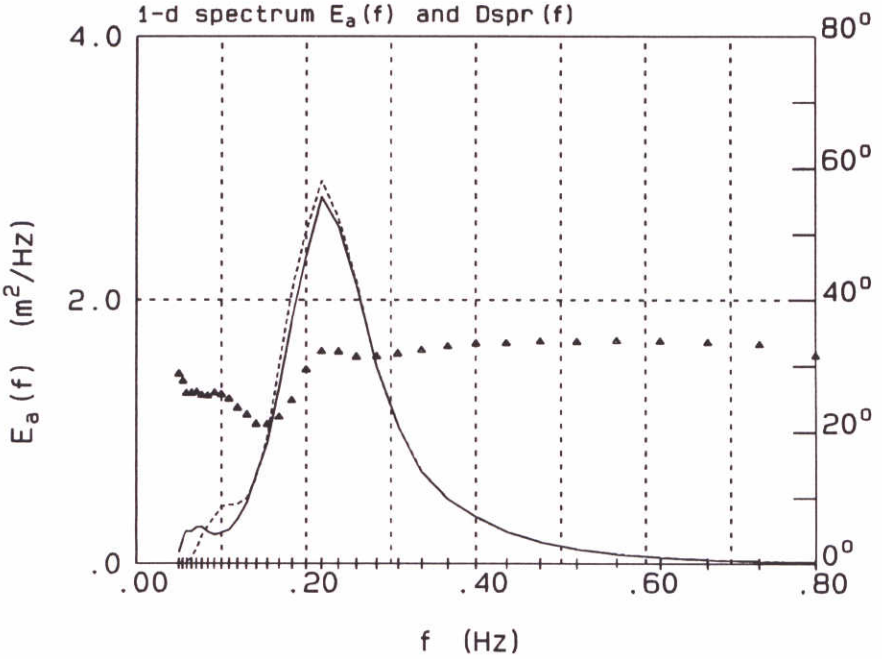

Parameters of $E_a(f)$

f_p	=	.22 (Hz)
Emax	=	2.79 (m^2/Hz)
H_s	=	2.47 (m)
T_{m02}	=	3.38 (s)
T_p	=	4.59 (s)
Dir	=	309.00 (^{0}N)
Dspr	=	32.97 (^{0})
kappa	=	.31
depth	=	19.42 (m)

Wave spectra in Friesche Zeegat computed by SWAN Case b6-f: Higher peak period Location 5 x=200567.2 , y=608977.0	b6-f Superstorm
DELFT HYDRAULICS/DELFT UNIVERSITY OF TECHNOLOGY	H2368 Fig. 4.23

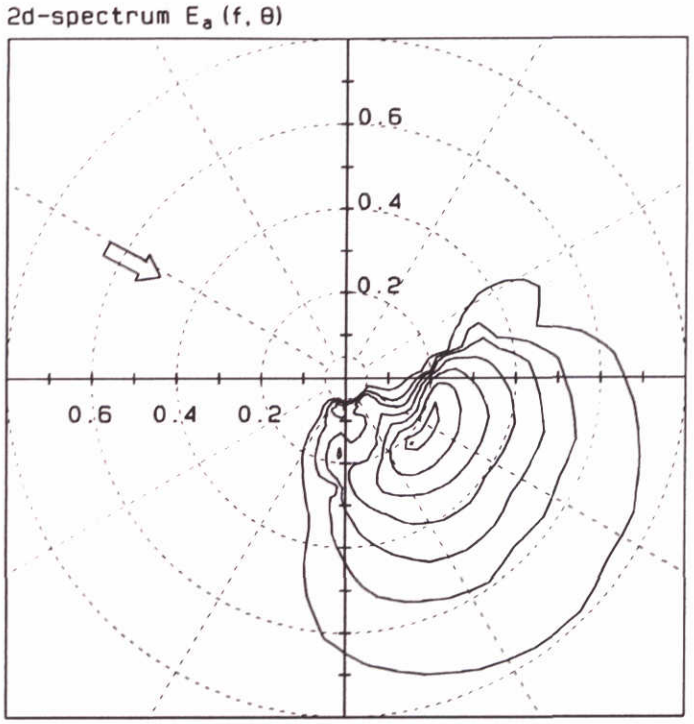

Contour levels:

0.99	$E_{a,max}$
0.90	$E_{a,max}$
0.50	$E_{a,max}$
0.25	$E_{a,max}$
0.125	$E_{a,max}$
0.0625	$E_{a,max}$
0.03125	$E_{a,max}$
0.01	$E_{a,max}$

⇨ Wind direction

Wind speed = 33.0 (m/s)

Wind direction = 298. (^{0}N)

Freq. range .05- .80 (Hz)

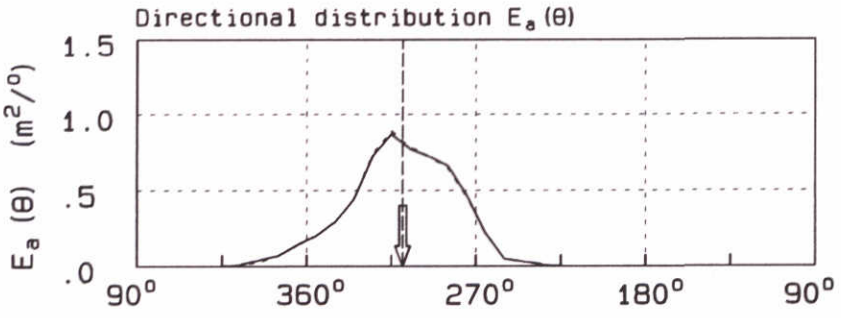

⇩ Mean wave direction

——— Case b6-f

..... Case b1-f

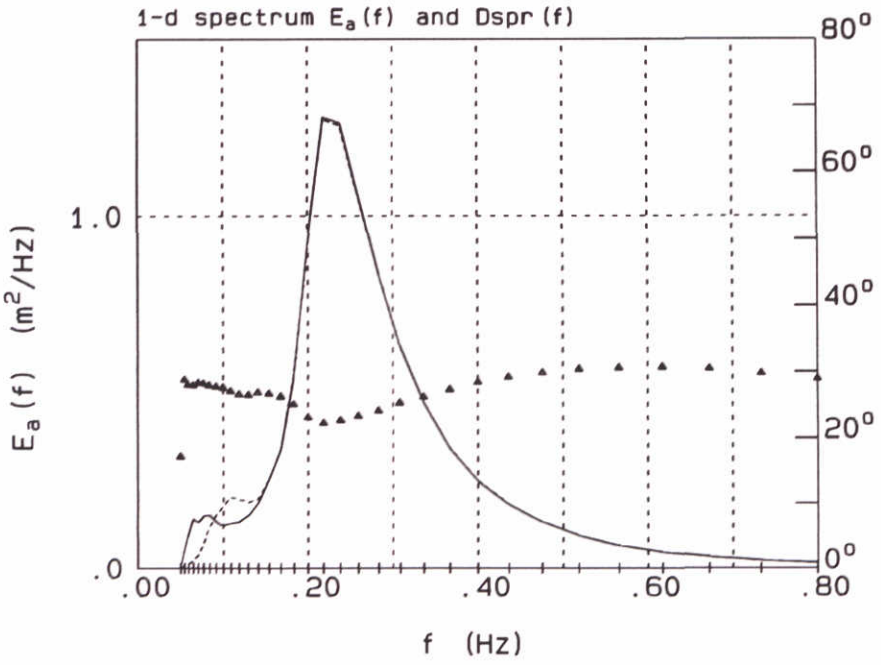

Parameters of $E_a(f)$

f_p	=	.22 (Hz)
Emax	=	1.28 (m^2/Hz)
H_s	=	1.77 (m)
T_{m02}	=	2.69 (s)
T_p	=	4.59 (s)
Dir	=	309.00 (^{0}N)
Dspr	=	26.45 (^{0})
kappa	=	.32
depth	=	4.63 (m)

Wave spectra in Friesche Zeegat computed by SWAN Case b6-f: Higher peak period Location 8 x=201457.1 , y=603243.0		b6-f
	Superstorm	
DELFT HYDRAULICS/DELFT UNIVERSITY OF TECHNOLOGY	H2368	Fig. 4.24

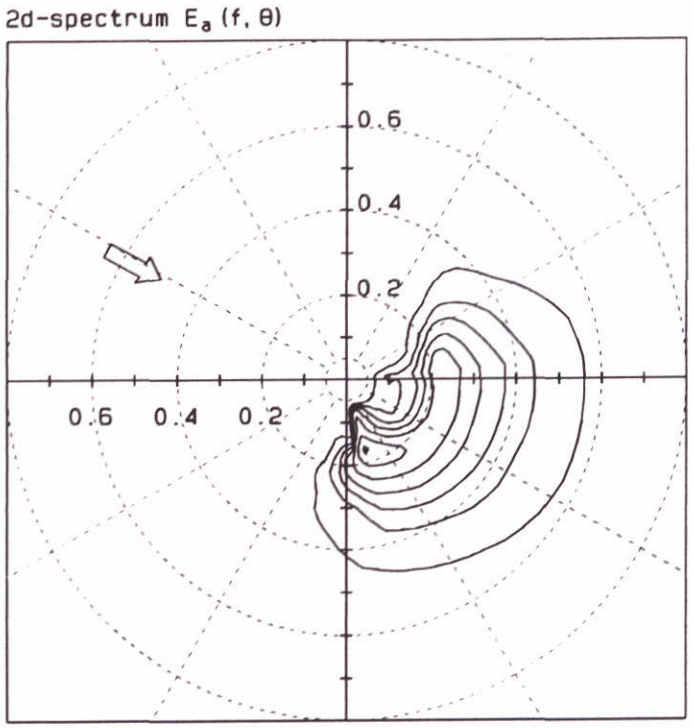

Contour levels:

0.99	$E_{a,max}$
0.90	$E_{a,max}$
0.50	$E_{a,max}$
0.25	$E_{a,max}$
0.125	$E_{a,max}$
0.0625	$E_{a,max}$
0.03125	$E_{a,max}$
0.01	$E_{a,max}$

⇨ Wind direction

Wind speed = 32.9 (m/s)

Wind direction = 299. (^oN)

Freq. range .05- .80 (Hz)

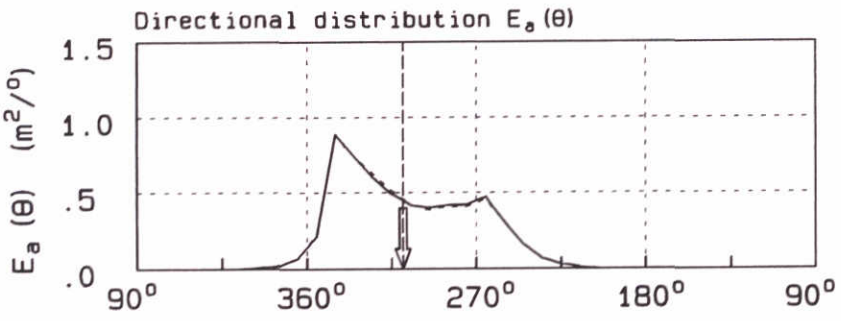

⇩ Mean wave direction

——— Case c3-f

..... Case b1-f

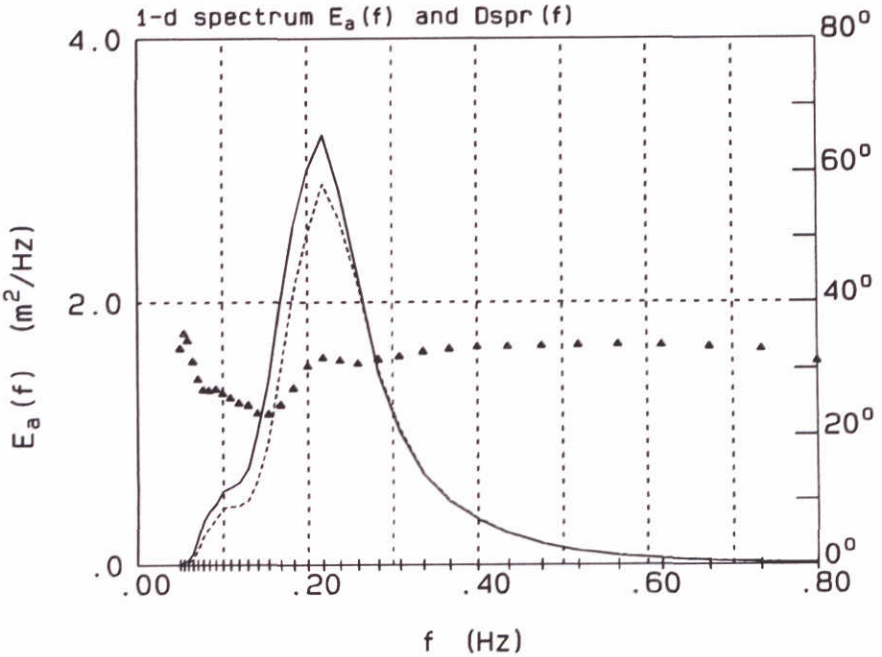

Parameters of $E_a(f)$

f_p	=	.22 (Hz)
Emax	=	3.28 (m^2/Hz)
H_s	=	2.67 (m)
T_{m02}	=	3.56 (s)
T_p	=	4.59 (s)
Dir	=	309.00 (^oN)
Dspr	=	32.60 (^{o})
kappa	=	.33
depth	=	19.42 (m)

Wave spectra in Friesche Zeegat computed by SWAN Case c3-f: higher $gamma_d$ Location 5 x=200567.2 , y=608977.0		c3-f
	Superstorm	
DELFT HYDRAULICS/DELFT UNIVERSITY OF TECHNOLOGY	H2368	Fig. 4.25

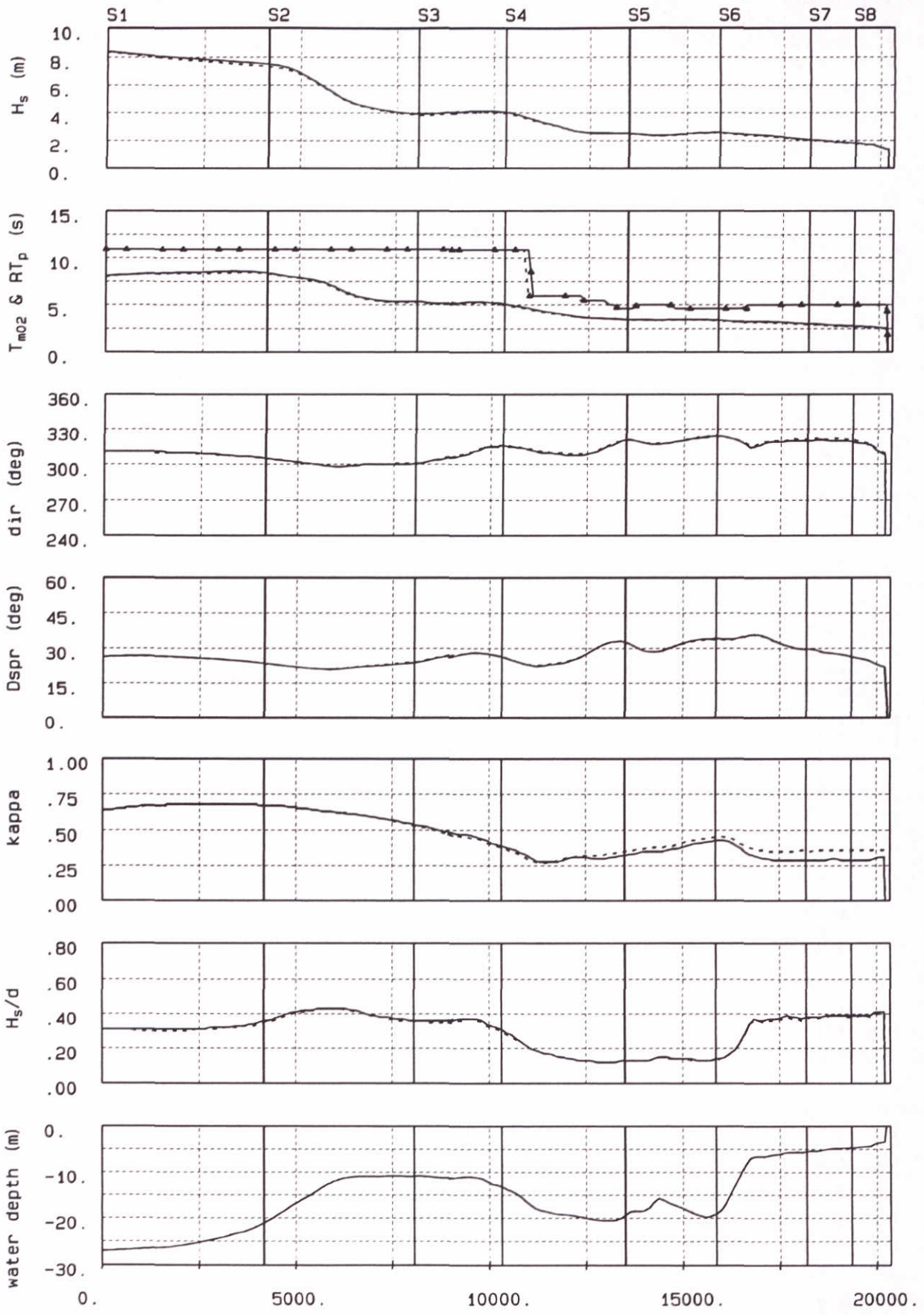

Wave parameters along rays in Friesche Zeegat
SWAN wave model computation, no bottom friction
Case c4 (solid line), Case b1 (dashed line)

Ray 1	Case c4
Superstorm	

DELFT HYDRAULICS/DELFT UNIVERSITY OF TECHNOLOGY	H2368	Fig. 4.26

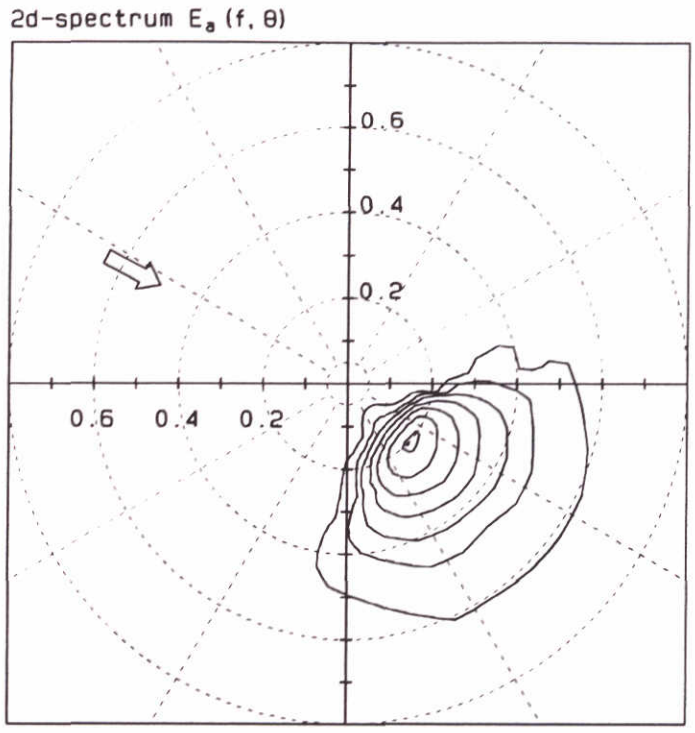

Contour levels:

0.99	$E_{a,max}$
0.90	$E_{a,max}$
0.50	$E_{a,max}$
0.25	$E_{a,max}$
0.125	$E_{a,max}$
0.0625	$E_{a,max}$
0.03125	$E_{a,max}$
0.01	$E_{a,max}$

⇨ Wind direction

Wind speed = 32.3 (m/s)

Wind direction = 297. (^{0}N)

Freq. range .05- .80 (Hz)

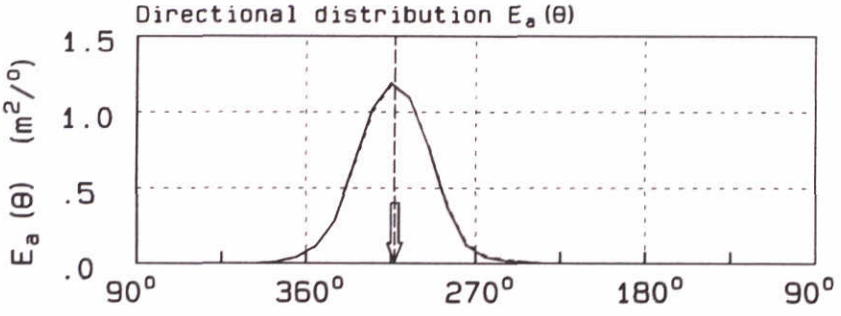

⇩ Mean wave direction

——— Case c4-f

..... Case b1-f

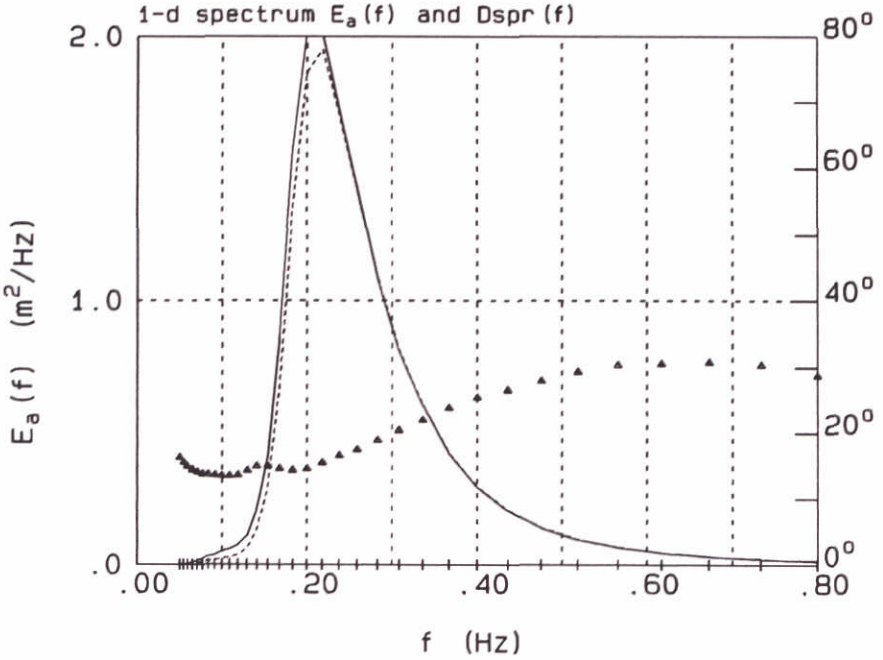

Parameters of $E_a(f)$

f_p	=	.20 (Hz)
Emax	=	2.02 (m^2/Hz)
H_s	=	2.08 (m)
T_{m02}	=	3.11 (s)
T_p	=	5.00 (s)
Dir	=	313.00 (^{0}N)
Dspr	=	19.12 (^{0})
kappa	=	.51
depth	=	7.17 (m)

Wave spectra in Friesche Zeegat computed by SWAN Case c4-f: no bottom friction Location 12 x=210108.0 , y=603044.0		c4-f
	Superstorm	
DELFT HYDRAULICS/DELFT UNIVERSITY OF TECHNOLOGY	H2368	Fig. 4.27

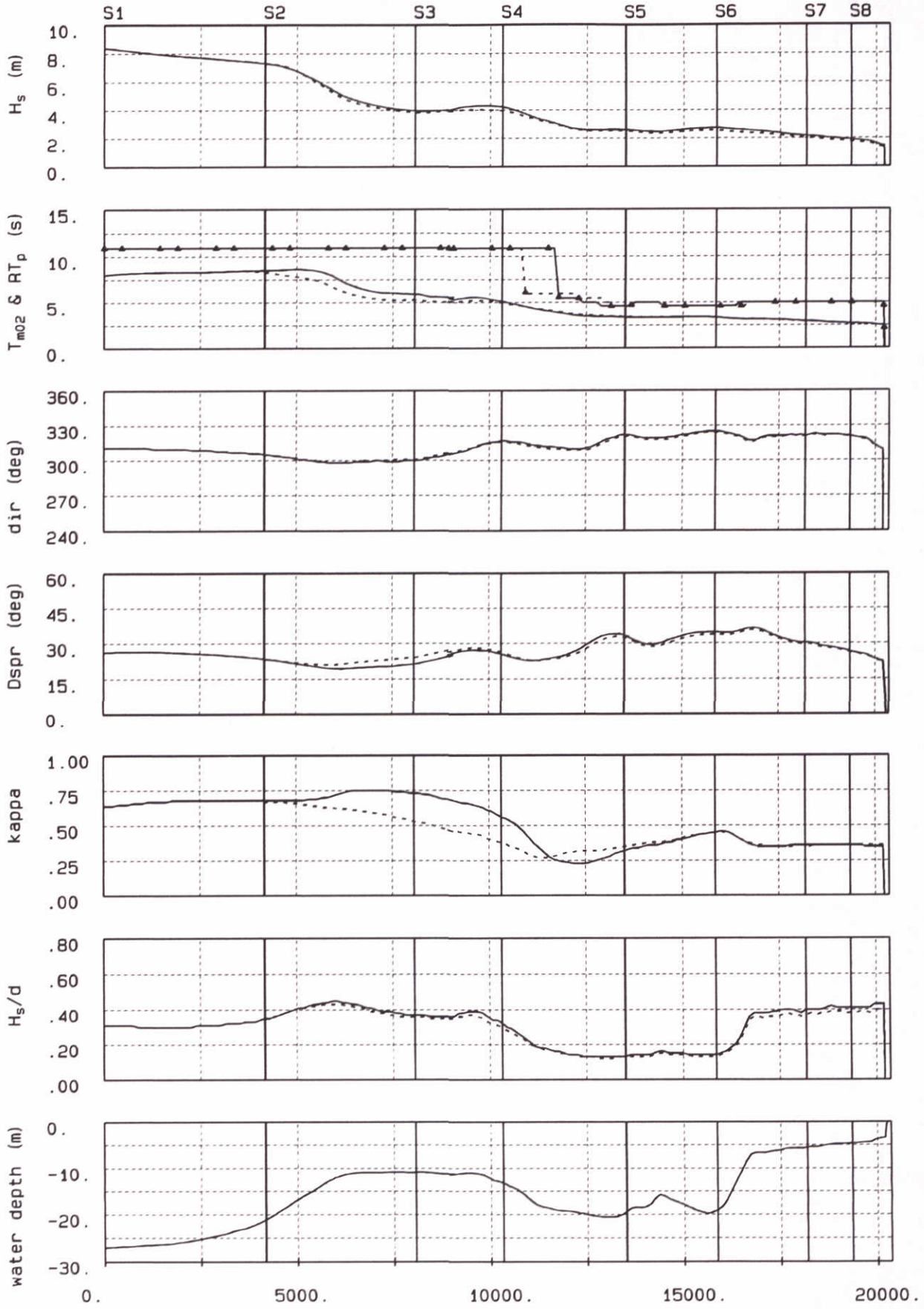

Wave parameters along rays in Friesche Zeegat SWAN wave model computation, no triads Case c5 (solid line), Case b1 (dashed line)	Ray 1	Case c5
	Superstorm	
DELFT HYDRAULICS/DELFT UNIVERSITY OF TECHNOLOGY	H2368	Fig. 4.28

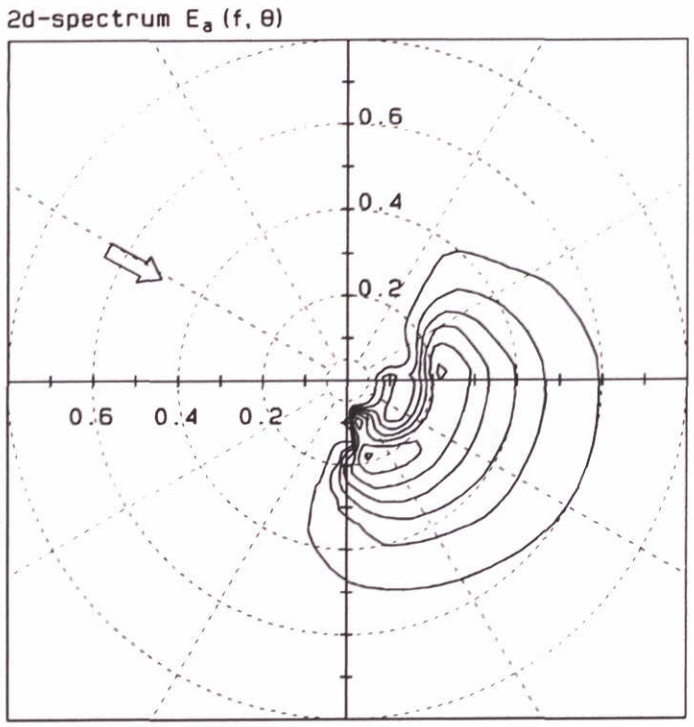

Contour levels:

0.99	$E_{a,max}$
0.90	$E_{a,max}$
0.50	$E_{a,max}$
0.25	$E_{a,max}$
0.125	$E_{a,max}$
0.0625	$E_{a,max}$
0.03125	$E_{a,max}$
0.01	$E_{a,max}$

⇨ Wind direction

Wind speed = 32.9 (m/s)

Wind direction = 299. (°N)

Freq. range .05- .80 (Hz)

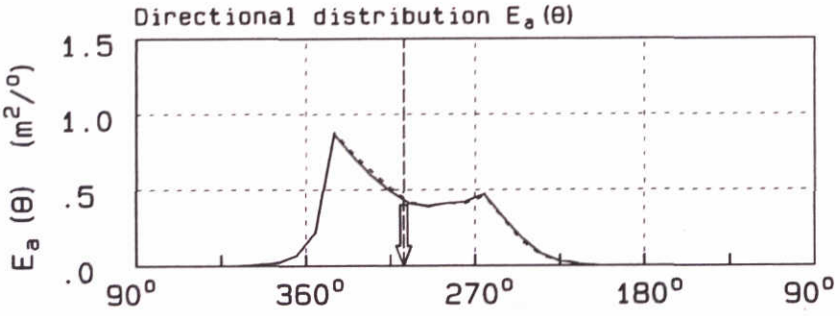

⇩ Mean wave direction

——— Case c5-f

..... Case b1-f

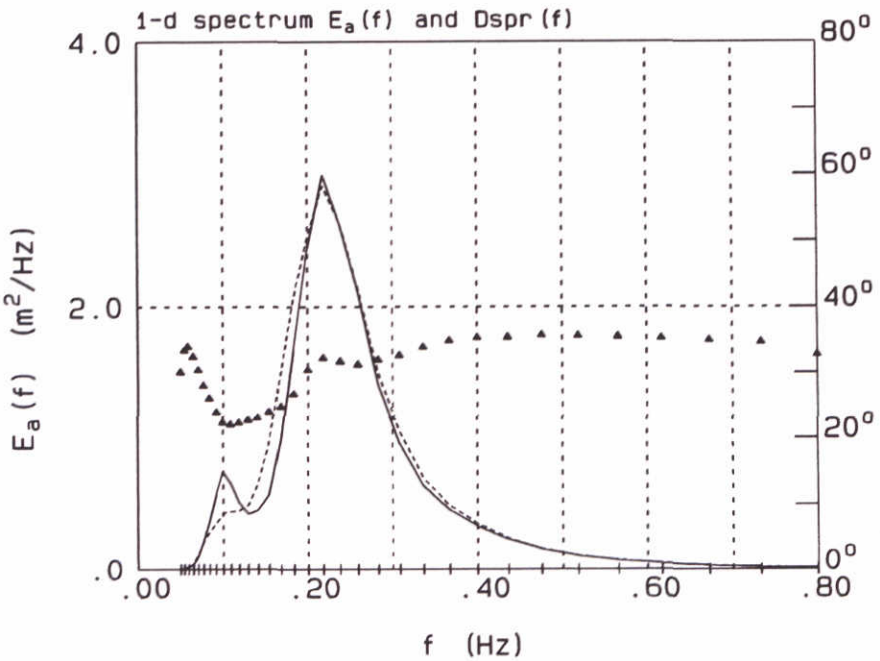

Parameters of $E_a(f)$

f_p	=	.22 (Hz)
Emax	=	2.99 (m^2/Hz)
H_s	=	2.61 (m)
T_{m02}	=	3.36 (s)
T_p	=	4.59 (s)
Dir	=	308.00 (°N)
Dspr	=	33.45 (°)
kappa	=	.32
depth	=	19.42 (m)

Wave spectra in Friesche Zeegat computed by SWAN Case c5-f: no triads Location 5 x=200567.2 , y=608977.0		c5-f
	Superstorm	
DELFT HYDRAULICS/DELFT UNIVERSITY OF TECHNOLOGY	H2368	Fig. 4.29

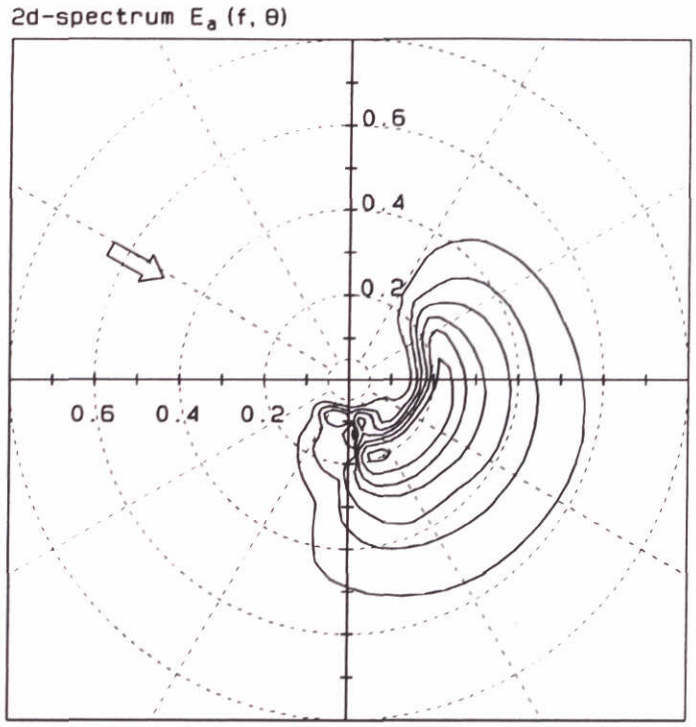

Contour levels:

0.99	$E_{a,max}$
0.90	$E_{a,max}$
0.50	$E_{a,max}$
0.25	$E_{a,max}$
0.125	$E_{a,max}$
0.0625	$E_{a,max}$
0.03125	$E_{a,max}$
0.01	$E_{a,max}$

⇨ Wind direction

Wind speed = 32.9 (m/s)

Wind direction = 299. (^oN)

Freq. range .05- .80 (Hz)

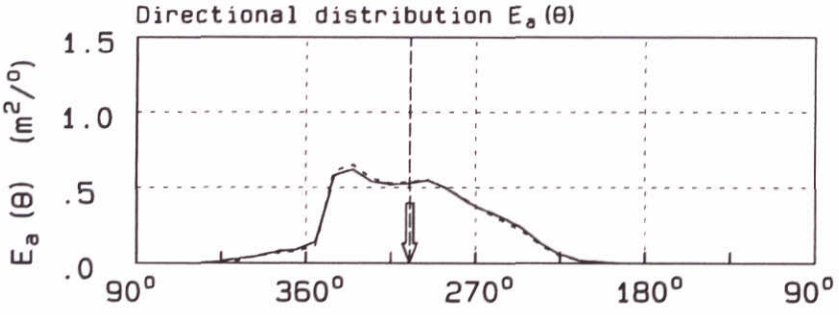

⇩ Mean wave direction

——— Case c5-f

..... Case b1-f

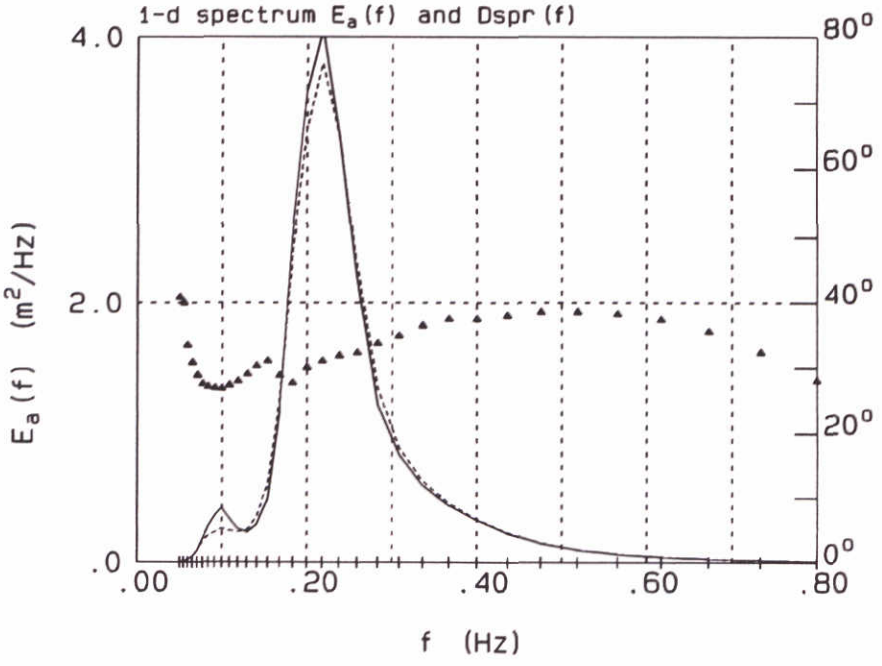

Parameters of $E_a(f)$

f_p	=	.22 (Hz)
Emax	=	4.06 (m^2/Hz)
H_s	=	2.73 (m)
T_{m02}	=	3.35 (s)
T_p	=	4.59 (s)
Dir	=	305.00 (^oN)
Dspr	=	34.70 (^{o})
kappa	=	.45
depth	=	19.07 (m)

Wave spectra in Friesche Zeegat computed by SWAN Case c5-f: no triads Location 6 x=201245.3 , y=606717.0		c5-f
	Superstorm	
DELFT HYDRAULICS/DELFT UNIVERSITY OF TECHNOLOGY	H2368	Fig. 4.30

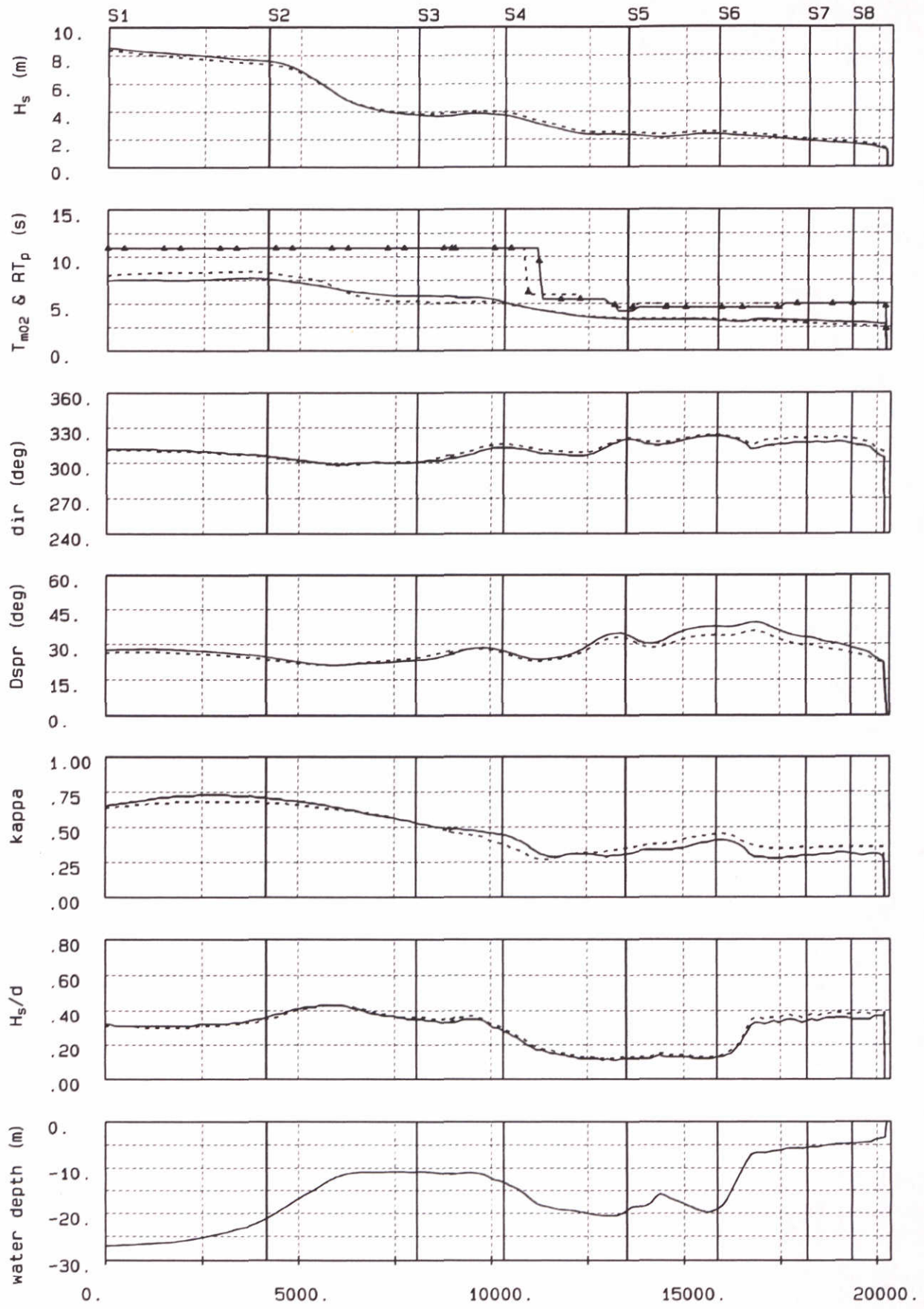

Wave parameters along rays in Friesche Zeegat SWAN wave model computation, WAM 3 settings Case c9 (solid line), Case b1 (dashed line)	Ray 1	Case c9
	Superstorm	
DELFT HYDRAULICS/DELFT UNIVERSITY OF TECHNOLOGY	H2368	Fig. 4.31

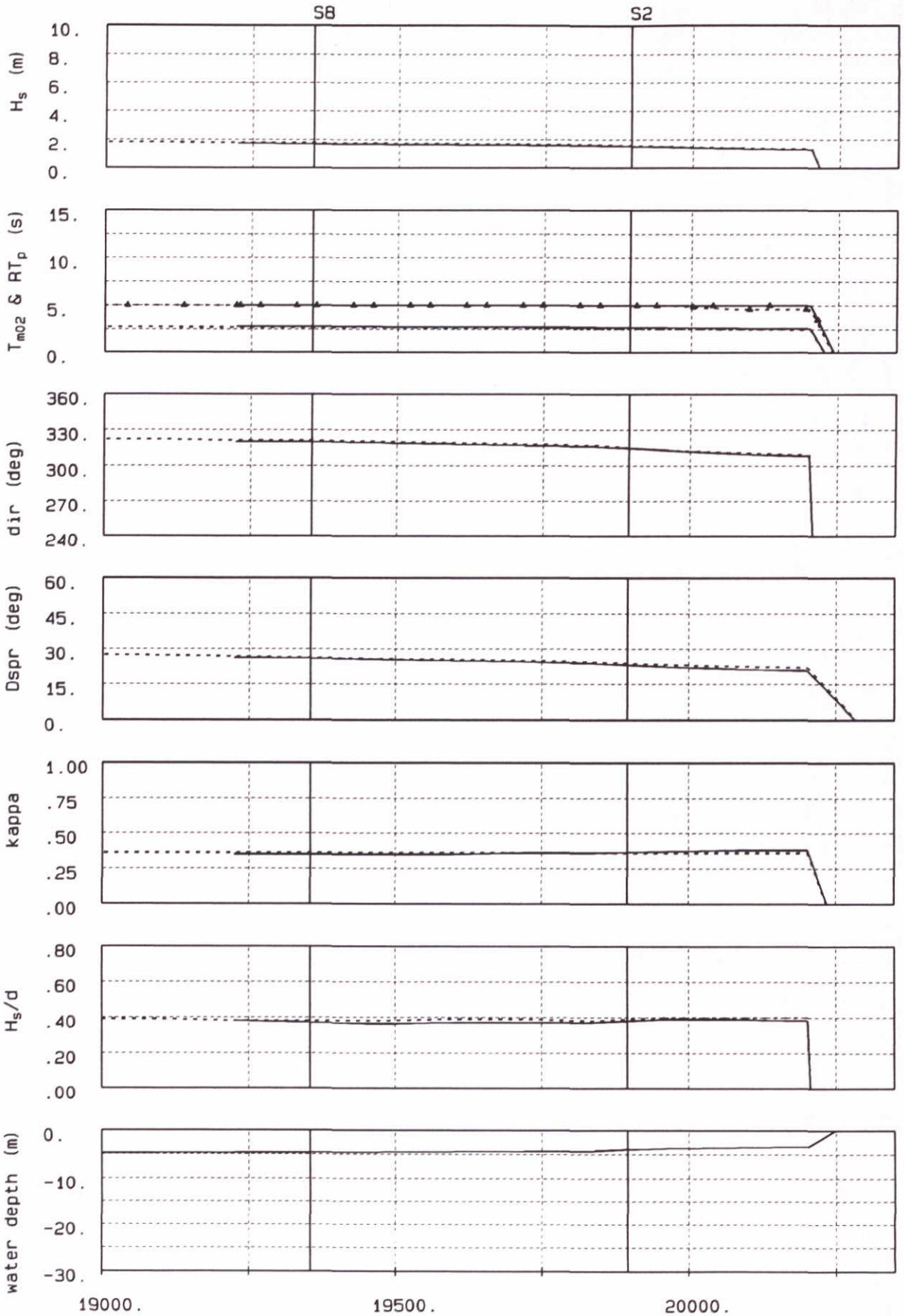

Wave parameters along rays in Friesche Zeegat SWAN wave model computation, extra fine grid Extra fine grid (solid line), fine grid (dashed line)	Ray 1	Case c11
	Superstorm	
DELFT HYDRAULICS/DELFT UNIVERSITY OF TECHNOLOGY	H2368	Fig. 4.32

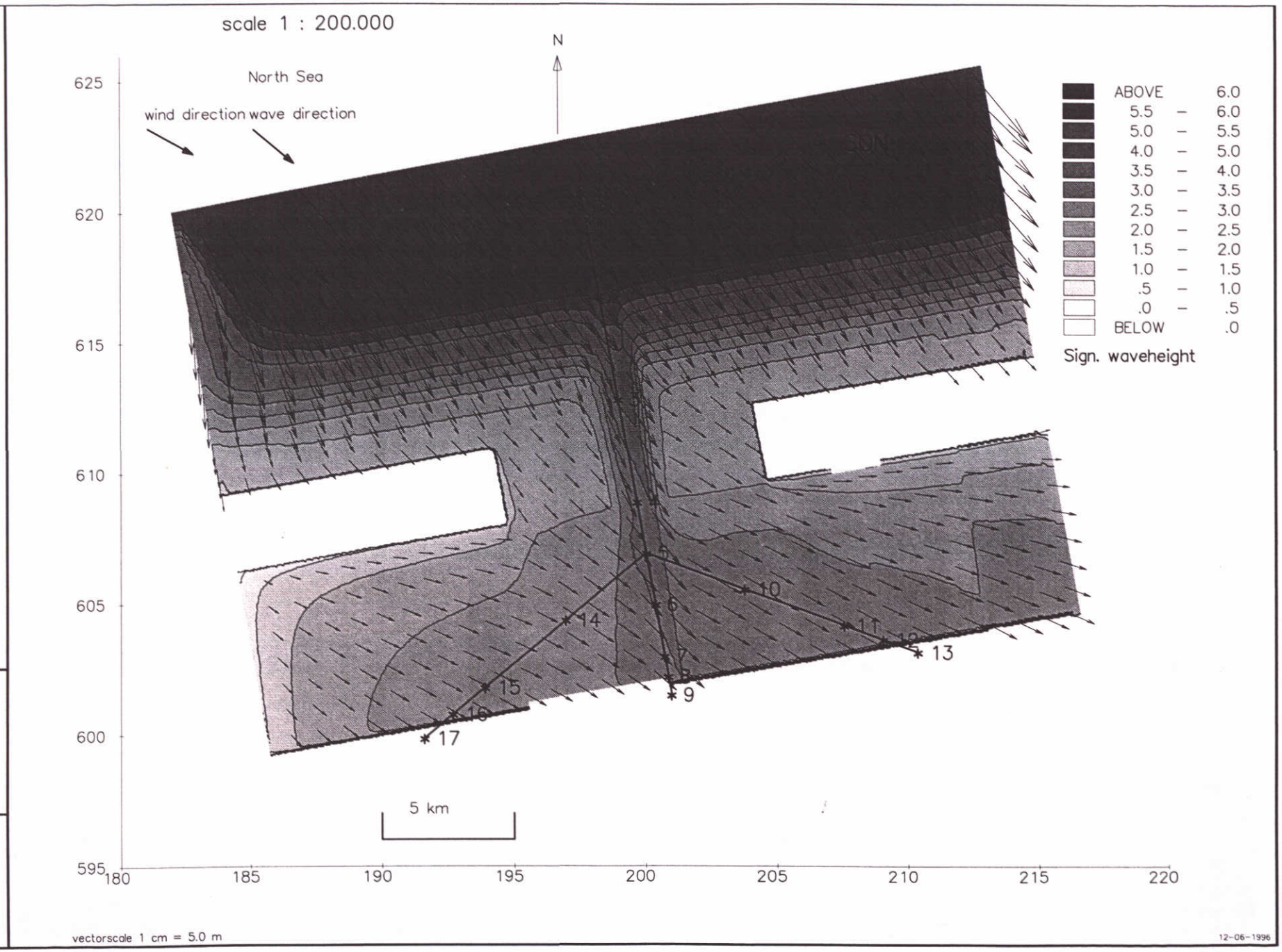

Wave model results Friesche Zeegat

SWAN wave model, course + fine grid , artificial topography

Significant wave height (m) and mean wave direction

case c13	SWAN
superstorm	
H2368	Fig. 4.33

DELFT HYDRAULICS + Delft University of Technology

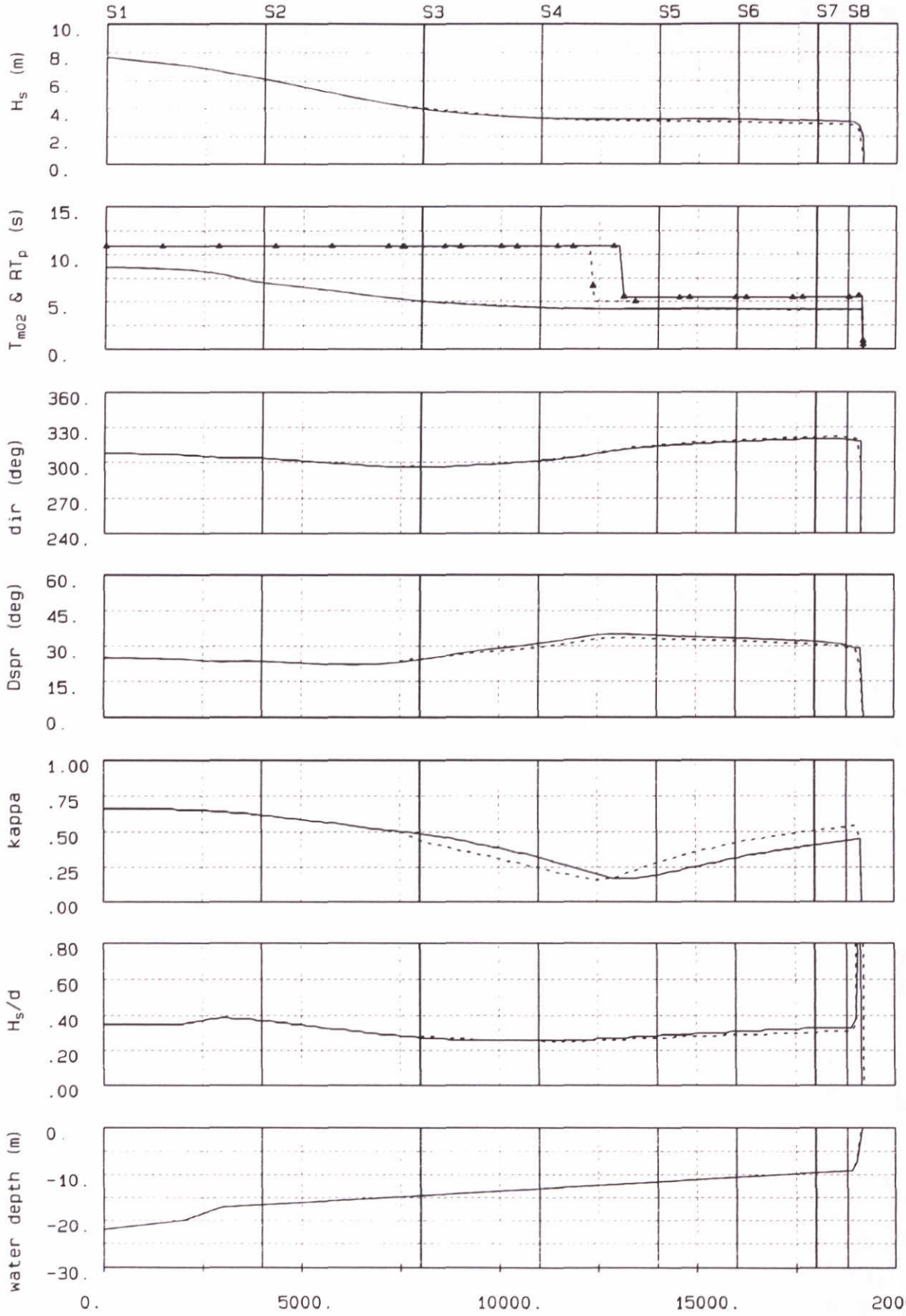

Wave parameters along rays in Friesche Zeegat SWAN wave model computation, Artifical bottom Coarse grid (solid line), fine grid (dashed line)	Ray 1	Case c13
	Superstorm	
DELFT HYDRAULICS/DELFT UNIVERSITY OF TECHNOLOGY	H2368	Fig. 4.34

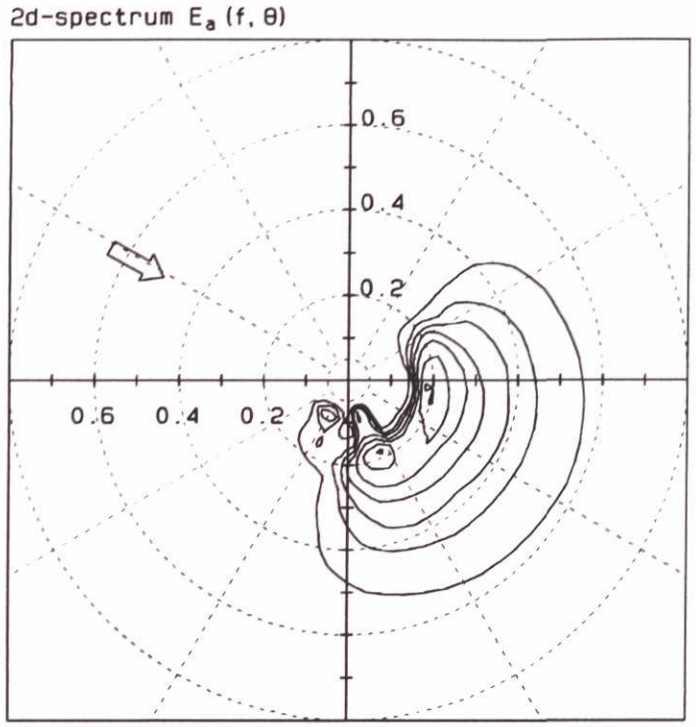

Contour levels:

0.99	$E_{a,max}$
0.90	$E_{a,max}$
0.50	$E_{a,max}$
0.25	$E_{a,max}$
0.125	$E_{a,max}$
0.0625	$E_{a,max}$
0.03125	$E_{a,max}$
0.01	$E_{a,max}$

⇨ Wind direction

Wind speed = 33.3 (m/s)

Wind direction = 299. (°N)

Freq. range .05- .80 (Hz)

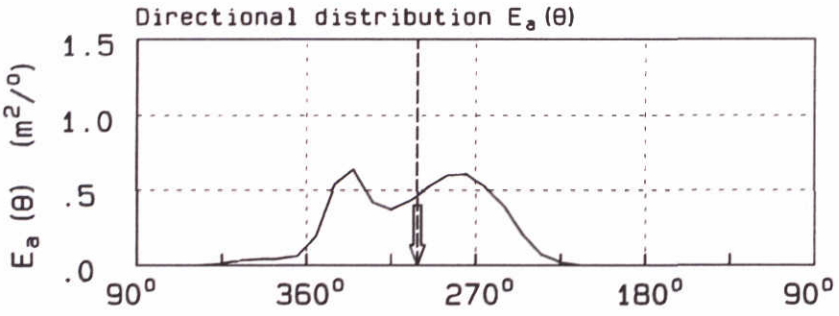

⇩ Mean wave direction

——— Case c13-f

..... Case c13-f

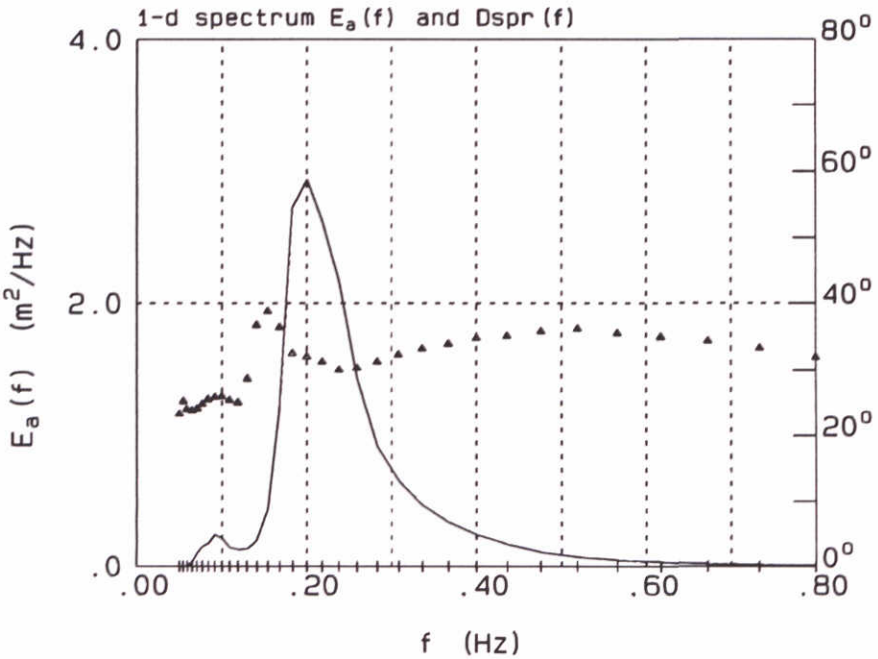

Parameters of $E_a(f)$

f_p	=	.20 (Hz)
Emax	=	2.94 (m^2/Hz)
H_s	=	2.38 (m)
T_{m02}	=	3.57 (s)
T_p	=	5.00 (s)
Dir	=	301.00 (°N)
Dspr	=	33.90 (°)
kappa	=	.48
depth	=	7.00 (m)

Wave spectra in Friesche Zeegat computed by SWAN Case c13-f: artificial topograph Location 14 x=196978.7 , y=604363.5		c13-f
	Superstorm	
DELFT HYDRAULICS/DELFT UNIVERSITY OF TECHNOLOGY	H2368	Fig. 4.35

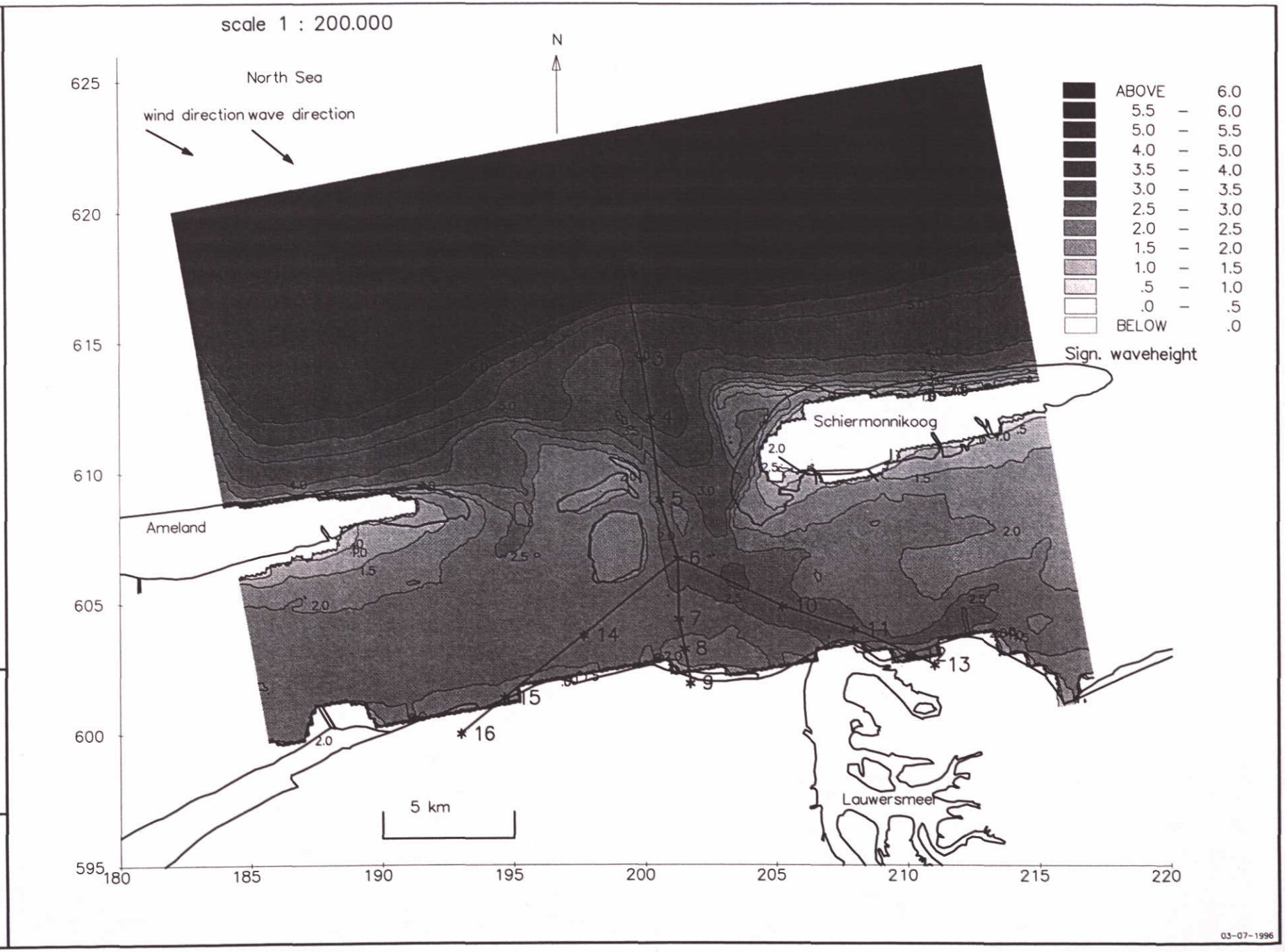

Phidias Wave model results Friesche Zeegat

Contour lines of significant wave height (m)

Time T07: 530131 2200

case T07	SWAN
superstorm	
H2368	Fig. 4.36

DELFT HYDRAULICS + Delft University of Technology

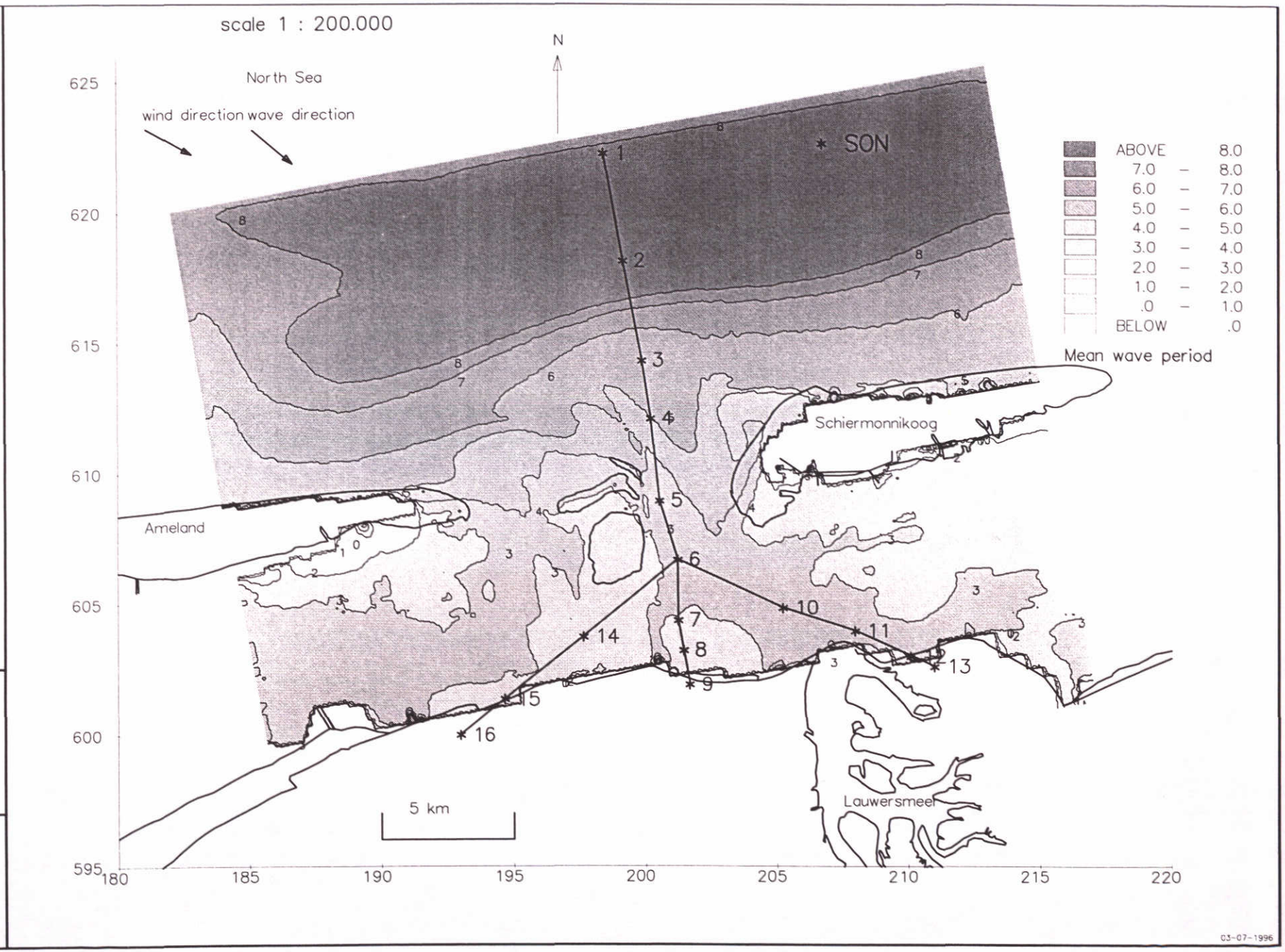

Phidias Wave model results Friesche Zeegat

Contour lines of mean wave period (s)

Time T07: 530131 2200

case T07	SWAN
superstorm	
H2368	Fig. 4.37

DELFT HYDRAULICS + Delft University of Technology

Phidias Wave model results Friesche Zeegat Contour lines of (absolute) peak period (s) Time T07: 530131 2200	case T07	SWAN
	superstorm	
DELFT HYDRAULICS + Delft University of Technology	H2368	Fig. 4.38

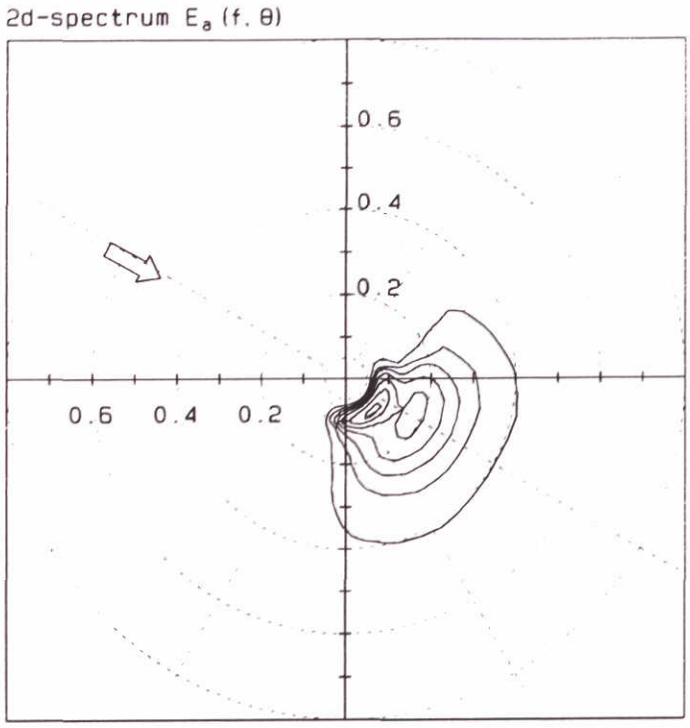

Contour levels:

0.99	$E_{a,max}$
0.90	$E_{a,max}$
0.50	$E_{a,max}$
0.25	$E_{a,max}$
0.125	$E_{a,max}$
0.0625	$E_{a,max}$
0.03125	$E_{a,max}$
0.01	$E_{a,max}$

⇨ Wind direction

Wind speed = 32.9 (m/s)

Wind direction = 299. (^{0}N)

Freq. range .05- .80 (Hz)

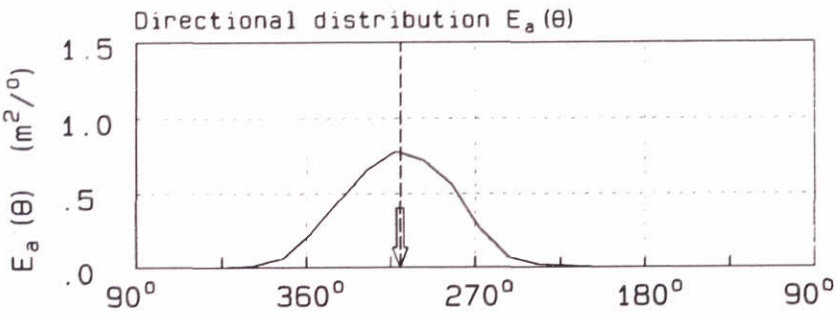

⇩ Mean wave direction

——— Case b1-t07

..... Case b1-t07

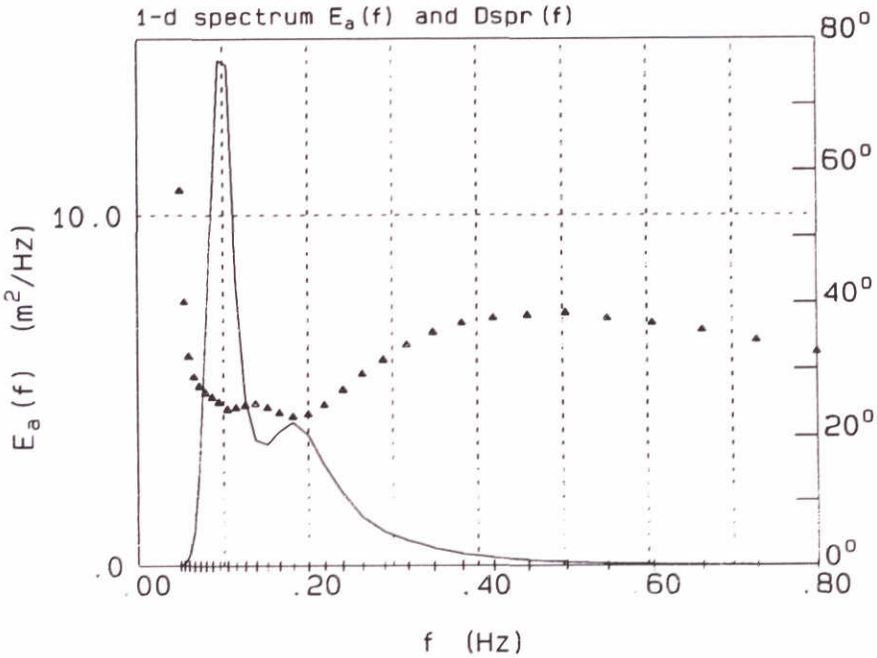

Parameters of $E_a(f)$

f_p	=	.09 (Hz)
Emax	=	14.40 (m^2/Hz)
H_s	=	4.21 (m)
T_{m02}	=	5.01 (s)
T_p	=	10.53 (s)
Dir	=	310.00 (^{0}N)
Dspr	=	26.78 (^{0})
kappa	=	.51
depth	=	13.21 (m)

Wave spectra in Friesche Zeegat, PHIDIAS Case b1-t07: Time run Location 4 x=200240.0 , y=612150.0		b1-t07
	Superstorm	
DELFT HYDRAULICS/DELFT UNIVERSITY OF TECHNOLOGY	H2368	Fig. 4.39

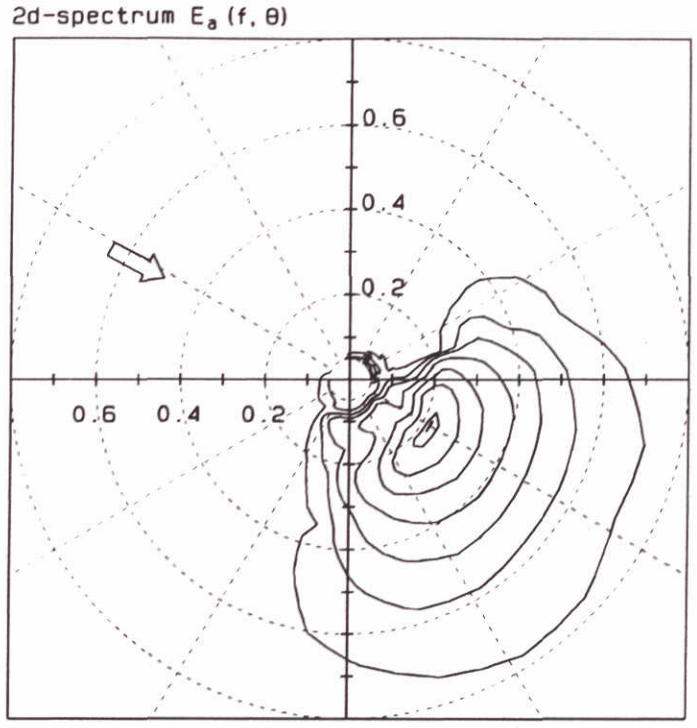

Contour levels:

0.99	$E_{a,max}$
0.90	$E_{a,max}$
0.50	$E_{a,max}$
0.25	$E_{a,max}$
0.125	$E_{a,max}$
0.0625	$E_{a,max}$
0.03125	$E_{a,max}$
0.01	$E_{a,max}$

⇨ Wind direction

Wind speed = 33.0 (m/s)

Wind direction = 298. (°N)

Freq. range .05- .80 (Hz)

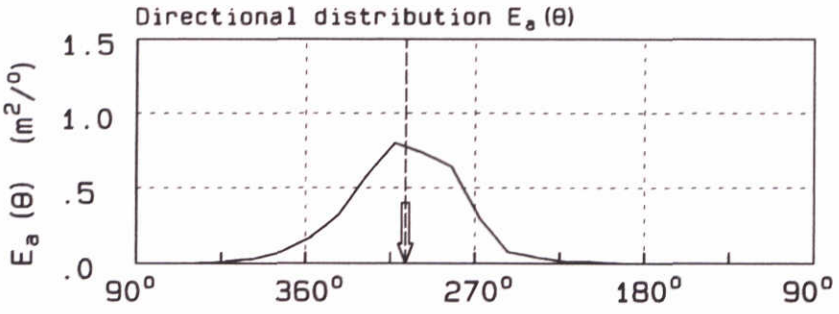

⇩ Mean wave direction

——— Case b1-t07

..... Case b1-t07

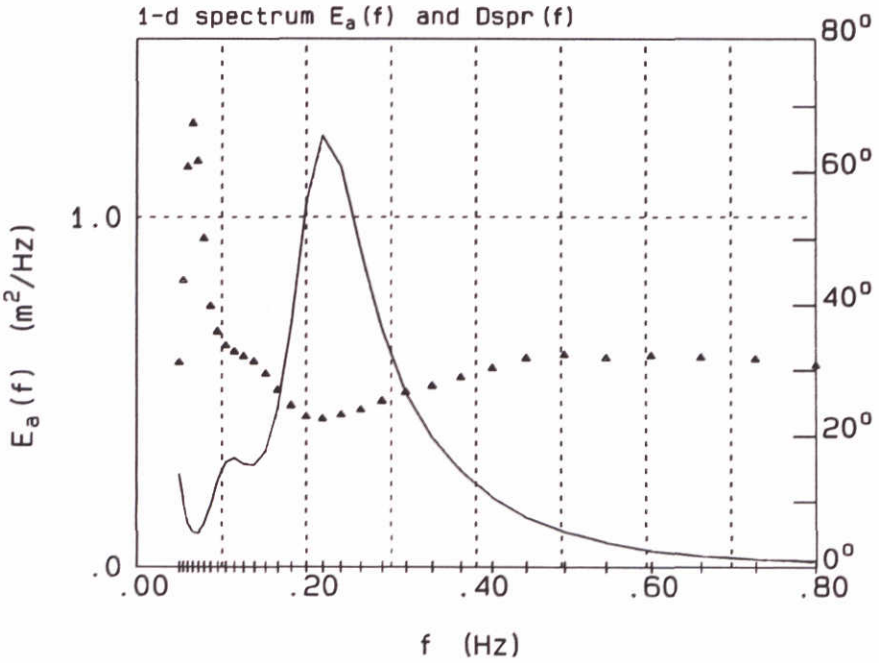

Parameters of $E_a(f)$

f_p	=	.22 (Hz)
Emax	=	1.23 (m^2/Hz)
H_s	=	1.90 (m)
T_{m02}	=	2.75 (s)
T_p	=	4.57 (s)
Dir	=	307.00 (°N)
Dspr	=	29.48 (°)
kappa	=	.24
depth	=	4.62 (m)

Wave spectra in Friesche Zeegat, PHIDIAS Case b1-t07: Time run Location 8 x=201457.1 , y=603243.0		b1-t07
	Superstorm	
DELFT HYDRAULICS/DELFT UNIVERSITY OF TECHNOLOGY	H2368	Fig. 4.40

Appendix I

Overview of flow models

Overview of flow models

The Continental Shelf Model (CSM)

The Continental Shelf Model covers a large part of the North West European Continental Shelf, with boundaries in deep water. See Figure A1.1. The model was originally build around 1984 in spherical coordinates. The resolution is now, 1/8th of a degree longitude and 1/12th of a degree latitude (approximately 9 by 9 km^2). The bathymetry in the North Sea was taken from the GENO model (Voogt, 1984), outside this area sea charts were used. The bathymetry was corrected for the difference between Chart Datum and Mean Sea Level. The bathymetry was consequently improved in recent years. The boundary conditions are prescribed in the form of harmonic constituents for the water levels. The model was calibrated on the basis of monthly runs by comparison of the harmonic constants from tidal analysis of model results in monitoring points with the harmonic constants from tidal analysis of measurements in coastal stations.

The Southern North Sea model (ZUNOWAQ-bol model)

The Southern North Sea model covers almost the entire part of the North Sea, South of the 54 degrees 30 minutes latitude. The model is nested into the CSM model. The model was originally build in 1984 in spherical coordinates. It has now a resolution of 1/24th of a degree longitude and 1/36th of a degree latitude (approximately 3 by 3 km^2). The bathymetry was updated many times with more recently available bathymetries and corrected for Mean Sea level. The boundary conditions in the form of harmonic constants for water levels were derived from the CSM model.

The curvi-linear Wadden model (Wadden-model)

The Wadden model covers an area of approximately 70 kilometres in a direction normal to the Wadden Islands and some 220 kilometres perpendicular to the Wadden Islands. The model reaches from Petten (south of Den Helder) till the German Wadden Island Norderney. An overview of the grid is shown in Figure A1.2. The curvi-linear model has a resolution which varies from 40 till 3526 metres in M-direction and from 63 till 1304 metres in N-direction. The bathymetry of the model, which was build in 1994, is constructed of a large amount of surveys in between 1987 and 1994. The model comprises approx. 69000 active computational grid points (DELFT HYDRAULICS, 1994a). The bathymetry refers to NAP. The boundary conditions in the form of harmonic constants for water levels were derived from the CSM model. A number of 22 constituents was used to drive the Wadden model.

The Friesche Zeegat model (FZ-model)

The Friesche Zeegat model was build in 1991 by "Rijkswaterstaat". It was one of the first examples of a recti-linear model with varying grid sizes. The model covers an area of approximately 32 by 20 km^2. An overview of the grid is shown in Figure A1.3. The boundary conditions for the model were derived from the curvi-linear Wadden model (500 by 500 m^2) resolution.

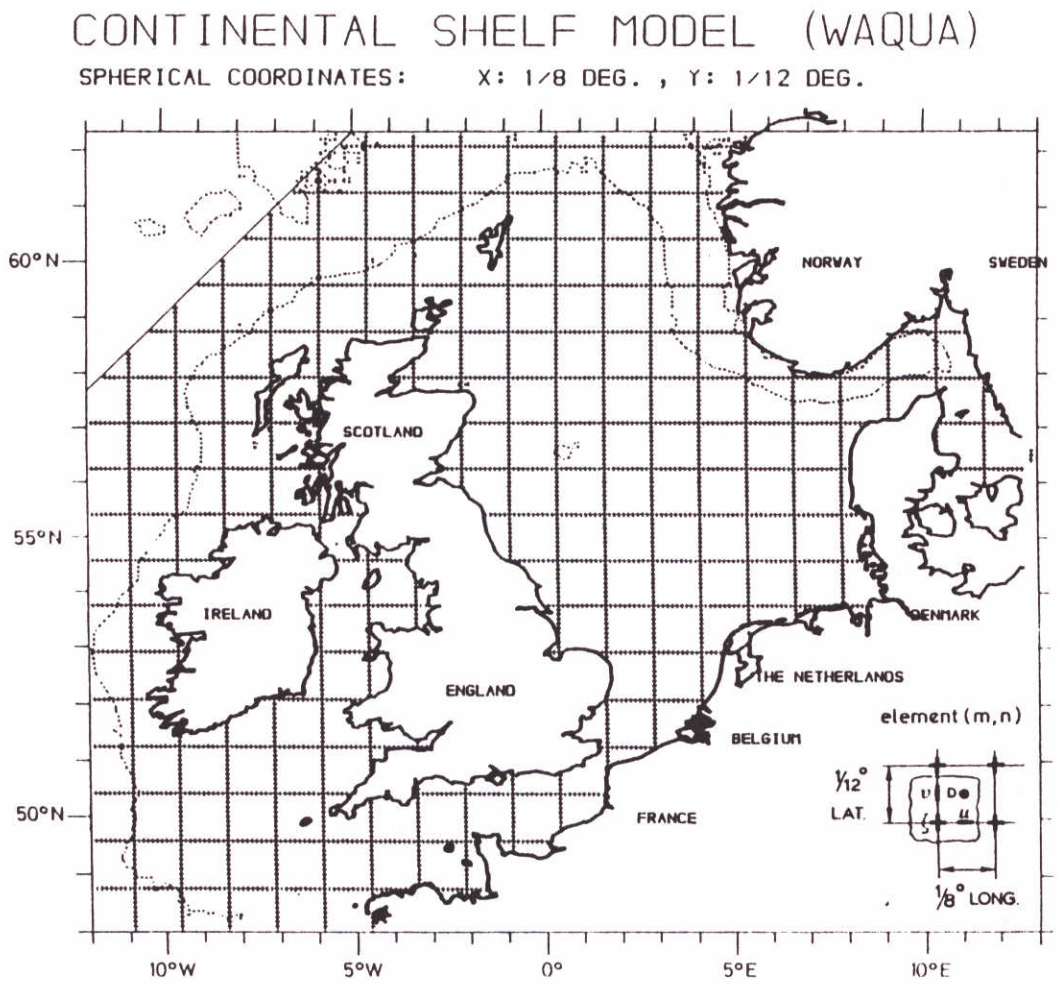

Computational area of CSM model

DELFT HYDRAULICS/DELFT UNIVERSITY OF TECHNOLOGY | H2368 | Fig. A1.1

Computational grid of WADDEN model

DELFT HYDRAULICS/DELFT UNIVERSITY OF TECHNOLOGY | H2368 | Fig. A1.2

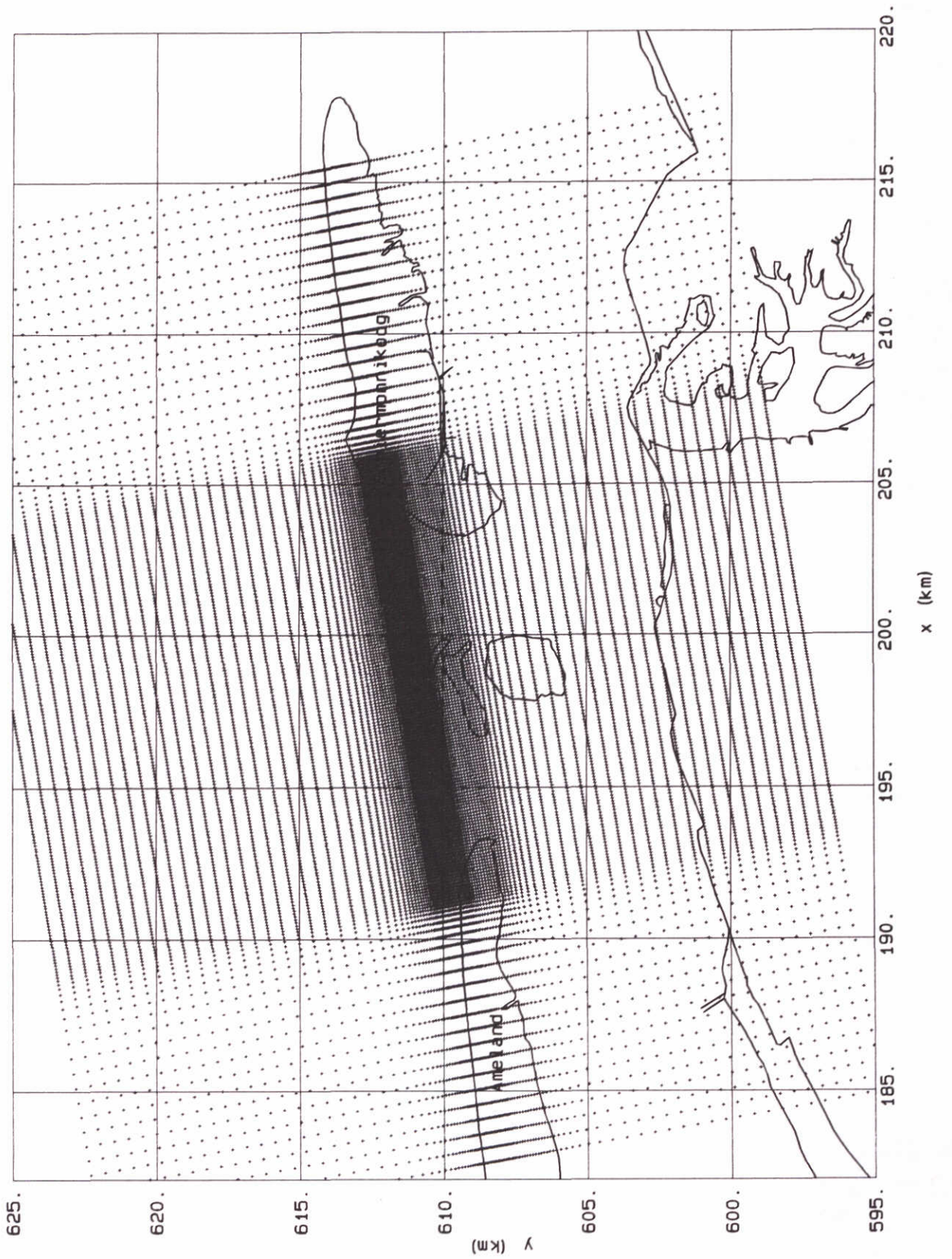

Grid points of the Friesche Zeegat flow model

DELFT HYDRAULICS/DELFT UNIVERSITY OF TECHNOLOGY | H2368 | Fig. A1.3

Appendix II

Modifications to SWAN for this project

Modifications to SWAN for this project

After a number of initial computations with SWAN in this project and after a number of verification computations outside this project, several modifications were made in the source code of SWAN for this project. These are listed here.

1 To maintain robustness (thus saving computing time) it was found that for such extreme conditions as in the super storm, the triads should be computed with an implicit scheme if their value is positive (receiving action from other frequencies) and with an explicit scheme if their value is negative (transferring action to other frequencies). The original numerical scheme (explicit for both positive and negative values) was correspondingly modified.

2 The magnitude of the triad wave-wave interaction has been reduced by 50%. The reasons are:
   — the original formulation in SWAN appeared to transfer too much action from low-frequencies to high frequencies in two observed field cases (Haringvliet and Friesche Zeegat),
   — the computational results of SWAN in the laboratory experiment of Battjes and Beji (1992) is only weakly sensitive to a variation in the magnitude of the triad interactions of a factor 2 (for the present formulation).

3 To save computing time, the triad interactions are not computed in the first iteration (the effect is a smoother (and therefore quicker) convergence of the results).

4 The first iteration in the original source code assumed a minimum wind speed in the wind generation module of SWAN to avoid overflow problems. This excluded the possibility to make calculations without wind. This has been solved by calling this module only whether the wind speed is more than 0.01 m/s.

5 The user-provided current field is not always consistent with the user-provided bathymetry. Two have therefore been added in SWAN:
   — set all current speeds at zero over land,
   — to avoid situations where all wave components (including the lowest discrete frequency) in a grid point in SWAN are swept down-current (causing numerical problems), current speeds which are larger than the shallow water action propagation speed (c = sqrt(gd) where g is gravitational acceleration and d is depth), are set this speed c.

6 Very little action occurred in some grid points in the SWAN computations for the super storm. This caused underflow problems which were solved by setting several auxiliary computation parameters at some minimum value.

It should be emphasized that all computations in the final report of this project have been carried out with these modifications in place.

Appendix III

Definitions of output variables

Definitions of output variables

In SWAN a number of variables, mostly related to waves are used in input and output. The definitions of these variables are conventional for the most part.

HSIGN significant wave height (H_s in m), defined as:

$$H_s = 4\sqrt{\int\int E(\omega,\theta)d\omega d\theta}$$

TM02 mean absolute wave period (in s) of $E(\omega,\theta)$, defined as:

$$T_{m02} = 2\pi \left[\frac{\int\int \omega^2 E(\omega,\theta)\, d\omega d\theta}{\int\int E(\omega,\theta) d\omega d\theta} \right]^{-1/2} = 2\pi \left[\frac{\int\int \omega^2 E(\sigma,\theta) d\sigma d\theta}{\int\int E(\sigma,\theta) d\sigma d\theta} \right]^{-1/2}$$

RTP peak period of $E(\sigma)$, equal to TP in the absence of currents. The character R refers to relative.

TP peak period of $E(\omega)$

KAPPA the normalized frequency narrowness of the spectrum. This parameter is known as the spectral wave groupiness parameter. It is defined by Battjes and van Vledder (1984) as:

$$\text{KAPPA} = \left| \int_0^\infty E(\omega) e^{i\omega\tau} d\omega \right| / E_{tot} \qquad \text{for } \tau = T_{m02}$$

The parameter KAPPA is a measure for the groupiness of wind waves and it is related to the width or narrowness of the frequency spectrum. The range of KAPPA is from 0 to 1. Broad frequency spectra have small values of KAPPA and relate to a small degree of wave groupiness. Narrow frequency spectra have high values of KAPPA and relate to a high degree of groupiness.

The parameter KAPPA is a relatively unknown parameter. To overcome this obscurity some additional numerical and graphical information is given for a number of typical JONSWAP spectra with various peak enhancement factors (Hasselmann et al., 1973). Based on a JONSWAP spectrum with $f_p = 0.1$ Hz, $\alpha = 0.01$, $\sigma_a = 0.07$ and $\sigma_b = 0.09$ a straightforward numerical integration has been performed in the frequency range 0.03-0.8 Hz to compute the parameter KAPPA for various values of the peak enhancement factor τ (GAMMA).

The results are given below:

τ	KAPPA
1.0	.422
2.0	.501
3.0	.555
3.3	.569
4.0	.596
5.0	.628
6.0	.654
7.0	.676
8.0	.694
9.0	.710
10.0	.724
15.0	.774
20.0	.805

The results for $\tau=1.0$ refer to a Pierson-Moskowitz spectrum. For $\tau=1.0$ and $\tau=20.0$ the corresponding normalized frequency spectra are shown below.

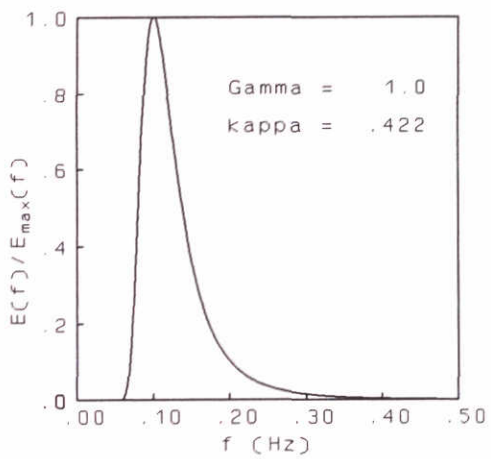

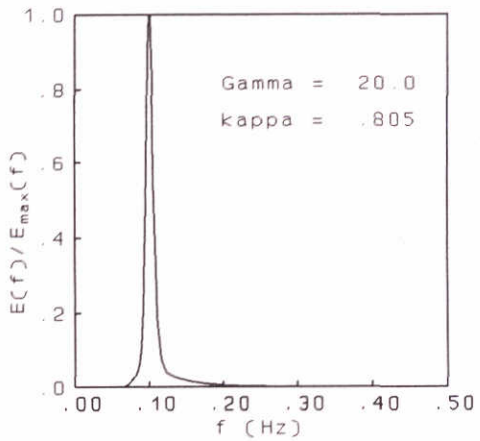

DIR mean wave direction (in rad internally in SWAN and in ^{0} in the output), as conventionally defined (see Kuik et al. 1988; this is the standard definition for WAVEC buoys) relative to x-axis of the problem coordinate system (counter-clockwise), except in the case of output with BLOCK command where the direction is relative to the x-axis of the output frame (measured counter-clockwise).

$$[\,\mathrm{DIR}\,] = \arctan\left[\int \sin(\theta)\,E(\sigma,\theta)\,d\sigma\,d\theta \Big/ \int \cos(\theta)\,E(\sigma,\theta)\,d\sigma\,d\theta\right]$$

This direction is the direction normal to the wave crests; note that, if currents are present, it is different from the direction of the energy transport

DSPR the directional width of the spectrum (directional spreading, in rad internally in SWAN and in ^{0} in the output), defined as

$$[\mathrm{DSPR}]^2 = \int_{-\pi/2}^{\pi/2} \{2\sin(\theta - \bar{\theta}/2)\}^2 D(\theta)\, d\theta$$

and computed as conventionally for pitch-and-roll buoy data (Kuik et al., 1988; this is the standard definition for WAVEC buoys):

$$[\mathrm{DSPR}]^2 = 2\left[1 - \left[\left(\int \sin(\theta) E(\sigma,\theta)\, d\sigma\, d\theta\right)^2 + \left(\int \cos(\theta) E(\sigma,\theta)\, d\sigma\, d\theta\right)^2\right]^{1/2}\right]$$

[MS] As input to the model in the command BOUNDARY (PARAM option) the directional distribution of incident wave energy is: $D(\theta) = A\ \{\cos(\theta)\}^{**}$[MS] at all frequencies. [MS] is not necessarily an integer number.
[MS] is, for this directional distribution, related to the directional spread of the waves (DSPR) as follows:

[MS]	DSPR (in ^{0})
1	37.5
2	31.5
3	27.6
4	24.9
5	22.9
6	21.2
7	19.9
8	18.8
9	17.9
10	17.1

Appendix IV

SWAN input file for case B1

SWAN input file for case B1

```
$
$ ******************* HEADING  ************************
$
PROJ 'SUPERSTORM' 'B1_C'
$
$   'standard run'
$
$  date: 31/1/53, time: 22.00
$
$ ******************* MODEL INPUT **********************
$
$ *** definition of computational grid :                    ***
$ *** xclen  yclen  mxc myc  xp     yp       alfa         mdc & ***

$ ***                                      flow   fhig     msc ***
GRID  24000. 31000. 96  124 182000. 620000. 280. CIRCLE 36 &
                                            .05   0.8      32
$
$ *** parameters for the three input grids :                  ***
$ ***                  xp      yp    alfa    mx    my     dx      dy ***
$
INPUT GRID WIND  180000. 590000.   0.    2     2    20000. 20000.
READ WIND 1. 'fzgwind2.dat' 4 1 FREE
$
INPUT GRID CURRENT 182000. 620000. 280.  240  310   100.   100.
READ CURRENT 1. 't07-uv.dat' 4 0 FREE
$
INPUT GRID BOTTOM  182000. 620000. 280.  240  310   100.   100.
READ BOTTOM 1. 't07-d.dat' 4 0 FREE
$
INPUT GRID WLEVEL  182000. 620000. 280.  240  310   100.   100.
READ WLEVEL 1. 't07-h.dat' 4 0 FREE
$
$ *** incident wave field ***
BOUNDARY LOW X JON PAR 8.54  10.52  310. 4.
$
$ *** processes activated ***
GEN3
BREAK
FRICTION
TRIAD
$
NUM ACCUR 0.03 0.03 0.03 97. 15
$
$ *************** OUTPUT REQUESTS **********************
$
$ *** 'fzeegat.loc' contains the 16 locations ***
```

```
POINTS 'locat' FILE 'fzeegat.loc'
$
$ *** definition of the nested grid:                    ***
$ ***          Lx     Ly     mx  my    x0     y0    alfa ***
NGRID 'nest1' 13000. 27750. 104 222 183650. 610645. 280.
NEST 'nest1' 'b1_cnest.rvw'
$
$ *** frame for output on computational grid ***
FRAME 'coarse' 24000. 31000. 182000. 620000. 280. 96 124
$
$ *** definition of the curves ***
$
CURVE 'R1'  198447.500000     622306.375000 33 &
            199178.818000     618195.254000 31 &
            199901.593750     614374.625000 18 &
            200240.0          612150.0      26 &
            200567.218000     608977.023000 19 &
            201245.296875     606717.000000 19 &
            201254.500000     604392.687500 9  &
            201457.093750     603243.000000 11 &
            201688.593750     601930.687500
$
CURVE 'R2'  201245.296875     606717.000000 37 &
            197643.593750     603756.000000 30 &
            194679.203125     601371.625000 18 &
            192975.0          600000.0
$
CURVE 'R3'  201245.296875     606717.000000 35 &
            205235.796875     604887.375000 23 &
            207966.203125     604002.312500 18 &
            210108.000000     603044.000000 8  &
            211000.0          602645.0
$
$ *** curve 1 in plot ***
LINE CONT 198447.500000     622306.375000 &
          199178.818000     618195.254000 &
          199901.593750     614374.625000 &
          200240.0          612150.0      &
          200567.218000     608977.023000 &
          201245.296875     606717.000000 &
          201254.500000     604392.687500 &
          201457.093750     603243.000000 &
          201688.593750     601930.687500
$
$ *** curve 2 in plot ***
LINE CONT 201245.296875     606717.000000 &
          197643.593750     603756.000000 &
          194679.203125     601371.625000 &
          192975.0          600000.0
```

```
$
$ *** curve 3 in plot ***
LINE CONT 201245.296875     606717.000000 &
          205235.796875     604887.375000 &
          207966.203125     604002.312500 &
          210108.000000     603044.000000 &
          211000.0          602645.0
$
$ *** definition of points on the three curves for plot ***
SITE 'S1'    198447.500000   622306.375000  TOWN
SITE 'S2'    199178.818000   618195.254000  TOWN
SITE 'S3'    199901.593750   614374.625000  TOWN
SITE 'S4'    200240.000000   612150.000000  TOWN
SITE 'S5'    200567.218000   608977.023000  TOWN
SITE 'S6'    201245.296875   606717.000000  TOWN
SITE 'S7'    201254.500000   604392.687500  TOWN
SITE 'S8'    201457.093750   603243.000000  TOWN
SITE 'S9'    201688.593750   601930.687500  TOWN
SITE 'S10'   205235.796875   604887.375000  TOWN

SITE 'S11'   207966.203125   604002.312500  TOWN

SITE 'S11x'  210108.000000   603044.000000  TOWN
SITE 'S12'   211000.0        602645.0       TOWN

SITE 'S13'   197643.593750   603756.000000  TOWN

SITE 'S14'   194679.203125   601371.625000  TOWN
SITE 'S15'   192975.0          600000.0     TOWN
$
$ *** block output ***
$
BLOCK 'coarse' FILE 'b1_c.blk' DEP HS TM02 RTP DSPR DIR FSPR
$
$ *** table output ***
TABLE 'R1' HEAD 'b1_c1.tbl'     XP YP WIND VEL DEP HS TM02 &
                                RTP DSPR DIR FSPR
TABLE 'R2' HEAD 'b1_c2.tbl'     XP YP WIND VEL DEP HS TM02 &
                                RTP DSPR DIR FSPR
TABLE 'R3' HEAD 'b1_c3.tbl'     XP YP WIND VEL DEP HS TM02 &
                                RTP DSPR DIR FSPR
TABLE 'locat' HEAD 'b1_c4.tbl' XP YP WIND VEL DEP HS TM02 &
                                RTP DSPR DIR FSPR
$
$ *** one-dimensional spectra ***
SPEC 'locat' SPEC1D ABS 'b1_c1d.spc'
$
$ *** two-dimensional spectra ***
SPEC 'locat' SPEC2D ABS 'b1_c2d.spc'
```

```
$
$ *** plots ***
$
PLOT 'COMPGRID' FILE 'b1_c.plt' 'depth and current' &
                                ISO DEP 2. 0. 100. &
                                VEC VEL dist=3  &
                                SITES LINES LOCATION 'nest1'
$
PLOT 'COMPGRID' FILE 'b1_c.plt' 'depth and wind' &
                                ISO DEP 2. 0. 100. &
                                VEC WIND dist=3 &
                                SITES LINES LOCATION 'nest1'
$
PLOT 'COMPGRID' FILE 'b1_c.plt' 'Hs and wave direction' &
                                ISO HS .5  0. 15. &
                                VEC DIR dist=3 &
                                SITES LINES LOCATION 'nest1'
$
PLOT 'locat'  FILE 'b1_c.plt' 'spectra at locations' &
              SPEC NORM 0.99 0.5 .1 0.02 0.004 0.0008 FREQ ABS
$
$                S1     S3     S5    S7     S10    S13
TEST 3,0 POINTS 2,67, 35,67, 56,66, 76,65, 76,81, 76,50
$
COMP
STOP
```

Appendix V

PHIDIAS input file

PHIDIAS input file

```
*.....................................................................
*
*    PHIDIAS input file PHUSER: file contains user input data
*
*.....................................................................
*
*    0. run IDENTIFICATION
*
     'RUNID'
*
*    0.1 Run description
*
*1
     'H2368'     'Super storm '
*
*    0.2 Run period
*
*1
     'period of the run (yyymmddhhmmss)' '530131180000' '530201020000'
*
*    0.2 Problem dimensions
*
*4
     'no of grid points in x direction'          156
     'no of grid points in y direction'          121
     'no of spectral frequencies'                30
     'no of spectral directions'                 24
*.....................................................................
*
*    1. OUTPUT selection
*
     'OUTPUT'
*10
     'time series to PHTIME'              'yes'
     'maps to PHMAPx'                     'yes'
     'spectra to PHSPEC'                  'yes'
     'optional print output to PHPRNT'    'no'
     'extensive logging to PHLOGS'        'no'
     'extensive logging to SCREEN'        'no'
     'error messages to PHERRS'           'yes'
     'error messages to SCREEN'           'no'
     'restart spectra to PHREST'          'yes'
     'plot spectra'                       'no'
```

```
*
*     1.1 time series
*
*4
     'no of parameters'                    0
     'parameter codes'                     'HM0'
     'no of grid points'                   0
     'pairs of x-y indices'                2  2
*
*     1.2 maps
*
*3
     'no of parameters'                    7
     'parameter codes'           'HH' 'HM0' 'TM02' 'TM02'  'FP1D'
                                 'DS' 'KA02'
     'output window SW and NE corner'      1 1   156  121
*
*     1.3 spectra
*
*4
     'no of spectra'                       1
     'spectrum codes'                      'E_a'
     'no of grid points'                   16
     'pairs of x-y coordinates'       198447.500000   622306.375
                                      199178.818000   618195.254
                                      199901.593750   614374.625
                                      200240.000000   612150.000
                                      200567.218000   608977.023
                                      201245.296875   606717.000
                                      201254.500000   604392.687
                                      201457.093750   603243.000
                                      201688.593750   601930.687
                                      205235.796875   604887.375
                                      207966.203125   604002.312
                                      210108.000000   603044.000
                                      211000.0        602645.0
                                      197643.593750   603756.000
                                      194679.203125   601371.625
                                      192975.0          600000.0
*
*     1.4 optional print output
*
*2
     'no of parameters'           0
     'parameter codes'
*.....................................................................
*
```

```
*     2. Activation or de-activation of PHYSICAL PROCESSES
*
      'PROCESS'
*
*     2.1 external conditions
*
*4
      'wind'                      'yes'
      'flow'                      'yes'
      'surge'                     'yes'
      'open boundary from file'   'yes'
*
*     2.2 wave generation and dissipation
*
*5
      'bottom friction'           'yes'
      'wave breaking'             'yes'
      'white capping'             'yes'
      'wind input'                'yes'
      'wave interaction'          'yes'
*
*     2.3 wave propagation
*
*4
      'propagation in xy_space'   'yes'
      'use boundary spectra'      'yes'
      'propagation in k_space'    'yes'
      'propagation in Ú_space'    'yes'
*.....................................................................
*
*     3. Selection of NUMERICAL ALGORITHMS
*
      'NUMERICAL'
*
*     3.1 wave generation and dissipation
*
*11
      'explicit scheme'                                 'no'
      'hybrid WAM scheme'                               'yes'
      'bottom friction diagonal'                        'yes'
      'wave breaking diagonal'                          'yes'
      'white capping diagonal'                          'yes'
      'wind input diagonal'                             'yes'
      'wave interaction diagonal'                       'yes'
      'energy growth limitation'                        'yes'
      'hf tail after wave generation'                   'yes'
      'conservative elimination after generation'       'yes'
      'hf tail basic integrals'                         'yes'
```

```
*
*     3.2 wave propagation
*
*2
      'conservative elimination after propagation'   'yes'
      'hf tail after wave propagation'               'yes'
*.....................................................................
*
*     4. FORMULATIONS used
*
      'FORMULAS'
*
*     4.1 bottom friction
*
*2
      'Qbo<1>= JONSWAP                                          'yes'
      'Qbo<2>= Madsen                                           'no'
*
*     4.2 wave breaking
*
*2
      'Qbr<1>= -α.Qb.fm.Hmax²/(4.m0).N'                         'no'
      'Qbr<2>= ..........'                                      'yes'
*
*     4.3 white capping
*
*2
      'Qwc<1>= -cwc.σms.[k/kms].[α/αpm]².N'                     'YES'
      'Qwc<2>= ..........'                                      'NO'
*
*     4.4 wind input
*
*2
      'Qin<1>= max {0,¼.pa/pw.[28.u*/σ.k.cos(θ-θu*)]}.E'        'YES'
      'Qin<2>= ..........'                                      'NO'
*
*     4.5 wave interaction
*
*2
      'Qnl<1>= quadruple wave-wave interaction'                 'YES'
      'Qnl<2>= ..........'                                      'NO'
*
*     4.6 dispersion relation
*
*2
      'σ²<1> = gktanh(kd)'                                      'YES'
      'σ²<2> = ..........'                                      'NO'
```

```
*
*     4.7 computation flow in line with waves
*
*2
      'u//<1> = u.cos(θ-θu)'                                    'YES'
      'u//<2> = ..........'                                     'NO'
*
*     4.8 transformation u10 -> u*
*
*2
      'u*<1>= drag law'                                         'YES'
      'u*<2>= ........'                                         'NO'
*
*     4.9 computation Hmax for Qbr
*
*2
      'Hmax<1>= τ1/km.tanh[τ2/τ1.km.d]'                         'NO'
      'Hmax<2>= τ1.d'                                           'YES'
*.....................................................................
*
*     5. TIME steps
*
      'TIME STEPS'
*
*     5.1 unit ('S' for seconds 'M' for minutes)
*
      'unit'    'S'
*
*     5.2 computational steps
*
*3
      'basic model step'              2
      'propagation'                   2
      'source term integration'      60
*
*     5.3 external conditions
*
*4
      'wind input'                 3600
      'flow input'                 3600
      'surge input'                3600
      'open boundary update'       3600
*
*     5.4 output
*4
      'time series'                3600
      'maps'                       3600
      'spectra'                    3600
      'restart'                   14400
```

```
*.....................................................................
*
*     6. INITIAL SPECTRA
*
      'INITIAL'
*
*     6.1 how to get the initial spectra
*
*5
      'read prepro E(fr,θ)'          'yes'
      'read restart N(k,θ)'          'NO'
      'set white noise E(fr,θ)'      'no'     0.000001
*
*     fp= 0.     means fp will be computed from wind speed
*     θp= 999.   means θp will be computed from wind direction
*
      'compute jonswap E(fr,θ)'      'yes'
          'Γ=' 3.3  'α=' 0.001 'm=' 5. 'σ≤fp=' 0.07 'σ>fp=' 0.09
          'fp= ' .25  'θp=' 0.
      'set single peak E(fr,θ)'      'NO'
          'E(ifr,iθ)=' 100.      'ifr=' 10  'iθ=' 1
*
*     6.2 relative frequency range and directions
*
*3
      'mean depth for fr -> k in m'   20.
      'fmin and fmax in Hz'           0.05 .8
      'directions θ in degrees'        0.   15.   30.   45.   60.   75.
                                       90.  105.  120.  135.  150.  165.
                                      180.  195.  210.  225.  240.  265.
                                      270.  295.  300.  315.  330.  345.
*.....................................................................
*
*     7. NUCLEUS PARAMETERS
*
      'NUCLEUS'
*
*     7.1 Energy growth (due to wave generation)
*
*1
      'energy increment limitation in % '    5.
*
*     7.2 High frequency tail (after propagation and generation)
*3
      'power of k in hf-tail'         -2.5
      'factor to multiply fm with'    2.5
      'factor to multiply fpm with'   4.
```

```
*
*     7.3 Source term computation
*
*     7.3.1 Wave breaking
*
*3
      'scaling factor α '              1.
      'coefficient γ1 for Hmax'        0.73
      'coefficient γ2 for Hmax'        0.80
*
*     7.3.2 White capping
*
*1
      'factor times 2.36E-5 '          1.
*
*      7.3.3 Wave interaction
*            Enter constants per configuration
*
*3
      'no of configurations'           1
      'lambda'                         0.25
      'factor times 0.0746 '           3000.
```

location Delft
Rotterdamseweg 185
p.o. box 177
2600 MH Delft
The Netherlands
telephone +31 15 2569353
telefax + 31 15 2619674
telex 38176 hydel-nl
e-mail info@wldelft.nl

location 'De Voorst'
Voorsterweg 28, Marknesse
p.o. box 152
8300 AD Emmeloord
The Netherlands
telephone +31 527 242922
telefax +31 527 243573
telex 42290 hylvo-nl
e-mail info@wldelft.nl